Structure-Function Relationships of Enzymes Involved in Starch Modification

Wang, Yu

Publication date:
2023

Document Version
Publisher's PDF, also known as Version of record

Structure-Function Relationships of Enzymes Involved in Starch Modification

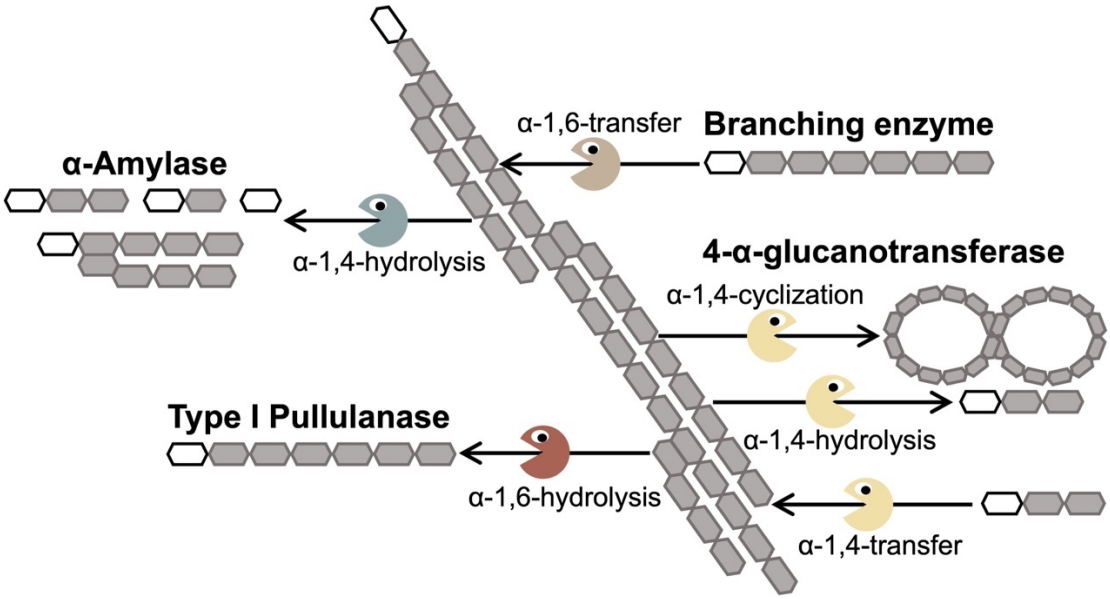

Yu Wang

PhD thesis

Supervisors: Birte Svensson & Marie Sofie Møller

Department of Biotechnology and Biomedicine

Technical University of Denmark – DTU

Kgs. Lyngby – Denmark

September 2023

Preface

The research presented in this PhD thesis was accomplished in the Enzyme and Protein Chemistry group at the Department of Biotechnology and Biomedicine - Technical University of Denmark, in the period from 1-10-2020 to 30-9-2023 under the supervision of main supervisor Prof. Birte Svensson, and co-supervisor Assoc. Prof. Marie Sofie Møller, with external stays at the University of Copenhagen and Jiangnan University.

The project was supported by Technical University of Denmark, and a China Scholarship Council (CSC) grant #202006790033 (to Yu Wang).

The PhD project was executed with the help of many collaborators:

- Prof. Andreas Blennow, Department of Plant and Environmental Sciences, University of Copenhagen, Denmark
- Prof. Peter Westh, Interfacial Enzymology, Department of Biotechnology and Biomedicine, Technical University of Denmark, Denmark
- Prof. Georges Feller, Laboratory of Biochemistry, Center for Protein Engineering-InBioS, University of Liège, Belgium
- Prof. Yuxiang Bai, School of Food Science and Technology, Jiangnan University, China
- Prof. Štefan Janeček, Laboratory of Protein Evolution, Institute of Molecular Biology, Slovak Academy of Sciences, Slovakia
- Asst. Prof. Chengfang Pang, Research Group for Genomic Epidemiology, National Food Institute, Technical University of Denmark, Denmark
- Dr. Hossein Mohammad-Beigi, Protein Biophysics, Department of Biotechnology and Biomedicine, Technical University of Denmark, Denmark
- Ph.D. candidate Yu Tian, Department of Plant and Environmental Sciences, University of Copenhagen, Denmark
- Dr. Xiaoxiao Li, School of Food Science and Technology, Jiangnan University, China
- Dr. Yuyue Zhong, Department of Plant and Environmental Sciences, University of Copenhagen, Denmark
- Dr. Stefan Jarl Christensen, Enzyme Technology, Department of Biotechnology and Biomedicine, Technical University of Denmark, Denmark

Acknowledgements

Finally, it is time to say goodbye to my PhD journey. I remember I wrote some words in the acknowledgment for my master thesis: I hold a sincere aspiration to perpetually nurture my love and optimism for academia and life. I am really happy that I made this decision to carry on my academia at Technical University of Denmark. I am super grateful to everyone who helped, encouraged, and accompanied me.

Firstly, I would like to start by expressing my deepest gratitude to my PhD supervisor, Prof. Birte Svensson. Thank you so much for giving me the opportunity to embark on this wonderful PhD project, which fits so well with my interest in applied enzymology. Thank you for always staying kind and patient, and for all the technical and less technical talks. You taught me a lot, not only about scientific work, but also about life. You are the one always be there to listen to me and encourage me when I was in trouble in my project. This thesis would not have been the same today without you.

Secondly, I'm extremely grateful to my co-supervisor and officemate, Assoc. Prof. Marie Sofie Møller. It was an amazing experience to share office with you since we can talk about my project anytime when I have some process, problem, or some new ideas, and you were always willing to talk and share your thought. You are so knowledgeable, and could always give me an answer. I have learnt so much from you about CAZymes and research in general. Thank you for helping me out from troubles during my PhD.

Thirdly, I want to give my special thanks to my amazing cooperators: Prof. Peter Westh and Asst. Prof. Chengfang Pang from Technical University of Denmark, Prof. Andreas Blennow and Dr. Yuyue Zhong from University of Copenhagen, and Prof. Georges Feller from University of Liège. You are so professional and knowledgeable, and I really enjoyed and appreciated the excellent cooperation. I also want to thank Prof. Yuxiang Bai, Dr. Xiaoxiao Li, and master students from Prof. Bai's lab in Jiangnan University for helping me with some experiments. I am also thankful to Prof. Štefan Janeček from Slovak Academy of Sciences, and Prof. Bernard Henrissat from DTU for helping me with some of the bioinformatic analyses.

Now, I want to say Tusind tak to my wonderful colleagues, Mette, Mikkel, Tobias, Andrew, Hossein, Karina, and Filip from the EPC group. It was such a nice time to work with you all. I will miss all the scientific and non-scientific talks, lunch, Monday cake, coffee break, Friday beer and many other fun times we had during the last three years. Most of my PhD work was carried out in the Department of Biotechnology and Biomedicine at DTU, and I am grateful for all the PIs and colleagues. There are many excellent PCET people I have met over the last three years, too numerous to point out individually here, unfortunately.

Finally, I would like to thank my parents, Zuhua Wang and Lanjiao Zhang. You have always been there encouraged me and listened to my complains. Now, words cannot express my love and gratitude to my girlfriend Yu Tian. We have shared almost the entire PhD journey together. We went through a lot of happiness, troubles and problems in our projects and daily lives. Thank you so much for always being there, listening to me, understanding me, and encouraging me. I couldn't image how the life would have been without you.

I would also like to thank Technical University of Denmark and China Scholarship Council for the financial support during my PhD project.

行文至此，三年的博士生涯也就告一段落了。感谢大家的陪伴与帮助，也感谢这个一直在追逐自己学术目标的自己。在此借用我硕士论文中的一句话：希望这篇博士论文不会是我学术和科研的终章，希望自己还能保持着对科研对生活的热爱和希望，希望前面的这些话不止是希望。

Yu Wang in Denmark, 26th September 2023

王禹 2023 年 9 月 26 日于丹麦

List of publications

Paper 1: **Yu Wang**, Yu Tian, Yuyue Zhong, Mohammad Amer Suleiman, Georges Feller, Peter Westh, Andreas Blennow, Marie Sofie Møller, Birte Svensson. Improved hydrolysis of granular starches by a psychrophilic α-amylase starch binding domain-fusion. (2023) *Journal of Agricultural and Food Chemistry*, 71, 9040–9050.
DOI: https://doi.org/10.1021/acs.jafc.3c01898

Paper 2: **Yu Wang**, Yazhen Wu, Stefan Jarl Christensen, Štefan Janeček, Yuxiang Bai, Marie Sofie Møller, Birte Svensson. Impact of starch binding domain fusion on activities and starch product structure of 4-α-glucanotransferase. (2023) *Molecules*, 23, 1320.
DOI: https://doi.org/10.3390/molecules28031320

Paper 3: **Yu Wang**, Yu Tian, Stefan Jarl Christensen, Andreas Blennow, Birte Svensson, Marie Sofie Møller. An enzymatic approach to quantify branching on the surface of starch granules by interfacial catalysis. (2024) *Food Hydrocolloids*, 146, 109162.
DOI: https://doi.org/10.1016/j.foodhyd.2023.109162

Paper 4: **Yu Wang**[1], Chengfang Pang[1], Hossein Mohammad-Beigi, Xiaoxiao Li, Yazhen Wu, Marie Karen Tracy Hong Lin, Yuxiang Bai, Marie Sofie Møller, Birte Svensson. Sequential starch modification by branching enzyme and 4-α-glucanotransferase improves retention of curcumin in starch-alginate beads. (2023) *Carbohydrate Polymers*, 323, 121387.
DOI: https://doi.org/10.1016/j.carbpol.2023.121387

Manuscript 1: **Yu Wang**, Birte Svensson, Bernard Henrissat, Marie Sofie Møller. Functional roles of N-terminal domains in pullulanase from human gut *Lactobacillus acidophilus*. Submitted to *Journal of Agricultural and Food Chemistry* on the 11th of September 2023 (Under review).

Manuscript 2: **Yu Wang**, Yu Tian, Stefan Jarl Christensen, Andreas Blennow, Peter Westh, Birte Svensson, Marie Sofie Møller. Sabatier Principle for Understanding the Effect of Enzyme Modification of Granular Starch. In preparation.

[1] These authors contributed equally to this work.

Not included in this thesis:

1. Yu Tian[1], **Yu Wang**[1], Yuyue Zhong, Marie Sofie Møller, Peter Westh, Birte Svensson, Andreas Blennow. Interfacial catalysis during amylolytic degradation of starch granules: Current understanding and kinetic approaches. (2023) *Molecules*, 28, 3799.
DOI: https://doi.org/10.3390/molecules28093799

2. Yu Tian, **Yu Wang**, Xingxun Liu, Klaus Herburger, Peter Westh, Marie Sofie Møller, Birte Svensson, Yuyue Zhong, Andreas Blennow. Interfacial enzyme kinetics reveals degradation mechanisms behind resistant starch. (2023) *Food Hydrocolloids*,140, 108621.
DOI: https://doi.org/10.1016/j.foodhyd.2023.108621

3. Xiaoxiao Li[1], **Yu Wang**[1], Jing Wu, Zhengyu Jin, Lubbert Dijkhuizen, Maher Abou Hachem, Yuxiang Bai. *Thermoproteus uzoniensis* 4-α-glucanotransferase catalyzed production of a thermo-reversible potato starch gel with superior rheological properties and freeze-thaw stability. (2023) *Food Hydrocolloids*, 134, 108026.
DOI: https://doi.org/10.1016/j.foodhyd.2022.108026

4. Xiaoxiao Li, **Yu Wang**, Jing Wu, Zhengyu Jin, Lubbert Dijkhuizen, Birte Svensson, Yuxiang Bai. Designing starch derivatives with desired structures and functional properties via rearrangements of glycosidic linkages by starch-active transglycosylases. (2023) *Critical Reviews in Food Science and Nutrition*, 1-14.
DOI: https://doi.org/10.1080/10408398.2023.2198604

[1] These authors contributed equally to this work.

Abstract

Starch, a sustainable and abundant energy storage source found in human food and animal feed, plays a crucial role in diverse applications such as biomaterials, biorefineries, and biomass feedstocks for fuel energy. To enhance its properties, starch can be subjected to enzymatic, chemical, or physical treatments through structural engineering. Enzyme treatment using starch-active enzymes is an environmentally friendly and attractive approach, improving thermal properties, digestion resistance, and complexation capacity. Enhancing catalytic efficiency of these enzymes can be achieved through mutations or constructing starch binding domain (SBD) fusions, which increase the affinity of the enzymes for the substrates and consequently improve their catalytic efficiency.

The thesis is divided into 5 chapters.

Chapter 1 is the Introduction, which starts by an overview of the multi-level structure of starch granules. Additionally, it delves into the realm of carbohydrate active enzymes (CAZymes), with a particular emphasis on the enzymes that were studied in this thesis. It is also explored how CAZymes find application in the modification of starch. Furthermore, it is delved into the understanding of SBDs, in terms both of their structural characteristics and functional roles, along with their innovative application through SBD fusions. As the essence of this thesis, we introduce the concept of interfacial catalysis and kinetics of starch granules, and shed light on its significance. To conclude, a comprehensive overview of the fundamental materials, enzymes, and methodologies in this thesis are provided.

Chapter 2 is the Result and divided into 3 subchapters.

Subchapter 2.1 comprises 2 papers (*Paper 1* and *Paper 2*). *Paper 1* focused on the impact of SBDs on the interfacial catalysis on granular starches by C-terminally fusing an SBD from either *Aspergillus niger* glucoamylase (SBD_{GA}) or *Arabidopsis thaliana* glucan, water dikinase 3 (SBD_{GWD3}) to a psychrophilic α-amylase, AHA, from the Antarctic bacterium *Pseudoalteromonas haloplanktis* TAB23. The Michaelis-Menten (MM) approach is used to determine kinetic parameters for α-amylase hydrolysis of granular starch. This suits soluble substrates having an excess substrate, but is challenging for insoluble starch with undefined molarity and limited enzyme accessibility. To overcome this, we applied interfacial kinetics analysis with enzyme-starch granule adsorption isotherms, inspired by cellulases acting on cellulose, to measure the attack site density ($^{kin}\Gamma_{max}$) and binding site density ($^{ads}\Gamma_{max}$) for various types of starch granules. According to the interfacial kinetics analysis, the AHA-SBD fusions increased the density of enzyme attack sites and binding sites on the starch granules

by up to 5- and 7-fold, respectively. *Paper 2* focused on the impact of an N-terminal SBD fusion on the activities and starch product structure of a thermophilic 4-α-glucanotransferase from *Thermoproteus uzoniensis* (TuαGT). The SBDs were the N-terminal tandem domains (SBD_{St1} and SBD_{St2}) from *Solanum tuberosum* disproportionating enzyme 2 (*St*DPE2), and the C-terminal domain (SBD_{GA}) of glucoamylase from *Aspergillus niger* (*An*GA). The results showed that SBD-TuαGT fusions had higher hydrolytic activity than TuαGT and higher affinity for starch granules. Among the *St*DPE2 SBD-fusions, SBD_{St2} significantly outperformed SBD_{St1} in enhancing TuαGT activity, substrate binding, and stability.

Subchapter 2.2 includes 1 paper and 2 manuscripts (*Paper 3*, *Manuscripts 1* and *2*). *Manuscript 1* focused on the impact of SBDs on interfacial catalysis of starch granules by pullulanase. In this manuscript, we identified the function of N-terminal domains (NTDs), including a CBM41 and two domains of unknown function (DUFs) in the pullulanase from *Lactobacillus acidophilus* NCFM (*La*Pul) by two recombinantly produced truncated variants, namely ∆41-*La*Pul (without CBM41) and ∆(41+DUFs)-*La*Pul (without CBM41 and two DUFs). Through analyzing the unfolding temperature, binding affinity to β-cyclodextrin (β-CD) and starch granules, as well as kinetics on soluble substrates and interfacial kinetics on insoluble starch granules, we established that CBM41 plays a role in substrate binding, while the DUFs contribute to stability. As inspired by *Manuscript 1*, we hypothesized that the attack site density ($^{kin}\Gamma_{max}$) for pullulanase on the granular starches can be used to represent the density of branch point on the surface of starch granules since type I pullulanase (PULI) is only active on α-1,6-linkages (*Paper 3*). In *Paper 3*, the kinetics analysis of heterogenous catalysis was adapted to enumerate α-1,6-linked branch points hydrolyzed by a commercial *Bacillus licheniformis* pullulanase (*Bl*Pul) on the surface of granules of waxy and normal maize starch (WMS and NMS). To validate this novel method, we also pretreated these granular maize starches using either branching enzyme from *Rhodothermus obamensis* that (*Ro*BE) catalyzes introduction of new α-1,6 linked branch chains or by TuαGT (produced in *Paper 2*). The results indicated that WMS showed 1.9-fold higher branch point density on the starch surface than NMS. Besides, the treatment by *Ro*BE increased the branch point density for WMS from 1.7 to 3.3 nmol/g starch granules, while the treatment by TuαGT did not affect the branch point density for the two maize starch granules. *Manuscript 2* is a continuous work after *Paper 3*, where the Sabatier principle was introduced as a tool to understand the enzymatic reaction on starch granules. In *Manuscript 2*, we used BE and 4αGT to modify three types of maize starches with different amylose content and analyzed the structure of these granular starches. By analyzing the relationship between the relative affinity and reaction rate to *Bl*Pul, it was found that the *Ro*BE-modified starches showed higher affinity and lower reaction rate, except for the *Ro*BE-modified waxy maize starch, than unmodified and TuαGT-modified starches. This change in

affinity and reaction rate might stem from the granular structure of the starches, including the crystallinity, surface order degree and chain length distribution.

Subchapter 2.3 includes 1 paper (*Paper 4*) and is different from subchapters 2.1 and 2.2, as it does not involve enzyme discovery and characterization. In *Paper 4*, a novel super-branched amylopectin was prepared by modifying gelatinized normal maize starch using *Ro*BE and TuαGT. This modified starch was used for co-entrapment of a curcumin-loaded emulsion in alginate beads (ABs). UV stability and *in vitro* simulated gastrointestinal digestion were evaluated for of all prepared types of ABs, and demonstrated the potential of using enzymatically modified starch and alginate as a versatile vehicle for co-encapsulation to obtained controlled release and targeted delivery of bioactive compounds.

Chapters 3, 4 and 5 are the general discussion, conclusion, and future perspectives of the thesis, respectively.

This thesis provided new knowledge about the function of SBDs in different starch-active enzymes, especially about the interfacial catalysis of granular starches. This interfacial kinetic analysis provided new insights in the understanding the enzymatic degradation and/or modification of starch granules. Besides, we also investigated the application of enzyme modified starches for encapsulation of bioactive compounds within alginate beads.

Dansk Resumé

Stivelse, en bæredygtig og rigelig energilagringskilde, findes i menneskers fødevarer og dyrefoder, og spiller en afgørende rolle i forskellige anvendelser såsom biomaterialer, bioraffinaderier og biomasseråvarer til brændstofenergi. For at forbedre stivelses egenskaber kan den gennemgå enzymatiske, kemiske eller fysiske behandlinger. Enzymbehandling ved hjælp af stivelsesaktive enzymer er en miljøvenlig og attraktiv tilgang, der kan forbedre termiske egenskaber, fordøjelsesresistens og kompleksdannelseskapacitet. Forbedring af katalytisk effektivitet kan opnås gennem enzymmutationer eller konstruktion af fusioner med et stivelsesbindende domæne (SBD), som øger enzymernes affinitet for substrater og derved forbedrer den katalytiske effektivitet.

Ph.d.-afhandlingen er opdelt i fem kapitler:

Kapitel I er introduktionen, hvor der startes med at give et overblik over stivelseskorns strukturelle niveauer. Derudover dykker vi ned i kulhydrataktive enzymer (CAZymes), med særlig vægt på de enzymer, der er blev undersøgt i denne ph.d.-afhandling og hvordan CAZymes bruges til modifikation af stivelse. Desuden dykker vi ned i forståelsen af stivelsesbindende domæner (SBD'er) med hensyn til deres strukturelle egenskaber og funktionelle roller, samt deres innovative anvendelse gennem SBD-fusioner. Med hovedvægt i denne afhandling introduceres begrebet grænsefladekatalyse og kinetik og dets betydning. Afslutningsvis gives et omfattende overblik over de anvendte materialer, enzymer og metoder.

Kapitel 2 er Resultater og opdelt i 3 underkapitler.

Underkapitel 2.1 omfatter to artikler (Artikel 1 og Artikel 2). Artikel 1 fokuserede på SBD'ers virkning på grænsefladekatalyse for stivelseskorn i form af C-terminal fusionering af SBD fra enten *Aspergillus niger* glucoamylase (SBD_{GA}) eller *Arabidopsis thaliana* glucan, waterdikinase 3 (SBD_{GWD3}) til AHA, en psykrofil amylase, fra den antarktiske bakterie *Pseudoalteromonas haloplanktis* TAB23. Michaelis-Menten (MM) metoden er almindeligt benyttet til at bestemme kinetiske parametre for α-amylase-katalyseret hydrolyse af stivelseskorn. Det passer til opløselige substrater med overskydende substrat, men er udfordret for uopløselig stivelse, hvor substratets molaritet er svær at definere ligesom det er vanskeligt tilgængeligt for enzymet. Vi har derfor benyttet grænsefladekinetik-analyse kombineret med enzym-adsorptionsisotermer, inspireret af cellulasers reaktion med cellulose. Det har muliggjort bestemmelse af tætheden af enzymets angrebssteder ($^{kin}\Gamma_{max}$) og tætheden af dets bindingssteder ($^{ads}\Gamma_{max}$) for forskellige typer af stivelseskorn. Ifølge grænseflade-kinetik-analysen forøgede AHA-SBD-fusionerne tætheden af enzymangrebssteder og

bindingssteder på stivelseskorn med henholdsvis op til 5 og 7 gange. Artikel 2 fokuserede på N-terminal SBD-fusions effekt på aktiviteter og stivelsesprodukt-strukturer af en termofil 4-α-glucanotransferase fra *Thermoproteus uzoniensis* (TuαGT). SBD'erne omfattede de N-terminale tandemdomæner (SBD_{St1} og SBD_{St2}) fra *Solanum tuberosum* disproportionerende enzym 2 (*St*DPE2) og det C-terminale domæne (SBD_{GA}) af glucoamylase fra *Aspergillus niger* (*An*GA). Resultaterne viste, at SBD-TuαGT-fusioner havde højere hydrolytisk aktivitet end TuαGT og højere affinitet for stivelseskorn. Blandt *St*DPE2 SBD-TuαGT-fusionerne var SBD_{St2} betydeligt bedre end SBD_{St1} med hensyn til at forbedre TuαGTs aktivitet, substratbinding og stabilitet.

Underkapitel 2.2 omfatter en artikel og to manuskripter (Artikel 3, Manuskript 1 og 2). Manuskript 1 fokuserede på SBD'ers indflydelse på en pullulanases grænsefladekatalyse af stivelseskorn. I dette manuskript identificeredes funktionen af N-terminale domæner (NTD'er), herunder CBM41 og to domæner med ukendt funktion (DUF'er) i en pullulanase fra *Lactobacillus acidophilus* NCFM (*La*Pul) ved at fremstille to rekombinante forkortede varianter, nemlig ∆41-*La*Pul (uden CBM41) og ∆(41+DUF'er)-*La*Pul (uden CBM41 og to DUF'er). Ved analyse af udfoldningstemperatur, affinitet for β-cyclodextrin og stivelseskorn, samt kinetik for opløseligt substrat og grænsefladekinetik for stivelseskorn, blev det vist, at CBM41 spiller en afgørende rolle for substratbinding, mens DUF'erne bidrager til stabilitet.

Inspireret af Manuskript 1 antog vi, at angrebsstedstæthed ($^{kin}\Gamma_{max}$) for pullulanase på stivelseskorn kan repræsentere tætheden af forgreningspunkter, da type I pullulanase (PULI) kun er aktiv overfor α-1,6-bindinger (Artikel 3). I Artikel 3 har vi brugt kinetik for heterogen katalyse til at måle α-1,6-forgreningspunkter, som hydrolyseres af en kommerciel *Bacillus licheniformis* pullulanase (*Bl*Pul) på overfladen af ”waxy” og normale majsstivelseskorn (WMS og NMS). For yderligere at validere denne nye metode blev de to majsstivelser modificeret enten med *Rhodothermus obamensis* forgreningsenzym (*Ro*BE), der katalyserer introduktion af nye α-1,6-forbundne grenkæder, eller med TuαGT fremstillet som beskrevet i Artikel 2. Resultaterne understregede, at WMS har 1,9 gange højere forgreningspunktstæthed end NMS. Desuden forøgede behandlingen med *Ro*BE forgreningspunkttætheden for WMS fra 1,7 til 3,3 nmol/g stivelseskorn, mens behandlingen med TuαGT ikke påvirkede forgreningspunkttætheden. Manuskript 2 er en fortsættelse af Artikel 3, hvor Sabatier-princippet introduceres som værktøj til at forstå enzymreaktionen med stivelseskorn. I Manuskript 2 blev BE og 4αGT brugt til at modificere tre typer majsstivelseskorn med forskelligt amyloseindhold og analysere deres struktur. Ved at analysere forholdet mellem den relative affinitet og reaktionshastighed for *Bl*Pul vistes det, at *Ro*BE-modificerede stivelser førte til højere affinitet og lavere reaktionshastighed sammenlignet med umodificerede og TuαGT-modificerede stivelser, dog med undtagelse af *Ro*BE-modificeret ”waxy” majsstivelse.

Disse ændringer i affinitet og reaktionshastighed kan skyldes stivelseskornenes struktur, herunder krystalliniteten, overfladeordensgraden og kædelængdefordelingen.

Underkapitel 2.3 omfatter én artikel (Artikel 4). Det er forskellig fra de to tidligere kapitler, idet det ikke handler om enzym-opdagelse og -karakterisering. I Artikel 4 fremstilledes et nyt superforgrenet amylopektin ved modificering af gelatineret normal majsstivelse med *Ro*BE og TuαGT. Den modificerede stivelse blev brugt til indkapsling af en curcumin-emulsion i alginatperler. Analyse af UV-stabilitet og *in vitro* simuleret mave-tarm fordøjelse af de forskellige alginatperler viste potentialet af en kombination af enzym-modificeret stivelse og alginat til indkapsling og kontrolleret og målrettet frigivelse af bioaktive forbindelser.

Kapitlerne 3, 4 og 5 er henholdsvis den generelle diskussion, konklusion og fremtidsperspektiv for ph.d.-arbejdet.

Denne afhandling gav ny viden om funktionen af SBD'er i forskellige stivelsesaktive enzymer, især om grænsefladekatalyse af stivelseskorn. Denne kinetiske grænsefladeanalyse gav ny forståelse af den enzymatiske nedbrydning og/eller modifikation af stivelseskorn. Desuden undersøgte vi anvendelsen af enzymmodificeret stivelse kombineret med alginat til indkapsling af bioaktive forbindelser i perler.

Abbreviations

4αGT	4-α-glucanotransferase
A/B ratio	density of attack sites/density of binding sites ratio
AE	high-amylose maize starch AE 35
AFM	atomic force microscopy
AHA	α-amylase from *Pseudoalteromonas haloplanktis* TAB23
*An*GA	glucoamylase from *Aspergillus niger*
β-CD	β-cyclodextrin
BE	branching enzyme
*Bl*Pul	pullulanase from *Bacillus licheniformis*
CAZy	Carbohydrate-Active enZYmes Database
CAZyme	carbohydrate active enzyme
CBM	carbohydrate binding module
CD	catalytic domain
CLD	chain length distribution
CS_B-AB	curcumin-loaded MMS-B alginate beads
CS_{BT}-AB	curcumin-loaded MMS-BT alginate beads
CS_C-AB	curcumin-loaded alginate beads
CS_N-AB	curcumin-loaded NMS alginate beads
CS_T-AB	curcumin-loaded MMS-T alginate beads
CTD	C-terminal domain
CV	column volumes
G50	high-amylose maize starch Australia G50
G80	high-amylose maize starch Australia G80
DBE	debranching enzyme
DP	degree of polymerization
DUF	domain of unknown function
GH	glycoside hydrolase
GIT	gastrointestinal tract
HPAEC-PAD	high-performance anion-exchange chromatography with pulsed amperometric detection
HPPS	high-amylose/high-phosphate potato starch
iTOL	Interactive Tree Of Life
*La*Pul	pullulanase from *Lactobacillus acidophilus* NCFM
LR-CD	large-ring cyclodextrin
MM	Michaelis-Menten

MMS-B	NMS modified by BE
MMS-T	NMS modified by 4αGT
MMS-BT	NMS sequentially modified by BE followed by 4αGT
Mw	molecular weight
NMS	normal maize starch
NPS	normal potato starch
NTD	N-terminal domain
NWS	normal wheat starch
PUL	pullulanase
PULI	type I pullulanase
PULII	type II pullulanase
RDS	rapidly digested starch
*Ro*BE	branching enzyme from *Rhodothermus obamensis*
RS	resistant starch
SBD	starch binding domain
SBD_{GA}	starch binding domain from *Aspergillus niger* glucoamylase
SBD_{GWD3}	starch binding domain from *Arabidopsis thaliana* glucan, water dikinase 3
SDBE	starch-debranching enzyme
SDS	slowly digested starch
SEC	size-exclusion chromatography
SEM	scanning electron microscope
SGF	simulated gastric fluid
SIF	simulated intestinal fluid
SLAP	surface layer association protein
SPR	surface plasmon resonance
SSF	simulated salivary fluid
*St*DPE2	disproportionating enzyme 2 from *Solanum tuberosum*
Tm	melting temperature
TuαGT	4-α-glucanotransferase from *Thermoproteus uzoniensis*
WMS	waxy maize starch
WPS	waxy potato starch

Objectives of thesis

The overall objective of this PhD thesis entitled “Structure-function relationships of enzymes involved in starch modification” is to investigate the relationship between structure of different starch-active enzymes and the effects of enzymatic treatments on starch using these starch-active enzymes. Specifically, the thesis aims to focus on the impact of SBDs on the interfacial catalysis of granular starches when enzyme is fused with SBDs, or SBDs truncated from various starch-active enzymes.

The results chapter (Chapter 2) in this thesis comprises three subchapters, covering the effect of SBDs on the enzymatic degradation of starches using different starch-active enzymes, including α-amylase, 4αGT, and PULI, as well as a more applied investigations describing how molecular structure of starch influence the gel network of starch-alginate hydrogel beads, and applying these starch-alginate hydrogel beads for encapsulation of curcumin.

Chapter 2.1 focused on the effect of SBDs on the enzymatic properties of different starch-active enzymes and contained 2 published papers, covering the following headlines:

1. To select and utilize SBDs for targeting starch-active enzymes to starch.
2. To understand the effects of SBDs in the catalytic process of starch-active enzymes on starch.
3. To describe interactions of starch-active enzymes with starch granules by applying principles of interfacial enzymology.

Chapter 2.2 focused on the interfacial catalysis on granular starches of pullulanase and contained 1 published paper and 2 manuscripts, of which one is submitted, and one is in preparation. They cover the following headlines:

1. To understand the diverse functions of the NTDs on the properties of PULI by truncating the NTDs.
2. To understand the diverse functions on starch granules of the NTDs of PULI by applying interfacial kinetics.
3. To develop a novel method using pullulanase to enumerate α-1,6-linked branch points on the surface of granular starch by using interfacial kinetic analysis.
4. To describe the enzymatic modification processes on gelatinized and granular starches of BE and 4αGT

Chapter 2.3 focused on the effect of modification on gelatinized starch by *Ro*BE and TuαGT and evaluate its potential for co-entrapment of a curcumin-loaded emulsion in alginate beads for controlled release and targeted delivery of bioactive compounds. This chapter contains 1 paper. It covers the following headlines:

1. To produce a novel enzyme-modified starch with increased α-1,6-linkage content and elongated exterior chains.
2. To apply these enzymes modified starches in encapsulation of curcumin in starch-alginate hydrogel beads.
3. To understand the relationship between molecular structure of starch and gel network of starch-alginate hydrogel beads.

Contents

Chapter 1: Introduction

Starch is widely recognized as a sustainable source of energy storage and is abundantly present in human food and animal feed [1,2]. Additionally, it plays a crucial role in the development of innovative biomaterials, as well as in biorefineries to produce ethanol and other valuable chemicals. Moreover, it serves as a vital component of biomass feedstocks for fuel energy [3]. To impart new functionalities and enhance its positive characteristics, starch is subjected procedures for functional improvement through structural engineering, including enzymatic, chemical, or physical treatments. Notably, enzyme treatment of starch stands out as an environmentally friendly approach [4]. Additionally, it is highly appealing due to its ability to enhance starch with improved thermal properties, increased resistance to digestion, and enhanced complexation capacity.

Enzymatic catalysis on starch can be classified into two distinct situations: homogeneous catalysis, which involves gelatinized starch where both the substrate and enzyme are in solution, and heterogeneous catalysis, which pertains to insoluble substrates. In contrast to homogeneous catalysis, the enzymatic process on insoluble starch granules represents a heterogeneous (interfacial) catalytic process [5]. This process poses a unique challenge as the molar concentration of the substrate cannot be precisely defined, given the nature of the insoluble granules. The current thesis, motivated by heterogenous catalysis of cellulases acting on cellulose, focused on the interfacial catalysis by joining conventional Michaelis-Menten kinetics, where substrate is in excess, with an inverse kinetics approach having the enzyme in excess, combined with adsorption isotherms to extract densities of enzyme attack and binding sites on the starch granules [6].

This PhD thesis aimed to investigate the enzymatic degradation and/or modification of gelatinized and granular starch using hydrolases (discussed in **chapters 2.1** and **2.2**) and glucanotransferases (explored in **chapters 2.1** and **2.3**). Chapters 2.1 and 2.2 focused on investigating the impact of SBD on the interfacial catalysis of starch granule surfaces, employing α-amylase and PULI. The study utilized interfacial kinetics to gain insights into this process. Moving forward, chapters 2.1 and 2.3 delved into investigating the effects of starch binding domains on the enzymatic properties of a 4αGT, the modification of gelatinized and granular starch using BE and 4αGT, or a combination using BE followed by 4αGT, as well as the application of modified starch in encapsulation of guest compounds.

1.1 Starch

The starch granule is a highly organized and dense energy source made up of polysaccharides [1]. It is a key component of most plant foods and holds great importance for human well-being [2]. At various levels of its structure, the starch granule exhibits specific features. On a molecular level, it is primarily composed of the linear α-glucan amylose and the branched α-glucan known as amylopectin [7]. At the scale of 8–11 nm, the granule showcases crystalline and amorphous lamellar structures, while at the size of 0.1 μm, it exhibits alternating amorphous and semi-crystalline growth rings. The overall size of starch granule ranges from 1 to 100 μm, depending on the botanical origin [8] (Figure 1).

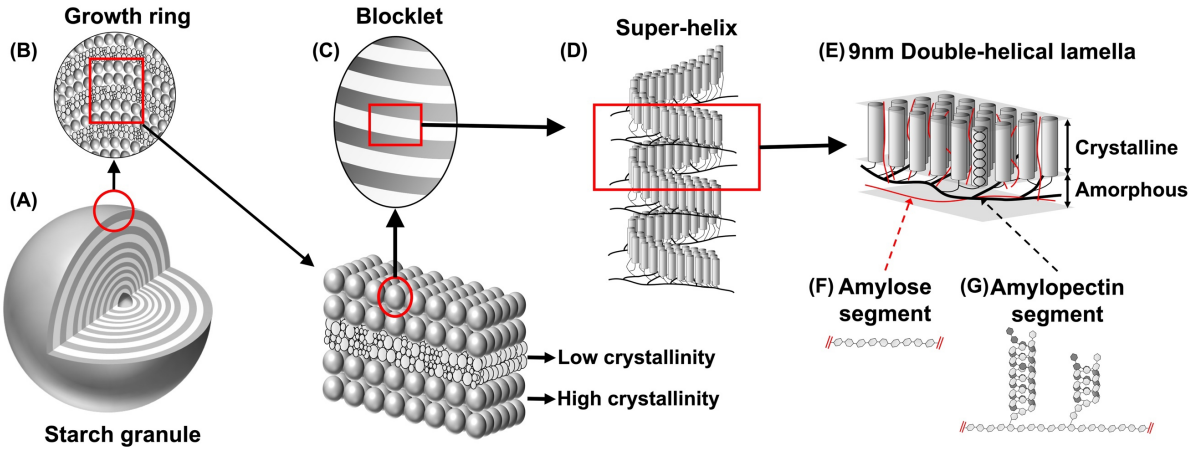

Figure 1. The multi-level structure of the starch granule as depicted by the blocklet [9] **organization**. This figure is adapted from a figure from Tian et al [5]. (A) Starch granule; (B) Growth rings as a repeating layered structure with a period of a few hundred nanometers contain a semi-crystalline region (high crystallinity) and an amorphous region (low crystallinity); (C) Spherical blocklets with a diameter between 10 and 300 nm in the semi-crystalline regions; (D) Left-handed amylopectin super-helix consists of alternating crystalline lamellae (containing the linear parts of the chains) and amorphous lamellae (containing most of the branch points) which stack with a periodicity of ~8–11 nm (E); Molecular structure of (F) amylose and (G) amylopectin.

There are ongoing discussions and debates surrounding models and representations of the different structural levels of starch granules [10]. Of particular significance is the molecular structure of amylopectin, which is subject to differing interpretations: the cluster model [11–13] and the more recent building block backbone model [8]. In both models, the double helices within amylopectin are oriented perpendicularly to the surface of the starch granules. The cluster model proposes a radial tree-like clustering arrangement of the branch chains within the amylopectin molecule. Conversely, the backbone model suggests that long backbone chains run tangentially to the direction of the double-helical structures of the branch chains (Figure 1E). In the backbone structure, the long chains form two-dimensional sheets, with non-clustered branched building blocks attached. From these building blocks, shorter segments of chain protrude in a perpendicular direction, allowing for the formation and crystallization of

parallel double helices. These segments are thought to be randomly distributed and have inter-branch spaces of less than nine glucose residues (degree of polymerization (DP), DP < 9 (5–8)) [8]. In the cluster model, the long chains can penetrate several layers of double helices and have a similar orientation to the double helices themselves. These segments, known as lamellae, are approximately 9 nm thick and contribute to the concentric structures observed within the starch granule [7,8,14]. The branching of amylopectin, the ratio of amylose to amylopectin, and the length of the branched chains all play important roles in determining the granular architecture. Amylose is believed to be dispersed throughout the granular matrix, primarily in amorphous regions. However, there is limited understanding of how different molecular structures influence the architecture of the granule and its susceptibility to enzymatic modification.

1.1.1 Topography and Morphology of the Starch Granules

The inner structure of starch is highly conserved across species, but the factors influencing the diverse morphologies and sizes of starch granules are not fully understood [15]. Storage starches vary greatly in granule size: quinoa, amaranth, and cow cockle have small granules (0.3–2 μm) [16,17], while oat, rice, and buckwheat have granules of 2–10 μm [15,16]. Medium-sized granules (5–30 μm) are found in cassava, barley, corn, and sorghum, and large granules (up to 100 μm) are present in tubers like potatoes [18,19]. Mutant plants with high amylose content exhibit morphological variations such as elongated, hollow, and aggregated granules [20,21]. These granules can possess distinct properties, with higher amylose content and enhanced resistance to heat and enzymatic degradation. Within a species, starch granules can differ in size, morphology, and number across different organs and tissues [20,22]. Many starch granules have surface pores, especially in A-type crystallinity starches, forming channels that reach an internal cavity [23,24]. However, the presence of pores on B-type crystallinity starches has also been observed [23,25–27]. The organization of amylose and amylopectin within granules is complex and varies depending on genotypes and mutations. Starch granules contain proteins and lipids that can affect granule degradation, digestibility, and gelatinization properties. These multi-level structures and non-starch compounds collectively influence starch digestibility. Starches containing amylose produce nanocrystals with slightly distorted symmetry, indicating that amylose influences the crystal structure [8].

1.1.2 Nano-Level Structures

At the nano-level, starch granules consist of A- and B-type crystalline systems. A-type is found in cereal grains, while B-type is in tuber and root starches, high-amylose starches, and a

mixture of A- and B-type called C-type is in pulses [14]. High amylose starches may also have a Vh-type polymorph with single helices and lipids. Small angle X-ray scattering reveals 4–6 nm thick crystalline lamellae rich in double-helices, and 3–6 nm thick amorphous lamellae with branch linkages and amylose. Light and electron microscopy show 0.1–1 μm thick growth rings with varying crystallinity. The granules, 1–100 μm in size, have concentrically deposited growth rings [28]. However, the relationship between structural levels and granule morphology remains unclear. Starch granules exhibit structural heterogeneity with varying degrees of compactness among starch molecules at different scales, observed within and between granules of the same plant [29].

1.1.3 Blocklet Structures

The surface structures of starch granules are not well understood, hindering our knowledge of enzyme-granule molecular interactions. However, an intermediate organizational structure called ellipsoidal blocklets has been observed between lamellar and growth ring structures [30,31]. Blocklets, visible through atomic force microscopy (AFM) and scanning electron microscope (SEM), are nodules of various sizes (10–500 nm) on the granule surface [32–35] (Figure 1C). Blocklet sizes vary among species, ranging at 40–100 nm in wheat [34], 10–300 nm in potato [36,37], 130–250 nm in pea [38], and 10–30 nm in maize [32]. The hypothesis suggests that differently structured blocklets form the growth rings, with amorphous rings consisting of smaller/less ordered blocklets and crystalline layers containing larger/more compact blocklets [30]. These surface structures may define variations in starch granules among plants and impact biosynthesis and enzyme degradation.

1.1.4 Amylose and Amylopectin

Starch is composed of two main types of polymeric components: amylose and amylopectin (Figure 1 F and G). These biomacromolecules are α-glucans consisting of α-D-glucosidic units linked together in larger polymeric structures. Amylopectin is the predominant component by weight and is formed through α-1,4- and α-1,6-linkages. Its molecular size is considerable compared to amylose. The amylose content in most normal starches ranges from 15 to 30%. Waxy starches have minimal or no amylose [39,40], while certain high amylose starches contain a much higher amylose content (> 50%), including genetically modified amylose-only starch [41,42]. The ratios and fine structure of these polymers influence the functional properties of starch, determining its various applications in the food industry.

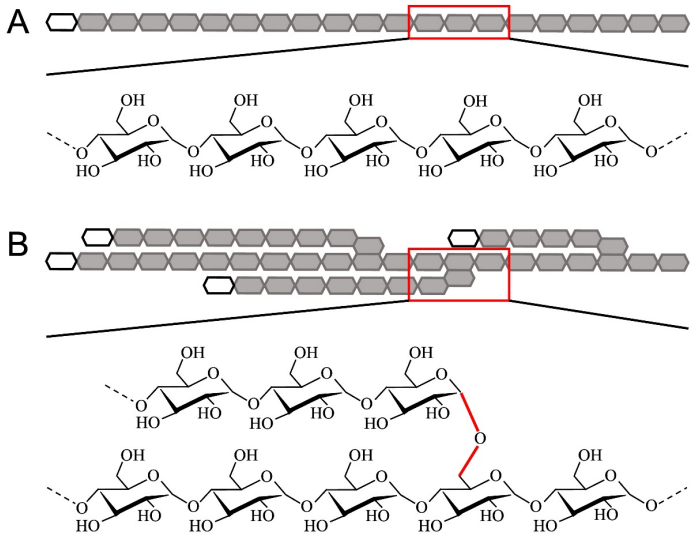

Figure 2. Molecular structure of amylose (A) and amylopectin (B). Open hexagon in (A) and (B) represents the non-reducing end residue. An α-1,6-linkage in (B) is shown in red.

Amylose, consists of α-1,4-linkages (around 99%) and a small portion of α-1,6-linkages (about 1%), is the minor and linear component of starch, resulting in a relatively long, predominantly linear polysaccharide (Figure 2A). The fine structure of amylose is characterized by its molecular size and branching pattern. The molecular size is often determined by techniques such as measuring the DP. The molecular weight of amylose varies among different botanical sources, typically ranging from 1.3×10^5 to 5×10^5 [43]. As for the branching pattern, some amylose molecules exhibit slight branching with 5–20 chains. Branched amyloses generally show larger molecular sizes compared to linear amyloses, but the chain length of linear amylose is longer on average than that of branched amylose. The localization of amylose within starch granules remains a topic of discussion. While it is generally believed that amylose is present in the amorphous region within the granules, its specific distribution is still debated. Jane and colleagues suggested that in both potato and maize starch granules, amylose is more concentrated in the peripheral regions compared to the interior [44,45]. In contrast, by using confocal laser scanning microscopy and 8-amino-1,3,6-pyrenetrisulfonic acid (APTS) as a fluorescent probe for reducing ends, Blennow et al. concluded that amylose is primarily confined to the interior regions of starch granules derived from potato, tapioca, maize, wheat, barley, and peas [29].

Amylopectin, consists of α-1,4-linkages (around 95%) and α-1,6-linkages (about 5%), is the major, highly branched component in starch, plays a crucial role in the internal structure of starch granules and adopts a semi-crystalline form (Figure 2B) [43,46]. Amylopectin consists of numerous short chains of α-1,4-linked D-glucose units, with each chain containing approximately from 6 to 35 glucose units. These chains are interconnected to form clusters. Various physicochemical techniques, including light scattering, viscometry, and

ultracentrifugation, indicate that the weight average molecular weight (Mw) of amylopectin is typically in the range of 10^7 to 10^8 Da depending on the botanical origin [47,48]. Size-exclusion chromatography (SEC), high-performance anion-exchange chromatography with pulsed amperometric detection (HPAEC-PAD), and fluorophore-assisted carbohydrate electrophoresis (FACE) are analytical methods used to analyze the distribution of amylopectin chains after debranching. By comparing debranched amylopectin, it was proposed to fractionate the chain units into four categories based on their length, including A-chains (DP 6–12), B1-chains (DP 13–24), B2-chains (DP 25–36), and B3-chains (DP > 36) [49].

1.2 Carbohydrate Active Enzymes

Carbohydrate active enzymes (CAZymes), a series of enzymes responsible for the synthesis, degradation, and modification of carbohydrates, such as starch, cellulose, chitin, and also various glycoproteins, play a crucial role in the metabolism of carbohydrates. CAZymes have been found in all different kinds of organisms, including bacteria, archaea, fungi, plants, and animals.

According to the catalytic mechanism, CAZymes can be classified into five different classes, namely glycoside hydrolases (GHs), glycosyltransferases (GTs), polysaccharide lyases (PLs), carbohydrate esterases (CEs), and Auxiliary activities (AAs) [50]. Among these classes, the GHs, with 183 families, represent unambiguously the largest CAZymes class in the CAZy database [50]. These enzymes catalyze the hydrolysis and/or rearrangement of glucosidic bonds via transglycosylation. GHs are involved in diverse processes such as digestion, biosynthesis, cellular signaling, and pathogen defense.

In this PhD thesis, four different GHs members with hydrolytic and/or transglycosylation activity were investigated: namely α-amylase, pullulanase, branching enzyme, and 4-α-glucanotransferase.

1.2.1 α-Amylase

α-amylases (EC 3.2.1.1) are endo-acting, catalyze hydrolysis of internal α-1,4-linkages in starch to generate maltooligosaccharides and occur widely in bacteria, archaea, plants and animals [51]. α-Amylase catalyzes the cleavage of an a-1,4-glucan, resulting in the formation of a glycosyl-enzyme intermediate in the first part of the catalytic cycle (Figure 3A). Subsequently, the intermediate is broken down via reaction with water as an acceptor resulting in hydrolysis (Figure 3C). In living organisms, α-amylase is crucial for carbohydrate digestion and absorption. In the human digestive system, salivary α-amylase initiates starch breakdown in the mouth, while pancreatic α-amylase continues the process in the small intestine [52]. The resulting glucose and maltodextrins are then absorbed into the bloodstream to serve as an essential energy source for bodily functions.

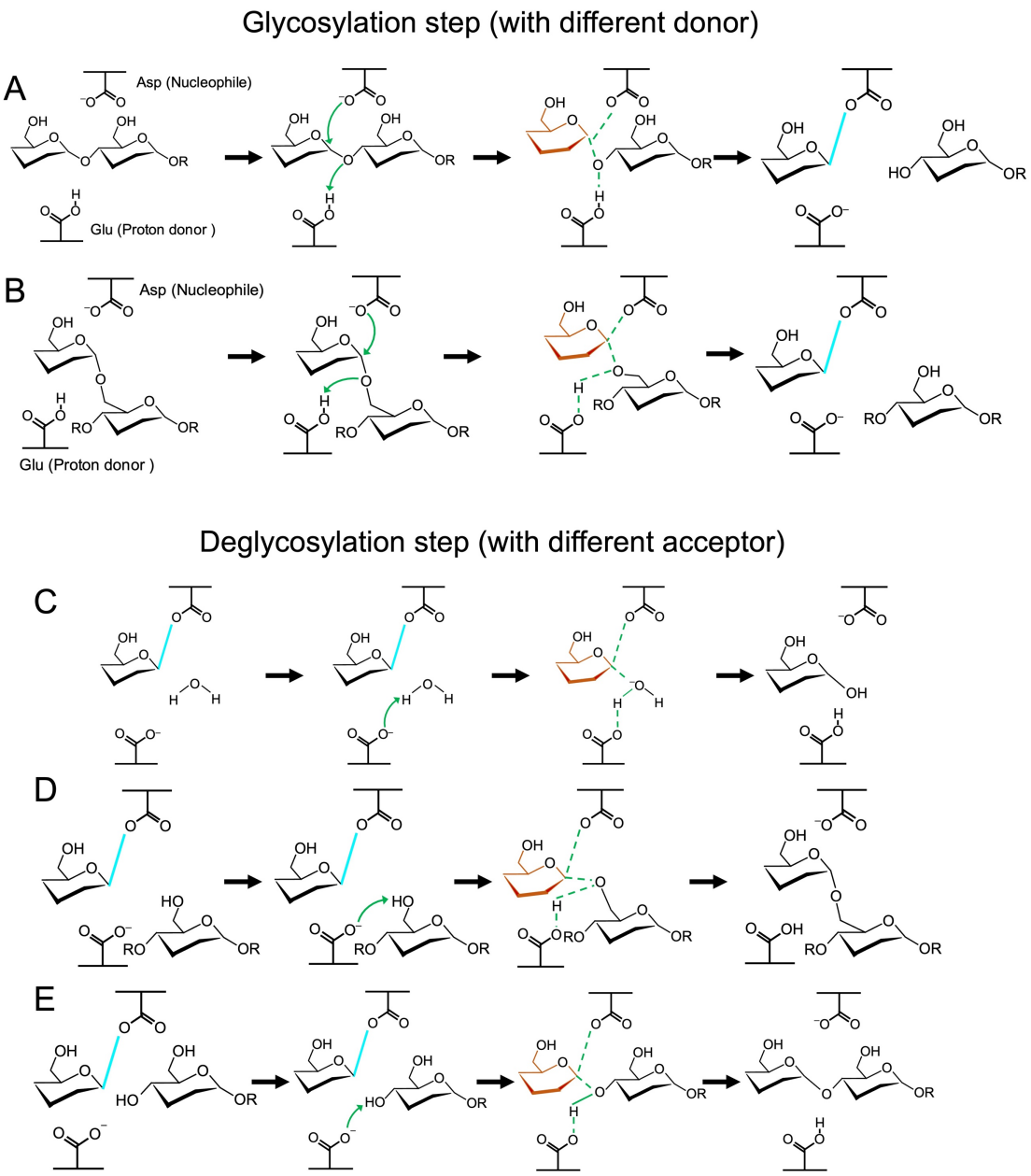

Figure 3. Reaction mechanism of enzymes involved in the thesis. Glycosylation step and formation of covalent intermediate for (A) α-amylase, branching enzyme and 4-α-glucanotransferase and (B) pullulanase. Deglycosylation step when (C) H_2O, (D) C6 in an α-glucose unit, or (E) C4 in an α-glucose unit act as an acceptor. The colour legend: transition of proton (green arrow), formation of an oxocarbenium ion-like intermediate (green dash line and brown glucose unit), and formed covalent intermediate (cyan solid line).

α-amylases mostly belong to the glycoside hydrolase family 13 (GH13) as organized in the CAZy (http://www.cazy.org/) database [50]. Besides, there are also α-amylases present in GH57, 119, and 126 [50].

GH13 is by far the largest GH family and is currently divided into 46 subfamilies harboring about 30 different specificities [53]. Among these subfamilies, α-amylases are found in 16 subfamilies (GH13_1, 5, 6, 7, 10, 15, 19, 21, 24, 27, 28, 32, 36, 37, 43, 45) [50]. Industrially significant liquefying and saccharifying bacterial α-amylases are classified under GH13_5 and GH13_28. Fungal α-amylases, such as those from *Aspergillus oryzae* and *Aspergillus niger*, fall under GH13_1. Plant α-amylases are categorized within GH13_6, while animal and mammalian digestive α-amylases are grouped under GH13_15 and GH13_24, respectively (***Paper 1***) [50,54]. Firstly, all α-amylases studied to date have been shown to employ a retaining reaction mechanism. From a mechanism point of view, GH13 α-amylases share the same type of active site cleft, containing two aspartic acid (Asp) and one glutamic acid (Glu) as catalytic residues. One of the Asp residues is the catalytic nucleophile, Glu is the proton donor and the second Asp residue is a transition state stabilizer [55]. Moreover, all members of GH13 exhibit a similar three-domain structure: domains A, B, and C. Domain A, with its characteristic $(\beta/\alpha)_8$-barrel (TIM-barrel), directs most enzyme activities and houses the active region essential for starch breakdown [56,57]. Domain B, composed mainly of β-strands, aids in Ca^{2+} binding in some α-amylases [58]. Domain C, located at the C-terminus of domain A, primarily adopts a β-sandwich fold, and varies the most among α-amylases. Domain C stabilizes the enzyme and can assist in substrate attachment (Figure 4K) [59].

Enzymes of the GH57 family, another α-amylase family, display clear distinctions from those in family GH13. While both GH57 and GH13 α-amylases utilize a retaining reaction mechanism, the crystal structure of a GH57 α-amylase remains unsolved. However, other GH57 members, such as the branching enzyme and 4-α-glucanotransferase, exhibit a $(\beta/\alpha)_7$-barrel, often referred to as an incomplete TIM-barrel (as seen in Figure 6G [60] and Figure 7A [61]). This suggests that GH57 α-amylases likely share this $(\beta/\alpha)_7$-barrel fold, a hypothesis supported by the AlphaFold2 model of an α-amylase from *Methanocaldococcus jannaschii* DSM 2661 (Figure 4R) [62].

GH119 represents the third α-amylase family, inaugurated in 2006 around the α-amylase IgtZ from *Bacillus circulans* [63]. To date, only 60 enzymes belong to this group, with α-amylase IgtZ being the sole experimentally characterized [50]. Similar to the GH13 and 57 α-amylases, GH119 employs a retaining mechanism. Structurally, α-amylase IgtZ showed two C-terminal CBM25 and one C-terminal CBM20 which are both starch binding domain family (Figure 4S and 11) [63].

The GH126, established in 2011, is the fourth GH family recognized as an α-amylase family [50]. Its inception was based on a study detailing the 3D structure of the CPF_2247 protein from the *Clostridium perfringens* genome [64]. Firstly, it was inferred that the GH126 α-amylases showed an inverting reaction mechanism, as opposed to the other α-amylase

families. Infact, the inverting mechanism is still under consideration since no ligand complex was defined for the crystal structure of the GH126 α-amylases [64]. Structurally, an $(\alpha/\alpha)_6$-barrel was found for the GH126 CPF_2247 protein [64]. However, based on the enzymatic characterization, whether GH126 members are α-amylases remains uncertain [51].

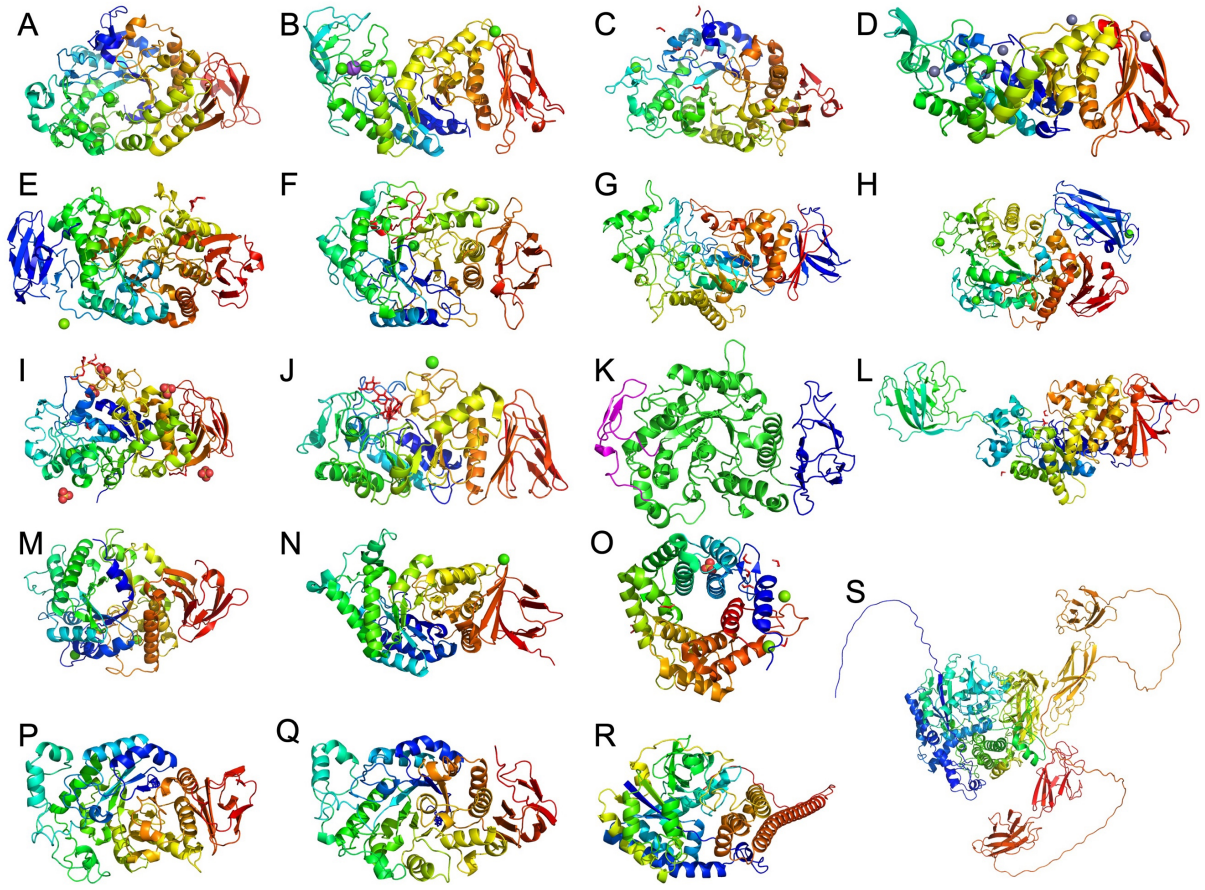

Figure 4. Gallery of experimentally determined structures and AlphaFold2 model of α-amylases from individual GH families. The entire polypeptide chain of an enzyme is coloured spectrally from N-terminus (blue) to C-terminus (red) using Pymol with Ca^{2+} (displayed if present as a green globule) and SO_4^{2-} (displayed if present as a red-yellow ion). The TIM-barrel domain A, domain B, and domain C for *Pseudoalteromonas haloplanktis* TAB23 α-amylase AHA are colored green, magenta, and blue, respectively in (K).
Experimentally determined structures for (A) GH13_1: *Aspergillus niger* α-amylase (PDB: 2AAA, [65]); (B) GH13_5: *Bacillus licheniformis* α-amylase (PDB: 1BLI, [66]); (C) GH13_6: *Hordeum vulgare* (barley) α-amylase (PDB: 1HT6, [67]); (D) GH13_7: *Pyrococcus woesei* α-amylase (PDB: 1MWO, [68]); (E) GH13_10: *Deinococcus radiodurans α-amylase* (PDB: 2BHU, [69]); (F) GH13_15: *Tenebrio molitor* α-amylase (PDB: 1CLV, [70]); (G) GH13_19: *Escherichia coli* α-amylase (PDB: 8IM8, [71]); (H) GH13_21: *Thermoactinomyces vulgaris* R-47 α-amylase (PDB: 1IZJ, [72]); (I) GH13_24: *Eisenia fetida* α-amylase (PDB: 6M4K, [73]); (J) GH13_28: *Bacillus subtilis* α-amylase (PDB: 1BAG, [74]); (K) GH13_32: *Pseudoalteromonas haloplanktis* TAB23 α-amylase (PDB: 1AQH, [75]); (L) GH13_36: *Bacteroides thetaiotaomicron* VPI-5482 α-amylase (PDB: 3K8K, [76]); (M) GH13_37: uncultured bacterium α-amylase (AmyP, PDB: 5H05, [77]); (N) GH13_45: *Anoxybacillus* sp. SK3-4 α-amylase (PDB: 5A2A, [78]); (O) GH126: *Clostridium perfringens* α-amylase (PDB: 3REN, [64]).
AlphaFold2 models for (P) GH13_27: *Aeromonas hydrophila* α-amylase (Accession: AAA21936.1, [79]); (Q) GH13_43: *Haloarcula hispanica* α-amylase (Accession: CAI64586.1, [80]); (R) GH57: *Methanocaldococcus jannaschii* DSM 2661 α-amylase (Accession: AAB99631.1, [62]); (S) GH119: *Niallia circulans* α-amylase (GenBank accession: BAF37284.1, [63]).

1.2.2 Pullulanase

Pullulanase (PUL), also known as debranching enzyme, is a type of CAZyme that plays a significant role in carbohydrate metabolism, which belongs to the GH13 and GH57 families [50]. PUL catalyze the fragmentation of an α-1,6-glucan molecule, leading to formation of a glycosyl-enzyme complex during the initial phase of their catalytic process (Figure 3B). Following this, the complex undergoes decomposition through interaction with water, which acts as an acceptor, ultimately leading to hydrolysis (Figure 3C) [81]. PULs are widely occurring in a diverse array of microorganisms, including bacteria, yeast, and fungi. PULs are important in the digestion and utilization of complex carbohydrate in human gut. The human digestive system lacks enzymes that can efficiently break down α-1,6-linkages in certain complex carbohydrates, such as resistant starch. Such carbohydrates from food reach the large intestine mostly undigested. However, certain gut bacteria, like *Lactobacillus acidophilus* [82] and *Ruminococcus bromii* [83] produce pullulanase and possess the ability to degrade these complex carbohydrates, converting them into smaller, more digestible sugars that can be utilized by the host [84]. Moreover, PULs also play a crucial role in industries. For example, PULs are employed in the production of maltodextrins and glucose syrups from starch sources. Besides, in brewing, PULs are used to improve the fermentability of starch-based raw materials, such as malted barley. Interestingly, some PULs also showed transglycosylation activity, which has been applied in the pharmaceutical industry [85,86].

PULs are classified as two types according to the linkage specificity, namely pullulanase type I (PULI) and pullulanase type II (PULII), the latter also being known as amylopullulanase [87]. PULIs can only catalyze the hydrolysis of α-1,6-linkages in pullulan, starch, and other related branched carbohydrates, while PULII can catalyze the hydrolysis of both α-1,4- and α-1,6-linkages in α-glucans. PULIs are found in three GH13 subfamilies (GH13_12, 13, and 14) [81,88].

From a catalytic perspective, PULI enzymes exhibit a retaining mechanism characterized by three consistent catalytic site residues: Asp (serving as the nucleophile/base), Glu (acting as the proton donor), and another Asp involved in the distortion and stabilization of the transition state [81].

The crystal structure of PULI showcases its intricate three-dimensional arrangement and offers insights into its mechanism of action. It generally has a multi-domain architecture: one or several N-terminal domains (NTDs), including CBMs and some other domains of unknown function (DUFs), a catalytic domain shown as a TIM-barrel [$(\beta/\alpha)_8$-barrel] domain, and an additional domain C typical for most GH13 enzymes (Figure 5A) [88,89]. The CBM aids in substrate recognition, binding, stability, and oligomerization [90]. A CBM48 is always found N-

terminally to the CD with a few exceptions, such as *Nostoc punctiforme* PCC 73102 debranching enzyme (Figure 5L) [91]. No specific binding function has been identified for CBM48s in PULIs and they might also contribute to structural stability and protein production [92]. PULIs commonly possess at least one additional CBM, such as CBM20, CBM41, or CBM68 and moreover have DUFs not classified as CBMs. Some of the DUFs of a sorghum PULI (limit dextrinase) are reported to have an impact on the digestibility of sorghum starch [93].

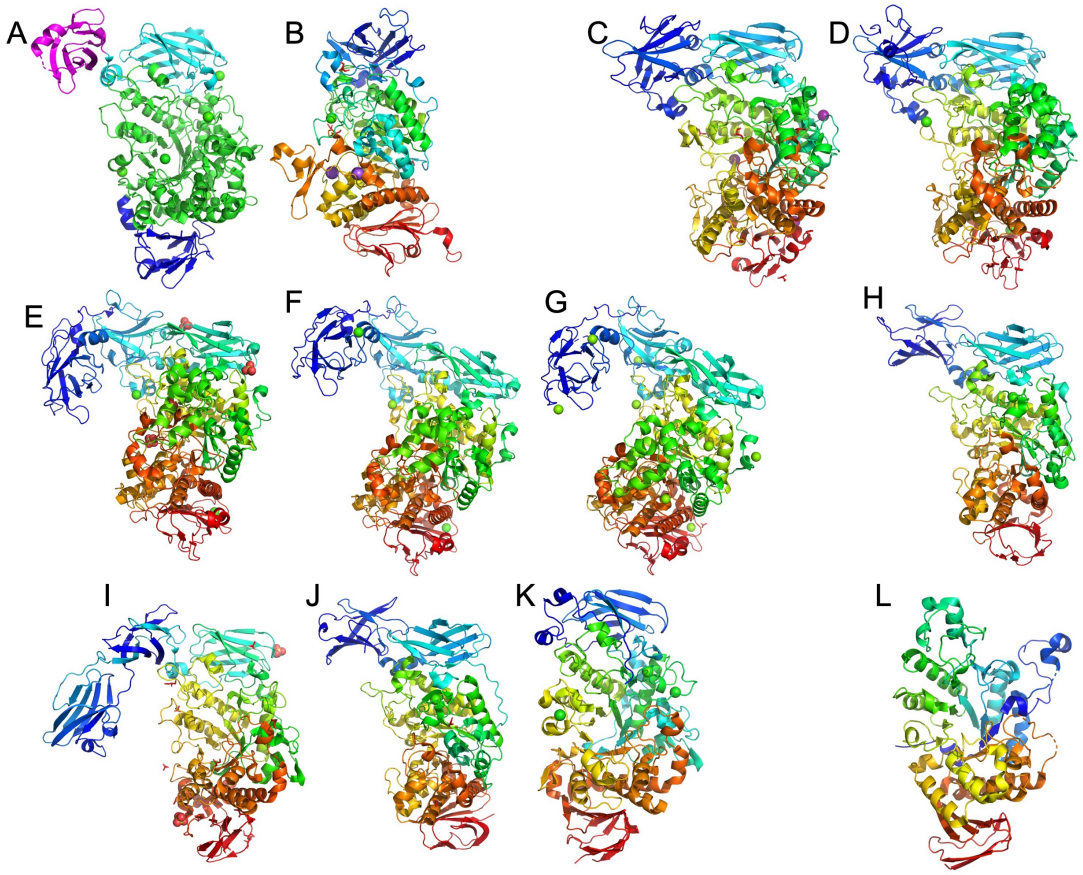

Figure 5. Gallery of experimentally determined structures of type I pullulanase (PULI) from individual GH13 subfamilies. The entire polypeptide chain of an enzyme is coloured spectrally from N-terminus (blue) to C-terminus (red) with Pymol with Ca^{2+} (displayed if present as green globule), I^{-1} (displayed if present as a purple globule) and SO_4^{2+} (displayed if present as a red-yellow ion). The domain N1, domain N2, TIM-barrel domain A, and domain C for *Streptococcus agalactiae* PULI are colored magenta, cyan, green, and blue, respectively in (A).
GH13_12 PUL: (A) *Streptococcus agalactiae* PULI (PDB: 3FAW, [94]); (B) *Streptococcus pneumoniae* PULI (PDB: 2YA0,[95]).
GH13_13 PUL: (C) *Hordeum vulgare* (barley) PULI (PDB: 4AIO, [96]); (D) *Klebsiella pneumoniae*/*aerogenes* PULI (PDB: 2FGZ, [97]); (E) *Klebsiella oxytoca*/*pneumoniae* UNF 5023 PULI (PDB: 2YOC, [98]); (F) *Klebsiella pneumoniae* P43212 PULI (PDB: 5YN2, [99]); (G) *Klebsiella pneumoniae* PULI (PDB: 6J33, [100]).
GH13_14 PUL: (H): *Anoxybacillus* sp. LM18-11 PULI (PDB: 3WDH, [101]); (I) *Bacillus acidopullulyticus* PULI (PDB: 2WAN, [102]); (J) *Bacillus subtilis* subsp. *subtilis* str. 168 PULI (PDB: 2E8Y, [103]). (K) *Paenibacillus barengoltzii* PULI (PDB: 6JHF, [104]).
GH13_20 PUL: (L) *Nostoc punctiforme* PCC 73102 debranching Enzyme (PDB: 2WC7, [91]).

Even though there are some reports showing that these extra CBMs in PULI, apart from CBM48, participated in the binding to substrate [95], the specific roles of the individual domains remain ambiguous, largely due to their intertwined interactions with each other and their substrates. In the PULI derived from *Geobacillus thermocatenulatus*, when CBM41 was truncated, there was a slight reduction in K_M and an increase in k_{cat} on pullulan, possibly attributed to an active site that is more exposed [105]. A similar outcome was observed when CBM41 was truncated in PULI from *Bacillus deramificans* [92]. However, for the PULI sourced from *Bacillus acidopullulyticus*, truncating CBM41 resulted in a doubled K_M on pullulan, suggesting that CBM41 plays a role in substrate affinity [106,107]. As far as we are aware, the effects of truncating non-CBM DUFs on the activity and stability of PULI remain unexplored. Furthermore, our comprehension is somewhat limited concerning the activity of PULIs, especially on granular starch. Apart from the effects on the substrate recognition, a CBM68-truncated *Anoxybacillus* sp. LM18-11 PULI also showed decreased thermostability compared with WT enzyme by showing 10 °C lower optimum temperature relative to the full length enzyme [101]. Hence, exploring the diverse roles of these NTDs in PUL is crucial. To address this, two truncated versions of a GH13_14 PULI were recombinantly produced. These truncations were studied for their impact on thermostability, activity towards soluble substrates, and interfacial kinetics on starch granules (***Manuscript 1***).

1.2.3 Branching Enzyme

Branching enzyme (BE, EC 2.4.1.18) belongs to glucoside hydrolase family 13 (GH13) mostly and to GH57, and occurs widely in animals, microorganisms and plants [108]. Other names in common use for BEs include the starch branching enzyme (SBE), glycogen-branching enzyme (GBE) and Q-enzyme. BE catalyzes the addition of α-1,6-linked branches in a transglycosylation reaction by cleaving an a-1,4-glucan for the formation of a glycosyl-enzyme covalent intermediate during the glycosylation step (Figure 3A). The intermediate is then broken down via reaction with C6 in an α-1,4-glucan as an acceptor (Figure 3D).

Firstly, all BEs studied to date have shown to employ a retaining reaction mechanism. From the structural point of view, the BEs from GH13 showed a $(\beta/\alpha)_8$-barrel of the catalytic domain [109], while BEs from GH57 showed a $(\beta/\alpha)_7$-barrel [110] (Figure 6). The GH13 BEs comprise three distinct domains: Firstly, the CBM48, pivotal in regulating oligosaccharide transfer length. Second, a central CD characterized by a $(\beta/\alpha)_8$-barrel structure, which is a shared feature in the GH13 α-amylase family, albeit with diverse manifestations among its members [89]. Lastly, a C-terminal domain (CTD) engages in substrate attachment and catalytic capability [111,112] (Figure 6A). Regarding the GH57 BEs, they typically comprise a $(\beta/\alpha)_7$-barrel structure. This $(\beta/\alpha)_7$-barrel can be categorized into three distinct domains: domain A (CD), domain B (an α-

helix domain) situated between β2 and α5 of domain A, and domain C (an α-helix domain) (Figure 6G-I) [60,110,113].

BEs are important in organisms, particularly in the metabolism and storage of carbohydrates. These enzymes are essential for the synthesis of branched polysaccharides, such as starch in plants and glycogen in animals [112]. In plants, the SBEs are involved in the synthesis of amylopectin, which is the major component of starch [114,115]. In animals, the GBE are responsible for glycogen synthesis in tissues like the liver and muscles [116,117]. BEs control the distance between and position of α-1,6 branch points in α-glucan chains during starch biosynthesis. SBEs can be applied in industrial processes to modify the structure of starches having impact on functional properties of these complex carbohydrates [112].

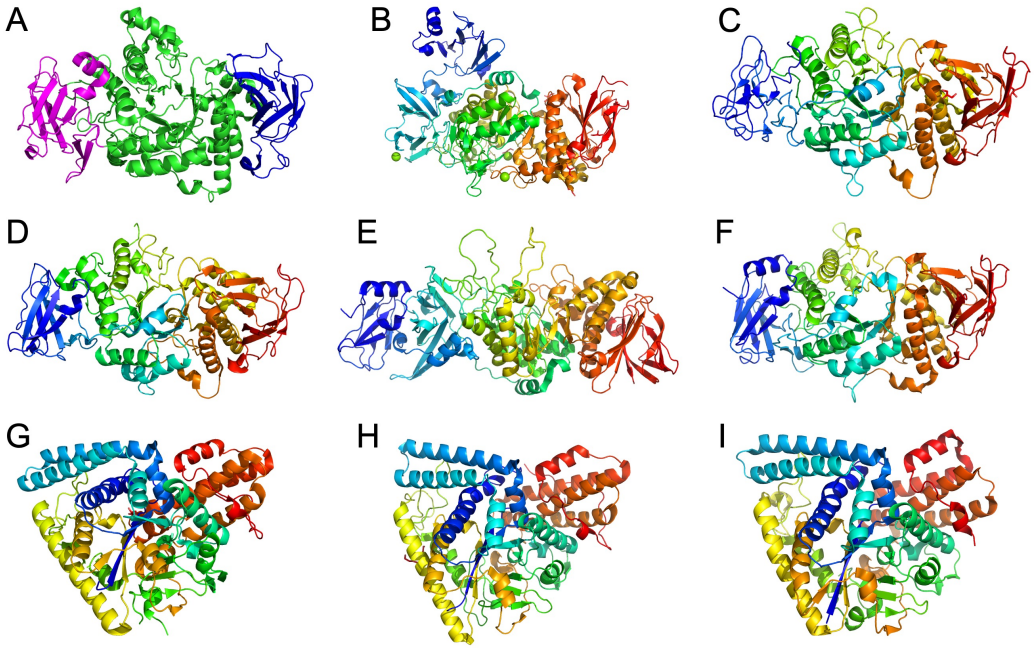

Figure 6. Gallery of experimentally determined structures of branching enzyme (BE) from individual GH families. The entire polypeptide chain of an enzyme is coloured spectrally from N-terminus (blue) to C-terminus (red) using Pymol. Ca^{2+} is displayed if present as a green globule. The domain N, TIM-barrel domain A, and domain C for *Crocosphaera subtropica* ATCC 51142 branching enzyme are colored magenta, green, and blue, respectively in (A).
GH13 BE: (A) GH13: *Crocosphaera subtropica* ATCC 51142 BE (PDB: 7XSY); (B) *Cyanothece* sp. ATCC 51142 BE (PDB: 5GQU, [118]); (C) *Escherichia coli* BE (PDB: 5E6Y, [109]); (D) *Escherichia coli* BE (PDB: 1M7X, [119]); (E) *Mycobacterium tuberculosis* H37RV BE (PDB: 3K1D, [120]); (F) *Rhodothermus obamensis* STB05 BE (PDB: 6JOY, [121]).
GH57 BE: (G) *Pyrococcus horikoshii* BE (PDB: 5WU7, [60]); (H) *Thermococcus kodakaraensis* BE (PDB: 3N8T, [110]); (I) *Thermus thermophilus* HB8 BE (PDB: 1UFA, [113]).

1.2.4 4-α-Glucanotransferase

4-α-glucanotransferases (4αGT, EC 2.4.1.25), also known as amylomaltase (AM) in microorganisms and disproportionating enzyme (D-enzyme) in plants, are found in glycoside

hydrolase families 13, 57, and 77 as based on their sequence in the CAZy (http://www.cazy.org/) database [50].

In the context of the α-amylase enzyme family, researchers commonly posit a tripartite composition consisting of domains A, B, and C. However, distinctive characteristics emerge within 4-α-glycosyltransferases due to the absence of domain C (Figure 7). In the absence of domain C, the GH13 and 77 4αGTs have been subdivided the structural domain of 4-α-glycosyltransferase into four domains: A, B1, B2, and B3 (Figure 7D). Domain A shows typical features of α-amylase family enzymes, displaying a $(\beta/\alpha)_8$-barrel structure [122,123]. Unique to 4-α-glycosyltransferase, domain B2 plays a pivotal role in substrate specificity and DP of the product. Notably, a conserved region dubbed the "250s loop" resides within domain B1. This flexible loop significantly influences substrate binding and particularly impacts large-ring cyclodextrins (LR-CDs) generation [124,125]. Besides, another 460 loop was also proved to be important for the initial substrate recognition during the transglycosylation reactions [126]. Different from GH13 and 77 4αGTs, GH57 4αGTs are composed of two domains: an N-terminal CD, which showed a $(\beta/\alpha)_7$ barrel, and a CTD, which showed a twisted β-sandwich fold [61]. Despite the uncertain role of the CTD, it could potentially contribute to the transglycosylation reactions of GH57 4αGTs. This speculation is rooted in the observation that the β-sandwich domain of *E. coli* β-galactosidase is implicated in transglycosylation reactions [127].

4αGT catalyzes four different reactions: cyclization, coupling, hydrolysis, and disproportionation. The catalytic process of 4αGTs involves two steps: (1) cleave an α-1,4-glucosidic linkage to release a linear glucan chain and form covalent intermediate (Figure 3A), (2) transfer the glucosyl unit to the non-reducing end of a different position, generating a new glucan (Figure 3E) [128,129].

4αGTs play an important role in diverse biological processes. In plants, they are involved in starch granule architecture, biosynthesis and degradation rates of starch [130]. In microorganisms, these enzymes are involved in glycogen metabolism, serving as the storage form of glucose and utilization of maltooligosaccharides [131]. The unique ability of 4αGTs to modify carbohydrate structures has attracted interest from the industrial sector. It plays a crucial role in catalyzing the cyclization reaction, specifically intramolecular transglycosylation, using substrates such as amylose or amylopectin. This enzymatic process results in the formation of large-ring cyclodextrins (LR-CDs) with a DP ranging from 9 to several hundred. The DP and yield of LR-CDs depend on various factors, including the specific enzyme, substrate selection, and reaction conditions.

4αGT is an important enzyme involved in the metabolism of maltooligosaccharides and glycogen in microorganisms. It plays a role in synthesizing long-chain maltooligosaccharides from short-chain ones, facilitating their metabolism [131]. Notably, the D-enzyme is another enzyme present in the plant starch biosynthesis pathway, sharing remarkable similarities in amino acid sequences and enzymatic characteristics with amylomaltase. Both enzymes are involved in glucan transfer to the novel 4-position acceptor (disproportionation reaction) from α-1,4-glucan, as well as synthesizing cyclic α-1,4-glucans of varying DPs (cyclization reaction). Besides, 4αGT can also catalyze disproportionation reactions cleaving amylose into shorter fragments, which are transferred to the nonreducing ends of amylopectin resulting in longer exterior chains. For example, modification of starch by 4αGT can improve the retrogradation and digestibility of starch [132], as well as water binding capacity, gel properties and freeze-thaw stability of starch-based hydrogels [128,129].

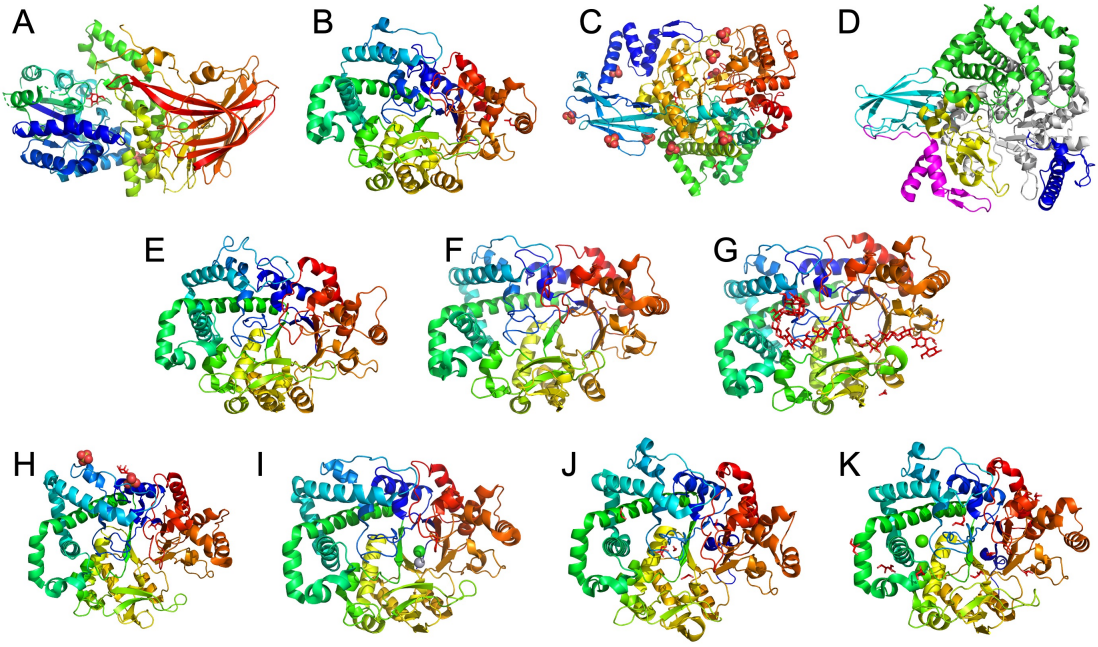

Figure 7. Gallery of experimentally determined structures of 4-α-glucanotransferase (4αGT) from individual GH families. The entire polypeptide chain of an enzyme is coloured spectrally from N-terminus (blue) to C-terminus (red) using Pymol. Ca^{2+} is displayed if present as a green globule), SO_4 (displayed if present in red-yellow molecule), and ligand (displayed if present in red glucan). The TIM-barrel domain A, subdomains N1, N2, and B1, B2 and B3 are colored gray, magenta, cyan, and green, yellow and blue, respectively in (D).
GH57 4αGT: (A) *Thermococcus litoralis* 4αGT (PDB: 1K1W, [61]).
GH77 4αGT: (B) *Aquifex aeolicus* 4αGT (PDB: 1TZ7, [133]); (C) *Corynebacterium glutamicum* 4αGT (PDB: 5B68, [123]); (D) *Escherichia coli* 4αGT (PDB: 4S3P, [122]); (E) *Streptococcus agalactiae* 4αGT (PDB: 6M6T, [122]); (F) *Thermus aquaticus* 4αGT in complex with a 34-meric cycloamylose (PDB: 1CWY, [134]); (G) *Thermus aquaticus* 4αGT in complex with a 34-meric cycloamylose (PDB: 1CWY, [126]); (H) *Thermus brockianus* 4αGT (PDB: 2X1I, [135]); (I) *Thermus thermophilus* HB8 4αGT (PDB: 1FP8, [125]); (J) *Arabidopsis* 4αGT (PDB: 5CPQ, [136]); (K) *Solanum tuberosum* (potato) 4αGT (PDB: 1X1N, [137]).

1.3 Enzymatic Modification of Starch

Starch can be modified to achieve desired properties by altering the content and molecular structures of amylose and amylopectin through change of chain length, adjustment of branching points, and formation of novel glucosidic linkages which does not exist in natural starch (e.g. α-1,3-linkages [138]). Modification methods include physical, chemical, and biological treatments. Physical treatments such as osmotic pressure, deep freezing and thawing, and pulsed electric field are considered safe but less efficient. Chemical modification of starch, including cross-linking, oxidation, and acid hydrolysis, offers high efficiency and product diversity. However, these modification approaches may be detrimental to the environment and requires recycling [4].

Enzymatic modification, being mild, safe, and environmentally friendly, is the most promising approach. Hydrolases and glucanotransferases capable of hydrolysis and/or transglycosylation, respectively, classified in GH families, are used in starch processing. It is worth mentioning that while hydrolases and transferases are typically associated with their specific functions, many hydrolases can also facilitate transfer reactions under specific conditions, and transferases commonly exhibit hydrolytic activity as well.

Among the hydrolases commonly employed for starch modification, the primary classification revolves around enzymes that degrade α-1,4-linkages. These include, for example, the endo-acting α-amylase (EC 3.2.1.1) [51], the exo-acting β-amylase (EC 3.2.1.2) [139], and the exo-acting glucoamylase (EC 3.2.1.3) [140]. Moreover, there are α-1,6-linkage degrading enzymes such as PULI (EC 3.2.1.41) and isoamylase (EC 3.2.1.68) [96]. In addition to these enzymes that specifically target one type of linkage, there are also enzymes like PULII (amylopullulanase, EC 3.2.1.41) and neopullulanase (EC 3.2.1.135), which can act on both α-1, 4- and α-1, 6-linkages [141,142].

Glucanotransferases, including BE (EC 2.4.1.18), cyclodextrin glycosyltransferase (CGTase, EC 2.4.1.19), 4αGT (EC 2.4.1.25), and GH70 4,3-α-glucanotransferase (EC 2.4.1.-), 4,6-α-glucanotransferase (EC 2.4.1.-), and amylosucrase (EC 2.4.1.4), play essential roles in cleaving α-1,4 bonds within a donor molecule and transferring the released portion onto a glycosyl acceptor. These processes can lead to the formation of new α-1,3-, α-1,4-, or α-1,6-linkages.

1.3.1 Enzymatic Modification of Granular Starch

Enzymatic modification of gelatinized starch systems is more efficient compared with granular starch systems due to the disruption of granular and semi-crystalline structures. However,

maintaining the granular state of starch without gelatinization is desirable for energy savings, handling convenience, and prevention of retrogradation.

Generally, hydrolases disrupt the granular integrity and yield hydrolytic products that depend on reaction conditions and enzymes. Mild conditions result in porous starches with increased surface area, suitable for use as carriers for flavors, drugs, probiotics, oils, antioxidants, absorbents, wastewater treatment, and skincare [143]. Medium conditions further disrupt the starch structure, cleaving AP and AM molecules into branched and linear dextrin, valuable in candy, coffee, and ice cream production [144]. Under strong conditions, with high enzyme dosage and long incubation time, starch is cleaved into maltooligosaccharides, maltose, and glucose, which can be used for syrups and in beverage production [145].

Different from the popularity of using hydrolases on granular starch modification, the application of glucanotransferase is gaining increasing attention as this special enzymatic process endowed improved properties. For instance, 4αGT treatment increased the thermal resistance of pea starch, but had the opposite effect on cassava starch [146]. Maize starch granules modified by BE [147,148] have shown higher digestive resistance. Additionally, the treatment with BE did not alter the crystallinity and pores of granular rice starch after pretreatment with maltogenic α-amylase, whereas BE significantly increased both the crystallinity and number of pores in rice starch granules that were pretreated with hot ethanol [149]. Similarly with producing pores on the surface of granular starch by hydrolases, enzymatic modification by CGTase of granular maize starch led to structures with irregular surface and small pinholes [150]. Besides, CGTase modified maize starch granules were less susceptible to undergo α-amylase hydrolysis [150].

1.3.2 Enzymatic Modification of Gelatinized Starch

The compact semi-crystalline structure of granular starch poses a challenge for enzymes to efficiently catalyze chain transfer or hydrolytic reactions within its matrix. Consequently, the modification of starch through enzymatic means is typically carried out after the process of starch gelatinization, which significantly enhances its accessibility as a substrate.

The α-amylases are responsible for hydrolyzing α-1,4-linkages present in both AM and AP molecules. Besides, there are some specific maltooligosaccharide-forming α-amylase, such as maltotetraose-forming α-amylase (EC 3.2.1.60) [151], maltohexaose-forming α-amylase (EC 3.2.1.98) [152], and maltotriose-forming α-amylase (EC 3.2.1.116) [153]. Such enzymatic activity of α-amylases results in the formation of various linear maltooligosaccharides, branched α-limit dextrin, maltose, and glucose [154]. On the other hand, the β-amylases, from GH14, sequentially hydrolyze starch molecules from the non-reducing ends, leading to

production of maltose, β-limit dextrin, and small quantities of glucose [139]. In the GH15 enzyme family, glucoamylase primarily acts on α-1,4-linkages, liberating glucose from the non-reducing ends of starch. Although it can also catalyze α-1,6-linkage hydrolysis, its activity in this regard is considerably lower (less than 1%) [140].

Besides, during the debranching process of starch by PULI and isoamylase, linear chains are liberated from amylopectin, which facilitates molecular rearrangement and the formation of A- or B-type crystalline polymorphs, as well as gel networks. These released linear chains have the capacity to form complexes with helical host molecules, such as lipids and other hydrophobic compounds, resulting in the creation of V-type crystalline polymorphs [155,156]. These complexes demonstrate enhanced resistance to digestion and recrystallization, along with the ability to form high-strength gels that exhibit thermo-reversibility. As a result of these exceptional properties, they are utilized as tablet excipients, fat replacers, and additives in low-calorie foods [157]. Additionally, by cleavage of both α-1,4- and α-1,6-linkages by amylopullulanase and neopullulanase, the modified starch usually showed increased crystallinity and digestive resistance [141,142] (Table 1).

Apart from the application of hydrolases in starch modification, different glucanotransferases are gaining increasing attentions since these enzymes catalyze the formation of new α-1,3-, α-1,4-, or α-1,6-linkages, and therefore endow modified starch with novel properties, such as digestibility, gel properties, and encapsulation ability. CGTase has been widely used on large scale in the production of starch syrups, maltodextrins, and cyclodextrins [158]. BE was reported to catalyze the formation of the cyclic cluster dextrin, low-amylose starch, low-digestible starch, and glycogen-liked starch [159]. 4αGT has been reported to catalyze the cyclization reaction with substrate of amylose or amylopectin thus forming LR-CDs with DP from 9 to hundreds [160]. Besides, the modification on starch by 4αGT will also lead to the formation of low-amylose, low-digestible starch [128]. GH70 4,3- and 4,6-α-glucanotransferases demonstrate clear disproportionating activity on starch and maltodextrin substrates, resulting in linear or branched isomalto-oligosaccharide with various α-1,3 or α-1,6 linkages, respectively [138,161]. These polymers exhibit different types and degrees of branching, as well as diverse sizes and conformations and have been used for isomalto-oligosaccharide (Table 1).

Table 1. Characteristics of enzymes involved in starch degradation/modification and their main products using starch as substrate.

Type of enzyme	Enzyme	EC number	GH family	Main product
Hydrolase	α-amylase	3.2.1.1	GH13	Maltooligosaccharides, branched α-limit dextrin, maltose, and glucose
	Maltogenic amylase	3.2.1.133	GH13	α-D-maltose
	β-amylase	3.2.1.2	GH14	β-D-maltose
	Glucoamylase	3.2.1.3	GH15	Glucose
	PULI	3.2.1.41	GH13	Maltooligosaccharides
	Isoamylase	3.2.1.68	GH13	Maltooligosaccharides
	PULII (amylopullulanase)	3.2.1.41	GH13	Low-amylose starch, Maltooligosaccharides
	Neopullulanase	3.2.1.135	GH13	Low-amylose starch, iso-maltooligosaccharides
	Maltotetraose-forming α-amylase	3.2.1.60	GH13	Maltotetraose
	Maltohexaose-forming α-amylase	3.2.1.98	GH13	Maltohexaose
	Maltotriose-forming α-amylase	3.2.1.116	GH13	Maltotriose
Glucano transferase	BE	2.4.1.18	GH13, GH57	Glycogen, cyclic cluster dextrin, low-amylose starch, low-digestible starch
	CGTase	2.4.1.19	GH13	Cyclodextrin, low-digestible starch
	4αGT	2.4.1.25	GH13, GH57, GH77	Cycloamylose, low-amylose starch, low-digestible starch
	4,3-α-glucanotransferase	2.4.1.-	GH70	Isomalto-oligosaccharides
	4,6-α-glucanotransferase	2.4.1.-	GH70	Isomalto-oligosaccharides

1.4 Starch Binding Domains

Starch binding domains (SBDs) have been demonstrated to process the ability to bind onto raw, thermally untreated granular starch [162], although SBD is not necessary for all amylases to bind to starch granules [163–165]. SBDs are a defined group of carbohydrate binding modules (CBMs) without enzymatic activity which confer numerous starch-active enzymes with the ability to bind α-glucans, including starch granules [162,166]. Historically, SBD was first determined in glucoamylases from *Aspergillus awamori* [167], *Aspergillus niger* [140,168] and *Rhizopus oryzae* [169,170]. Currently, among the 98 CBM families in the CAZy database (http://www.cazy.org/) [50], 16 can be considered to have SBD functional characteristics: CBM20, 21, 25, 26, 34, 41, 45, 48, 53, 58, 68, 69, 74, 82, 83, and 98 [166,171].

1.4.1 Structure of Starch Binding Domains

The common structural motif found in SBDs is a β-sandwich fold (Figures 8 and 9). SBDs, except CBM74, are individual immunoglobulin-like fold domains of about 100 amino acid residues [166,172]. These β-sheets are composed of several β-strands that are connected by loops, and the entire structure is stabilized by hydrogen bonds and hydrophobic interactions. Moreover, some SBDs has two starch binding sites, while some only shows one. For example, typically two binding sites have been found in CBM20, 21, 25 and 34 (Figure 8A, B, C, and E; Figure 10A and B) [173–175]. Among the SBD families, SBDs from CBM74 differed as it consisted of ~350 amino acid, showed different structure having 21 β-strands and 13 short α-helices with a core β-sandwich fold of two sheets with five antiparallel β-strands (Figure 8K) [172,176].

1.4.2 Function of Starch Binding Domains

Functionally, SBDs typically bind to starch granules with micromolar affinity [177] and have been described to also disentangle interacting α-glucan chains on the starch granule, facilitating the enzymatic degradation [178]. Thus SBDs support enzymatic processes by bringing the active site on the catalytic domain (CD) in close contact with the substrate, which may include guiding α-glucan chains to be hydrolyzed to the active site crevice [179,180]. Besides, in plants, solitary SBD-containing proteins (e.g. PTST3) have been shown to play an important role in biosynthesis of starch, by helping to regulate the synthesis and storage of starch in different plant tissues [166,181].

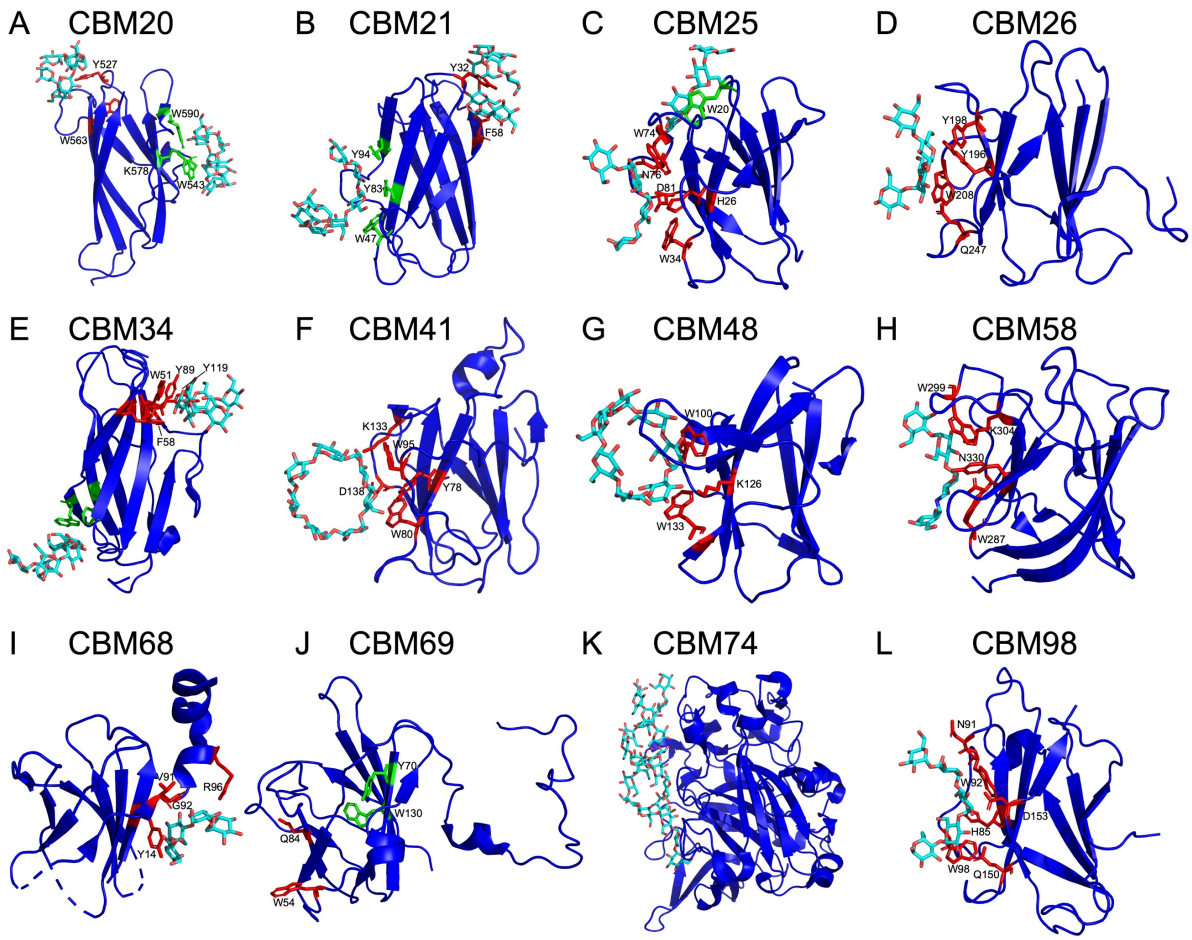

Figure 8. Gallery of experimentally determined structures of SBDs from individual CBM families. The entire polypeptide chain of a CBM is coloured in blue with highlighted side chains of residues involved in binding a carbohydrate (displayed if present in cyan); the residues being coloured red and green, respectively, for binding site 1 (BS1) or binding site 2 (BS2). (A) CBM20: *Aspergillus niger* glucoamylase (GH15, PDB: 1AC0, ligand: β-CD, [179]); (B) CBM21: *Rhizopus oryzae* glucoamylase (GH15, PDB: 2V8M, ligand: maltoheptaose, [182]); (C) CBM25: *Bacillus halodurans* maltohexaose-forming amylase (PDB: 2C3W, ligand: maltotetraose, [183]); (D) CBM26: *Eubacterium rectale* DSM 17629 α-amylase (PDB: 6B3P, ligand: maltopentose, [184]); (E) CBM34: *Thermoactinomyces vulgaris* α-amylase (PDB: 1UH4, ligand: maltopentose and maltohexaose, [185]); (F) CBM41: *Klebsiella pneumoniae* Pullulanase (PDB: 5YNC, ligand: β-CD, [99]); (G) CBM 48: *Rattus norvegicus* AMP-activated protein kinase (PDB:1Z0M; ligand: β-CD, [186]); (H) CBM58: *Bacteroides thetaiotaomicron* α-amylase (PDB: 6BS6; ligand: maltotetraose, [187]); (I) CBM68: *Anoxybacillus* sp. LM18-11 pullulanase (PDB: 3WDJ; ligand: maltotetraose, [101]); (J) CBM69: uncultured bacterium α-amylase (AmyP, PDB: 5X5S; ligand: none, [188]); (K) CBM 74: *Ruminococcus bromii* α-amylase (Sas6, PDB: 7UWV; ligand: maltodecaose); (L) CBM 98: *Bacteroides ovatus* α-amylase (PDB: 5DL1; ligand: maltoheptaose, [171]).

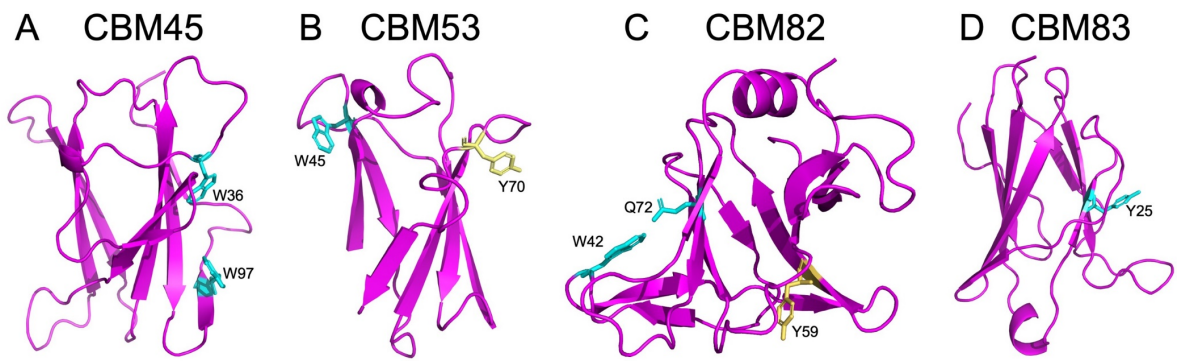

Figure 9. Gallery of Alphafold2 models of SBDs from individual CBM families. The entire polypetide chain of a CBM is coloured by magenta with highlighted side-chains of residues predicted to be involved in binding a carbohydrate; the residues are coloured cyan and yellow, respectively, for binding site 1 (BS1) or binding site 2 (BS2). (A) CBM45: *Arabidopsis thaliana* α-amylase (GenBank accession: Q94A41.1); (B) CBM53: *Arabidopsis thaliana* Starch synthase 3 (GenBank accession: F4IAG2.1); (C) CBM82: *Agathobacter rectalis* DSM 17629 α-amylase (GenBank accession: CBK91127.1; residues 44–172); (D) CBM83: *Agathobacter rectalis* DSM 17629 α-amylase (GenBank accession: CBK91127.1; residues 508–613).

1.4.3 CBM Families Involved in this PhD Thesis

Family CBM20

CBM20 stands as the quintessential SBD, initially recognized as a C-terminal SBD in glucoamylase in the early 1980s [189]. Its origins trace back to glucoamylases in *Aspergillus awamori* [167] and *Aspergillus niger* [140,168]. With over 3,678 members, CBM20 hosts 18 characterized three-dimensional structures. Bacterial representation dominates, followed by Eucarya and Archaea [50]. Although typically associated with enzymes from the α-amylase GH13 [190,191] or GH70/GH77 families [192], part of the GH-H clan [50], CBM20 modules also appear in GH14 β-amylases [193], GH15 glucoamylases [194], GH57 amylopullulanase [195], and the GH119 α-amylase IgtZ from *Bacillus circulans* [63]. Besides, CBM20s are found in other non-GH proteins, such as laforin from *Homo sapiens* [196], AA13 lytic polysaccharide monooxygenase [197], and phosphoglucan, water dikinase 3 (GWD3) from *Arabidopsis thaliana* (*At*GWD3) [198]. From the domain architecture, it was found that the CBM20s have always been found located at the C-terminus of CD (Figure 11). By contrast, in plant 4-α-glucanotransferase (DPE2) and GH57 amylopullulanase, two or three copies of the CBM20 module are positioned N-terminally. CBM20 is frequently encountered as a singular occurrence within a protein, often presenting without concurrent presence of SBDs from other CBM families within the same protein molecule. However, instances of concurrent existence have been noted alongside CBM25 (Figure 11), as well as CBM34 and CBM48 [199,200]. In terms of structure, CBM20 adopts a β-sandwich fold (Figure 8A), recognized as the immunoglobulin-like fold [201]. This particular fold is widely acknowledged as a defining characteristic of CBMs [202]. Functionally, two binding sites were found in CBM20s [194], while there are also some cases with only one binding sites [195]. The two binding sites may

serve distinct purposes for the enzymes they are associated with. The initial binding site, referred to as binding site 1, plays a crucial role in the affinity for raw starch, a trait supported by the presence of two tryptophan residues (Figure 10A). On the other hand, binding site 2, composed by two Trp and one Lys (Figure 10B), is believed to function in directing starch chains towards the active site [166]. CBM20s from different organisms showed significantly different affinity. For example, CBM20 from *At*GWD3 showed around 50-times lower affinity than CBM20 from *An*GA on β-CD (Table 2) [198]. This substantial contrast in affinity played a pivotal role in our selection of these two CBM20s for the construction of SBD-fusions in ***Paper 1***.

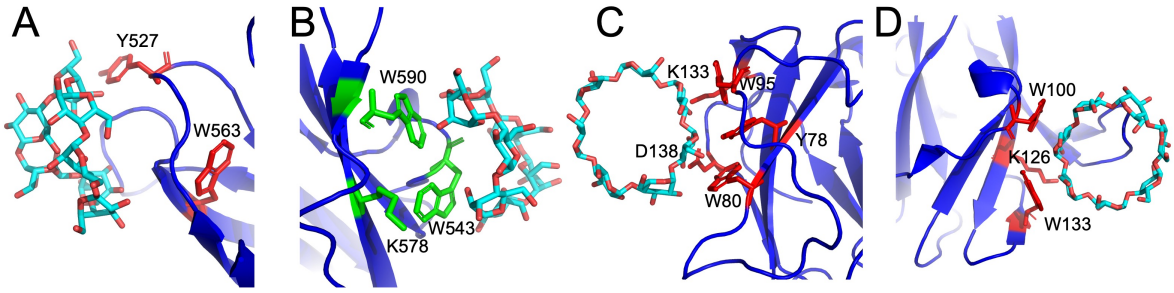

Figure 10. Close-up of binding sites in selected CBMs. (A) Binding site 1 in CBM20: *Aspergillus niger* glucoamylase (GH15, PDB: 1AC0, ligand: β-CD, [179]); (B) Binding site 2 in *An*GA CBM20; (C) CBM41: *Klebsiella pneumoniae* Pullulanase (PDB: 5YNC, ligand: β-CD, [99]); (D) CBM 48: *Rattus norvegicus* AMP-activated protein kinase (PDB:1Z0M; ligand: β-CD, [186]). The entire polypeptide chain of the CBM is coloured in blue with highlighted side chains of residues involved in binding a carbohydrate (displayed if present in cyan); the residues for binding site 1 and binding site 2 (displayed if present) are coloured in red and green, respectively.

Family CBM41

CBM41 stands out as one of the larger CBM families, with 6,747 members from the *Bacteria*. Besides, there are an additional 8 CBM41s identified within green/red algae, along with a solitary CBM41 found in liverwort [50]. Typically, the positioning of the CBM41 module within proteins occurs at the N-terminus, occasionally manifesting as tandem repeats. This strategic placement is in proximity to the catalytic TIM-barrel domain inherent to pullulanases and akin GH13 enzymes (Figure 11). However, there are also some other cases, e.g., in the GH13_41 α-amylase from *Micrococcus* sp. 207, which features two CBM41s positioned in tandem at the C-terminus (Figure 11) [203]. Beyond this, CBM41 interfaces with various other CBM families, such as CBM25, CBM26, CBM48, CBM69, CBM82, and CBM83 [81,166,184]. Structurally, CBM41 exhibits a characteristic β-sandwich structure, adopting a distorted β-barrel configuration akin to an immunoglobulin fold. This arrangement comprises a singular α-glucan

binding site (Figure 8F), involves stacking interactions with two aromatic residues, Trp80 and Trp95, and hydrogen bond contacts contributed by Tyr78, Lys133 and Asp138 in *Klebsiella pneumoniae* PULI (Figure 10C, PDB: 5YNC [99]). Functionally, Given that the majority of experimentally elucidated CBM41s are found as integral components of debranching enzymes belonging to the GH13 subfamilies, namely GH13_12, GH13_13, and GH13_14, it is plausible to hypothesize that these modules have the capability to accommodate α-glucans containing glucose residues connected through α-1,6 linkages [204]. In debranching enzymes, CBM41 was reported to participate in substrate recognition by showing dramatically reduced affinity after truncation of CBM41 (Table 2) (***Manuscript 1*** and [92]).

Family CBM48

The CBM48 family, with more than 57,327 members, represents unambiguously the largest SBD CBM family and it is the second biggest CBM family in CAZy [50]. More than 55,720 members originate from *Bacteria*, the rest are from *Eucarya* (~2,635), *Archaea* (~226) and *Viruses* (~5) [50]. The first experimental evidence of α-glucan binding to CBM48 was obtained by solving the crystal structure of the CBM48 module from the β1-subunit of the rat AMP-activated protein kinase (AMPK) in complex with β-CD (Figure 8G) [186]. As shown in Figure 11, CBM48s were found N-terminally in diverse proteins, mostly from the α-amylase family GH13, including pullulanase, isoamylase, maltooligosyltrehalose trehalohydrolase, cyclomaltodextrinase, and α-glucan branching enzyme [50]. CBM48s were also found at the N-terminus of feruloyl esterase [205] and AMPK [186]. Besides, C-terminal CBM48s were found in glucan phosphatase starch-excess 4 protein (SEX-4) [206] and *Arabidopsis thaliana* proteins targeting to starch 2 and 3 (PTST2 and 3) [207]. Similar to CBM41, CBM48 also interfaces with various other CBM families within SBDs, such as CBM25, CBM34, CBM41, CBM68, CBM69, CBM82, and CBM83 [166]. In the CBM48s from the α-amylase family GH13, CBM48s were positioned immediately upstream of the CDs, except for in the cyclomaltodextrinase from *Pyrococcus furiosus* DSM 3638 [208]. Structurally, CBM48 showed a classical β-sandwich immunoglobulin-like fold (Figure 8G). This arrangement comprises a single α-glucan binding site involving stacking interactions with two aromatic residues, Trp100 and Trp133, and hydrogen bond contacts contributed by Lys578, as seen for the CBM48 from rat AMPK β1 (Figure 10D) [186]. Functionally, Mesbah et al. concluded that CBM48 is essential for binding branched substrates and for the enzyme stability showing lower activity on branched substrate after truncation of CBM48 in *Alkalilimnicola* sp. NM-DCM-1 amylopullulanase [209]. Besides, CBM48 is crucial for the expression of PULI by showing no expression after truncation of CBM48 in *Thermotoga maritima* MSB8 PUL [210].

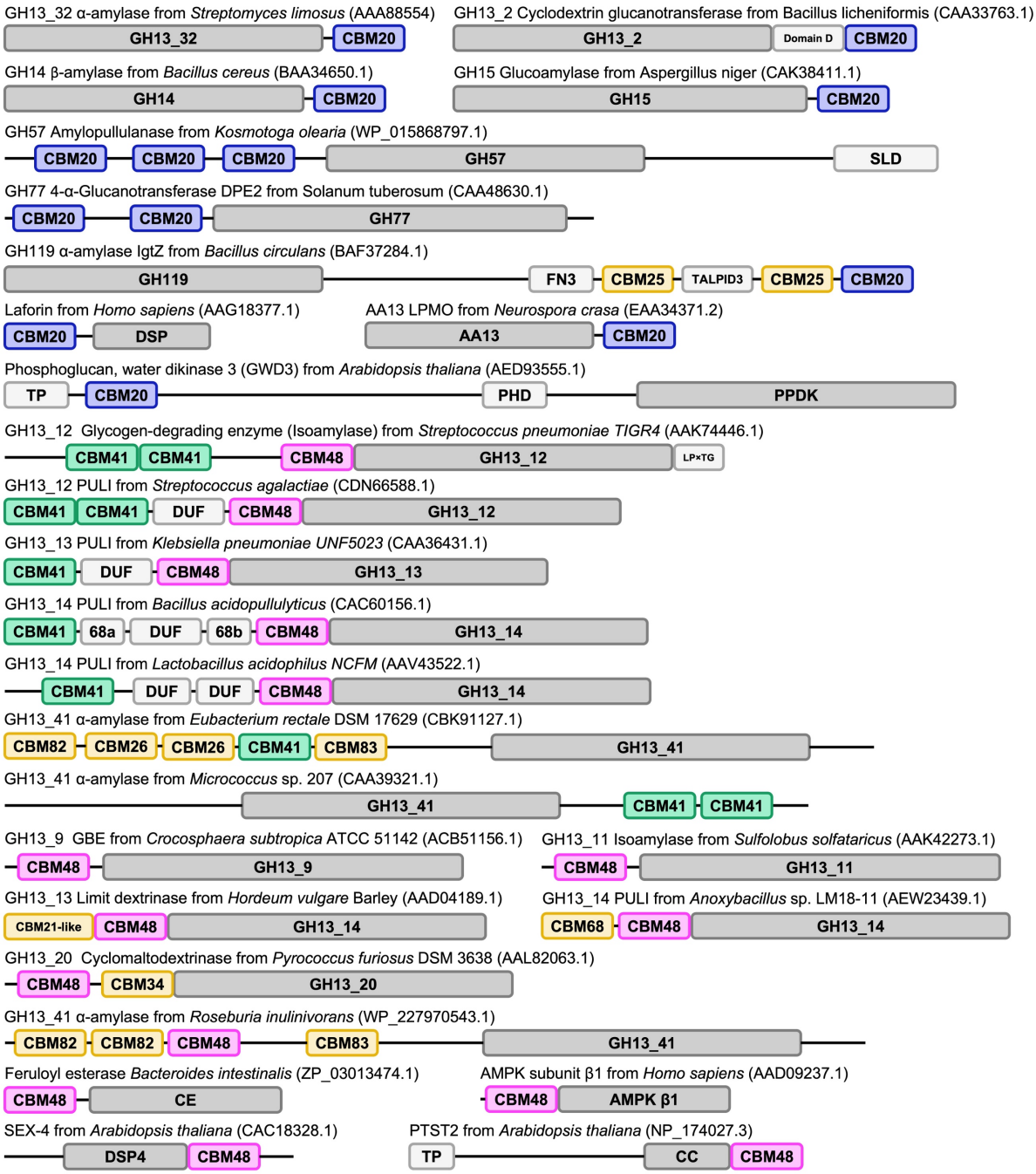

Figure 11. Domain architecture of representative enzymes containing CBM20, 41, and 48. This figure is inspired by a figure from Janeček et al [166]. CBM20, CBM41, CBM48 and other CBM families were colored in blue, green, magenta, and yellow, respectively. CDs and other domains with or without known function are colored gray and white in each case. The NCBI database (https://www.ncbi.nlm.nih.gov/) accession number of every protein is given in parenthesis. The abbreviations other than GH and CBM are as follows: AA13, auxiliary activity family 13; AMPK β1, AMP-activated protein kinase β-subunit; CC, Coiled coil-containing regions; CE, carbohydrate esterase; DSP4, dual specificity phosphatase domain of laforin; DUF, domain of unknown function; SLD, surface-layer homology bearing domain; LPxTG, cell wall anchor motif; PHD, phosphohistidine domain; PPDK, pyruvate phosphate dikinase; PTST, protein targeting to starch; SEX-4, glucan phosphatase starch-excess 4 protein; TP, transit peptide.

Table 2. Binding of CBMs to different ligands.

CBM family	Protein	Organism	Ligand	K_d	Method/ condition	Ref.
20	GA[a] (CBM20)	*A. niger*	Maltose	6.3 mM	Ultraviolet (UV) difference spectroscopy, pH 4.5, 25 °C	[211]
			Maltoheptaose	2.38 mM		
			Maltododecaose	10.5 μM		
			β-CD	1.7 μM		[212]
	GA (CBM20)	*A. niger*	β-CD	14.4 μM	UV difference spectroscopy, pH 4.5, 25 °C	[213]
	GA (CBM20 W590K)		β-CD	6.4 μM		
	GA (CBM20 W563K)		β-CD	28 μM		
	GWD3[b] (CBM20)	*A. thaliana*	β-CD	380 μM	SPR, pH 5.5	[198]
	GA (CBM20)	*A. niger*	β-CD	7.5 μM		
	GA (CBM20)	*A. niger*	Maize starch	19.6 μM	Pull down assay, pH 3.6, 2 °C	[214]
	GA (CBM20)	*A. niger*	Maize starch	3.2 μM	Pull down assay, 25 °C	[177]
	GA (CBM20)	*A. niger*	Potato starch	3.3 μM		
41	PULI (CBM41-DUFs-CBM48-CD)	*L. acidophilus* NCFM	β-CD	48.3 μM	SPR pH 5, 25 °C	*M1*[c]
			WMS	0.12 μM	Pull down assay, pH 5, 4 °C	
			NMS	1.08 μM		
	PULI (DUFs-CBM48-CD)		β-CD	>1000 μM	SPR pH 5, 25 °C	
			WMS	0.36 μM	Pull down assay, pH 5, 4 °C	
			NMS	1.8 μM		
	CBM41-CBM41-X	*S. pyogenes*	Maize starch	K_a=2.2 M^{-1}	Solid-state depletion isotherm method	[215]
	CBM41-CBM41-X	*S. pneumoniae*	Maize starch	K_a=1.1 M^{-1}		
48	PTST2[d]	*A. thaliana*	β-CD	1–3.3 μM	ITC, pH 7.5, 22 °C	[207]
	PTST2 (CBM48)	*A. thaliana*	β-CD	1.7–4 μM		
	AMPK β1		β-CD	5.5 μM	CBM48 fluorescence (NMR), pH 7, 25 °C	[216]
	AMPK β2		β-CD	0.5 μM		
	AMPK β1	*Rattus norvegicus*	β-CD	4.39 μM	ITC, pH 6.8, 25 °C	[217]
			Glc-β-CD	4.4 μM		
	AMPK β2		β-CD	0.98 μM		
			Glc-β-CD	0.32 μM		
	BE (CBM41-CBM48-CD)	*Ostreococcus tauri*	Starch	K_{ad}=10.9 mL/g	Pull down assay, pH 6.9, room temperature	[218]
			Amylose	K_{ad}=6.0 mL/g		
			Amylopectin	K_{ad}=1.6 mL/g		
	BE (CBM48-CD)		Starch	K_{ad}=4.6 mL/g		
			Amylose	K_{ad}=8.1 mL/g		
			Amylopectin	K_{ad}=3.1 mL/g		
	BE (CBM48)		Starch	K_{ad}=12.6 mL/g		
			Amylose	K_{ad}=8.5 mL/g		
			Amylopectin	K_{ad}=4.2 mL/g		

[a] GA: glucoamylase. [b] GWD3: phosphoglucan, water dikinase 3. [c] *M1*: *Manuscript 1.* [d] PTST2: protein targeting to starch 2.

1.5 Starch Binding Domain Fusion

1.5.1 Structural Design of Starch Binding Domain Fusion

Proteins are large macromolecules consisting of polypeptide chains, which play diverse roles in organisms. When designing protein fusions, the sequential arrangement of protein domains and the linkers between them are crucial for successful recombinant protein expression and production.

Order of protein domains

The translation of proteins begins at the N-terminus and progresses towards the C-terminus. Proteins often contain self-contained units called domains that have distinct structures and functions. The positioning of fused domains can impact protein expression since translation and folding occur simultaneously. Interactions between different domains occur through various bonds, such as non-covalent hydrogen bonding and hydrophobic interactions, or covalent disulfide bridges. The specific sequence and arrangement of domains determine the overall structure and function of the protein. Some domains stabilize the structure of protein, prevent unfolding, or regulate protein-protein interactions and activity. Additionally, the sequence of domains can influence post-translational modifications that affect protein function. The location of fused domains can affect protein expression, as observed in a study by Palmer et al., where N-terminal fusion proteins showed incorrect localization compared to correctly localized C-terminal fusion proteins [219]. This suggests that N-terminal fusions may disrupt the folding of target proteins, while C-terminal fusions do not interfere since they are folded lastly [220]. In the design of protein fusions, the location of substrate-binding domains (SBDs) relative to the acceptor protein is often considered. According to the reported work, most SBDs are fused to the C-terminus of the acceptor protein, regardless of their location in the SBD donor protein (Table 3) [221–223]. However, the relative positioning of SBDs with respect to the acceptor protein can also impact their function.

Linkers between protein domains

Linkers between protein domains are crucial in protein fusion design. They play a role in expression and proper folding of fusion proteins. Natural linkers can be either rigid or flexible to maintain distance between domains and minimize unwanted interactions. Artificial linkers can be designed using DNA technology to control the proximity and interaction between domains. Linkers can be classified as flexible, rigid (α-helix), or cleavable, each with specific structural and functional properties [224]. Flexible linkers often contain small and polar residues like Gly, Ser, and Thr [225–227]. Rigid linkers can be formed by α-helices or specific amino acid sequences like (EAAAK)n or Pro-rich linkers [228–230]. Cleavable linkers can be

used to release functional domains after cleavage, offering advantages in terms of steric obstruction and altered bioactivity [231,232]. Linkers also serve as functional domains in fusion proteins [227]. They can improve folding, stability, expression yield, and bioactivity of fusion proteins [233,234]. Proper linker design helps maintain appropriate distances between domains, reducing interference and enhancing protein function.

Overall, the sequential arrangement of protein domains and the choice of linkers are critical considerations in protein fusion design, affecting protein expression, folding and stability.

1.5.2 Applications of Starch Binding Domain Fusion

The specific binding ability of the SBD enables SBD fusion to fulfill various functions (Table 3). First and most importantly, as a binding module [235], SBDs are widely applied in altering substrate affinity and enzyme activity, directing proteins to starch-rich environments, and introducing new interaction modes [221,236,237]. For example, Firouzabadi et al. investigated the effect of CBM20-mutansucrase fusions on the biosynthesis of potato starch and found that the morphology of potato starch was severely altered when mutansucrase was fused with CBM20 [238]. SBD fusion can also change the affinity and substrate specificity of α-amylase [221] (***Paper 1***). Besides, SBDs also excel in protein purification, with SBD-containing proteins efficiently isolated using starch-based affinity columns, selectively excluding non-specific proteins [239,240]. While highly effective, their applicability is limited to bacterial and plant cell-expressed proteins, occasionally requiring additional purification methods. Commercial starch-based resins can also be costly. For example, the amylose resin costs 661 USD/1,000 mL (NEBExpress, UK) [239]. In some cases, SBDs further enhance protein stability and solubility, mitigating degradation by cellular proteases and increasing solubility, aiding in purification [222,241]. Yamaguchi et al. found that the two N-terminally fused SBDs improved the solubility of the target protein by 4-times [242]. Beyond these applications, innovative uses of SBD fusions include antigen carriers and hydrogel formation, highlighting their untapped potential in biotechnology [243,244].

Table 3. Information on SBDs and recombinant protein fusions.

CBM family	SBD donor (Organism)	Acceptor protein (Organism)	Position of SBD	Linker	Impact of SBD	Ref.
20	*An*GA[a]	*Hordeum vulgare* (Barley) α-amylase	C-TER[b]	QRS	Improved affinity (5-fold) and initial rate of hydrolysis (15-fold) on barley starch granules	[221]
	*An*GA	β-galactosidase	C-TER	ND[c]	Enhanced affinity to native starch (18-fold)	[236,237]
	Bacillus circulans strain 251 CGTase[d]	Mutansucrase from potato amyloplasts (*Gtfl*CAT)	N-TER & C-TER	P-T-rich linker	Alter the morphology of amylose-free potato starch granules	[238]
	*An*GA	*E. coli* GBE glycogen branching enzyme[e] (glgB)	N-TER	ND	Improve the branching degree of the transgenic starch by introducing more α-1,6-glucosidic bonds during starch biosynthesis	[245]
	Bacillus sp. strain TS-23 α-amylase	*Bacillus stearothermophilus* leucine aminopeptidase II	C-TER	ND	(1) Enhanced half-time at 70°C from 5 min to 30 min, (2) No binding to native starch for acceptor protein, improved binding ability for SBD-fusion. (3) Increased catalytic activity (2-fold).	[222]
	Bacillus sp. strain TS-23 α-amylase	*Bacillus kaustophilus* leucine aminopeptidase	C-TER	ND	Improved purification	[240]
	Bacillus sp. strain TS-23 α-amylase	*Bacillus stearothermophilus* leucine aminopeptidase II	C-TER	ND	Improved purification	[246]
	N- terminally truncated forms of Bacillus sp. strain TS-23 α-amylase	*Bacillus licheniformis* γ-glutamyltranspeptidase	C-TER	ND	(1) Helped the purification, (2) No binding to native starch for acceptor protein, improved binding ability for SBD-fusion.	[247]
	*An*GA	*Saccharomyces cerevisiae* GA	C-TER	No	Increased activity (10-fold) Increased binding (close to native *An*GA)	[248]
	Cryptococcus sp. S-2 α-amylase	Marine metagenome α-amylase (AmyP)	C-TER (C-TER His-tag)	TPS-ASG-LTK-VEF	(1) Enhanced thermostability at 40°C by 2.6-fold, (2) Improved activity on raw starches (from 1.6-fold to 4.4-fold on different native starches), (3) Improved binding capacity to starch (2.7-fold).	[241]
	Alkalimonas amylolytica α-amylase	*Paenibacillus macerans* CGTase	C-TER	SSG-G	Improved AA-2G yield by 3.9 (CGTΔE-CBM_{Amy})–5.9 (CGT-CBM_{Amy})-fold	[249]
	E-domain and DE-domains from of *Bacillus*	*Thermus aquaticus* YT-1 4αGT[f]	C-TER	*Eco*RI[g]	Enhanced molar specific activity toward amylose	[250]

	stearothermophilus ET1 CGTase					
	Bacillus circulans strain 251 CGTase	*Geobacillus* sp. CGTΔE	C-TER	No	Enhanced catalytic efficiency on soluble starch (2-fold) and native potato starch (4.7-fold)	[223]
	*An*GA	GFP	C-TER	ND	(1) Location of starch granule, (2) Determination of starch-protein interaction.	[251]
	Bacillus sp. *strain TS-23* α-*amylase*	Arg-Gly-Asp (RGD) peptide	C-TER	No	Used for preparation of dextrin-based hydrogel, improved fibroblast adhesion and spreading on the hydrogel surface	[244]
	*An*GA G1	*Clostridium cellulovorans* cellulose binding domain	C-TER	SVP-GVG-VPG-VGV-PGV-GVP-GVG-VP	Cellulose/Starch Cross bridging demonstrated cross-bridging ability in different model systems composed of insoluble or soluble starch and cellulose	[252]
	Saccharophagus degradans maltopentaose-forming amylase	*Bacillus megaterium* maltopentaose-forming amylase	C-TER	ND (17 AA)	(1) Improved hydrolysis activity (2-fold), (2) Improved catalytic efficiency on different substrates (1.4–5.9-fold), (3) Enhanced maltooligo-saccharide convertion rate (up to 5.3-fold).	[253]
21	*Rhizopus oryzae* GA[f]	GFP	N-TER & C-TER	ND	Helped purification of GFP	[254]
25	*Microbacterium aurum* α-amylase	Potato granule-bound starch synthase I (GBSSI)	C-TER	RGS (His)6-tag	The binding affinity of GBSSI can change the morphology of potato starch granules	[175]
	Kocuria varians α-amylase	GFP	N-TER	Thro-mbin site	Improved solubility (4-fold)	[242]
53	*A. thaliana* Starch synthase	*Agrobacterium tumefaciens* glycogen synthases	N-TER	ND	Enhanced glycogen accumulation *in vivo* (4-fold)	[255]
ND	ND	(1) GFP (2) tetanus toxin fragment C (3) *Entamoeba histolytica* Cys-rich protein	C-TER	No	Helped purification of acceptor proteins	[239]
ND	ND	*Mycobacterium tuberculosis* α crystallin (Acr)	C-TER	ND	Helped the delivery and presentation of vaccine	[243]

[a] *An*GA: *Aspergillus niger* glucoamylase. [b] TER: terminus. [c] ND: Not described. [d] CGTase: cyclodextrin glycosyltransferase. [e] GBE: glycogen branching enzyme. [f] 4αGT: 4-α-glucanotransferase. [g] Restriction enzyme site. [f] Glucoamylase.

1.6 Interfacial Catalysis of Granular Starch

Interfacial enzyme catalysis, also known as heterogeneous enzyme catalysis, represents a fascinating and distinct aspect of enzymatic reactions. Unlike homogeneous catalysis, where the enzyme and substrate are present in the same phase (i.e., both in the soluble state), allowing direct interaction and reaction between them, interfacial catalysis involves a scenario where the enzyme and substrate exist in different phases, with the enzyme typically being in a soluble form and the starch in its solid granular form. This unique arrangement gives rise to dynamic interactions at the interface between the enzyme and the substrate, which significantly impacts the reaction kinetics and mechanisms. One of the most notable examples of interfacial enzyme catalysis is in fact the hydrolysis of insoluble substrates, such as starch granules, cellulose, and lipid droplets [256].

1.6.1 Process of Interfacial Enzyme Catalysis of Granular Starch

The enzymatic hydrolysis of starch granules is intricately influenced by the diverse structures of the granule surface and matrix, as well as the substrate recognition and catalytic activity of the hydrolase. A crucial aspect to consider is the presence of accessible glucan chains at the granular starch surface, which can serve as efficient binding sites and substrates for starch-active enzymes [257,258]. The overall rate of hydrolysis is influenced by three key factors: (1) diffusion of the enzyme toward the granule surface, (2) the adsorption of enzymes onto the starch granule surface, (3) the catalysis of glycoside bonds within the starch structure, and (4) the subsequent desorption of enzymes from the starch granule surface (Figure 12) [6].

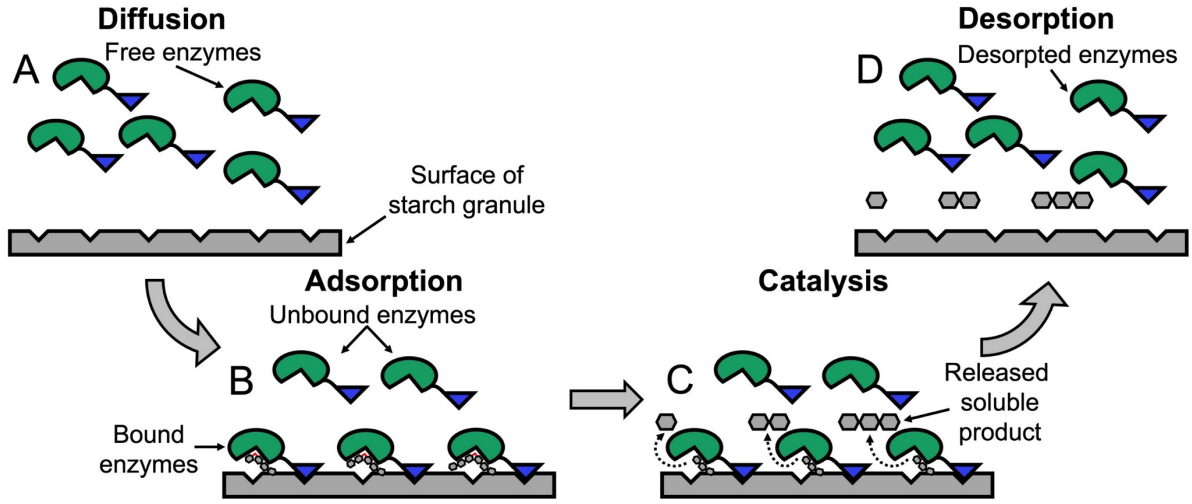

Figure 12. Interfacial catalysis of granular starch by starch-active enzymes during (A) diffusion, (B) adsorption, (C) catalysis, and (D) desorption.

Enzyme Diffusion

Diffusion plays a vital role in interfacial biocatalysis, where achieving the highest possible reaction rate hinges on finding the right equilibrium between the speed and degree of enzyme binding and the pace of movement across the surface [259]. When reactions are limited by adsorption, it is typically because there are not enough enzyme molecules available. Conversely, when surface concentrations are high, as seen with materials like granular starch, surface diffusion is slowed down, making it harder for enzymes to encounter and interact with catalytic sites. This slowing of surface diffusion is caused by restricted lateral movement and an increase in the strength of electrostatic interactions between the enzyme and the substrate [260].

Enzyme Adsorption

In interfacial enzyme catalysis, enzymes in a soluble state adsorb onto the starch granule surface through non-covalent interactions, such as aromatic stacking interaction, hydrogen bonding, and van der Waals forces [189,261]. Factors like enzyme concentration, substrate structure, temperature, and pH influence the adsorption. Sufficient enzyme concentration and sufficient substrate accessibility are crucial for effective adsorption [262,263]. Besides, optimal temperatures and pH can enhance the enzyme-substrate interactions and increase the overall rate of enzymatic adsorption [82]. With regard to the Sabatier principle, when the enzyme exhibits weak substrate binding, it violates the Sabatier principle, which states that optimal catalytic efficiency requires the formation of a stable enzyme-substrate complex. Insufficient binding hinders proper alignment of the substrate within the active site of the enzyme, leading to reduced catalytic activity and efficiency (Figure 13) [264].

Catalysis of Glycoside Bond Hydrolysis

Once adsorbed onto the substrate, the enzyme initiates the hydrolysis of glycoside bonds in the insoluble substrate. In starch granules, enzymes hydrolyze α-1,4- and α-1,6-glucosidic bonds, eventually breaking down the starch molecules into soluble fragments.

Enzyme Desorption

Following the hydrolysis of glucosidic bonds, the enzyme-product complex dissociates from the substrate surface, with release of soluble products. Desorption is influenced by factors such as product concentration, substrate structure, and competitive binding. It is crucial for desorption to occur efficiently to complete the catalytic cycle, allowing the enzyme to bind to

and catalyze multiple substrate molecules in quick succession. However, if the enzyme binds too strongly to the substrate, it can lead to a desorption limited situation, preventing the enzyme to dissociate and find the next binding site, and continue the next catalytic process (Figure 12D) [264].

Overall, the three steps of enzyme adsorption, catalysis of glucosidic bonds, and subsequent desorption are intricately interconnected and determine the overall efficiency of interfacial enzyme catalysis.

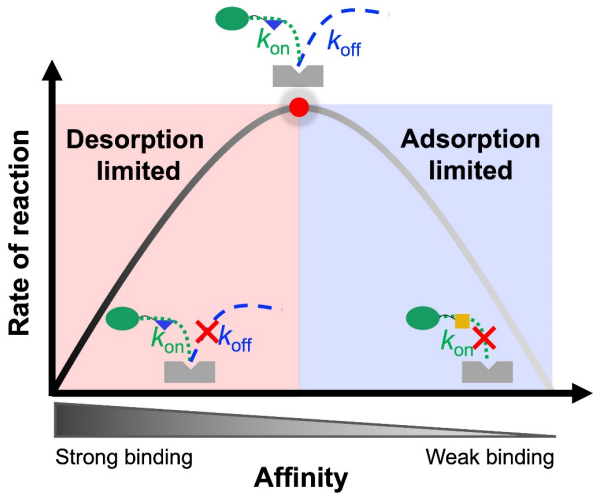

Figure 13. A volcano plot illustrating the Sabatier principle. This figure is inspired by a figure from Kari et al. [264].The pink part represents desorption limited catalysis, where higher affinity for substrate leads to lower rate of reaction. The blue part represents adsorption limited catalysis, where higher affinity for substrate leads to higher rate of reaction. The red dot between the desorption and adsorption limited regions represents the best affinity for substrate of the enzyme to have the highest rate of reaction.

1.6.2 Factors Influencing Interfacial Enzyme Catalysis

Interfacial Properties

In the case of starch, the properties of the surface of granular starches, such as accessibility of glucan chains, degree of order, crystallinity, and surface area, play a critical role in catalysis by affecting the enzyme-substrate interactions [5]. Certainly, an augmentation in surface area can result in a greater extent of exposed binding sites. This, as a result, leads to a higher quantity of enzymes being adsorbed onto the surface [265]. Besides, the changes in the degree of order on the surface can also influence the binding affinity between the enzyme and the substrate [266].

Enzyme Structure and Affinity for Substrate

The structure of the enzyme itself is an important factor in granular starch catalysis. Enzymes often undergo structural rearrangements upon interaction with the interface, which can

modulate their catalytic activity. The flexibility of the enzyme structure can allow optimal positioning and orientation of the active site towards the substrate, leading to enhanced catalytic efficiency [267,268]. Besides, the affinity for starch is crucial for formation of a stable enzyme-substrate complex. By modifying the CDs or adding specific SBDs, enzymes can be tailored for enhanced affinity and activity towards starch granules [221].

Apart from changing the substrate and enzyme, the interactions between the enzyme and other components present at the interface, such as surfactants, lipids, or nanoparticles, can influence interfacial enzyme catalysis [269]. These interactions can alter the enzyme stability, conformation, and activity. Surfactants, for example, can promote the adsorption and orientation of enzymes at interfaces, thereby enhancing their catalytic efficiency [270]. For example, by addition of surfactant (Cetrimonium bromide) in different concentration, Bååth et al. were able to control the affinity between poly(ethylene terephthalate) (PET) waste and PET hydrolases according to Sabatier principle, thus to improve the catalytic efficiency of PET hydrolases [271].

1.6.4 Strategies for Analyzing Interfacial Enzyme Catalysis—Interfacial Kinetics

The application of classical Michaelis-Menten (MM) kinetics to analyze amylolytic hydrolysis of granular starch, a two-phase system with a heterogeneous interface, requires caution [272]. Applying conventional MM approaches to such systems, like amylase acting on insoluble starch granule, similar to cellulases acting on insoluble cellulose, raises concerns [6]. The fundamental requirement for the quasi-steady-state assumption (QSSA) of the conventional MM approach assumes substrate in excess, which is hard to fulfill experimentally for heterogeneous systems due to ambiguous substrate molar concentration. Recent studies propose an alternative approach, varying enzyme concentration instead of substrate concentration and introducing a factor, ${}^{kin}\Gamma_{max}$, enumerating enzyme attack sites per gram of substrate (eq. 3). To obtain this parameter, interfacial catalysis was applied involving joining the conventional Michaelis-Menten kinetics (Figure 14A, eq. 1), where substrate is in excess, with an inverse kinetics approach having the enzyme in excess (Figure 14B, eq. 2). Please for detailed derivation of the equations see the earlier report [6].

Experiments with substrate in excess were analyzed using the conventional MM equation, eq. 1, where S_0^{mass} is the substrate mass load, V_{max} is the maximum velocity in the conventional experiments, and $K_{1/2}$ is the mass load at substrate half-saturation.

$$v_0 = \frac{V_{max} \times S_0^{mass}}{K_{1/2} + S_0^{mass}} \quad (1)$$

To analyze the inverse experiments, we expressed the inverse MM equation as eq. 2, where E_0 is the initial enzyme concentration, ${}^{inv}V_{max}$ is the maximum velocity in the inverse experiments, and K_M is the enzyme concentration at enzyme half-saturation.

$$v_0 = \frac{{}^{inv}V_{max} \times E_0}{K_M + E_0} \tag{2}$$

The ${}^{kin}\Gamma_{max}$ was determined using V_{max} (eq. 1) and ${}^{inv}V_{max}$ (eq. 2) by eq. 3 [6].

$$\frac{\frac{{}^{inv}V_{max}}{S_0^{mass}}}{\frac{V_{max}}{E_0}} = {}^{kin}\Gamma_{max} \tag{3}$$

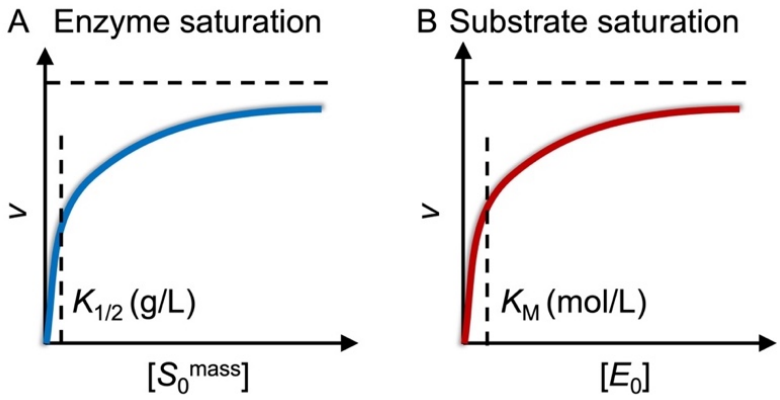

Figure 14. Schematics of the interfacial MM kinetics principle. This figure is inspired by a figure from Kari et al. [264]. (A) Conventional MM kinetic with substrate in excess; (B) Inverse MM kinetic with enzyme in excess.

This approach, combined with Langmuir isotherm binding data, allows calculation of attack site and binding site densities related to different surface structures [6,273,274]. The gained insight sheds light on the amylolytic reaction mechanism for various starch substrates, particularly on assessing whether the reaction is limited by binding or catalysis. This modified approach bridges starch structure and enzyme hydrolytic efficiency in interfacial systems, providing valuable experimental data for biologically relevant situations.

1.7 Essential Materials and Methods

1.7.1 Starches

Waxy maize starch (WMS) was a kind gift of Cargill, USA, normal maize starch (NMS) of Archer Daniels Midland (ADM, Decatur, IL) and high-amylose maize starches G50 and G80 of Penford Australia, Ltd. (Lane Cove, NSW, Australia). High-amylose maize starch AE35 (AE) and high-amylose wheat starch (HWS) were obtained from experimental fields of Northwest A&F University, Yangling, China. Waxy wheat starch (WWS) was generously provided by the Chinese Academy of Sciences, China [275]. Normal wheat starch (NWS) was a kind gift of Lantmännen, Sweden. Normal potato starch (NPS) and high-amylose/high-phosphate potato starch (HPS) were extracted from the cultivar Dianella respectively a dual RNA interference starch branching enzyme I and II line in the Dianella genetic background, as previously described [276,277]. Starch from an RNA interference GBSS line (waxy potato starch, WPS) was a kind gift of Lyckeby Stärkelsen, Sweden. Two varieties of barley, Cinnamon (waxy barley starch; WBS) and Golden Promise (normal barley starch; NBS), were cultivated under normal diurnal (16 h light) or constant light growing conditions in a greenhouse at the University of Copenhagen (Copenhagen, Denmark). Amylose-only barley starch (AOBS) was obtained by gene modification as described [41]. The amylose content and crystalline polymorph were previously determined for the starch granules (Table 4) [276–279].

Table 4. Characteristics of starch granules

Name of starch type	Abbreviation	Amylose content (%)	Crystalline polymorph
Waxy maize starch	WMS	0.7	A-type
Normal maize starch	NMS	20.7	A-type
High-amylose maize starch G50	G50	40.5	B-type
High-amylose maize starch G80	G80	50.5	B-type
High-amylose maize starch AE35	AE	72.2	B-type
Waxy wheat starch	WWS	0.2	A-type
Normal wheat starch	NWS	33.1	A-type
High-amylose wheat starch	HWS	67.4	B-type
Waxy barley starch	WBS	0.3	A-type
Normal barley starch	NBS	27.9	A-type
Amylose-only barley starch	AOBS	97.5	B-type
Waxy potato starch	WPS	1.9	B-type
Normal potato starch	NPS	26.3	B-type
High-amylose potato starch	HPS	35.2	B-type

1.7.2 Commercial Enzymes

Pullulanase M2 from *Bacillus licheniformis* (*Bl*Pul, E-PULBL, 900 U/mL) was purchased from Megazyme Co. Ltd (Wicklow, Ireland). Pancreatin from porcine pancreas (P7545, 8 × USP), α-amylase from human saliva (A1031), amyloglucosidase from *Aspergillus niger* (A7095) were purchased from Sigma-Aldrich Co. Ltd (St. Louis, MO, USA). Branching enzyme from

Rhodothermus obamensis (*Ro*BE, 5.98 U/mg) was a kind gift of Novozymes (Bagsvaerd, Denmark).

1.7.3 Construction, Production, and Purification of Recombinant Enzymes

α-amylase

The α-amylase from *Pseudoalteromonas haloplanktis* TAB23 (AHA, GenBank Accession: CAA41481.1), and SBD-fusions, AHA-SBD_{GA} and AHA-SBD_{GWD3}, were produced recombinantly essentially as described [280]. The fusions contained full length AHA connected C-terminally to the SBD from *Aspergillus niger* glucoamylase or *Arabidopsis thaliana* glucan, water dikinase 3 via a decapeptide linker, TSSASGLTKV. See ***Paper 1*** for details on construction, production, and purification of AHA and AHA-SBD fusions.

TuαGT

The 4αGT from *Thermoproteus uzoniensis* (TuαGT, GenBank Accession: WP_013679179.1), and SBD-fusions, SBD_{St1}-TuαGT, SBD_{St2}-TuαGT, and SBD_{GA}-TuαGT, were produced recombinantly essentially as described [128]. The fusions contained full length TuαGT connected N-terminally to the SBD from *Solanum tuberosum* disproportionating enzyme 2 (*St*DPE2), and the *An*GA via an 18-residues linker, TTGESRFVVLSDGLMREM, which naturally connects the SBD_{St1}–SBD_{St2} tandem with the CD in *St*DPE2. See ***Paper 2*** for details on construction, production, and purification of TuαGT and SBD-TuαGT fusions.

LaPul

The PULI from *Lactobacillus acidophilus* NCFM (*La*Pul, GenBank Accession: AAV43522.1) and two N-terminally truncated forms (Δ41-*La*Pul and Δ41+ND-*La*Pul) were expressed in *Escherichia coli* Rosetta (DE3) and the recombinantly produced proteins were purified essentially as described [82]. See ***Manuscript 1*** for details on construction, production, and purification of *La*Pul and N-terminally truncated forms.

1.7.4 Bioinformatics Analysis

α-amylases

Protein sequences for all α-amylases from different subfamilies of GH13 in the CAZy database [50] were retrieved from NCBI (156 sequences). A multiple sequence alignment of the sequences was generated using the CLC Main Workbench 7 (QIAGEN). Phylogenetic analysis was performed using the maximum likelihood method from the CLC Main Workbench

7. The tree was visualized using the Interactive Tree Of Life (iTOL) online tool (https://itol.embl.de/; [281]).

Type I pullulanases

Protein sequences encompassing all members of GH13_14 within the CAZy database [50] were sourced from NCBI, resulting in a total of 4263 sequences. To mitigate redundancy, CD-HIT [282] was applied with a 90% identity cut-off, which yielded 731 sequences for constructing a preliminary phylogenetic tree (Figure S1 in ***Manuscript 1***). Subsequently, the sequence set was further pruned using a 55% identity cut-off, resulting in 109 sequences, which facilitated creation of a more intricate phylogenetic tree accompanied by domain architectures (See Figure 1 in ***Manuscript 1***). For the alignment of multiple sequence data of CDs, as anticipated by dbCAN3 [283], the CLC Main Workbench 7 from QIAGEN was employed for the maximum likelihood method. The tree visualization was accomplished using the iTOL online tool (https://itol.embl.de/; [281])

CBM20s

Protein sequences for CBM20 domains from 65 different amylolytic and related enzymes in the CAZy database [50] were retrieved from GenBank (https://www.ncbi.nlm.nih.gov/genbank/; [284]) and UniProt (https://www.uniprot.org/; [285]) databases (87 sequences) based on prior investigations focused on GH77 DPE2s and various starch-binding domain CBM families [166,286–289] (See ***Paper 2*** for details about the choice of sequences). A multiple sequence alignment was performed using the program Clustal-Omega (https://www.ebi.ac.uk/Tools/msa/clustalo/; [290]) and the output was used for calculating the maximum-likelihood evolutionary tree by the bootstrapping procedure with 1000 bootstrap trials [291], implemented in the MEGA-X package [292]. The tree was visualized using the iTOL online tool (https://itol.embl.de/; [281]).

1.7.5 Interfacial Kinetics for Starch Granules

Two complementary methods, conventional and inverse MM analyses, were employed to study the enzyme kinetics for hydrolysis of starch granules. In the conventional MM experiments, starch granule samples (135 µL, final substrate concentration in Table 5) were pre-incubated (10 min, 1100 rpm, temperature in Table 5) and then enzyme was added (15 µL, final enzyme concentration Table 5) and incubated (1100 rpm, temperature in Table 5). By contrast, in inverse MM kinetics, a constant starch granule concentration (final substrate concentration in Table 5) was used, and seven different enzyme concentrations (final enzyme concentration in Table 5) were assayed. After 30 min, aliquots were transferred to new tubes and mixed with 20 µL 1.8 M Na_2CO_3 to terminate the reaction. The resulting mixture was

centrifuged (10000 *g*, 5 min), and the concentration of reducing sugar in the supernatant was determined using the PAHBAH method with glucose (0–1000 µM) as the standard [293]. The linear range in MM kinetics was not shown, and data were collected accordingly.

Table 5. Experimental conditions for interfacial kinetics and starch granule adsorption

	Conventional MM		Inverse MM		Langmuir isotherm	
Enzyme	S_0^{mass} (g/L)	E_0 (nM)	S_0^{mass} (g/L)	E_0 (nM)	[S] (g/L)	E_0 (nM)
AHA	25–150	30	25	30–150	15	40–2000
AHA-SBD_{Ga}						40–200
AHA-SBD_{GWDs}						40–2000
*Bl*Pul	15–150	62.5	20	0.3–625		
*La*Pul	15–150	50	20	50–5000	25	50–1500
Δ41-*La*Pul						50–4000
Δ(41+DUFs)-*La*Pul						50–2000

Experiments with substrate in excess were analyzed using the conventional MM equation, eq. 1, where S_0^{mass} is the substrate mass load, V_{max} is the maximum velocity in the conventional experiments, and $K_{1/2}$ is the mass load at substrate half-saturation. Eq.1 was used for non-linear regression analyses of the conventional MM data, and this analysis returned values of V_{max} (in $M \cdot s^{-1}$) and $K_{1/2}$ (in $g \cdot L^{-1}$).

$$v_0 = \frac{V_{max} \times S_0^{mass}}{K_{1/2} + S_0^{mass}} \quad (1)$$

To analyze the inverse experiments, we expressed the inverse MM equation as eq. 2, where where E_0 is the initial enzyme concentration, ${}^{inv}V_{max}$ is the maximum velocity in the inverse experiments, and K_M is the enzyme concentration at enzyme half-saturation. Eq.2 was used for the nonlinear regression analysis of inverse MM data, and this returned the parameters ${}^{inv}V_{max}$ (in $g \cdot L^{-1} \cdot s^{-1}$) and K_M (in M).

$$v_0 = \frac{{}^{inv}V_{max} \times E_0}{K_M + E_0} \quad (2)$$

The ${}^{kin}\Gamma_{max}$ was determined using V_{max} (eq. 1) and ${}^{inv}V_{max}$ (eq. 2) by eq. 3 [6].

$$\frac{\frac{{}^{inv}V_{max}}{S_0^{mass}}}{\frac{V_{max}}{E_0}} = {}^{kin}\Gamma_{max} \quad (3)$$

1.7.6 Adsorption to Starch Granules

The binding capacity of starch granules (25 mg/mL (w/v), 135 µL) was determined under the same conditions as used for the activity assay by adding 15 µL enzyme to seven different final concentrations (final enzyme concentration in Table 5). After 30 min incubation (4 °C, 1100

rpm), the mixtures were centrifuged (10,000 *g*, 5 min) and 100 µL supernatant was added to 100 µL 2.5-fold diluted Protein assay dye reagent (Bio-Rad). The enzyme in solution was quantified from the ratio of absorbance values at 590 over 450 nm using relative enzyme as standards [294]. The results were fitted to the Langmuir isotherm (eq. 4) using GraphPad Prism 6, where K_d is the dissociation constant and ${}^{ads}\Gamma_{max}$ is the (apparent) saturation coverage (density of binding site in this thesis) [6].

$$\Gamma = \frac{{}^{ads}\Gamma_{max} \times E_{free}}{K_d + E_{free}} \quad (4)$$

1.7.7 Chain Length Distribution Analysis

For CLD analysis of the granular starch surface, starch (50 mg/mL, w/v) was resuspended in 50 mM sodium acetate (pH 5.5) and debranched by 50 nM (final concentration) *Bl*Pul (25 °C, 30 min), followed by centrifugation (10000 *g*, 5 min).

For CLD analysis of gelatinized starch, starch (5 mg/mL, w/v) was suspended in 50 mM sodium acetate (pH 5.5), gelatinized (99 °C, 1100 rpm, 30 min) and cooled to 42 °C. The gelatinized starches were debranched by 50 nM (final concentration) *Bl*Pul (42 °C, 2 h) and centrifuged (10000 *g*, 5 min).

The supernatants were analyzed by HPAEC-PAD to determine the CLD as described [295].

1.7.8 Cryo-Scanning Electron Microscopy (cryo-SEM)

For cryo-SEM analysis, a specimen was prepared as follows: An alginate bead was affixed onto a sample holder connected to a transfer rod, which was swiftly frozen by submerging it into slushy liquid nitrogen at a chilling temperature of –210 °C. The frozen sample was then transported to the preparation chamber stage, maintained at –180 °C, using the Quorum PP2000 Cryo Transfer System. Subsequently, the frozen sample was cleaved using a cold knife, which exposed a fractured surface for examination. To facilitate imaging, sublimation was carried out at –80 °C for a duration of 15 min. The sample was subsequently coated with a layer of platinum (Pt) using a current of 4.5 mA for 30 s. Following this preparation, the sample was transferred to the SEM stage in the Field Emission Scanning Electron Microscope (FEI Quanta 200 ESEM FEG) within a vacuum environment. The imaging was conducted at an acceleration voltage of 10 kV, utilizing an Everhart-Thornley detector (ETD). The resulting images were used to analyze the distribution of pores on the bead. This analysis of pore distribution was carried out using ImageJ software, version 1.50b (National Institutes of Health, USA).

Chapter 2: Results

2.1 Impact of Starch Binding Domain Fusions on Interfacial Catalysis and Enzymatic Properties of Starch-Active Enzymes

This chapter is comprised of 2 papers (***Paper 1*** and ***Paper 2***), both concerning the impact of SBDs on enzymatic properties of starch-active enzymes. In this section, it is shown that SBDs play an important role on protein thermostability, product profile, substrate recognition, and interfacial catalysis for the degradation of granular starches.

Paper 1 investigated the effects of SBDs on a psychrophilic α-amylase from the Antarctic bacterium *Pseudoalteromonas haloplanktis* TAB23 (AHA) by fusing two different SBDs of CBM20 from either *Aspergillus niger* glucoamylase (SBD_{GA}) or *Arabidopsis thaliana* glucan, water dikinase 3 (SBD_{GWD3}) to the C-terminus of AHA. The optimum reaction conditions, for activities and kinetics analysis of different soluble and insoluble substrates were studied. Most importantly, we focused on the effects of SBDs on the interfacial catalysis for the degradation of granular starches by AHA and AHA-SBD fusions. The strategy to study the process of interfacial catalysis of granular starches was discussed in section 1.6.4. More details can be also seen in ***Paper 1***. By combining conventional MM kinetics, having substrate in excess, and inverse kinetics, having enzyme in excess, with enzyme-starch granule adsorption isotherms, we found that the AHA-SBD fusions resulted in increased density of enzyme attack sites ($^{kin}\Gamma_{max}$) and binding sites ($^{ads}\Gamma_{max}$) on the starch granules by up to 5- and 7-fold, respectively, compared with AHA. The increase in enzyme attack sites for AHA-SBD fusions compared to AHA alone has resulted in a higher k_{cat} (catalytic turnover rate) for AHA-SBD fusions. This is attributed to the increased availability of authentic substrates (enzyme attack sites) for AHA-SBD fusions to interact with. The increased activity of the AHA-SBD fusions correlated with higher affinity for the starch granules, which suggests adsorption-limited behavior in line with the Sabatier principle.

Different from ***Paper 1*****,** focusing on catalysis of granular starches, ***Paper 2*** was concerned with the impact of fused SBD on the enzyme properties and activity on soluble substrates and starches of a thermophilic 4-α-glucanotransferase from *Thermoproteus uzoniensis* (TuαGT).

Three phylogenetically distinct SBDs from *St*DPE2 and *An*GA were fused individually to the N-terminus of the thermophilic TuαGT using an 18-residue linker. This resulted in altered substrate binding and activity for TuαGT. Bioinformatics revealed that SBD_{St1}, SBD_{St2}, and SBD_{GA} are evolutionarily distant, belonging to unique clusters of related enzymes. The SBD_{St2} fusion enhanced thermostability of TuαGT and doubled its disproportionation activity on amylose. However, all SBD fusions reduced activity for maltotriose. The SBD_{GA} fusion exhibited the highest affinity for starch granules, possibly due to its two binding sites containing

canonical aromatic residues. Structure analysis of starch showed that SBD_{St1} and SBD_{St2} fusions increased hydrolysis and had a significant impact on starch chain alterations by TuαGT compared to SBD_{GA}. The modified starches may offer nutritional benefits similar to resistant starch dietary fibers. Given their evolutionary divergence and varied functional impacts, SBD_{St1} and SBD_{St2} may have unique roles in *St*DPE2 that are yet to be identified.

Notably, we also found that SBD can alter the product profile of the enzymes. This fusing SBDs to AHA lead to release of more glucose during degradation on WMS, whereas AHA alone released mostly maltose and maltotriose. We concluded that the SBD-fusion altered the product profile and possibly the C-terminal SBD orients non-reducing ends of α-glucan chains on WMS towards the active site on the CD of AHA to release the terminal glucose, whereas the AHA alone maintained the endo-action mode (***Paper 1***). By contrast, only minor changes were found between the product profile of TuαGT and the SBD-TuαGT fusions (***Paper 2***).

2.1.1 Paper 1 – Improved Hydrolysis of Granular Starches by a Psychrophilic α-Amylase Starch Binding Domain-Fusion

This paper was accepted for publication in *Journal of Agricultural and Food Chemistry* on the 24th of May 2023. The paper presents results on the effect of SBD-fusion on the interfacial catalysis of different maize starch granules by a psychrophilic α-amylase. The supporting information can be found at the end of the paper. The permission to reuse this article in this PhD thesis was obtained from the publisher.

JOURNAL OF AGRICULTURAL AND FOOD CHEMISTRY

pubs.acs.org/JAFC Article

Improved Hydrolysis of Granular Starches by a Psychrophilic α-Amylase Starch Binding Domain-Fusion

Yu Wang, Yu Tian, Yuyue Zhong, Mohammad Amer Suleiman, Georges Feller, Peter Westh, Andreas Blennow, Marie Sofie Møller,* and Birte Svensson*

Cite This: J. Agric. Food Chem. 2023, 71, 9040−9050 Read Online

ACCESS | Metrics & More | Article Recommendations | Supporting Information

ABSTRACT: Degradation of starch granules by a psychrophilic α-amylase, AHA, from the Antarctic bacterium *Pseudoalteromonas haloplanktis* TAB23 was facilitated by C-terminal fusion to a starch-binding domain (SBD) from either *Aspergillus niger* glucoamylase (SBD_{GA}) or *Arabidopsis thaliana* glucan, water dikinase 3 (SBD_{GWD3}) via a decapeptide linker. Depending on the waxy, normal or high-amylose starch type and the botanical source, the AHA-SBD fusion enzymes showed up to 3 times higher activity than AHA wild-type. The SBD-fusion thus increased the density of enzyme attack-sites and binding-sites on the starch granules by up to 5- and 7-fold, respectively, as measured using an interfacial catalysis approach that combined conventional Michaelis−Menten kinetics, with the substrate in excess, and inverse kinetics, having enzyme in excess, with enzyme-starch granule adsorption isotherms. Higher substrate affinity of the SBD_{GA} compared to SBD_{GWD3} was accompanied by the superior activity of AHA-SBD_{GA} in agreement with the Sabatier principle of adsorption limited heterogenous catalysis.

KEYWORDS: *carbohydrate-binding module, waxy starch, normal starch, high-amylose starch, Pseudoalteromonas haloplanktis α-amylase, heterogenous catalysis, Sabatier principle*

1. INTRODUCTION

Starch is regarded as a sustainable form of energy storage and one of the most abundant components in human food and animal feed. Starch also serves as a constituent of novel biomaterials in biorefineries for production of ethanol as well as other chemical commodities and as part of biomass feedstocks for fuel energy.[1−3] Storage starch is synthesized and deposited in seeds, roots, and tubers as compact supramolecular granules of different shapes and sizes ranging from about 1 μm to more than 100 μm having conspicuous alternating concentric amorphous and crystalline layers.[4,5] Normal starch contains in a ratio of about 1:3 (w:w) the essentially linear α-1,4-linked α-glucan amylose of 250−10^3 kDa and amylopectin of 10^4−10^6 kDa, that has about 5% α-1,6-branch points connecting α-1,4-linked chains.[6]

Starch is hydrolyzed by α-amylases (EC 3.2.1.1) and different enzymes acting on α-1,4 and α-1,6-glucosidic linkages with formation of linear and branched maltooligosaccharides, maltose, and glucose.[7] Heterogeneous enzyme catalysis of starch granule degradation occurs *in planta* during seed germination and to secure night-time respiration in leaves, by starch utilization in animal and human digestive tracts and by microbial attack on plant-biomass.[8,9] In industry, the raw starch is gelatinized at elevated temperatures to disintegrate the granular structure and ease the contact between substrate and catalytic domains (CDs) of amylolytic enzymes.[10] α-Amylases occur widely in bacteria, archaea, plants, and animals,[11] and most belong to glycoside hydrolase family 13 (GH13) as organized in the carbohydrate-active enzymes database, CAZy (http://www.cazy.org/).[12] Enzymes from psychrophilic bacteria hold promise for energy-saving operations on raw starch at moderate temperature,[13] even though conventionally, the microbial α-amylases selected for industrial processes are thermostable and/or active at extreme pH values.[14] Notably, psychrophilic enzymes usually have up to 10-fold higher activity at low and moderate temperatures as compared to their mesophilic homologues.[15] Since enzymes hydrolyse granular starch less efficiently than gelatinized starch,[16] one strategy to enhance degradation efficacy is by increasing the substrate contact such as through fusion of starch binding domains (SBDs) to the CDs by protein engineering.

SBDs are carbohydrate binding modules (CBMs) found in many multimodular enzymes with the ability to bind to and convert α-glucans, including starch granules, soluble polysaccharides, and the starch mimic β-cyclodextrin.[17,18] SBDs are organized in 15 sequence-based CBM families (http://www.cazy.org/),[12] all, except for the larger CBM74, having an immunoglobulin-like fold of about 100 amino acid residues.[18] SBDs can bind onto starch granules with micromolar affinity[19] and were hypothesized to disentangle double helical α-glucan chains, which facilitates reaction with the CD,[18,20,21] as well as to guide the single chains to the active site crevice.[22,23] Engineered α-amylase SBD-fusions in fact imitate natural α-amylases possessing SBDs.[24] In this manner, barley α-amylase was added a C-terminal SBD and obtained 2.3-fold increased

Received: March 24, 2023
Revised: May 23, 2023
Accepted: May 24, 2023
Published: June 2, 2023

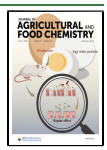

activity on starch granules[25] by enhancing its endogenous affinity controlled by a couple of surface binding sites.[20,26] Different ways to boost α-amylase activity toward starch granules exemplify interfacial catalysis of vital natural processes.[8,9,27]

Earlier studies used the Michaelis−Menten (MM) approach to determine kinetic parameters of α-amylase hydrolysis of granular starch.[28] As for enzymes acting on soluble substrates,[29] MM analysis may be applicable on granular starch when the substrate is in (molar) excess. However, this requirement is not readily assessed for an insoluble substrate that represents an undefined molarity and where only a small and unknown fraction is accessible to the enzyme.[30] To address this situation, we here, motivated by heterogenous catalysis of cellulases acting on cellulose,[31] applied interfacial kinetics analysis to measure the attack site density, ${}^{kin}\Gamma_{max}$, for granules of different starch types. Recently, we used interfacial kinetics to describe the mechanism of the glucoamylase from *Aspergillus niger*, serving as a model for degradation of nutritionally important resistant starch in the gut.[32] The ${}^{kin}\Gamma_{max}$ parameter (in mol/g) enumerates loci on the substrate surface where the enzyme forms a productive complex. As deduced from cellulase−cellulose systems,[33] we anticipated that ${}^{kin}\Gamma_{max}$ depends on the properties of both the enzyme and substrate such as binding strength of enzyme−starch granule complexes, granule surface area, crystallinity, etc. In practice, ${}^{kin}\Gamma_{max}$ provides a conversion factor between the mass load of a solid substrate (which is usually known from experimental data) and an apparent molar concentration of attack sites. This opens for a more stringent kinetic analysis[31,34] as exemplified in Materials and Methods (Section 2.5. Interfacial Kinetics Analysis on Granular Starch).

Enzyme reaction on granular starch is attractive, as it avoids dealing with issues related to high viscosity and instability due to retrogradation of α-glucan chains,[35] and also represents a clean and energy-saving advancement compared to processes using heat-gelatinized starch. Here, one of the best characterized psychrophilic α-amylases, AHA, from the Antarctic bacterium *Pseudoalteromonas haloplanktis* TAB23 having maximum activity at 25 °C,[36−39] is chosen for degradation of starch granules after C-terminal fusion with SBDs of family CBM20 from either *Aspergillus niger* glucoamylase (AHA-SBD_{GA}) or glucan water dikinase 3 (phosphoglucan, water dikinase) (AHA-SBD_{GWD3}) from *Arabidopsis thaliana*.[21,22,40,41] The interfacial kinetic analysis of AHA-SBD_{GA} and AHA-SBD_{GWD3} describes the positive impact by the SBD-fusion on starch granule hydrolysis. This application of the inverse MM approach gave new insights into the heterogeneous catalysis providing a foundation for rational improvement of hydrolysis of starch granules from different crops and of different types by α-amylases.

2. MATERIALS AND METHODS

2.1. Substrates. Amylose, amylopectin, and soluble starch (all from potato), oyster glycogen, and α-, β-, and γ-cyclodextrins were purchased from Sigma-Aldrich Co., Ltd. (St. Louis, MO, USA). Normal potato starch (NPS) and high-amylose/high-phosphate potato starch (HPPS) were extracted from the cultivar Dianella, a dual RNA interference starch branching enzyme I and II line in the Dianella genetic background, respectively, as previously described.[42,43] Starch from an RNA interference GBSS line (waxy potato starch, WPS) was a kind gift of Lyckeby Stärkelsen, Sweden. Normal wheat starch (NWS) was generously provided by Lantmännen, Sweden. Waxy maize starch (WMS) was a kind gift of Cargill, USA, normal maize starch (NMS) of Archer Daniels Midland (ADM, Decatur, IL), and high-amylose maize starches G50 and G80 of Penford Australia, Ltd. (Lane Cove, NSW, Australia). The high-amylose maize starch AE 35 was obtained from experimental fields of Northwest A&F University, Yangling, China. The amylose content and crystalline polymorph were previously determined of the starch granules (Table 1).[42−45]

Table 1. Characteristics of Starch Granules

name of starch type	abbreviation	amylose content (%)	crystalline polymorph
waxy maize starch	WMS	0.7	A-type
normal maize starch	NMS	20.7	A-type
Australia G50	G50	40.5	B-type
Australia G80	G80	50.5	B-type
AE 35 maize starch	AE	72.2	B-type
normal potato starch	NPS	26.3	B-type
high-amylose/high-phosphate potato starch	HPPS	35.2	B-type
waxy potato starch	WPS	1.9	B-type
normal wheat starch	NWS	33.1	A-type

2.2. Construction, Production, and Purification of AHA and AHA-SBD Fusions. The AHA α-amylase from *Pseudoalteromonas haloplanktis* TAB23 (GenBank Accession CAA41481.1), AHA-SBD_{GA} and AHA-SBD_{GWD3} were produced recombinantly essentially as described.[46] The fusions contained full length AHA connected C-terminally to the SBD via a decapeptide linker, TSSASGLTKV (see Supporting Information for details on construction, production, and purification). Protein concentrations were determined spectrophotometrically at 280 nm (Nanodrop Lite, Thermo Scientific, USA) using predicted molar extinction coefficients (ε) of 94,310, 125,250, and 123,300 M^{-1} cm^{-1} for AHA, AHA-SBD_{GA}, and AHA-SBD_{GWD3} having theoretical molecular masses of 49,343.1, 61,703.7, and 61,231.5 Da, respectively (https://web.expasy.org/protparam/). The purity of AHA, AHA-SBD_{GA}, and AHA-SBD_{GWD3} was verified by SDS-PAGE.

2.3. Activity Assays. Amylose (40 mg) in 1 mL MilliQ water was dissolved by adding 1 mL of 2 M NaOH and neutralized before use by 1:1 (v:v) 1 M HCl. For the standard activity assay, 100 μL of enzyme (20 nM, final concentration) acted on 1 mg/mL amylose in 900 μL of assay buffer: 100 mM Hepes, 50 mM NaCl, 10 mM $MgCl_2$, pH 7.1 (25 °C, 300 rpm, 30 min). The reaction was stopped by the addition of DNS reagent (1:1 (v:v)) and heated (95 °C, 5 min), as previously described.[47] After cooling, absorbance was measured at 520 nm using a microplate reader (PowerWave XS, BIO-TEK). One unit of activity was defined as the amount of enzyme releasing 1 μmol/s, reducing sugar under the above conditions using glucose (0−5 mM) for the standard curve. The pH activity dependence was determined at the optimum temperature 25 °C using the standard assay in universal buffer,[48] 20 mM MES, 20 mM Hepes, 150 mM NaCl, pH 4.0−10.0. Temperature activity dependence was determined at the optimum pH 7.0 in the above buffer.

The specific activity of 20 nM enzyme was determined toward 1 mg/mL (w:v) amylose, amylopectin, glycogen, soluble starch, and α-, β-, and γ-cyclodextrins as described above. Soluble starch (1 mg/mL) and amylopectin (1 mg/mL) were gelatinized (75 °C, 30 min, 1100 rpm) and cooled to 25 °C before the assay. Kinetic parameters were determined at six concentrations of amylose (0.625−2.5 mg/mL, 1 mL assay volume) for 20 nM enzyme (final concentration) in assay buffer (25 °C, 300 rpm). Aliquots (100 μL) were removed at 1, 2, 5, 10, and 15 min, mixed with DNS reagent (100 μL), heated (95 °C, 5 min), and cooled, and the absorbance was measured at 520 nm as above. V_{max}, K_M, and k_{cat} were calculated by fitting of the MM equation to initial rates of product formation and substrate concentrations (GraphPad Prism 6, GraphPad Software Inc).

2.4. Activity on Starch Granules. Granules of NPS, WPS, HPPS, NMS, WMS, AE, and NWS (25 mg/mL (w/v), 1 mL) were washed twice with MilliQ water and once with assay buffer. Enzyme

https://doi.org/10.1021/acs.jafc.3c01898
J. Agric. Food Chem. 2023, 71, 9040−9050

(100 μL, 20 nM final concentration) was added to granule samples and incubated (25 °C, 24 h, 1100 rpm), and the reaction was stopped by 200 μL of 1.8 M Na_2CO_3 followed by centrifugation (10,000g, 5 min). Reducing sugar in the supernatant was determined using the DNS assay as described above. One unit of activity was defined as the amount of enzyme releasing 1 nmol/s reducing sugar under the above conditions and with glucose as standard. Products released by 20 nM AHA, AHA-SBD_{GA}, and AHA-SBD_{GWD3} from WMS (25 mg/mL (w:v)) after 30 min (25 °C, 1100 rpm) were analyzed by thin layer chromatography (TLC Silica gel 60 (Merck, USA); mobile phase, 1-butanol: ethanol: MilliQ water = 5:5:3). Released glucose was quantified using the GOPOD assay (D-glucose assay kit, Megazyme) with glucose as standard.[49]

2.5. Interfacial Kinetics Analysis on Granular Starch. The kinetics on the insoluble substrates were studied by two complementary methods denoted as conventional and inverse MM analyses. In conventional MM, the initial rates are measured in a series of experiments with a fixed, low enzyme concentration and gradually increasing substrate loads. This is the usual MM framework, and saturation implies that all enzyme is engaged in a substrate complex. In the inverse approach, using a constant, low substrate load initial rates were measured for gradually increasing enzyme concentrations. In this case, saturation indicated that all available attack sites on the substrate surface are in complex with enzyme. We applied these two kinetic approaches to five types of maize starch granules of WMS, NMS, and three high-amylose maize starches (G50, G80, AE) with varying amylose contents and crystalline polymorphs (Table 1). In conventional MM experiments, starch granules at six different loads (25−150 mg/mL (w/v), 135 μL) were preincubated (10 °C, 15 min, 1100 rpm), added enzyme (15 μL, final concentration 30 nM), and incubated (10 °C, 1100 rpm). For inverse MM kinetics, 135 μL of starch granules (25 mg/mL (w/v)) was added enzyme (15 μL) to six final concentrations (30−150 nM) and incubated (10 °C, 1100 rpm). After 30 min (within a linear reaction range according to MM kinetics, data not shown), aliquots (100 μL) were transferred to new tubes, mixed with 20 μL of 1.8 M Na_2CO_3 to terminate the reaction, and centrifuged (10,000 g, 5 min). The concentration of reducing sugar in the supernatant was determined using the DNS assay with glucose as standard.

The overall output of these measurements was 30 saturation curves: 15 conventional MM curves with the initial rates vs substrate load and 15 inverse curves with initial rates vs enzyme concentration. These plots were analyzed by nonlinear regression (GraphPad Prism 6, GraphPad Software Inc) against the conventional (eq 1) and inverse (eq 2) MM equations. Different aspects of the application of these equations to solid substrates have been discussed in more detail elsewhere,[31,34,50] and here, we briefly reiterate pertinent facets. The approach rests on the claim that a steady-state description of enzyme reactions with a solid substrate requires three kinetic parameters. Two of them are k_{cat} (in s^{-1}) and K_M (in M), while the third is the attack site density, ${}^{kin}\Gamma_{max}$ (in mol/g).

Experiments with substrate excess can be analyzed by the conventional MM equation, eq 1, where S_0^{mass} is the substrate mass load and $K_{1/2}$ is the mass load at substrate half-saturation. Equation 1 was used for nonlinear regression analyses of the data, and this analysis returned values of $k_{cat}{\cdot}E_0$ (in M·s^{-1}) and $K_{1/2}$ (in g·L^{-1}).

$$v_0 = \frac{k_{cat} \times E_0 \times S_0^{mass}}{K_{1/2} + S_0^{mass}} \quad (1)$$

Since ${}^{kin}\Gamma_{max}$ specifies the number of attack sites (mole) per gram substrate, a conversion of $K_{1/2}$ to K_M in molar units was conducted using eq 5. In eq 5, K_M is the molar concentration of attack sites that gives half-saturation in conventional experiments, but due to the symmetry of E and S in the reaction scheme and the fact that one enzyme only occupies one attack site, this value is the same at the molar concentration of enzyme that gives half saturation in the inverse experiments.[31]

$$K_M = K_{1/2} \times {}^{kin}\Gamma_{max} \quad (2)$$

To analyze the inverse experiments, we expressed the inverse MM equation as eq 2, which was used in the nonlinear regression analysis of inverse MM data giving the parameters K_M (in M) and ${}^{inv}k_{cat} \times S_0^{mass}$ (in g·L^{-1}·s^{-1}).

$$v_0 = \frac{{}^{inv}k_{cat} \times E_0 \times S_0^{mass}}{K_M + E_0} \quad (3)$$

This returned k_{cat} (from conventional MM) and K_M (from inverse MM), but the analysis also opens a way to find the attack site density. Thus, as both $K_{1/2}$ in eq 1 and K_M in eq 2 were calculated, the ${}^{kin}\Gamma_{max}$ could be determined as the ratio of these parameters, ${}^{kin}\Gamma_{max} = K_M/K_{1/2}$. Analogous arguments have shown that ${}^{kin}\Gamma_{max}$ can also be derived from the ratio of the two maximal specific rates.[31]

It was concluded that the combined use of conventional and inverse kinetic analyses allowed a stringent kinetic description with three kinetic parameters k_{cat}, $K_{1/2}$, and ${}^{kin}\Gamma_{max}$. We will use these parameters for comparative analyses of the three AHA forms with particular focus on the functional roles of the SBD-fusions.

2.6. Adsorption to Starch Granules. The enzyme binding capacity of starch granules (25 mg/mL (w:v), 135 μL) was determined under the same conditions as used for the activity assay by adding 15 μL of enzyme to seven different final concentrations in the range of 10−100 nM. After 10 min of incubation (10 °C, 1100 rpm), the mixtures were centrifuged (10,000 g, 5 min) and 100 μL supernatant was added to 100 μL 2.5-fold diluted protein assay dye reagent (Bio-Rad). The enzyme in solution was quantified from the ratio of absorbance values at 590 over 450 nm[51] using AHA, AHA-SBD_{GA}, and AHA-SBD_{GWD3} (0−2.0 μM) as standards. The results were fitted with the Langmuir isotherm (eq 3) using GraphPad Prism 6 (GraphPad Software Inc), where K_d is the dissociation constant and ${}^{ads}\Gamma_{max}$ is the (apparent) saturation coverage.[31]

$$\Gamma = \frac{{}^{ads}\Gamma_{max} \times E_{free}}{K_d + E_{free}} \quad (4)$$

2.7. Homology Modeling. SWISS-MODEL (https://swissmodel.expasy.org/) was used for homology modeling. *A. niger* SBD_{GA} (PDB: 1AC0) was used as template to generate an SBD_{GWD3} homology model. The GGQ domain of YaeJ protein from *Escherichia coli* (PDB: 2RTX) was used as a template to obtain a homology model for the TSSASGLTKV linker.

2.8. Statistical Analysis. Interfacial kinetics was analyzed in duplicate and all other experiments in triplicate. The statistical significance was assessed with one-way analysis of variance (ANOVA) using SPSS 20.0 (SPSS Inc., Chicago, USA). p values of <0.05 were considered statistically significant throughout the study.

3. RESULTS

3.1. Selection of α-Amylase and SBD Fusions. Different amylolytic enzymes of which α-amylases are the most prominent in catalyzing the hydrolysis of α-1,4-glucosidic linkages in the starch α-glucans (amylose and amylopectin), glycogen, and related oligosaccharides. α-Amylases are organized in four glycoside hydrolase (GH) families, GH13, GH57, GH119, and GH126 in the CAZy database of carbohydrate-active enzymes (http://www.cazy.org/).[11,12] GH13, by far the largest family, is divided into 46 subfamilies harboring about 30 different specificities.[52] α-Amylases are found in 16 subfamilies (GH13_1, 5, 6, 7, 10, 15, 19, 21, 24, 27, 28, 32, 36, 37, 43, 45)[12] as shown in a phylogenetic tree (Figure 1). Fungal α-amylases, e.g., from *Aspergillus niger* are found in subfamily GH13_1; bacterial liquefying and saccharifying α-amylases also used industrially are in GH13_5 and GH13_28. Plant α-amylases belong to GH13_6; mammalian digestive and animal α-amylases belong to GH13_15 and GH13_24.[12,53] Notably, AHA from *Pseudoalteromonas haloplanktis* TAB23 and other Arctic and Antarctic bacterial cold-adapted α-amylases, which

https://doi.org/10.1021/acs.jafc.3c01898
J. Agric. Food Chem. 2023, 71, 9040−9050

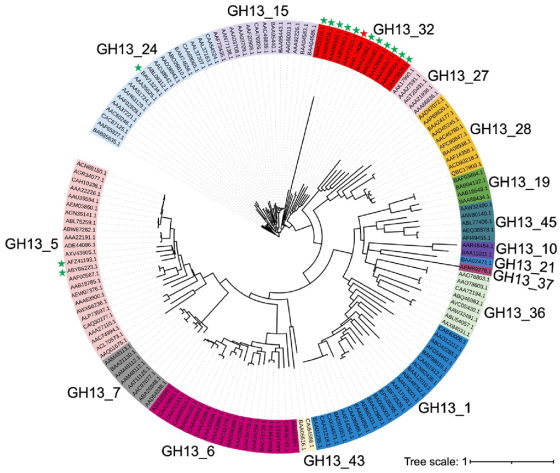

Figure 1. Phylogenetic tree of characterized α-amylases in glycoside hydrolase (GH) family 13 subfamilies.[12,46] The origins are fungi and yeasts, GH 13_1; bacteria, GH 13_5, GH13_19, GH13_21, GH13_27, GH13_28, GH13_32, GH13_36, GH13_37, GH13_43, and GH13_45; plants, GH13_6; archaea, GH13_7, GH13_10; insects, GH13_15; mammals and other animals, GH13_24. AHA from *Pseudoalteromonas haloplanktis* TAB23 (red asterisk) and other psychrophilic bacterial enzymes (green asterisks) are marked. Gene sequences and accession numbers were obtained from the NCBI database (https://www.ncbi.nlm.nih.gov/).

receive attention for starch conversion in energy-saving processes,[54] group in GH13_32, although some are found in GH13_5 and GH13_24 (asterisks in Figure 1). Psychrophilic enzymes of GH13_32 are suitable for hydrolytic degradation of granular starches with optimum activity at 10−50 °C (Table S1), compared to typical starch gelatinization performed at 60−90 °C. We selected the well-characterized AHA[55] for SBD-fusion and analysis of heterogenous catalysis of starch granules. AHA has attractive pH and temperature activity optima of pH 7.0 and 25 °C and excellent stability at 25 °C (Figure S1).[38,39]

Two SBDs of CBM20 with different affinities for the starch mimic β-cyclodextrin were C-terminally fused to AHA (Figure 2).[40,41,46] SBD_{GA} from *A. niger* glucoamylase, widely used in industrial production of glucose syrups from starch, has been described in great detail,[21,56] while the SBD_{GWD3} from *Arabidopsis thaliana* glucan, water dikinase 3, is involved in starch granule mobilization *in planta*.[41,43] We used the decapeptide linker, TSSASGLTKV, which was found suitable for fusing a marine α-amylase of GH13_37 (AmyP) from *Cryptococcus* sp. S-2 to an SBD of CBM69.[57,58]

The SBD-fusions and wild type AHA were produced in 0.15−0.25 mg yields per 5 g *E. coli* cells. AHA, AHA-SBD_{GA}, and AHA-SBD_{GWD3} migrated in SDS-PAGE as single protein bands estimated to 49, 61, and 61 kDa, respectively, in agreement with the theoretical molecular masses (Figure S2). Both starch binding sites on the SBDs appear to be exposed in the multimodular AHA-SBD architectures (Figure 2A,B). Superposition of SBD_{GA} and SBD_{GWD3} showed that tryptophan residues at SBD_{GWD3} putative starch binding sites 1 (W48) and 2 (W35 and W75) (GWD3 numbering; PDB: 1AC0 as template) co-localize with tryptophans in SBD_{GA} binding sites 1 (W543 and W590) and 2 (W563) (PDB: 1AC0) (Figure 2A,C−E).

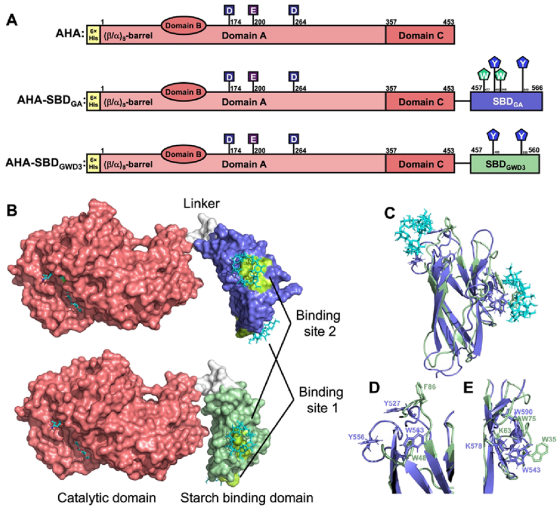

Figure 2. Domain architecture of AHA, AHA-SBD_{GA}, and AHA-SBD_{GWD3}. (A) Schematics including the three catalytic acids Asp174, Glu200, and Asp264 (squares)[38] and identified, predicted aromatic residues at binding sites on SBD_{GA}[40] and SBD_{GWD3} (pentagons).[41] (B) Surface representation of 3D models of AHA-SBD_{GA} and AHA-SBD_{GWD3}. AHA (red) with the inhibitor acarbose (light blue sticks) bound at the active site (PDB: 1AQH), SBD_{GA} (blue; PDB: 1 AC0), SBD_{GWD3} model (green; PDB: 1 AC0 as template), and the decapeptide linker (TSSASGLTKV) model (white: PDB: 2RTX as template). (C) Superposition of SBD_{GA} (blue; PDB: 1 AC0) in complex with β-cyclodextrin (cyan) and the modeled SBD_{GWD3} (green; PDB: 1 AC0 as template). Close-up of superposition of SBD_{GA} and SBD_{GWD3} showing aromatic residues at (D) binding site 1 and (E) binding site 2.

3.2. Activity and Kinetics on Soluble Substrates.

Fusion with the SBDs reduced the activity of AHA on amylose by 16−20%, whereas AHA wild type and the SBD-fusions all showed the same 2−5-fold lower activities on amylopectin, glycogen, and soluble starch (Table 2). The starch mimics α-, β-, and γ-cyclodextrins were poor substrates showing 1−2% of the activity level on amylose (Table 2).

The kinetic parameters K_M and k_{cat} on amylose were very similar for the three AHA forms (Table 3). Thus, AHA-SBD_{GA} displayed slightly higher k_{cat} and K_M than AHA, while k_{cat} was the same and K_M 1.5-fold higher for AHA-SBD_{GWD3} compared to AHA. Overall, the SBD-fusion seemed neither to improve

Table 2. Specific Activity of AHA, AHA-SBD_{GA}, and AHA-SBD_{GWD3} toward Soluble α-Glucans and Cyclodextrins at 25 °C and pH 7.1

substrate[a]	AHA	AHA-SBD_{GA}	AHA-SBD_{GWD3}
amylose	247 ± 32[b] (100[c])	199 ± 8 (80.6)	207 ± 5 (83.8)
amylopectin	75 ± 5 (30.4)	69 ± 9 (27.9)	73 ± 2 (29.6)
soluble starch	90 ± 6 (36.4)	90 ± 1 (36.4)	92 ± 2 (37.2)
glycogen	47 ± 12 (19.0)	45 ± 4 (18.2)	41 ± 1 (16.6)
α-cyclodextrin	4 ± 0.04 (1.6)	4 ± 1 (1.6)	2 ± 1 (0.8)
β-cyclodextrin	3 ± 1 (1.2)	2 ± 0.3 (0.8)	2 ± 0.2 (0.9)
γ-cyclodextrin	4 ± 0.04 (1.6)	1 ± 1 (0.4)	3 ± 0.4 (1.2)

[a]Substrates are described in Materials and Methods (Section 2.1.). [b]Specific activity (μmol/s)/μmol protein. [c]The percentage of the specific activity of AHA on amylose (100%) is given in parenthesis.

https://doi.org/10.1021/acs.jafc.3c01898
J. Agric. Food Chem. 2023, 71, 9040−9050

Table 3. Kinetic Parameters of AHA, AHA-SBD$_{GA}$, and AHA-SBD$_{GWD3}$ towards Amylose at 25 °C and pH 7.1

	AHA	AHA-SBD$_{GA}$	AHA-SBD$_{GWD3}$
K_M (mg/L)	145 ± 21	190 ± 13	217 ± 52
k_{cat} (s^{-1})	2310 ± 81	2939 ± 64	2432 ± 319
k_{cat}/K_M (L·[mg·s]$^{-1}$)	16 ± 2	16 ± 0.1	11 ± 1

nor hamper the action of AHA on soluble substrates (Tables 2 and 3).

3.3. Activity on Starch Granules. The α-amylase activity on starch granules varied by two orders of magnitude with the starch types and botanical sources. The SBDs actually contributed specificity differences; thus, AHA wild type was most active on waxy maize starch (WMS) and the SBD-fusions on normal maize starch (NMS) granules (Table 4). Moreover,

Table 4. Specific Activity of AHA, AHA-SBD$_{GA}$, and AHA-SBD$_{GWD3}$ toward Different Starch Granules at 25 °C and pH 7.1

substrate[a]	AHA	AHA-SBD$_{GA}$	AHA-SBD$_{GWD3}$
NWS	398 ± 19[b] (100[c])	754 ± 10 (189.4)	629 ± 9 (158.0)
WPS	16 ± 4 (4.0)	15 ± 8 (3.8)	19 ± 9 (4.8)
NPS	10 ± 3 (2.5)	19 ± 6 (4.8)	13 ± 3 (3.3)
HPPS	4 ± 1 (1.0)	7 ± 5 (1.8)	9 ± 2 (2.3)
WMS	462 ± 5 (116.1)	589 ± 51 (148.0)	535 ± 31 (134.4)
NMS	83 ± 6 (20.9)	148 ± 44 (37.2)	135 ± 16 (33.9)
AE	9 ± 7 (2.3)	29 ± 7 (7.3)	11 ± 4 (2.8)

[a]Substrates are described in Materials and Methods (Section 2.1). [b]Specific activity (nmol/s)/μmol protein. [c]Percentage of the specific activity of AHA on NWS (100%) is given in parenthesis.

AHA-SBD$_{GA}$ and AHA-SBD$_{GWD3}$ were 1.6−1.9-fold more active on NMS and normal wheat starch (NWS) and 1.2−1.3-fold more active on WMS granules than AHA (Table 4). Although, specific activity of AHA toward granules of waxy, normal, and high amylose potato starch (WPS, NPS and HPPS) and high amylose maize starch (AE) was only 0.9−3.3% of the activity for WMS, still, among these four notoriously poor substrates, AHA-SBD$_{GWD3}$ doubled activity for HPPS and AHA-SBD$_{GA}$ tripled activity for AE compared to AHA (Table 4). Notably, the activity decreased dramatically with increasing amylose content of the maize starch granules (Tables 1 and 4).

Distinct features of the two CBM20 domains and the substrates are assumed to cause the relatively better improvement for AHA-SBD$_{GWD3}$ toward WPS, NPS, and HPPS and for AHA-SBD$_{GA}$ toward WMS, NMS, and AE (Table 4). Although it is well-known that starch granules are recalcitrant for α-amylolytic hydrolysis, the highest activity of AHA, which was further increased by the SBD-fusions, was on the waxy starch (WMS, WPS) granules, despite its activity on soluble amylopectin being only 30% of the activity toward soluble amylose (Table 2). Clearly, diversity in structural features of the different starch granules seems to determine recognition and susceptibility to hydrolysis for the AHA forms and the various activity differences are proposed to be associated with granular morphologies and microstructures.[59] WMS and NMS are of the A-type, while AE is of B-type crystalline polymorph (Table 1).[45] In addition, the surface of the amylose-rich AE granules is smooth, whereas the amylopectin-rich WMS and NMS granules have more wrinkles on the surface.[60] Wrinkled surfaces are speculated to possess more enzyme attack sites, as also supported by the attack site density parameter we established by interfacial kinetics analysis (see Section 3.5.). Notably, the AHA-SBD$_{GA}$ and AHA-SBD$_{GWD3}$ released large amounts of 1854 ± 28 and 986 ± 64 μM glucose, respectively, during 30 min of reaction on WMS, whereas AHA released mostly maltose and maltotriose and only 218 ± 30 μM glucose (Figure S3A). Thus, the SBD-fusion altered the product profile and possibly the C-terminal SBD orients nonreducing ends of α-glucan chains on WMS toward the active site on the AHA CD, leading to the release of terminal glucose residues, whereas the AHA wild type maintained the endo-action mode (Figure S3B,C). Previously, preference for phosphorylating shorter chains was observed for potato glucan water, dikinase 1 (GWD1) after truncation of the natural SBD of family CBM45, indicating that the SBD supported interaction of longer chains with the enzyme CD, in turn influencing the substrate specificity.[61]

3.4. Adsorption to Starch Granules. SBD-fusion to AHA conferred increased binding to granular maize starches, illustrated by 3−7-fold higher binding site density ($^{ads}\Gamma_{max}$) depending on the starch type (Figure 3 and Table 1). For example, binding site density on WMS was 4.0- and 2.7-fold higher for AHA-SBD$_{GA}$ and AHA-SBD$_{GWD3}$ than for AHA (Figure 3B) and the affinity ($1/K_d$) increased by 16- and 2.3-fold for AHA-SBD$_{GA}$ and AHA-SBD$_{GWD3}$ (Figure 3D), a trend agreeing with K_d-values of 7.5 and 380 μM for β-cyclodextrin binding to SBD$_{GA}$ and SBD$_{GWD3}$, respectively.[41] This 50-fold difference indicated from binding to the SBDs alone rather than the 7-fold difference in K_d between AHA-SBD$_{GWD3}$ and AHA-SBD$_{GA}$ probably reflects distinct structural binding motifs of β-cyclodextrin and the starch granule surface and rigidity constraints contributed by the short decapeptide linker (Figure 3D).

For protein fusions, intuitively, a flexible linker would allow substantial inter-domain dynamics having impact on functionality, binding, and orientation preferences. However, barley α-amylase AMY1 fused C-terminally to SBD$_{GA}$ via a long natural linker (37 residues) from *A. niger* glucoamylase had just 5-fold higher affinity for barley starch granules than AMY1 itself.[25] In that light, the overall 7.6−16-fold decreases in K_d for starch granules obtained by AHA-SBD$_{GA}$ are substantial (Figure 3).

3.5. Interfacial Kinetics of Granular Starch Hydrolysis. Initially, the heterogeneous catalysis by AHA-SBD$_{GA}$ of the WMS, NMS, and AE granular starches was analyzed at the temperature optimum of the enzyme of 25 °C (Figure S1A). Here, we introduced $K_{1/2}$ as the mass load at substrate half-saturation and K_M as the molar concentration of enzyme that gives half-saturation in inverse MM experiments (for a detailed explanation, see Materials and Methods, Section 2.5. Interfacial Kinetics Analysis on Granular Starch). This analysis of conventional and inverse MM kinetics gave the highest $k_{cat}/K_{1/2}$ of AHA-SBD$_{GA}$ toward WMS, followed by NMS and AE (Table S2). WMS also contained the highest attack site density of 0.80 followed by 0.64 and 0.27 nmol/g for NMS and AE, respectively. The superior substrate accessibility on WMS, may explain the faster degradation of this substrate (Figure S4 and Table S2). However, most of the experiments at 25 °C did not approach enzyme saturation, hence, only allowing for specificity constants ($k_{cat}/K_{1/2}$) and not k_{cat} and $K_{1/2}$ to be extracted (Figure S4 and Table S2). To address this weakness, the same kinetic experiments were conducted at 10 °C, where the three AHA forms displayed 70−80% of their respective

https://doi.org/10.1021/acs.jafc.3c01898
J. Agric. Food Chem. 2023, 71, 9040−9050

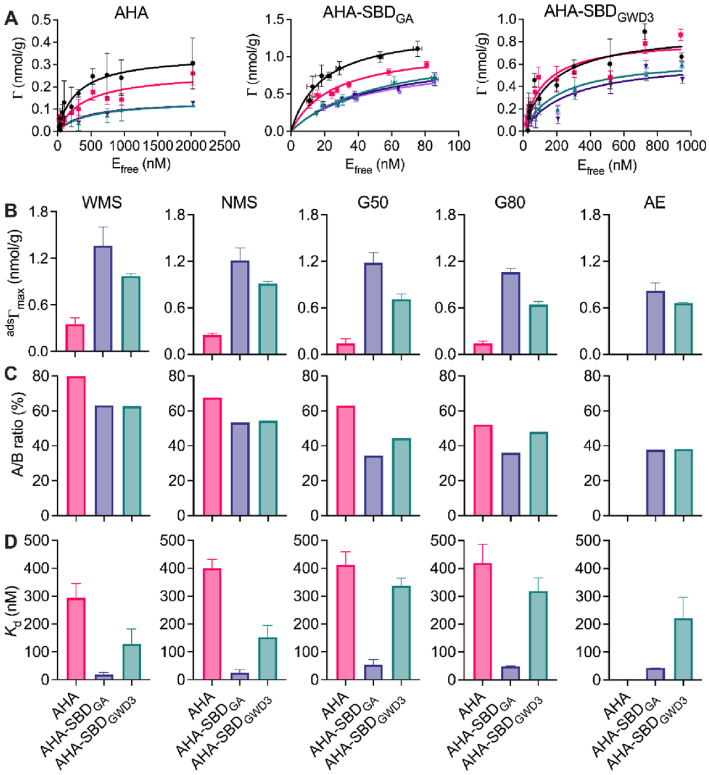

Figure 3. Adsorption to different granular maize starches by AHA wild type and SBD-fusions at 10 °C and pH 7.1. (A) Binding isotherms for AHA, AHA-SBD_{GA}, and AHA-SBD_{GWD3}. Lines represent best fits of the Langmuir equation (eq 3) for the starches (see Table 1) WMS, black; NMS, red; G50, green; G80, dark purple; AE, light purple (AHA was not analyzed on AE starch). Parameters for AHA (red), AHA-SBD_{GA} (purple), and AHA-SBD_{GWD3} (green) with the different starches (B) $^{ads}\Gamma_{max}$ (binding site density). (C) Attack site density/binding density site (A/B ratio; see also section 3.5). (D) K_d.

maximum activities at 25 °C (Figure S1A). Now, $K_{1/2}$ and K_M were consistently lower and in practice; this meant that we could get data to support linear regression of eqs 1 and 2. The MM curves from both conventional and inverse kinetics and the derived kinetic parameters (Figure 4A,B and Table S3) demonstrated all $K_{1/2}$ and K_M values to be within the used concentration range of the WMS granules, while it was reduced by 4−5-fold for the value of NMS and even more reduced for the high amylose starches, i.e., 8−11-fold for G50 and G80, and 12−15-fold for AE (AE was not analyzed for AHA wild type because the experiment did not approach enzyme saturation) (Figure 4E and Table S3).

The inverse kinetics experiments were conducted to determine and compare the number of attack sites ($^{kin}\Gamma_{max}$) on the granules (Figure 4F and Table S3). Different, albeit consistent, trends were observed both regarding the influence of the SBD-fusion and the type of substrate. For the effects of the different substrates, several properties followed the sequence WMS > NMS > G50 > G80. This decrease tendency was found for both binding ($^{ads}\Gamma_{max}$) and attack ($^{kin}\Gamma_{max}$) site densities, and we therefore conclude that accessibility of susceptible bonds is much higher in WMS than for the more amylose-rich substrates G50 and G80.

The difference between the substrates fell in the range from 1.5- to 4-fold higher accessibility for WMS compared to G80. We did not detect any clear effect of the SBD type on this trend. In other words, the lower accessibility associated with more amylose-rich granular starches was not offset by the SBD. Also for glucoamylase from *A. niger*, Tian et al. noted a similar effect of decreasing accessibility with increasing amylose content.[32] The higher accessibility found for WMS is in line with the rapid degradation of this substrate in the activity measurements (Table 4). However, the kinetic data (Figure 4C and Table S3) revealed that WMS is also characterized by a faster turnover rate. Hence, k_{cat} decreased gradually for all three AHA forms with increasing amylose content and was typically an order of magnitude higher on WMS compared to G80 starch. It follows that the rapid degradation of WMS (Table 4) relies on additive effects of accessibility and turnover. It is of interest to consider the densities of binding and attack sites through the series of the five maize substrates. Thus, the enzyme obviously needs to be in an adsorbed state to form a productive complex, but not all adsorbed enzyme molecules seem capable of attack. If there is a population of adsorbed but catalytically unproductive enzyme, we would expect that $^{ads}\Gamma_{max} > {}^{kin}\Gamma_{max}$ as also illustrated by the A/B ratio (Figure 3C). Inspection of the data (Figure 3C and Table S3) revealed that this is consistently the case, and we conclude that a fraction of the adsorbed enzymes is catalytically unproductive for all investigated systems. However, this fraction is not large. Thus, on WMS, the productive population ranges from about three quarters for AHA wild type to two thirds for the AHA-

https://doi.org/10.1021/acs.jafc.3c01898
J. Agric. Food Chem. 2023, 71, 9040−9050

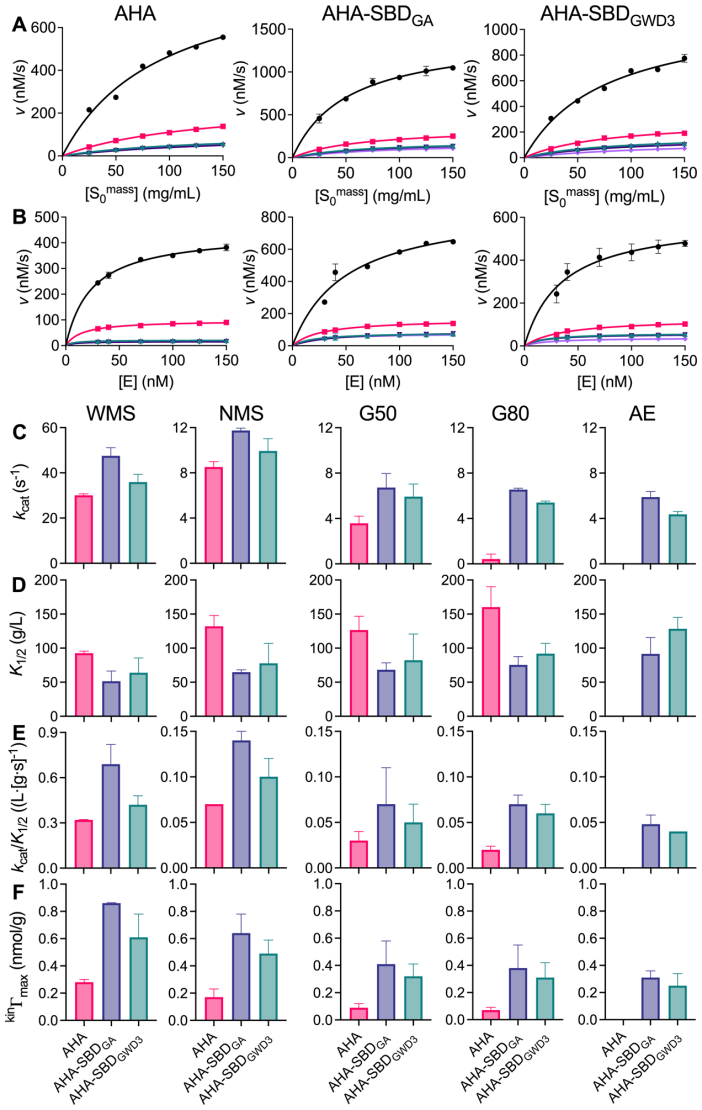

Figure 4. Interfacial catalysis of granular starches by AHA wild type and SBD fusions at 10 °C and pH 7.1. (A) Conventional and (B) inverse kinetics for AHA, AHA-SBD$_{GA}$, and AHA-SBD$_{GWD3}$ on WMS (black), NMS (red), G50 (green), G80 (dark purple), and AE (light purple). Lines represent best fits of the Michaelis−Menten kinetics. (C) k_{cat}, (D) $K_{1/2}$, (E) $k_{cat}/K_{1/2}$, and (F) $^{kin}\Gamma_{max}$ for AHA (red), AHA-SBD$_{GA}$ (purple), and AHA-SBD$_{GWD3}$ (green) for the different granular starches. AHA was not analyzed with AE starch.

SBD enzymes. Interestingly, the productive population was lower on the high amylose substrates and fell between one third and half on G80. This observation implies that less accessible substrates, such as G50 and G80, challenge reactivity by both lower accessibility and a larger fraction of unproductively adsorbed enzyme.

3.6. Application of the Sabatier Principle in Starch Granule Degradation. According to the Sabatier principle, optimal catalysis occurs when the interactions between the catalyst and substrate are of intermediary strength.[34] To study the relationship between binding strength and turnover number, a relative standard free energy of enzyme−substrate binding ($\Delta\Delta G^{\circ}$) was calculated according to eq 4, where $K_{1/2,i}$ is the Michaelis constant for the enzyme in question and $K_{1/2,ref}$ is the value for a reference,[34] here chosen as the $K_{1/2}$ for AHA-SBD$_{GA}$ acting on different starches.

$$\Delta\Delta G^{\circ} = RT\ln\left(\frac{K_{1/2,i}}{K_{1/2,ref}}\right) \quad (5)$$

The relationship between k_{cat}, $^{inv}k_{cat}$, and $\Delta\Delta G^{\circ}$ using different enzymes and substrates (Figure 5 and Figure S5) for all fits showed that k_{cat} was negatively correlated with $\Delta\Delta G^{\circ}$, which means that the degradations of the starch granules by AHA and its SBD-fusions were adsorption-limited reactions according to the Sabatier principle as described below.

The Sabatier principle has been used to analyze the relationship between catalysts and substrates of varying

https://doi.org/10.1021/acs.jafc.3c01898
J. Agric. Food Chem. 2023, 71, 9040−9050

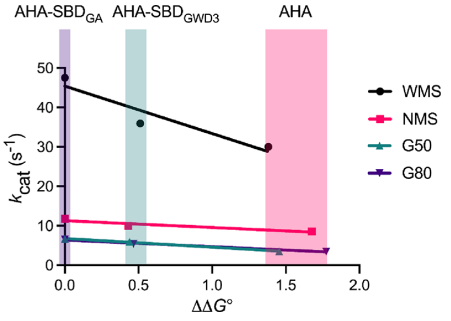

Figure 5. Fitting of k_{cat} with $\Delta\Delta G°$ for AHA and AHA-SBD fusions acting on different starch granules at 10 °C and pH 7.1. Lines represent best linear fits. $K_{1/2}$ for AHA-SBD$_{GA}$ acting on individual starches were selected as $K_{1/2,ref}$ to fix the $\Delta\Delta G°$ for AHA-SBD$_{GA}$ as zero (eq 4).

intermediary binding strength.[62] For example, the hydrolysis of cellulose using different cellulases as presented by a so-called volcano plot (Figure S6), is characteristic for the Sabatier principle.[34] There are two situations applying to the Sabatier principle, namely, desorption-limited and adsorption-limited reactions. For desorption-limited reactions, the higher the affinity for the substrate, the lower the activity. By contrast, in adsorption-limited reactions, higher affinity between the catalyst and substrate leads to higher activity. The fitting between k_{cat} or $^{inv}k_{cat}$ and $\Delta\Delta G°$ for the three AHA forms showed that when the SBD-fusion increased the affinity (lower $\Delta\Delta G°$) for starch granules, the rate of degrading (k_{cat}) and the density of attack sites ($^{inv}k_{cat}$) was faster and higher, respectively, than for the AHA. In addition, the higher affinity of AHA-SBD$_{GA}$ for starch granules led to both higher k_{cat} and $^{inv}k_{cat}$, in accordance with enzyme adsorption limited catalysis (Figure 5 and Figure S5).

4. DISCUSSION

Notably, the SBD-fusion did not essentially adversely affect the performance of AHA on soluble substrates. Previously, C-terminal fusion of SBD$_{GA}$ to barley α-amylase also did not alter activity for soluble starch, except at very low substrate concentration where the activity was doubled.[25] Even though fusion with CBMs, in this case, SBDs of family CBM20, may be expected to ameliorate interactions between enzyme and polysaccharide substrates, cases are reported of CBMs having been understood to hamper the interaction between CDs of naturally occurring multidomain enzymes and good substrates.[63] However, for a cold-active α-amylase from *Saccharophagus degradans* 2-40T that naturally contains a C-terminal linker-connected CBM20, in fact, the removal of linker and CBM20 dramatically reduced activity toward both solid and soluble substrates,[64] in agreement with AHA in its own right allowing the functionally improving SBD-fusion.

Then, with focus on heterogenous α-amylase-catalyzed degradation of starch granules from different crops and of different types, we assessed impact of the SBD-fusion to AHA on the performance through comparing activity and kinetic parameters (Figure 4 and Table S3). Quite expectedly, connecting AHA to an SBD consistently improved affinity for granular starches. This was manifested, for example, in marked reduction in K_d and concomitant positive fold-changes in both binding site density ($^{ads}\Gamma_{max}$) and density of attack sites ($^{kin}\Gamma_{max}$) for the two AHA-SBD variants. As concluded from these data, we note that addition of an SBD led to systematic, albeit moderate, increases in k_{cat}. This effect further adds to the overall functional advantage of having an SBD. Notably, the impact of SBD-fusion was the strongest for high-amylose substrates where the turnover went up by a factor of 2. The SBD fusions moreover had increased density of attack sites ($^{kin}\Gamma_{max}$) for all the solid substrates and relatively most so for the high-amylose granular starches, which were overall characterized by rather low density of attack sites (Figure 4F and Table S3).

Looking closer into these parameters, we noticed that the catalytically productive fraction (determined as the ratio of $^{kin}\Gamma_{max}$ over $^{ads}\Gamma_{max}$ (Figure 3C, A/B ratio) was lower for SBD-fusions on all substrates, compared to the AHA wild type. Hence, we conclude that the SBDs promoted both enzyme accumulation on the surface of the granules and ability to create enzyme−ligand complexes but that the catalytic performance was to some degree counteracted by an enlarged population of adsorbed unproductive enzymes. The productive interaction of the CD on starch granules is presumed to happen between the active site and substrate α-glucan chains adopting a suitable conformation in the enzyme complex. Thus, the CD had a clear preference for interacting with so-called attack sites. By contrast, the SBDs, as well as possible additional surface binding sites (SBSs) on the CD,[20] seem capable of binding to sites on the substrates without leading to catalytic cleavage by the CD.[65] Similar results were obtained in heterogeneous catalysis of cellulose degradation by multimodular cellobiohydrolases; thus, truncation of the natural CBM1 of Cel7A from *Trichoderma reesei* resulted in an 8-fold decrease in its binding capability.[31] However, all in all, the negative effect of SBD-fusion on performance was minor compared to the improved ability to recognize attack sites. Notably, attack and binding site densities ($^{kin}\Gamma_{max}$ and $^{ads}\Gamma_{max}$) for the three AHAs forms were in the nmol/g range, corresponding with the level observed for glucoamylase acting on starch granules,[32] whereas $^{kin}\Gamma_{max}$ and $^{ads}\Gamma_{max}$ for cellulases degrading cellulose were in the μmol/g range.[31] It has been shown that cellulase attacks in processive mode from the nonreducing end of the β-1,4-glucan chain until degradation is arrested due to a much reduced chain length.[66] However, the surface of starch granules is a more open structure than crystalline cellulose and the bonds susceptible to the CD are less concentrated. Second, α-amylase seems to act near the nonreducing ends possibly after unwinding double helical α-1,4-glucan chains (Figure S3), which also contributes to the lower $^{kin}\Gamma_{max}$ and $^{ads}\Gamma_{max}$ than those found for cellulases.

In conclusion, compared to AHA, SBD-fusion improved activity on both A- and B-type starch crystalline polymorphs, even though the AHA-SBDs had slightly reduced activity on amylose, the best soluble substrate. Interfacial kinetics analysis demonstrated that SBD-fusion increased attack and binding site densities of AHA on all types of starch granules by up to 5- and 7-fold, respectively. Elevated activity of the AHA SBD-fusions accompanied the increase in affinity for the starch granules according to the Sabatier principle of adsorption limited behavior. The understanding gained from the careful analysis of the mode of action of AHA and SBD-fusions has general relevance for enzyme-catalyzed natural and biotechnological utilization of granular starch.

https://doi.org/10.1021/acs.jafc.3c01898
J. Agric. Food Chem. 2023, 71, 9040−9050

■ ASSOCIATED CONTENT

Supporting Information

The Supporting Information is available free of charge at https://pubs.acs.org/doi/10.1021/acs.jafc.3c01898.

Construction, production and purification of AHA and AHA-SBD fusions; amino acid sequences for AHA, AHA-SBD_{GA} and AHA-SBD_{GWD3}; temperature and pH activity dependency of AHA and SBD-fusions (Figure S1); SDS-PAGE of purified enzymes (Figure S2); product profile of AHA and AHA-SBDs (Figure S3); conventional and inverse kinetics on granular maize starches at 25 °C and pH 7.1 (Figure S4); fitting of k_{cat} and $^{inv}k_{cat}$ with $\Delta\Delta G°$ for AHA and AHA-SBD fusions degrading starch granules (Figure S5); volcano plot illustrating the Sabatier principle Figure S6); properties of α-amylases from psychrophilic bacteria and an earthworm (Table S1); interfacial kinetics parameters for AHA and the SBD-fusions at 25 °C and pH 7.1 (Table S2); and interfacial kinetics parameters for AHA and the SBD-fusions at 10 °C and pH 7.1 (Table S3) (PDF)

■ AUTHOR INFORMATION

Corresponding Authors

Marie Sofie Møller − *Applied Molecular Enzyme Chemistry, Department of Biotechnology and Biomedicine, Technical University of Denmark, DK-2800 Kgs. Lyngby, Denmark*; Phone: +45 45252741; Email: msmo@dtu.dk

Birte Svensson − *Enzyme and Protein Chemistry, Department of Biotechnology and Biomedicine, Technical University of Denmark, DK-2800 Kgs. Lyngby, Denmark*; orcid.org/0000-0002-2993-8196; Phone: +45 45252740; Email: bis@bio.dtu.dk

Authors

Yu Wang − *Enzyme and Protein Chemistry, Department of Biotechnology and Biomedicine, Technical University of Denmark, DK-2800 Kgs. Lyngby, Denmark*; orcid.org/0000-0002-0019-6889

Yu Tian − *Department of Plant and Environmental Sciences, University of Copenhagen, DK-1871 Frederiksberg C, Denmark*

Yuyue Zhong − *Department of Plant and Environmental Sciences, University of Copenhagen, DK-1871 Frederiksberg C, Denmark*

Mohammad Amer Suleiman − *Enzyme and Protein Chemistry, Department of Biotechnology and Biomedicine, Technical University of Denmark, DK-2800 Kgs. Lyngby, Denmark*

Georges Feller − *Laboratory of Biochemistry, Center for Protein Engineering-InBioS, University of Liège, B4000 Liège-Sart Tilman, Belgium*

Peter Westh − *Interfacial Enzymology, Department of Biotechnology and Biomedicine, Technical University of Denmark, DK-2800 Kgs. Lyngby, Denmark*

Andreas Blennow − *Department of Plant and Environmental Sciences, University of Copenhagen, DK-1871 Frederiksberg C, Denmark*

Complete contact information is available at: https://pubs.acs.org/10.1021/acs.jafc.3c01898

Author Contributions

B.S. conceived the study with A.B. and P.W. Y.W. designed and performed experiments, collected data, and drafted the manuscript. Y.T. and Y.Z. contributed with experimental design. M.A.S. performed experiments. G.F. provided expertise on AHA. All other authors contributed to the writing of the manuscript and approved the final version. M.S.M., B.S., and P.W. developed the theoretical framework. M.S.M. and B.S. provided supervision and edited the final version of the manuscript.

Funding

This work was supported by a China Scholarship Council (CSC) grant #202006790033 and the Technical University of Denmark (Y.W.), by a China Scholarship Council (CSC) grant #202003250068 (Y.T.), and the project "HIAMBA - grain, flour, bread & bakery products preventing type 2 diabetes", Innovation Fund Denmark (Project 9067-00004A) (Y.Z.).

Notes

The authors declare no competing financial interest.

■ ACKNOWLEDGMENTS

Karina Jansen (Department of Biotechnology and Biomedicine, Technical University of Denmark) is gratefully thanked for technical assistance.

■ ABBREVIATIONS

AHA, α-amylase from *Pseudoalteromonas haloplanktis* TAB23; A/B ratio, density of attack sites/density of binding sites; AE, high-amylose maize starch AE 35; CBM, carbohydrate binding module; CD, catalytic domain; G50, high-amylose maize starch Australia G50; G80, high-amylose maize starch Australia G80; GH, glycoside hydrolase; HPPS, high-amylose/high-phosphate potato starch; MM, Michaelis−Menten; NMS, normal maize starch; NPS, normal potato starch; NWS, normal wheat starch; SBD, starch binding domain; SBD_{GA}, starch binding domain from *Aspergillus niger* glucoamylase; SBD_{GWD3}, starch binding domain from *Arabidopsis thaliana* glucan, water dikinase 3; WMS, waxy maize starch; WPS, waxy potato starch

■ REFERENCES

(1) Kaimal, A. M.; Mujumdar, A. S.; Thorat, B. N. Resistant starch from millets: Recent developments and applications in food industries. *Trends Food Sci. Technol.* **2021**, *111*, 563−580.

(2) Ståhl, M.; Berghel, J.; Frodeson, S.; Granström, K.; Renström, R. Effects on pellet properties and energy use when starch is added in the wood-fuel pelletizing process. *Energy Fuels* **2012**, *26*, 1937−1945.

(3) Falua, K. J.; Pokharel, A.; Babaei-Ghazvini, A.; Ai, Y.; Acharya, B. Valorization of starch to biobased materials: A review. *Polymer* **2022**, *14*, 2215.

(4) Chi, C.; Li, X.; Huang, S.; Chen, L.; Zhang, Y.; Li, L.; Miao, S. Basic principles in starch multi-scale structuration to mitigate digestibility: A review. *Trends Food Sci. Technol.* **2021**, *109*, 154−168.

(5) Irshad, A.; Guo, H.; Rehman, S. U.; Wang, X.; Wang, C.; Raza, A.; Zhou, C.; Li, Y.; Liu, L. Soluble starch synthase enzymes in cereals: An updated review. *Agronomy* **2021**, *11*, 1983.

(6) Bertoft, E. Understanding starch structure: Recent progress. *Agronomy* **2017**, *7*, 56.

(7) DeMartino, P.; Cockburn, D. W. Resistant starch: Impact on the gut microbiome and health. *Curr. Opin. Biotechnol.* **2020**, *61*, 66−71.

(8) Kartal, Ö.; Ebenhöh, O. A generic rate law for surface-active enzymes. *FEBS Lett.* **2013**, *587*, 2882−2890.

(9) Warren, F. J.; Butterworth, P. J.; Ellis, P. R. The surface structure of a complex substrate revealed by enzyme kinetics and Freundlich

constants for α-amylase interaction with the surface of starch. *Biochim. Biophys. Acta, Gen. Subj.* **2013**, *1830*, 3095−3101.
(10) Pasqualone, A.; Costantini, M.; Labarbuta, R.; Summo, C. Production of extruded-cooked lentil flours at industrial level: Effect of processing conditions on starch gelatinization, dough rheological properties and techno-functional parameters. *LWT* **2021**, *147*, No. 111580.
(11) Janeček, Š.; Svensson, B. How many α-amylase GH families are there in the CAZy database? *Amylase* **2022**, *6*, 1−10.
(12) Drula, E.; Garron, M. L.; Dogan, S.; Lombard, V.; Henrissat, B.; Terrapon, N. The carbohydrate-active enzyme database: Functions and literature. *Nucleic Acids Res.* **2022**, *50*, D571−D577.
(13) Lee, H. W.; Jeon, H. Y.; Choi, H. J.; Kim, N. R.; Choung, W. J.; Koo, Y. S.; Ko, D. S.; You, S. G.; Shim, J. H. Characterization and application of BiLA, a psychrophilic α-amylase from *Bifidobacterium longum*. *J. Agric. Food Chem.* **2016**, *64*, 2709−2718.
(14) Sindhu, R.; Binod, P.; Madhavan, A.; Beevi, U. S.; Mathew, A. K.; Abraham, A.; Pandey, A.; Kumar, V. Molecular improvements in microbial α-amylases for enhanced stability and catalytic efficiency. *Bioresour. Technol.* **2017**, *245*, 1740−1748.
(15) Feller, G.; Gerday, C. Psychrophilic enzymes: Hot topics in cold adaptation. *Nat. Rev. Microbiol.* **2003**, *1*, 200−208.
(16) Warren, F. J.; Royall, P. G.; Gaisford, S.; Butterworth, P. J.; Ellis, P. R. Binding interactions of α-amylase with starch granules: The influence of supramolecular structure and surface area. *Carbohydr. Polym.* **2011**, *86*, 1038−1047.
(17) Ueda, S. Fungal glucoamylases and raw starch digestion. *Trends Biochem. Sci.* **1981**, *6*, 89−90.
(18) Janeček, Š.; Mareček, F.; MacGregor, E. A.; Svensson, B. Starch-binding domains as CBM families−history, occurrence, structure, function and evolution. *Biotechnol. Adv.* **2019**, *37*, No. 107451.
(19) Paldi, T.; Levy, I.; Shoseyov, O. Glucoamylase starch-binding domain of *Aspergillus niger* B1: molecular cloning and functional characterization. *Biochem. J.* **2003**, *372*, 905−910.
(20) Cockburn, D.; Nielsen, M. M.; Christiansen, C.; Andersen, J. M.; Rannes, J. B.; Blennow, A.; Svensson, B. Surface binding sites in amylase have distinct roles in recognition of starch structure motifs and degradation. *Int. J. Biol. Macromol.* **2015**, *75*, 338−345.
(21) Southall, S. M.; Simpson, P. J.; Gilbert, H. J.; Williamson, G.; Williamson, M. P. The starch-binding domain from glucoamylase disrupts the structure of starch. *FEBS Lett.* **1999**, *447*, 58−60.
(22) Sorimachi, K.; Le Gal-Coëffet, M.-F.; Williamson, G.; Archer, D. B.; Williamson, M. P. Solution structure of the granular starch binding domain of *Aspergillus niger* glucoamylase bound to β-cyclodextrin. *Structure* **1997**, *5*, 647−661.
(23) Penninga, D.; Van Der Veen, B. A.; Knegtel, R. M. A.; Van Hijum, S. A. F. T.; Rozeboom, H. J.; Kalk, K. H.; Dijkstra, B. W.; Dijkhuizen, L. The raw starch binding domain of cyclodextrin glycosyltransferase from *Bacillus circulans* strain 251. *J. Biol. Chem.* **1996**, *271*, 32777−32784.
(24) Kamitori, S.; Kondo, S.; Okuyama, K.; Yokota, T.; Shimura, Y.; Tonozuka, T.; Sakano, Y. Crystal structure of *Thermoactinomyces vulgaris* R-47 α-amylase II (TVAII) hydrolyzing cyclodextrins and pullulan at 2.6 Å resolution. *J. Mol. Biol.* **1999**, *287*, 907−921.
(25) Juge, N.; Nøhr, J.; Le Gal-Coëffet, M. F.; Kramhøft, B.; Furniss, C. S. M.; Planchot, V.; Archer, D. B.; Williamson, G.; Svensson, B. The activity of barley α-amylase on starch granules is enhanced by fusion of a starch binding domain from *Aspergillus niger* glucoamylase. *Biochim. Biophys. Acta, Proteins Proteomics* **2006**, *1764*, 275−284.
(26) Cockburn, D.; Wilkens, C.; Dilokpimol, A.; Nakai, H.; Lewińska, A.; Abou Hachem, M.; Svensson, B. Using carbohydrate interaction assays to reveal novel binding sites in carbohydrate active enzymes. *PLoS One* **2016**, *11*, No. e0160112.
(27) Xiao, H.; Wang, S.; Xu, W.; Yin, Y.; Xu, D.; Zhang, L.; Liu, G. Q.; Luo, F.; Sun, S.; Lin, Q.; Xu, B. The study on starch granules by using darkfield and polarized light microscopy. *J. Food Compos. Anal.* **2020**, *92*, No. 103576.
(28) Butterworth, P. J.; Bajka, B. H.; Edwards, C. H.; Warren, F. J.; Ellis, P. R. Enzyme kinetic approach for mechanistic insight and predictions of *in vivo* starch digestibility and the glycaemic index of foods. *Trends Food Sci. Technol.* **2022**, *120*, 254−264.
(29) Schnell, S. Validity of the Michaelis−Menten equation−steady-state or reactant stationary assumption: That is the question. *FEBS J.* **2014**, *281*, 464−472.
(30) Govindaraju, I.; Chakraborty, I.; Baruah, V. J.; Sarmah, B.; Mahato, K. K.; Mazumder, N. Structure and morphological properties of starch macromolecule using biophysical techniques. *Starch/Staerke* **2021**, *73*, 2000030.
(31) Kari, J.; Andersen, M.; Borch, K.; Westh, P. An inverse Michaelis-Menten approach for interfacial enzyme kinetics. *ACS Catal.* **2017**, *7*, 4904−4914.
(32) Tian, Y.; Wang, Y.; Liu, X.; Herburger, K.; Westh, P.; Møller, M. S.; Svensson, B.; Zhong, Y.; Blennow, A. Interfacial enzyme kinetics reveals degradation mechanisms behind resistant starch. *Food Hydrocolloids* **2023**, *140*, No. 108621.
(33) Eibinger, M.; Ganner, T.; Plank, H.; Nidetzky, B. A biological nanomachine at work: watching the cellulosome degrade crystalline cellulose. *ACS Cent. Sci.* **2020**, *6*, 739−746.
(34) Kari, J.; Olsen, J. P.; Jensen, K.; Badino, S. F.; Krogh, K. B. R. M.; Borch, K.; Westh, P. Sabatier principle for interfacial (heterogeneous) enzyme catalysis. *ACS Catal.* **2018**, *8*, 11966−11972.
(35) Wang, S.; Li, C.; Copeland, L.; Niu, Q.; Wang, S. Starch retrogradation: A comprehensive review. *Compr. Rev. Food Sci. Food Saf.* **2015**, *14*, 568−585.
(36) Feller, G.; Payan, F.; Theys, F.; Qian, M.; Haser, R.; Gerday, C. Stability and structural analysis of α-amylase from the Antarctic psychrophile *Alteromonas haloplanctis* A23. *Eur. J. Biochem.* **1994**, *222*, 441−447.
(37) Gerday, C.; Aittaleb, M.; Bentahir, M.; Chessa, J. P.; Claverie, P.; Collins, T.; D'Amico, S.; Dumont, J.; Garsoux, G.; Georlette, D.; Hoyoux, A.; Lonhienne, T.; Meuwis, M. A.; Feller, G. Cold-adapted enzymes: From fundamentals to biotechnology. *Trends Biotechnol.* **2000**, *18*, 103−107.
(38) Aghajari, N.; Feller, G.; Gerday, C.; Haser, R. Structures of the psychrophilic *Alteromonas haloplanctis* α-amylase give insights into cold adaptation at a molecular level. *Structure* **1998**, *6*, 1503−1516.
(39) D'Amico, S.; Sohier, J. S.; Feller, G. Kinetics and energetics of ligand binding determined by microcalorimetry: Insights into active site mobility in a psychrophilic α-amylase. *J. Mol. Biol.* **2006**, *358*, 1296−1304.
(40) Giardina, T.; Gunning, A. P.; Juge, N.; Faulds, C. B.; Furniss, C. S. M.; Svensson, B.; Morris, V. J.; Williamson, G. Both binding sites of the starch-binding domain of *Aspergillus niger* glucoamylase are essential for inducing a conformational change in amylose. *J. Mol. Biol.* **2001**, *313*, 1149−1159.
(41) Christiansen, C.; Abou Hachem, M.; Glaring, M. A.; Viksø-Nielsen, A.; Sigurskjold, B. W.; Svensson, B.; Blennow, A. A CBM20 low-affinity starch-binding domain from glucan, water dikinase. *FEBS Lett.* **2009**, *583*, 1159−1163.
(42) Blennow, A.; Wischmann, B.; Houborg, K.; Ahmt, T.; Jørgensen, K.; Engelsen, S. B.; Bandsholm, O.; Poulsen, P. Structure function relationships of transgenic starches with engineered phosphate substitution and starch branching. *Int. J. Biol. Macromol.* **2005**, *36*, 159−168.
(43) Kozlov, S. S.; Blennow, A.; Krivandin, A. V.; Yuryev, V. P. Structural and thermodynamic properties of starches extracted from GBSS and GWD suppressed potato lines. *Int. J. Biol. Macromol.* **2007**, *40*, 449−460.
(44) Htoon, A.; Shrestha, A. K.; Flanagan, B. M.; Lopez-Rubio, A.; Bird, A. R.; Gilbert, E. P.; Gidley, M. J. Effects of processing high amylose maize starches under controlled conditions on structural organisation and amylase digestibility. *Carbohydr. Polym.* **2009**, *75*, 236−245.
(45) Tian, Y.; Qu, J.; Zhou, Q.; Ding, L.; Cui, Y.; Blennow, A.; Zhong, Y.; Liu, X. High pressure/temperature pasting and gelling of

https://doi.org/10.1021/acs.jafc.3c01898
J. Agric. Food Chem. 2023, 71, 9040−9050

starch related to multilevel structure-analyzed with RVA 4800. *Carbohydr. Polym.* **2022**, *295*, No. 119858.
(46) Feller, G.; Le Bussy, O.; Gerday, C. Expression of psychrophilic genes in mesophilic hosts: assessment of the folding state of a recombinant-amylase. *Appl. Environ. Microbiol.* **1998**, *64*, 1163−1165.
(47) Clayton, J. W.; Meredith, W. O. S. The effect of thiols on the dinitrosalicylic acid test for reducing sugars. *J. Inst. Brew.* **1966**, *72*, 537−540.
(48) Brooke, D.; Movahed, N.; Bothner, B. Universal buffers for use in biochemistry and biophysical experiments. *AIMS Biophys.* **2015**, *2*, 336.
(49) Huggett, A. S.; Nixoh, D. A. Use of glucose oxidase, peroxidase, and O-dianisidine in determination of blood and urinary glucose. *Lancet* **1957**, *273*, 368−370.
(50) Andersen, M.; Kari, J.; Borch, K.; Westh, P. Michaelis−Menten equation for degradation of insoluble substrate. *Math. Biosci.* **2018**, *296*, 93−97.
(51) Ernst, O.; Zor, T. Linearization of the Bradford protein assay. *J. Visualized Exp.* **2010**, *38*, 1918.
(52) Stam, M. R.; Danchin, E. G. J.; Rancurel, C.; Coutinho, P. M.; Henrissat, B. Dividing the large glycoside hydrolase family 13 into subfamilies: Towards improved functional annotations of α-amylase-related proteins. *Protein Eng., Des. Sel.* **2006**, *19*, 555−562.
(53) Janeček, Š.; Svensson, B.; MacGregor, E. A. α-Amylase: an enzyme specificity found in various families of glycoside hydrolases. *Cell. Mol. Life Sci.* **2014**, *71*, 1149−1170.
(54) Ottoni, J. R.; e Silva, T. R.; de Oliveira, V. M.; Passarini, M. R. Z. Characterization of amylase produced by cold-adapted bacteria from Antarctic samples. *Biocatal. Agric. Biotechnol.* **2020**, *23*, No. 101452.
(55) Aghajari, N.; Feller, G.; Gerday, C.; Haser, R. Crystal structures of the psychrophilic α-amylase from *Alteromonas haloplanctis* in its native form and complexed with an inhibitor. *Protein Sci.* **1998**, *7*, 564−572.
(56) Svensson, B.; Svendsen, T. G.; Svendsen, I. B.; Sakai, T.; Ottesen, M. Characterization of two forms of glucoamylase from *Aspergillus niger*. *Carlsberg Res. Commun.* **1982**, *47*, 55−69.
(57) Peng, H.; Li, R.; Li, F.; Zhai, L.; Zhang, X.; Xiao, Y.; Gao, Y. Extensive hydrolysis of raw rice starch by a chimeric α-amylase engineered with α-amylase (AmyP) and a starch-binding domain from *Cryptococcus* sp. S-2. *Appl. Microbiol. Biotechnol.* **2018**, *102*, 743−750.
(58) Feller, G.; D'Amico, S.; Benotmane, A. M.; Joly, F.; Van Beeumen, J.; Gerday, C. Characterization of the C-terminal propeptide involved in bacterial wall spanning of α-amylase from the psychrophile *Alteromonas haloplanctis*. *J. Biol. Chem.* **1998**, *273*, 12109−12115.
(59) Chen, P.; Yu, L.; Chen, L.; Li, X. Morphology and microstructure of maize starches with different amylose/amylopectin content. *Starch/Staerke* **2006**, *58*, 611−615.
(60) Altay, F.; Gunasekaran, S. Influence of drying temperature, water content, and heating rate on gelatinization of corn starches. *J. Agric. Food Chem.* **2006**, *54*, 4235−4245.
(61) Mikkelsen, R.; Suszkiewicz, K.; Blennow, A. A novel type carbohydrate-binding module identified in α-glucan, water dikinases is specific for regulated plastidial starch metabolism. *Biochemistry* **2006**, *45*, 4674−4682.
(62) Ooka, H.; Huang, J.; Exner, K. S. The Sabatier principle in electrocatalysis: basics, limitations, and extensions. *Front. Energy Res.* **2021**, *9*, 155.
(63) Møller, M. S.; El Bouaballati, S.; Henrissat, B.; Svensson, B. Functional diversity of three tandem C-terminal carbohydrate-binding modules of a β-mannanase. *J. Biol. Chem.* **2021**, *296*, No. 100638.
(64) Ding, N.; Zhao, B.; Ban, X.; Li, C.; Venkataram Prasad, B. V.; Gu, Z.; Li, Z. Carbohydrate-binding module and linker allow cold adaptation and salt tolerance of maltopentaose-forming amylase from marine bacterium *Saccharophagus degradans* 2-40^T. *Front. Microbiol.* **2021**, *12*, 1948.
(65) Guillén, D.; Santiago, M.; Linares, L.; Pérez, R.; Morlon, J.; Ruiz, B.; Sánchez, S.; Rodríguez-Sanoja, R. Alpha-amylase starch binding domains: Cooperative effects of binding to starch granules of multiple tandemly arranged domains. *Appl. Environ. Microbiol.* **2007**, *73*, 3833−3837.
(66) Kari, J.; Molina, G. A.; Schaller, K. S.; Schiano-di-Cola, C.; Christensen, S. J.; Badino, S. F.; Sørensen, T. H.; Røjel, N. S.; Keller, M. B.; Sørensen, N. R.; Kolaczkowski, B.; Olsen, J. P.; Krogh, K. B. R. M.; Jensen, K.; Cavaleiro, A. M.; Peters, G. H. J.; Spodsberg, N.; Borch, K.; Westh, P. Physical constraints and functional plasticity of cellulases. *Nat. Commun.* **2021**, *12*, 1−10.

https://doi.org/10.1021/acs.jafc.3c01898
J. Agric. Food Chem. 2023, 71, 9040−9050

Supporting Information for

Improved Hydrolysis of Granular Starches by a Psychrophilic α-Amylase Starch Binding Domain-Fusion

*Yu Wang [a], Yu Tian [b], Yuyue Zhong [b], Mohammad Amer Suleiman [a], Georges Feller [c], Peter Westh [d], Andreas Blennow [b], Marie Sofie Møller [e, *], Birte Svensson [a, *]*

[a] Enzyme and Protein Chemistry, Department of Biotechnology and Biomedicine, Technical University of Denmark, DK-2800, Kgs. Lyngby, Denmark

[b] Department of Plant and Environmental Sciences, University of Copenhagen, DK-1871, Frederiksberg C, Denmark

[c] Laboratory of Biochemistry, Center for Protein Engineering-InBioS, University of Liège, B4000 Liège-Sart Tilman, Belgium

[d] Interfacial Enzymology, Department of Biotechnology and Biomedicine, Technical University of Denmark, DK-2800, Kgs. Lyngby, Denmark

[e] Applied Molecular Enzyme Chemistry, Department of Biotechnology and Biomedicine, Technical University of Denmark, DK-2800, Kgs. Lyngby, Denmark

* Corresponding authors:

Marie Sofie Møller: msmo@dtu.dk; phone: +45 45252741

Birte Svensson: bis@bio.dtu.dk; phone: +45 45252740

EXPERIMENTAL SECTION

Construction, Production and Purification of AHA and AHA-SBD Fusions. Codon-optimised genes for *Escherichia coli* encoding AHA (GenBank accession CAA41481.1, amino acid residues 25–477), AHA-SBD_{GA} and AHA-SBD_{GWD3} (see protein sequences below) were purchased and cloned into the expression vector pET-28a (+) using NheI and XhoI the restriction sites (GenScript, Leiden, The Netherlands) in frame with the N-terminal His-tag. The AHA, AHA-SBD_{GA} and AHA-SBD_{GWD3} encoding plasmids were transformed into *E. coli* BL21(DE3)* and screened on LB agar plates containing 50 μg/mL kanamycin. A starter culture (10 mL) made by inoculating LB medium (1% tryptone, 0.5% yeast extract, 0.5% NaCl, 50 μg/mL kanamycin, 10 mM glucose) with a single colony and incubating (37 °C, shaking at 170 rpm, overnight) was used to inoculate 800 mL LB medium containing 10 mM glucose and 50 μg/mL kanamycin in shake flasks. Recombinant protein was produced (18 °C, shaking at 160 rpm, 24 h) following addition of 0.1 mM isopropyl-β-D-thiogalactopyranoside (IPTG) for induction at an optical density of 0.6 at 600 nm. Cells were harvested by centrifugation (4,000 *g*, 30 min) and stored at –20 °C until protein purification.

Cells (5 g) were resuspended in 20 mL HisTrap equilibration buffer (20 mM Hepes, 250 mM NaCl, 1 mM $CaCl_2$, 10% glycerol, pH 7.5), lysed by sonication (500 W, 20 kHz, 2 min), added 3 μL Benzonase Nuclease (Sigma-Aldrich) and centrifuged (40,000 *g*, 4 °C, 30 min). AHA, AHA-SBD_{GA} and AHA-SBD_{GWD3} were purified by mixing supernatants (20 mL) with 2 mL HisPur™ nickel-nitrilotriacetic acid resin (Thermo Fisher Scientific), pre-equilibrated with equilibration buffer, and washed with 20 mL washing buffer (35 mM imidazole in equilibration buffer). Bound protein was eluted by 10 mL elution buffer (300 mM imidazole in equilibration buffer), buffer-exchanged to the ion exchange chromatography equilibration buffer (20 mM MES, 1 mM $CaCl_2$, 10% glycerol, pH 6.5) using Amicon® Ultra-15 Centrifugal Filter Unit (Ultracel-30 regenerated cellulose membrane, 15 mL sample volume, Merck), concentrated to

2 mL (30 kDa MWCO; Amicon® Ultra), filtered (0.45 µm), loaded onto a Resource Q column (1 mL, Cytiva, pre-equilibrated by 15 column volumes (CV) of equilibration buffer) and eluted by 50 CV of a linear gradient from 0 to 800 mM NaCl in equilibration buffer. Fractions showing activity towards amylose (see Activity assays) were verified by SDS-PAGE to contain AHA, AHA-SBD_{Ga} and AHA-SBD_{GWD3} with theoretical molecular mass (https://web.expasy.org/protparam/) of 49,343.1, 61,703.7 and 61,231.5Da, respectively.

Amino Acid Sequences for AHA, AHA-SBDGA and AHA-SBDGWD3:

AHA (GenBank Accession CAA41481.1, residues 25–477):

TPTTFVHLFEWNWQDVAQECEQYLGPKGYAAVQVSPPNEHITGSQWWTRYQPVSY
ELQSRGGNRAQFIDMVNRCSAAGVDIYVDTLINHMAAGSGTGTAGNSFGNKSFPIYS
PQDFHESCTINNSDYGNDRYRVQNCELVGLADLDTASNYVQNTIAAYINDLQAIGVK
GFRFDASKHVAASDIQSLMAKVNGSPVVFQEVIDQGGEAVGASEYLSTGLVTEFKYS
TELGNTFRNGSLAWLSNFGEGWGFMPSSSAVVFVDNHDNQRGHGGAGNVITFEDG
RLYDLANVFMLAYPYGYPKVMSSYDFHGDTDAGGPNVPVHNNGNLECFASNWKC
EHRWSYIAGGVDFRNNTADNWAVTNWWDNTNNQISFGRGSSGHMAINKEDSTLTA
TVQTDMASGQYCNVLKGELSADAKSCSGEVITVNSDGTINLNIGAWDAMAIHKNAK
LNTSSAS

AHA-SBD_{GA} (GenBank Accession CAA41481.1, residues 25–477, linker TSSASGLTKV, and GenBank Accession P69328.1, residues 538–639):

TPTTFVHLFEWNWQDVAQECEQYLGPKGYAAVQVSPPNEHITGSQWWTRYQPVSY
ELQSRGGNRAQFIDMVNRCSAAGVDIYVDTLINHMAAGSGTGTAGNSFGNKSFPIYS
PQDFHESCTINNSDYGNDRYRVQNCELVGLADLDTASNYVQNTIAAYINDLQAIGVK
GFRFDASKHVAASDIQSLMAKVNGSPVVFQEVIDQGGEAVGASEYLSTGLVTEFKYS
TELGNTFRNGSLAWLSNFGEGWGFMPSSSAVVFVDNHDNQRGHGGAGNVITFEDG
RLYDLANVFMLAYPYGYPKVMSSYDFHGDTDAGGPNVPVHNNGNLECFASNWKC

EHRWSYIAGGVDFRNNTADNWAVTNWWDNTNNQISFGRGSSGHMAINKEDSTLTA

TVQTDMASGQYCNVLKGELSADAKSCSGEVITVNSDGTINLNIGAWDAMAIHKNAK

LNTSSASGLTKVCTTPTAVAVTFDLTATTTYGENIYLVGSISQLGDWETSDGIALSAD

KYTSSDPLWYVTVTLPAGESFEYKFIRIESDDSVEWESDPNREYTVPQACGTSTATVT

DTWR

AHA-SBD$_{GWD3}$ (GenBank Accession CAA41481.1, residues 25–477, linker TSSASGLTKV, and GenBank Accession Q6ZY51.1, residues 83–164):

TPTTFVHLFEWNWQDVAQECEQYLGPKGYAAVQVSPPNEHITGSQWWTRYQPVSY

ELQSRGGNRAQFIDMVNRCSAAGVDIYVDTLINHMAAGSGTGTAGNSFGNKSFPIYS

PQDFHESCTINNSDYGNDRYRVQNCELVGLADLDTASNYVQNTIAAYINDLQAIGVK

GFRFDASKHVAASDIQSLMAKVNGSPVVFQEVIDQGGEAVGASEYLSTGLVTEFKYS

TELGNTFRNGSLAWLSNFGEGWGFMPSSSAVVFVDNHDNQRGHGGAGNVITFEDG

RLYDLANVFMLAYPYGYPKVMSSYDFHGDTDAGGPNVPVHNNGNLECFASNWKC

EHRWSYIAGGVDFRNNTADNWAVTNWWDNTNNQISFGRGSSGHMAINKEDSTLTA

TVQTDMASGQYCNVLKGELSADAKSCSGEVITVNSDGTINLNIGAWDAMAIHKNAK

LNTSSASGLTKVDGSGTKVRLNVRLDHQVNFGDHVAMFGSAKEIGSWKKKSPLNW

SENGWVCELELDGGQVLEYKFVIVKNDGSLSWESGDNRVLKVPNSGNFSVVCHWD

ATRE

SUPPLEMENTARY FIGURES AND TABLES

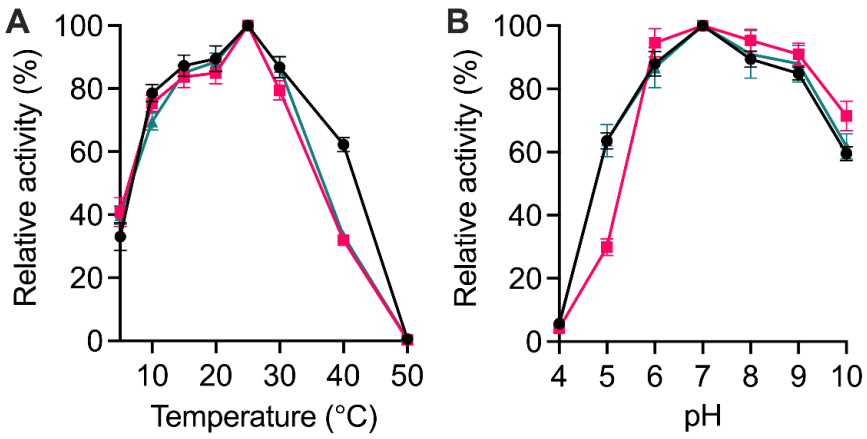

Figure S1. Temperature and pH dependence of activity for AHA and AHA-SBD-fusions on amylose using standard assay. (A) Temperature (5–50 °C). (B) pH 4.0–10.0. AHA (black), AHA-SBD$_{GA}$ (red), AHA-SBD$_{GWD3}$ (green). Maximum activity was defined for the individual enzymes as 100%. AHA, AHA-SBD$_{GA}$ and AHA-SBD$_{GWD3}$ all have highest activity for amylose at 25 °C, 80–90% of this activity at 15–20 and 30 °C, and 35–40% at 5 °C (Fig. S2). All three enzymes lost activity completely at 50 °C. The activity was highest at pH 7.0 and > 85% was retained throughout pH 6.0–9.0.

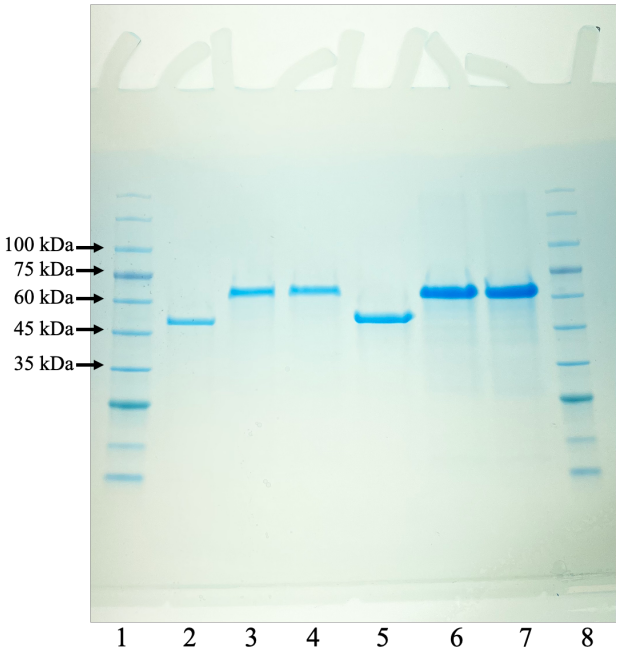

Figure S2. SDS-PAGE of purified recombinant enzymes. Lanes 1 and 8: Marker, Lane 2: AHA (1.3 µg), Lane 3: AHA-SBD$_{GA}$ (1.3 µg), Lane 4: AHA-SBD$_{GWD3}$ (1.3 µg), Lane 5: AHA (6.5 µg), Lane 6: AHA-SBD$_{GA}$ (6.5 µg), Lane 7: AHA-SBD$_{GWD3}$ (6.5 µg). Theoretical values of AHA, AHA-SBD$_{GA}$ and AHA-SBD$_{GWD3}$ are 49343.1, 61703.7 and 61231.5 Da, respectively (https://web.expasy.org/protparam/).

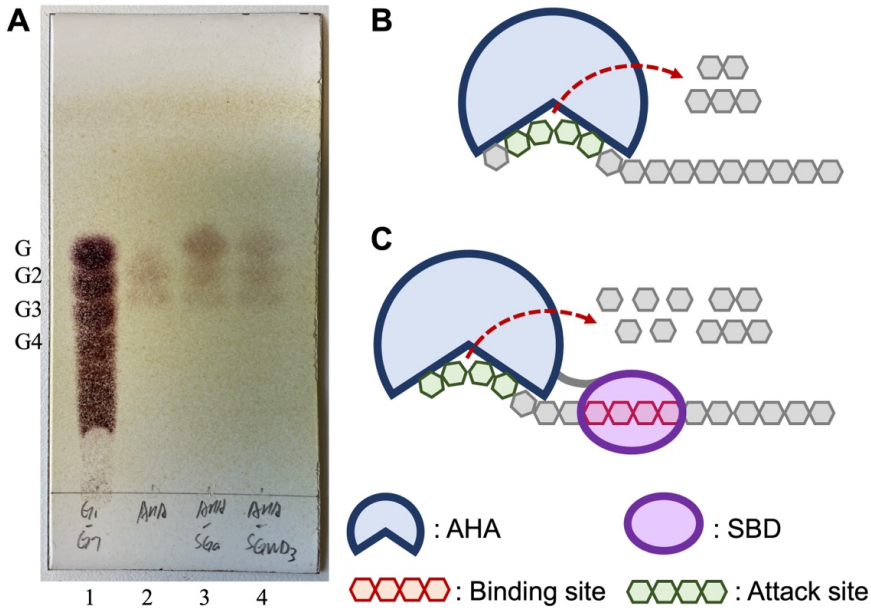

Figure S3. Products released by AHA and AHA-SBDs acting on waxy maize starch (WMS) granules at 25°C and pH 7.1 for 30 min. (A) TLC of soluble reaction products. Lane 1: Marker: Glucose (G) through maltoheptaose. Products of: Lane 2: AHA, Lane 3: AHA-SBD_{GA}, and Lane 4: AHA-SBD_{GWD3}. Cartoon illustrating a proposed mechanism behind the change in product profile from (B) AHA and (C) AHA-SBDs.

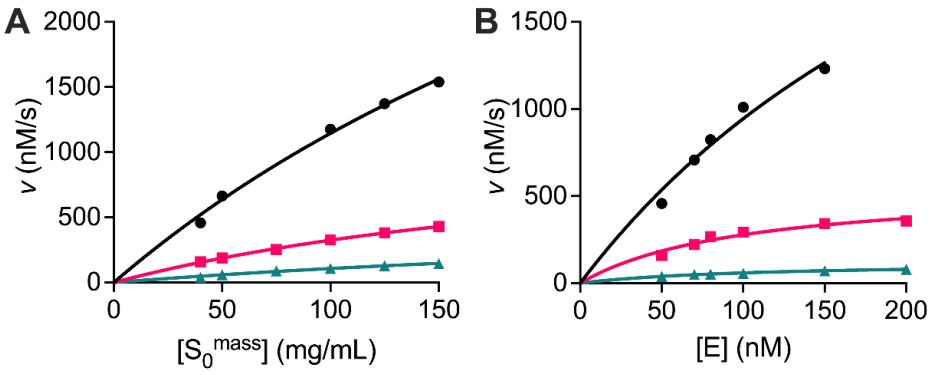

Figure S4. Initial rates of starch granule degradation by AHA-SBD_{GA} at 25°C and pH 7.1. (A) Conventional and (B) inverse kinetics (WMS, black; NMS, red; AE, green). Lines represent best fits of Michaelis-Menten kinetics.

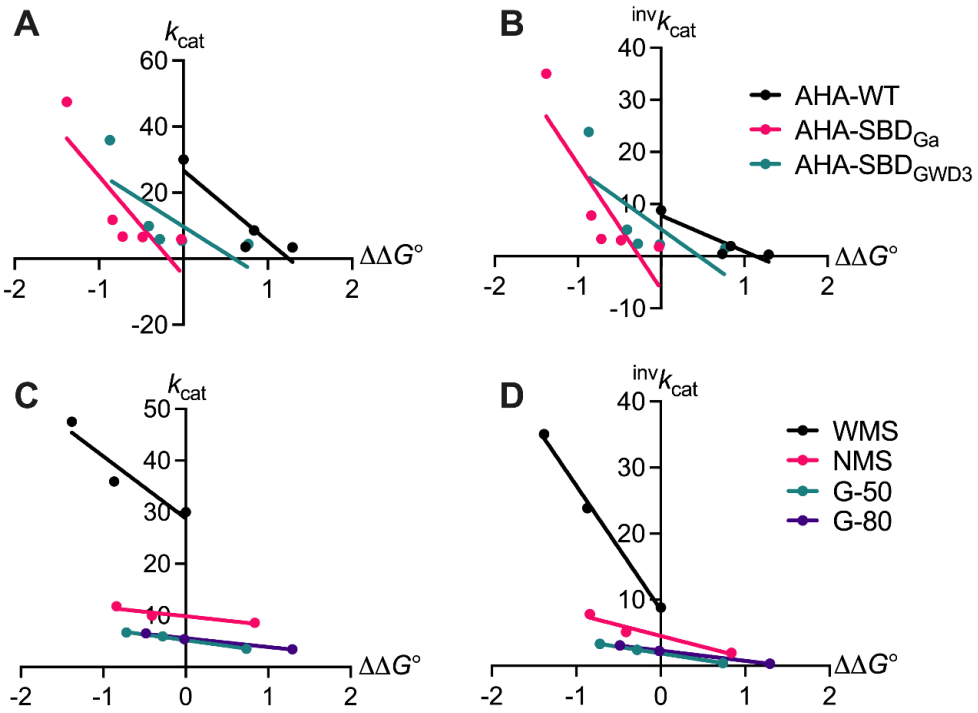

Figure S5. Fitting of k_{cat} (A and C) and $^{inv}k_{cat}$ (B and D) with $\Delta\Delta G°$ for AHA and AHA-SBD fusions (A and B) or starch granules (C and D) at 10°C and pH 7.1. Lines represent best linear fits. $K_{1/2}$ for AHA acting on WMS were selected as $K_{1/2,ref}$.[1]

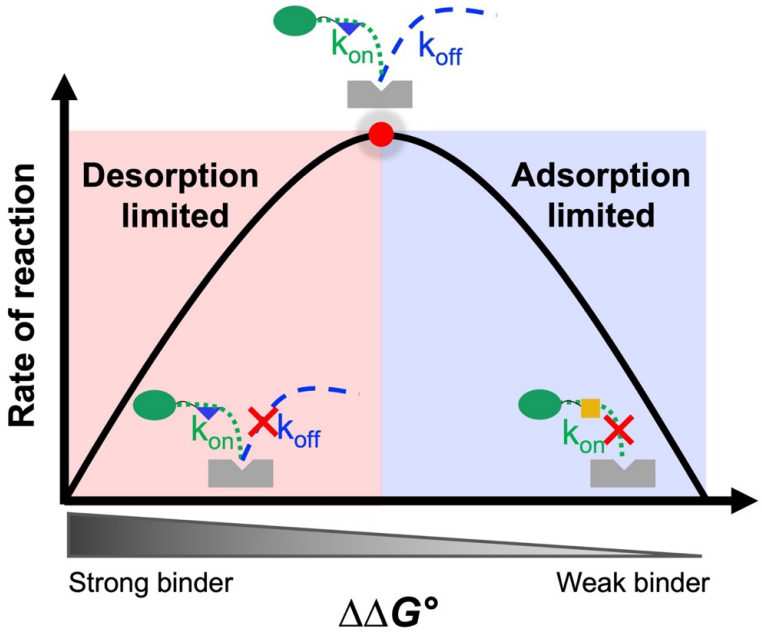

Figure S6. A volcano plot illustrating the Sabatier principle. This figure is inspired by a figure from Kari et al.[1].The pink part represents desorption limited catalysis, where higher affinity for substrate leads to lower rate of reaction. The purple part represents adsorption limited catalysis, where higher affinity for substrate leads to higher rate of reaction. The red dot between the desorption and adsorption limited regions represents the best affinity for substrate of the enzyme to have the highest rate of reaction.

Table S1. Enzyme Activity Properties of α-amylases from Psychrophilic Bacteria and an Earthworm

Organism	Optimum temperature (°C)	Optimum pH	Reference
Pseudoalteromonas sp. MY1	40	7.0	2
Nocardiopsis sp. 7326	35	8.0	3
Pseudoalteromonas arctica GS230	30	7.5	4
Arthrobacter agilis	30	3.0	5
Bacillus cereus	20	10.0	6
Pseudoalteromonas sp. 2-3	30	8.0	7
Pseudoalteromonas sp. M175	30	7.5	8
Bacillus sp. dsh19-1	20	6.0	9
Zunongwangia profunda	35	7.0	10
Aeromonas veronii NS07	10	4.0	11
Bifidobacterium longum	20	5.0	12
Shewanella sp. ISTPL2	40	8.0	13
Eisenia foetida (earthworm)	50	5.5	14
Microbacterium foliorum	20	9.0	6
Pseudoalteromonas haloplanctis TAB23	25	7.0	15, and this study

Table S2. Conventional and Inverse Kinetic Parameters of AHA-SBD_{GA} Acting on Starch Granules at 25 °C and pH 7.1

Enzyme	Substrate	WMS	NMS	AE
	Amylose content (%)	0.7	26.7	72.2
AHA-SBD_{GA}	k_{cat} (s^{-1})	113 ± 4	22 ± 1	11 ± 1
	$K_{1/2}$ (g/L)	398 ± 22	255 ± 2	421 ± 13
	K_m (nM)	311 ± 37	107 ± 3	99 ± 6
	$k_{cat}/K_{1/2}$ ($L\cdot[g\cdot s]^{-1}$)	0.28 ± 0.005	0.07 ± 0.004	0.03 ± 0.001
	${}^{kin}\Gamma_{max}$ (nmol/g)	0.80 ± 0.02	0.64 ± 0.14	0.27 ± 0.04

Table S3. Conventional and Inverse Kinetic Parameters of AHA, AHA-SBD$_{GA}$ and AHA-SBD$_{GWD3}$ Acting on Different Granular Starches at 10 °C and pH 7.1

Enzyme	Substrate	WMS	NMS	G50	G80	AE
	Amylose content (%)	0.7	26.7	40.5	50.5	72.2
AHA	k_{cat} (s^{-1})	30 ± 1	9 ± 1	4 ± 1	3 ± 0.4	ND
	$K_{1/2}$ (g/L)	93 ± 3	132 ± 16	127± 20	160 ± 30	ND
	K_M (nM)	24 ± 1	15 ± 7	7 ± 5	8 ± 3	ND
	$k_{cat}/K_{1/2}$ (L·[g·s]$^{-1}$)	0.32 ± 0.003	0.07 ± 0.00	0.03 ± 0.01	0.02 ± 0.004	ND
	$^{kin}\Gamma_{max}$ (nmol/g)	0.28 ± 0.02	0.17 ± 0.06	0.09 ± 0.03	0.07 ± 0.02	ND
	$^{ads}\Gamma_{max}$ (nmol/g)	0.35 ± 0.08	0.25 ± 0.02	0.14 ± 0.06	0.14 ± 0.03	ND
	A/B ratio (%)[b]	80	68	63	52	ND
	K_d (nM)	293 ± 52	400 ± 32	413 ± 46	420 ± 66	ND
AHA-SBD$_{GA}$	k_{cat} (s^{-1})	48 ± 4	12 ± 0.2	7 ± 1	7 ± 0.1	6 ± 1
	$K_{1/2}$ (g/L)	52 ± 15	65 ± 3	68 ± 10	75 ± 12	92 ± 24
	K_M (nM)	50 ± 10	40 ± 6	22 ± 3	22 ± 10	29 ± 8
	$k_{cat}/K_{1/2}$ (L·[g·s]$^{-1}$)	0.69 ± 0.13	0.14 ± 0.01	0.07 ± 0.04	0.07 ± 0.01	0.05 ± 0.01
	$^{kin}\Gamma_{max}$ (nmol/g)	0.86 ± 0.00	0.64 ± 0.14	0.41 ± 0.17	0.38 ± 0.17	0.31 ± 0.05
	$^{ads}\Gamma_{max}$ (nmol/g)	1.36 ± 0.24	1.21 ± 0.16	1.18 ± 0.13	1.06 ± 0.05	0.82 ± 0.10
	A/B ratio (%)	63	53	34	36	38
	K_d (nM)	19 ± 8	25 ± 12	54 ± 18	48 ± 2	43 ± 1
AHA-SBD$_{GWD3}$	k_{cat} (s^{-1})	36 ± 3	10 ± 1	6 ± 1	5 ± 0.1	4 ± 0.2
	$K_{1/2}$ (g/L)	64 ± 22	78 ± 29	82 ± 38	92 ± 15	128 ± 17
	K_M (nM)	35 ± 11	37 ± 5	19 ± 1	1 8 ± 3	21 ± 8
	$k_{cat}/K_{1/2}$ (L·[g·s]$^{-1}$)	0.42 ± 0.06	0.10 ± 0.02	0.05 ± 0.02	0.06 ± 0.01	0.04 ± 0.00
	$^{kin}\Gamma_{max}$ (nmol/g)	0.61 ± 0.17	0.49 ± 0.1	0.32 ± 0.09	0.31 ± 0.11	0.25 ± 0.09
	$^{ads}\Gamma_{max}$ (nmol/g)	0.97 ± 0.03	0.91 ± 0.003	0.71 ± 0.09	0.64 ± 0.04	0.66 ± 0.01
	A/B ratio (%)	63	54	44	48	38
	K_d (nM)	128 ± 54	153 ± 43	337 ± 28	319 ± 48	221 ± 76

[a] ND: Not determined; [b] A/B ratio: Density of attack sites/density of binding sites.

REFERENCES

(1) Kari, J.; Olsen, J. P.; Jensen, K.; Badino, S. F.; Krogh, K. B. R. M.; Borch, K.; Westh, P. Sabatier principle for interfacial (heterogeneous) enzyme catalysis. *ACS Catal.* **2018**, *8*, 11966–11972.

(2) Liu, X.; Xu, Y. Molecular cloning and characterization of an α-amylase with raw starch digestibility from *Bacillus* sp. YX-1. *Ann. Microbiol.* **2009**, *59*, 91–96.

(3) Zhang, J. W.; Zeng, R. Y. Purification and characterization of a cold-adapted α-amylase produced by *Nocardiopsis* sp. 7326 isolated from Prydz Bay, Antarctic. *Mar. Biotechnol.* **2008**, *10*, 75–82.

(4) Lu, M.; Wang, S.; Fang, Y.; Li, H.; Liu, S.; Liu, H. Cloning, expression, purification, and characterization of cold-adapted α-amylase from *Pseudoalteromonas arctica* GS230. *Protein J.* **2010**, *29*, 591–597.

(5) Kim, S.; Park, H.; Choi, J. Cloning and characterization of cold-adapted α-amylase from antarctic Arthrobacter agilis. *Appl. Biochem. Biotechnol.* **2017**, *181*, 1048–1059.

(6) Kuddus, M.; Roohi; Saima; Ahmad, I. Z. Cold-active extracellular α-amylase production from novel bacteria *Microbacterium foliorum* GA2 and *Bacillus cereus* GA6 isolated from Gangotri glacier, Western Himalaya. *J. Genet. Eng. Biotechnol.* **2012**, *10*, 151–159.

(7) Duarte, A. W. F.; Dos Santos, J. A.; Vianna, M. V.; Vieira, J. M. F.; Mallagutti, V. H.; Inforsato, F. J.; Wentzel, L. C. P.; Lario, L. D.; Rodrigues, A.; Pagnocca, F. C. Cold-adapted enzymes produced by fungi from terrestrial and marine Antarctic environments. *Crit. Rev. Biotechnol.* **2018**, *38*, 600–619.

(8) Wang, X.; Kan, G.; Shi, C.; Xie, Q.; Ju, Y.; Wang, R.; Qiao, Y.; Ren, X. Purification and characterization of a novel wild-type α-amylase from Antarctic sea ice bacterium *Pseudoalteromonas* sp. M175. *Protein Expr. Purif.* **2019**, *164*, 105444.

(9) Dou, S.; Chi, N.; Zhou, X.; Zhang, Q.; Pang, F.; Xiu, Z. Molecular cloning, expression, and biochemical characterization of a novel cold-active α-amylase from *Bacillus* sp. dsh19-1. *Extremophiles* **2018**, *22*, 739–749.

(10) Qin, Y.; Huang, Z.; Liu, Z. A novel cold-active and salt-tolerant α-amylase from marine bacterium *Zunongwangia profunda*: Molecular cloning, heterologous expression and biochemical characterization. *Extremophiles* **2014**, *18*, 271–281.

(11) Samie, N.; Noghabi, K. A.; Gharegozloo, Z.; Zahiri, H. S.; Ahmadian, G.; Sharafi, H.; Behrozi, R.; Vali, H. Psychrophilic α-amylase from *Aeromonas veronii* NS07 isolated from farm soils. *Process Biochem.* **2012**, *47*, 1381–1387.

(12) Lee, H. W.; Jeon, H. Y.; Choi, H. J.; Kim, N. R.; Choung, W. J.; Koo, Y. S.; Ko, D. S.; You, S. G.; Shim, J. H. Characterization and application of BiLA, a psychrophilic α-amylase from *Bifidobacterium longum*. *J. Agric. Food Chem.* **2016**, *64*, 2709–2718.

(13) Rathour, R.; Gupta, J.; Tyagi, B.; Thakur, I. S. Production and characterization of psychrophilic α-amylase from a psychrophilic bacterium, *Shewanella* sp. ISTPL2. *Amylase* **2020**, *4*, 1–10.

(14) Ueda, M.; Asano, T.; Nakazawa, M.; Miyatake, K.; Inouye, K. Purification and characterization of novel raw-starch-digesting and cold-adapted α-amylases from *Eisenia foetida*. *Comp. Biochem. Physiol. - B Biochem. Mol. Biol.* **2008**, *150*, 125–130.

(15) Feller, G.; Lonhienne, T.; Deroanne, C.; Libioulle, C.; Van Beeumen, J.; Gerday, C. Purification, characterization, and nucleotide sequence of the thermolabile α-amylase from the antarctic psychrotroph *Alteromonas haloplanctis* A23. *J. Biol. Chem.* **1992**, *267*, 5217–5221.

2.1.2 Paper 2 – Impact of Starch Binding Domain Fusion on Activities and Starch Product Structure of 4-α-Glucanotransferase

This paper was accepted for publication in *Molecules* on the 28th of January 2023. The paper presents results on the effect of SBD-fusion on the enzymatic properties and starch product structure of a thermophilic 4-α-glucanotransferase. The supporting information can be found at the end of the paper. The permission to reuse this article in this PhD thesis was obtained from the publisher.

molecules

MDPI

Article

Impact of Starch Binding Domain Fusion on Activities and Starch Product Structure of 4-α-Glucanotransferase

Yu Wang [1], Yazhen Wu [2], Stefan Jarl Christensen [3], Štefan Janeček [4,5], Yuxiang Bai [2], Marie Sofie Møller [6,*] and Birte Svensson [1,*]

1 Enzyme and Protein Chemistry, Department of Biotechnology and Biomedicine, Technical University of Denmark, DK-2800 Kongens Lyngby, Denmark
2 School of Food Science and Technology, Jiangnan University, Wuxi 214122, China
3 Protein Chemistry and Enzyme Technology, Department of Biotechnology and Biomedicine, Technical University of Denmark, DK-2800 Kongens Lyngby, Denmark
4 Laboratory of Protein Evolution, Institute of Molecular Biology, Slovak Academy of Sciences, SK-84551 Bratislava, Slovakia
5 Department of Biology, Faculty of Natural Sciences, University of SS. Cyril and Methodius, SK-91701 Trnava, Slovakia
6 Applied Molecular Enzyme Chemistry, Department of Biotechnology and Biomedicine, Technical University of Denmark, DK-2800 Kongens Lyngby, Denmark
* Correspondence: msmo@dtu.dk (M.S.M.); bis@bio.dtu.dk (B.S.)

Abstract: A broad range of enzymes are used to modify starch for various applications. Here, a thermophilic 4-α-glucanotransferase from *Thermoproteus uzoniensis* (TuαGT) is engineered by N-terminal fusion of the starch binding domains (SBDs) of carbohydrate binding module family 20 (CBM20) to enhance its affinity for granular starch. The SBDs are N-terminal tandem domains (SBD_{St1} and SBD_{St2}) from *Solanum tuberosum* disproportionating enzyme 2 (*St*DPE2) and the C-terminal domain (SBD_{GA}) of glucoamylase from *Aspergillus niger* (*An*GA). In silico analysis of CBM20s revealed that SBD_{GA} and copies one and two of GH77 DPE2s belong to well separated clusters in the evolutionary tree; the second copies being more closely related to non-CAZyme CBM20s. The activity of SBD-TuαGT fusions increased 1.2–2.4-fold on amylose and decreased 3–9 fold on maltotriose compared with TuαGT. The fusions showed similar disproportionation activity on gelatinised normal maize starch (NMS). Notably, hydrolytic activity was 1.3–1.7-fold elevated for the fusions leading to a reduced molecule weight and higher α-1,6/α-1,4-linkage ratio of the modified starch. Notably, SBD_{GA}-TuαGT and-SBD_{St2}-TuαGT showed K_d of 0.7 and 1.5 mg/mL for waxy maize starch (WMS) granules, whereas TuαGT and SBD_{St1}-TuαGT had 3–5-fold lower affinity. SBD_{St2} contributed more than SBD_{St1} to activity, substrate binding, and the stability of TuαGT fusions.

Keywords: 4-α-glucanotransferase; starch binding domain (SBD) fusion; starch modification; tandem SBDs; glycoside hydrolase family 77 (GH77); carbohydrate binding module family 20 (CBM20)

Citation: Wang, Y.; Wu, Y.; Christensen, S.J.; Janeček, Š.; Bai, Y.; Møller, M.S.; Svensson, B. Impact of Starch Binding Domain Fusion on Activities and Starch Product Structure of 4-α-Glucanotransferase. *Molecules* **2023**, *28*, 1320. https://doi.org/10.3390/molecules28031320

Academic Editor: Lesław Juszczak

Received: 9 January 2023
Revised: 26 January 2023
Accepted: 28 January 2023
Published: 30 January 2023

1. Introduction

4-α-glucanotransferases (4αGT, EC 2.4.1.25), belonging to the glycoside hydrolase family 77 (GH77) (http://www.CAZy.org, accessed on 23 December 2022) [1], catalyze four different reactions: cyclization, coupling, hydrolysis, and disproportionation [2]. The disproportionation is attractive as it involves a transfer of malto-oligosaccharides to suitable α-1,4-glucan acceptors. When the α-1,4-glucan acceptor is the α-glucan chain of the covalent enzyme-intermediate, a circular molecule is formed, named a large-ring cyclodextrin (LR-CD), by connecting the reducing and non-reducing ends [3]. When the acceptor in the disproportionation reaction is a different α-1,4-glucan chain, the transfer of a fragment to its non-reducing end can lead to elongation of exterior chains in branched α-glucan molecules [4].

Starch binding domains (SBDs), as a special group of carbohydrate binding modules (CBMs), provide numerous starch-active enzymes with enhanced affinity for different α-glucans [5]. Among the 94 CBM families (http://www.cazy.org/, accessed on 23 December 2022) [1], 15 were defined as SBDs, namely CBM20, 21, 25, 26, 34, 41, 45, 48, 53, 58, 68, 69, 74, 82, and 83 [5]. SBDs can have important affinity for α-glucans—including granular starches [6,7], show micromolar affinity for β-cyclodextrin (a starch model) [8,9], and are thought to be able to disentangle α-glucan chains of double helixes on the starch granule surface [5,8–10] offering an explanation for their stimulation of granular starch hydrolysis. Still, the main function of SBDs is considered to be molecular recognition and binding to starch granules. SBDs thus facilitate the reaction of the catalytic domains (CDs) by bringing the active site in close contact with substrate [11]. SBDs can also guide the α-glucan chain to be modified to the active site crevice on the CD [12].

The aim of the present work is to confer a thermophilic starch-modifying 4-α-glucanotransferase from *Thermoproteus uzoniensis* (TuαGT) [13] with novel functional properties by one-by-one fusion with three different SBDs, two from *Solanum tuberosum* (potato) disproportionating enzyme 2 (*St*DPE2) of the glycoside hydrolase family 77 (GH77) [14] and one from *Aspergillus niger* glucoamylase (*An*GA) of GH15 [15]. The effect on the different types of GH77 activities as obtained in the three fusions SBD_{St1}-TuαGT, SBD_{St2}-TuαGT, and SBD_{GA}-TuαGT was analysed by using maltotriose, amylose, gelatinised normal and waxy maize starches, and native waxy maize starch granules as substrates. In general, SBD-fusion increased the activity of TuαGT on amylose and gelatinised starch, but reduced the disproportionating activity on maltotriose. The SBD-TuαGTs had an increased affinity for granular starch but only slightly changed the chain length distribution of gelatinised NMS. The three SBDs exerted individual effects on the function of TuαGT. Especially, SBD_{St1} and SBD_{St2} showed different influences on the thermostability and binding affinity of TuαGT, suggesting that tandem SBDs from *St*DPE2 individually play different functional roles. Lastly, SBD-fusion can be a promising technology to change the substrate specificity and activity of enzymes.

2. Results and Discussion

2.1. 4-α-Glucanotransferase SBD Fusions

Several 4-α-glucanotransferases have been reported to contain starch binding domains (SBDs) [5,13]. To improve starch affinity and modification for TuαGT, three different fusion proteins were constructed by attaching SBDs of the family CBM20 to the N-terminus of the enzyme. Two SBDs from *Solanum tuberosum* disproportionating enzyme 2 (*St*DPE2) [14] (SBD_{St1}, the N-terminal, and SBD_{St2}, the second in tandem), and one (SBD_{GA}) from *Aspergillus niger* glucoamylase (*An*GA) [15] were used (Figure 1). The fusions of the CD and SBDs were performed via an 18-residues linker (TTGESRFVVLSDGLMREM) that naturally connects the SBD_{St1}_SBD_{St2} tandem with the CD in *St*DPE2 (Figure 1).

2.2. Bioinformatics Analysis

In order to put the three above-mentioned experimentally fused SBD_{St1}, SBD_{St2}, and SBD_{GA} into the overall context of the CBM20 family, 65 different starch hydrolases and related enzymes were selected for in silico analysis (Table 1). The emphasis was mainly on GH77 DPE2s, both from *Eukaryota* (including the *St*DPE2) and *Bacteria*, known to contain two recognizable CBM20s [16]. The set to be analysed was completed by various well-known CBM20s from amylolytic enzymes classified into several CAZy families (including *An*GA) as well as several non-CAZymes, such as phosphoglucan, water dikinase (GWD3), laforin, genethonin-1, etc. [5,16–19].

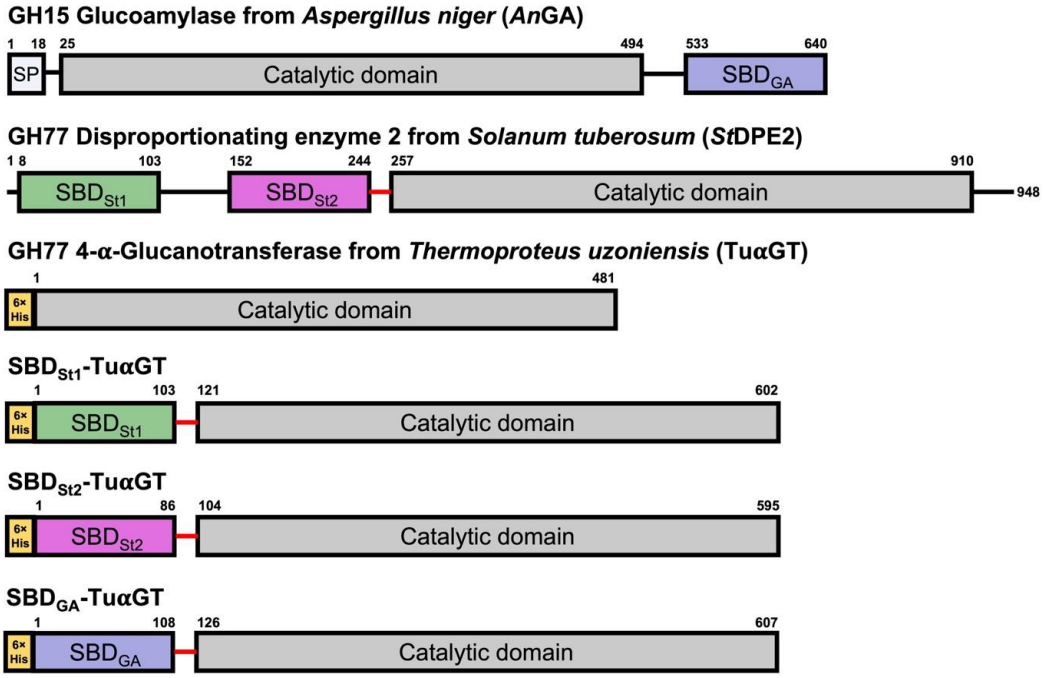

Figure 1. Domain architecture of amylolytic enzymes used in the present study. *Aspergillus niger* glucoamylase (*An*GA), *Solanum tuberosum* disproportionating enzyme 2 (*St*DPE2), 4-α-glucanotransferase from *Thermoproteus uzoniensis* (TuαGT), and the three SBD-TuαGT fusions (SBD_{St1}-TuαGT, SBD_{St2}-TuαGT, and SBD_{GA}-TuαGT) containing full length TuαGT and an SBD of family CBM20 connected to the N-terminus via an 18-residues linker (red: TTGESRFVVLSDGLMREM).

Table 1. The CBM20s originating from DPE2s, various other CAZymes, and related enzymes used in the present study [a].

No.	B/A/E [b]	Organism	Family [c]	Enzyme [d]	GenBank [e]	UniProt [e]	Length [f]	CBM20_1 [g]	CBM20_2 [g]	CBM20_3 [g]	Insert [h]
1	E	*Annona cherimola*	GH77	DPE2	ACN50178.1	C0L7E0	953	10–119	154–268		606–750
2	E	*Arabidopsis thaliana*	GH77	DPE2	AAL91204.1	Q8RXD9	955	13–122	157–270		608–752
3	E	*Chlamydomonas reinhardtii*	GH77	DPE2	EDO97689.1	A8JEI0	941	1–119	155–271		631–775
4	E	*Dictyostelium discoideum*	GH77	DPE2	EAL65318.1	Q54PW3	907	1–102	134–241		594–729
5	E	*Hordeum vulgare*	GH77	DPE2	BAJ94874.1	F2DIF3	931	1–108	143–257		595–739
6	E	*Linum tenue*	GH77	DPE2	CAI0439830.1	—	1137	10–119			499–643
7	E	*Micromonas* sp. RCC299	GH77	DPE2	ACO70268.1	C1FJ00	975	1–114	169–286		636–793
8	E	*Oryza sativa*	GH77	DPE2	BAD31425.1	Q69Q02	946	7–115	150–264		602–746
9	E	*Physcomitrella patens*	GH77	DPE2	EDQ55980.1	A9TKS8	1006	14–123	165–279		618–763
10	E	*Polysphondylium pallidum*	GH77	DPE2	EFA84397.1	D3B4Z9	1070		167–279		627–761
11	E	*Populus trichocarpa*	GH77	DPE2	EEF04969.1	B9IHJ8	975	10–119	155–268		606–750
12	E	*Ricinus communis*	GH77	DPE2	EEF38704.1	B9SCF0	901	10–119			533–676
13	E	*Selaginella moellendorffii*	GH77	DPE2	EFJ19739.1	D8S7D7	930	15–128			600–740
14	E	*Solanum tuberosum*	GH77	DPE2	AAR99599.1	Q6R608	948	1–112	147–259		597–741
15	E	*Sorghum bicolor*	GH77	DPE2	EER97686.1	C5X4T9	946	6–114	149–263		601–745
16	E	*Trichomonas vaginalis*	GH77	DPE2	EAY23705.1	A2D7I8	930	1–112	142–249		594–704
17	E	*Volvox carteri*	GH77	DPE2	EFJ42152.1	D8UDU0	995	51–178	214–329		671–786
18	B	*Alistipes finegoldii*	GH77	DPE2	AFL78258.1	I3YMP0	867		115–225		556–691
19	B	*Bacteroides thetaiotaomicron*	GH77	DPE2	AAO77253.1	Q8A5U2	893		119–235		573–714
20	B	*Barnesiella intestinihominis*	GH77	DPE2	EJZ64889.1	K0XAQ2	893	1–97	123–239		577–718

Table 1. *Cont.*

No.	B/A/E [b]	Organism	Family [c]	Enzyme [d]	GenBank [e]	UniProt [e]	Length [f]	CBM20_1 [g]	CBM20_2 [g]	CBM20_3 [g]	Insert [h]
21	B	*Dysgonomonas mossii*	GH77	DPE2	EGK04046.1	F8WZF9	888	1–95	119–231		571–712
22	B	*Elizabethkingia anophelis*	GH77	DPE2	EHM98897.1	H0KPQ2	885		119–225		572–711
23	B	*Flavobacteriaceae bacterium*	GH77	DPE2	ACU06866.1	C6X0I0	884		117–226		570–709
24	B	*Niastella koreensis*	GH77	DPE2	AEV98902.1	G8TPR9	895		127–241		579–720
25	B	*Ornithobacterium rhinotracheale*	GH77	DPE2	AFL98082.1	I4A298	874		109–217		563–698
26	B	*Paludibacter propionicigenes*	GH77	DPE2	ADQ79045.1	E4T2V1	897	1–101	128–243		582–722
27	B	*Parabacteroides distasonis*	GH77	DPE2	ABR41798.1	A6L7Y4	895	1–98	124–240		578–719
28	B	*Prevotella denticola*	GH77	DPE2	AEA21596.1	F2KWM4	897		126–233		581–722
29	B	*Succinatimonas hippei*	GH77	DPE2	EFY07743.1	E8LIB5	879		112–223		562–703
30	B	*Tannerella forsythia*	GH77	DPE2	AEW22695.1	G8UKR6	881		108–223		561–701
31	B	*Tannerella* sp. CT1	GH77	DPE2	EHL87887.1	G9S294	894		124–232		577–718
32	E	*Aspregillus kawachii*	GH13_1	AAMY	BAA22993.1	O13296	640	533–640			
33	B	*Bacillus circulans*	GH13_2	CGT	CAA55023.1	P43379	713	608–713			
34	B	*Geobacillus stearothermophilus*	GH13_2	MGA	AAA22233.1	P19531	719	609–719			
35	B	*Nostoc* sp. PC9229	GH13_2	CGT	AAM16154.1	Q8RMG0	642	534–642			
36	B	*Microbulbifer thermotolerans*	GH13_2	M3H	AID53183.1	A0A0A0Q4S7	761	657–761			
37	A	*Thermococcus* sp. B1001	GH13_2	CGT	BAA88217.1	Q9UWN2	739	629–739			
38	B	*Coralococcus* sp. EGB	GH13_6	M6H	AII00648.1	A0A076EBZ6	522	421–522			
39	B	*Streptomyces griseus*	GH13_32	AAMY	CAA40798.1	P30270	566	465–566			
40	B	*Geobacillus thermoleovorans*	GH13_39	APUL	AFI70750.1	I1WWV6	1655	1252–1349			
41	B	*Bacillus* sp. XAL601	GH13_39	APUL	BAA05832.1	Q45643	2032	1330–1427			
42	B	*Pseudomonas stutzeri*	GH13	M4H	AAA25707.1	P13507	548	446–548			
43	B	*Pseudomonas* sp. KO-8940	GH13	M5H	BAA01600.1	Q52516	614	509–614			
44	B	*Bacillus circulans*	GH13	ICGT	BAF37283.1	A0P8W9	995	888–995			
45	B	*Bacillus cereus*	GH14	BAMY	BAA75890.1	P36924	551	444–551			
46	B	*Bacillus megaterium*	GH14	BAMY	CAB61483.1	Q9RM92	545	444–545			
47	B	*Thermoanaerobacterium thermosulfurogenes*	GH14	BAMY	AAA23204.1	P19584	551	448–551			
48	E	*Aspergillus niger*	GH15	GAMY	CAA25303.1	P69328	640	533–640			
49	E	*Hormoconis resinae*	GH15	GAMY	CAA48243.1	Q03045	616	501–608			
50	E	*Penicillium oxalicum*	GH15	GAMY	EPS30575.1	S7ZIW0	616	508–616			
51	B	*Arthrobacter globiformis*	GH31	6AGT	BAD34980.1	Q6BD65	965	859–965			
52	B	*Kosmotoga_olearia*	GH57	APUL	ACR80150.1	C5CEB0	1354	32–136	155–258	267–372	
53	B	*Bacillus circulans*	GH119	AAMY	BAF37284.1	A0P8X0	1290	1183–1290			
54	E	*Aspergillus nidulans*	AA13	LPMO	CBF81866.1	Q5B1W7	385	278–385			
55	E	*Neurospora crassa*	AA13	LPMO	EAA34371.2	Q7SCE9	385	278–385			
56	A	*Thermococcus kodakarensis*	CE1	HYPO	BAD84711.1	Q5JF12	449	83–188			
57	E	*Arabidopsis thaliana*		GWD3	AAC26245.1	Q6ZY51	1196	66–166			
58	E	*Oryza sativa*		GWD3	ABA97816.2	Q2QTC2	1206	67–168			
59	E	*Branchiostoma floridae*		GPDP5	EEN65442.1	C3Y330	680	1–110			
60	E	*Homo sapiens*		GPDP5	BAA92672.1	Q9NPB8	672	1–115			
61	E	*Homo sapiens*		GEN1	AAC78827.1	O95210	358	258–358			
62	E	*Chondrus crispus*		LAF	CDF36183.1	R7QEI4	549	1–100	167–282	285–387	
63	E	*Cyanidioschyzon merolae*		LAF	BAM83396.1	M1UXX5	532	156–267	268–374		
64	E	*Homo sapiens*		LAF	AAG18377.1	O95278	331	1–124			
65	E	*Nematostella vectensis*		LAF	EDO32135.1	A7SVW9	324	1–125			

[a] Sixty-five enzyme sources resulting in eighty-seven CBM20 domains were included in the present study: (i) 17 GH77 DPE2s from *Eukarya* (numbers 1–17)—30 CBM20 sequences; (ii) 14 GH77 DPE2s from *Bacteria* (numbers 18–31)—18 CBM20 sequences; (iii) 25 enzymes representing various other CAZymes (especially amylolytic enzymes; numbers 32–56)—27 CBM20 sequences; and 9 non-CAZymes recognised as possessing CBM20 (numbers 57–65)—12 CBM20 sequences. [b] Bacterial (B), archaeal (A), or eukaryotic (E) origin. [c] CAZy family/subfamily (if known). [d] The abbreviations of enzymes are as follows: DPE2, disproportionating enzyme 2; AAMY, α-amylase; CGT, cyclodextrin glucanotransferase; MGA, maltogenic amylase; M3H, maltotriohydrolase; M6H, maltohexaohydrolase; APUL, amylopullulanase; M4H, maltotetraohydrolase; M5H, maltopentaohydrolase; ICGT, isocyclomaltooligosaccharide glucanotransferase; BAMY, β-amylase; GAMY, glucoamylase; 6AGT, 6-α-glucanotransferase; LPMO, lytic polysaccharide monooxygenase; HYPO, hypothetical protein; GWD3, glucan, water dikinase 3; GPDP5, glycerophosphodiester phosphodiesterase-5; GEN1, genethonin-1; LAF, laforin. [e] The Accession Nos. from the GenBank and UniProt databases. [f] The length of the protein, i.e., the number of amino acid residues. [g] The individual CBM20 copies. [h] The insert in DPE2 sequences. The individual groups are distinguished from each other by different colors corresponding to representatives shown in Figure 2 and Figure S1.

From the 65 selected enzymes, it was possible to sample 87 CBM20 sequences (see Table 1 for details). It is worth mentioning that although there was a stretch in almost each

DPE2 sequence (regardless the bacterial or eukaryotic origin) for two CBM20 copies at the N-terminus, only those not lacking most of the known CBM20 functionally important binding site residues [8,9,12] were taken into the analysis. Interestingly—based on a detailed inspection of their amino acid sequences—the hypothetical DPE2s from *Linum tenue* (GenBank Acc. No.: CAI0439830.1) and *Ricinus communis* (UniProt Acc. No.: B9SCF0) obviously contain only one CBM20 copy (data not shown). It is of note that of the two potential starch binding sites of CBM20, only starch binding site one, being formed by Trp543, Lys578, and Trp590 (GH15 *A. niger* glucoamylase numbering [8]), is well conserved (Figure S1), whereas residues forming starch binding site two may vary [5], as evidenced by the structural complexes of CBM20s from GH15 *A. niger* glucoamylase with cyclodextrin (Tyr527, Tyr556 and Trp563) [8] and GH13_2 *Bacillus circulans* cyclodextrin glucanotransferase with maltose (Tyr633 and Trp636) [19]—having only the tryptophan (Trp563 vs Trp 636) conserved (Figure S1). Of the SBD_{St1}, SBD_{St2}, and SBD_{GA} used in the present study, only SBD_{GA} from GH15 *A. niger* glucoamylase, that possesses all the key residues involved in binding (Figure S1), was previously demonstrated to bind starch [8]. SBD_{St1} and SBD_{St2} each lack one of the conserved residues at starch binding site one—the SBD_{St1} lysine (Lys578; *A. niger* GH15 CBM20 numbering) and the SBD_{St2} tryptophan (Trp590)—and only the tryptophan (Trp563) of starch binding site two is conserved in both; however, SBD_{St1} might have a stronger ability to bind since it has a tryptophan corresponding to Tyr527 at binding site two (Figure S1).

The evolutionary tree (Figure 2), constructed from the sequence alignment, illustrated several facts: (i) each of the two CBM20 copies from GH77 DPE2s forms its own cluster; (ii) all CBM20s from other CAZymes cluster together (including SBD_{GA} of *An*GA; cluster B) and separately from both groups covering the two CBM20 copies of GH77; (iii) the second CBM20 copy of GH77 DPE2s (including SBD_{St2} of *St*DPE2; cluster D) exhibits a closer relatedness to CBM20s from non-CAZymes (such as GWD3, laforin, genethonin-1, etc.; cluster C) than to those from other CAZyme families (cluster B); and (iv) the clade of the first CBM20 copy of GH77 DPE2s (including SBD_{St1} of *St*DPE2, cyan in Figure 2) covers also the second and the third CBM20 copies from laforins from *Cyanidioschyzon merolae* and *Chondrus crispus*, respectively, [18] (brown clade in cluster A, Figure 2) as well as the CBM20 from the four-domain GH13_2 cyclodextrin glucanotransferase from *Nostoc* sp. PC9229 [20] (green in cluster A, Figure 2). The results from the bioinformatics analysis thus indicate that the three CBM20s studied here, i.e., SBD_{St1}, SBD_{St2}, and SBD_{GA}, are positioned in three different clusters of the evolutionary tree (Figure 2) and may confer the parental enzyme TuαGT distinctly different biochemical properties by the fusion.

2.3. Biochemical Properties of TuαGT and SBD-TuαGT Fusions

The produced TuαGT, SBD_{St1}-TuαGT, SBD_{St2}-TuαGT, and SBD_{GA}-TuαGT migrated in SDS-PAGE as single protein bands estimated to 56, 68, 67, and 69 kDa (Figure 3A), respectively, in agreement with the theoretical values (see Section 3.5). The optimal reaction temperature and pH for the maltotriose disproportionation activity were around 70 °C and 7.0 for the different forms of TuαGT (Figure 3B,D). However, SBD_{GA}-TuαGT had a lower temperature optimum of 60 °C (Figure 3B). This is in good agreement with previously reported pH and temperature optima for the total activity on amylose and maltose of TuαGT at 6.0 and 75 °C [13]. TuαGT was nearly 100% active at 80 °C, indicating it is a thermophilic enzyme, which also showed significantly reduced activity at <60 °C. Notably, all three SBD-TuαGT fusions were relatively less active than TuαGT at >70 °C, but more active at <60 °C (Figure 3B). The improved affinity to starch of the SBD-fusions (see Section 2.4) may contribute to their relatively higher activity than the parent enzyme TuαGT at <60 °C, whereas the lower relative activity of the fusions at >70 °C may stem from their poorer thermostability as illustrated by the time progress for the loss of activity at 50 °C (Figure 3C). Notably, after 20 h at 50 °C, the parent TuαGT maintained ~35% activity. However, all SBD-TuαGT fusions lost more activity than TuαGT during the first 5 h at 50 °C and SBD_{St1}-TuαGT and SBD_{GA}-TuαGT retained only about 20% activity after 8 h, whereas

SBD_{St2}-TuαGT kept remarkably ~65% of its activity after 20 h (Figure 3C). Improved thermostability was previously found by N-terminal fusion of a CBM1 to β-mannanase from *Aspergillus usamii* YL-01-78 (reAuMan5A-CBM), having a temperature optimum at 75 °C compared with 70 °C for wild-type (reAuMan5A), indicating a stabilizing effect of the CBM1 on the CD [21]. In another study, Wang et al. [22] fused five different CBMs (of families CBM2, 3, 11, and 30) to the C-terminus of cis-epoxysuccinic acid hydrolase (CESH) and found a 5-times higher half-life for the CBM30-CESH than of wild-type CESH at 30 °C.

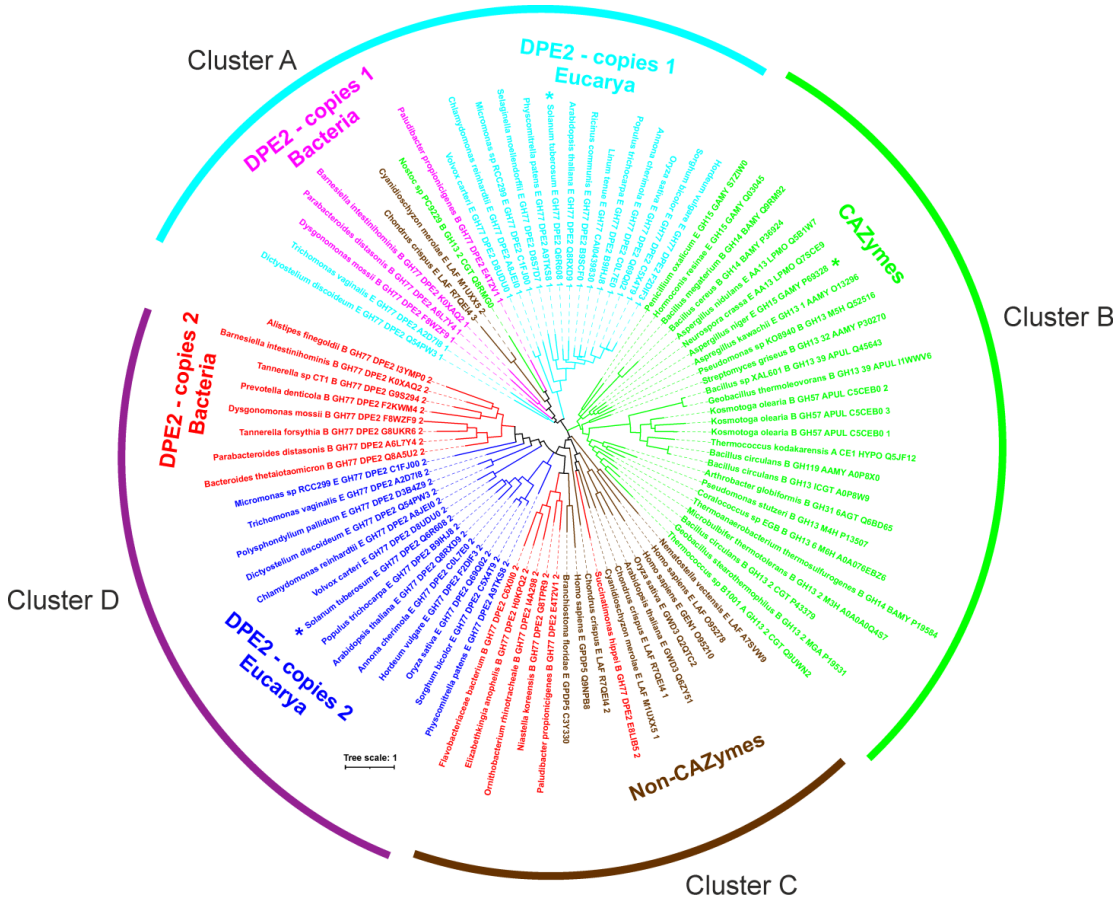

Figure 2. Phylogenetic tree of CBM20s with focus on GH77 DPE2s. The tree is based on the alignment of entire CBM20 sequences (Figure S1). The labels of protein sources consist of the name of the organism, letter "A", "B", or "E" for the archaeal, bacterial, and eukaryotic origin, respectively, CAZy family affiliation (if any), enzyme abbreviated name (for details, see Table 1), and the UniProt accession number. If there are more CBM20 copies in a single protein, the copies in the order of their appearance in the sequence are also indicated by the relevant number "1", "2", and "3" (at the end of the protein label). The three CBM20 domains, two from GH77 *Solanum tuberosum* DPE2 and one from GH15 *Aspergillus niger* glucoamylase, studied in the present work, are marked by an asterisk.

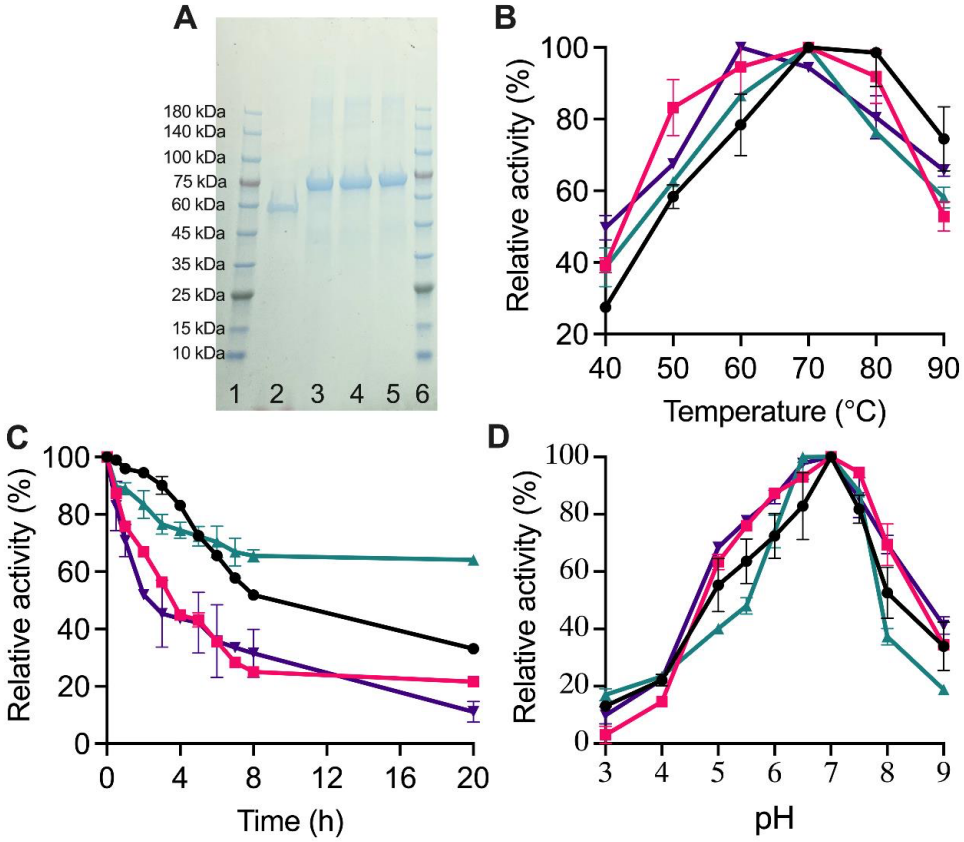

Figure 3. Biochemical characterization of TuαGT and SBD-TuαGT fusions. (**A**) SDS-PAGE of purified enzymes. Lanes 1 and 6: Marker, Lane 2: TuαGT (6.5 µg), Lane 3: SBD_{St1}-TuαGT (6.5 µg), Lane 4: SBD_{St2}-TuαGT (6.5 µg), Lane 5: SBD_{GA}-TuαGT (6.5 µg); (**B**) Temperature dependence for maltotriose disproportionation; (**C**) Thermostability at 50 °C; (**D**) pH dependence for maltotriose disproportionation. TuαGT (black), SBD_{St1}-TuαGT (red), SBD_{St2}-TuαGT (green), and SBD_{Ga}-TuαGT (purple). Activity at pH or temperature optima was defined as 100% for the individual enzymes.

2.4. Adsorption and Enzyme Kinetic Parameters

The binding capacity to WMS granules was increased for all three SBD-TuαGT fusions, revealing that the SBD domains were functional and fulfilling the purpose (Figure 4). Overall, SBD_{GA}-TuαGT had an almost 5 times higher binding capacity (B_{max}, Figure 4) and 10 times stronger affinity (K_d = 0.7 mg/mL) than TuαGT (K_d = 7.2 mg/mL). While SBD_{St1}-TuαGT and SBD_{St2}-TuαGT both had an essentially 3 times higher binding capacity to WMS granules than TuαGT, their affinity was quite similar and 5-fold larger, respectively, than of TuαGT (Figure 4). This agrees with SBD_{St1} lacking the lysine (Lys578, *An*GA numbering) and SBD_{St2} missing one of the two tryptophans (Trp590, *An*GA numbering) at starch binding site one, respectively, compared with SBD_{GA} (see Section 2.2; Figure S1). Notably, the positive effect of SBD_{St2} on binding was larger than of SBD_{St1} even though SBD_{St2} misses a tryptophan at binding site one, indicating that other features of these SBDs contribute to their binding determinants for WMS granules. This may likely include differences at the larger and more flexible binding site two, which is claimed for SBD_{GA} to be the tighter binding of the two sites [8,9]. Until now, there has been no report of different functions of the two SBDs arranged in tandem in *St*DPE2 or in other DPE2 enzymes.

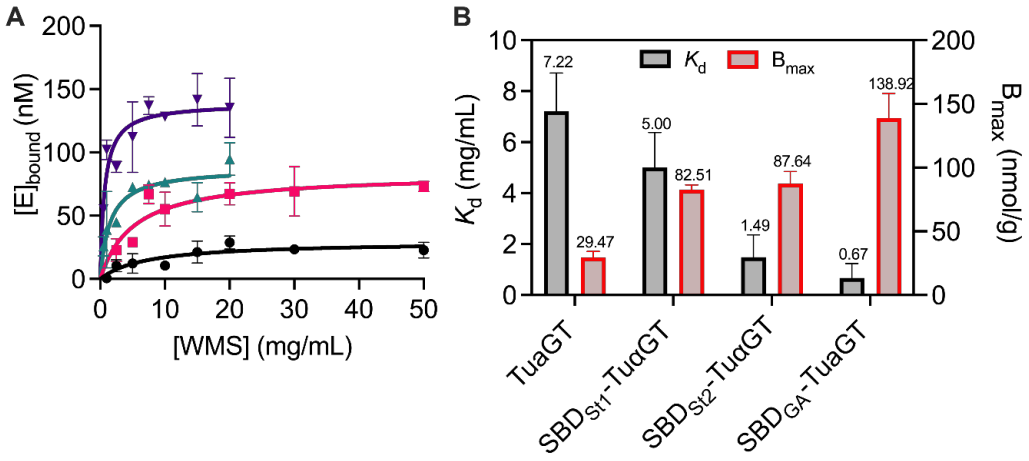

Figure 4. Binding capacity of TuαGT and SBD-TuαGT fusions on waxy maize starch (WMS) granules. (**A**) Binding isotherms on WMS granules for TuαGT (black), SBD_{St1}-TuαGT (red), SBD_{St2}-TuαGT (green), and SBD_{GA}-TuαGT (purple) at 25 °C and pH 7.0. Lines represent best fits of the Langmuir adsorption isotherm. (**B**) Dissociation constant (K_d) and (apparent) saturation coverage (B_{max}) on WMS granules.

The fusion of SBDs to TuαGT also influenced the enzymatic activity. Thus, the maltotriose disproportionation was reduced, SBD_{St2}-TuαGT and SBD_{GA}-TuαGT having slightly lower K_m than TuαGT, but 4-fold lower k_{cat}, and yielding 3-fold lower catalytic efficiency (k_{cat}/K_m) for these two fusion enzymes. Notably, k_{cat}/K_m for SBD_{St1}-TuαGT was 15-times reduced compared with TuαGT, due to a doubled K_m and an almost 9-fold lower k_{cat} (Table 2). By contrast, using amylose as a substrate, the SBD-fusion improved activity and kinetic parameters somewhat (Table 2). Thus, the similar K_m and higher k_{cat} of SBD_{St2}-TuαGT more than doubled the catalytic efficiency compared with TuαGT, whereas the overall outcome for SBD_{St1}-TuαGT and SBD_{GA}-TuαGT was essentially the same catalytic efficiency as of the parent enzyme. Overall, the kinetic analyses indicated that the SBD-fusion hampered the action of TuαGT on the oligosaccharide (maltotriose), but could improve it on the polysaccharide (amylose). Similarly, fusion of the SBD_{GA} to barley α-amylase, albeit via the much longer natural linker from *A. niger* glucoamylase (*An*GA), showed no adverse effect of the SBD on the active site integrity, as it did not change activity for soluble starch [23]. The improved catalytic efficiency for SBD_{St2}-TuαGT towards amylose may be caused by favourable polysaccharide binding to SBD_{St2}, increasing the local substrate concentration and perhaps also directing the substrate chain to the active site on the CD.

Table 2. Activity and kinetic parameters of TuαGT and SBD-TuαGT fusions towards maltotriose and amylose at 70 °C and pH 7.0.

Substrate	Parameter	TuaGT	SBD_{St1}-TuaGT	SBD_{St2}-TuaGT	SBD_{GA}-TuaGT
Maltotriose	Activity (U/mg)	27.5 ± 0.7	3.1 ± 0.5	10.3 ± 0.2	7.4 ± 0.4
	K_m (μM)	1.5 ± 0.1	3.5 ± 0.2	1.1 ± 0.1	1.4 ± 0.1
	k_{cat} (s^{-1})	0.04 ± 0.01	0.01 ± 0.0002	0.01 ± 0.002	0.01 ± 0.0005
	k_{cat}/K_m ($\mu M^{-1} \cdot s^{-1}$)	0.03 ± 0.004	0.002 ± 0.0003	0.01 ± 0.001	0.01 ± 0.0004
Amylose	Activity (U/mg)	1.3 ± 0.1	3.1 ± 0.2	2.5 ± 1.1	1.6 ± 0.9
	K_m (mg/mL)	0.6 ± 0.04	1.9 ± 0.1	0.6 ± 0.1	0.8 ± 0.02
	k_{cat} (s^{-1})	2.5 ± 0.3	7.0 ± 0.3	5.5 ± 0.4	3.3 ± 0.2
	k_{cat}/K_m ($mL \cdot [mg \cdot s]^{-1}$)	3.9 ± 0.2	3.6 ± 0.03	8.6 ± 0.4	4.0 ± 0.2

2.5. Hydrolysis and Cyclization Activities on Different Substrates

To gain insight into the modes of action of the SBD-TuαGT fusions on starch, the hydrolysis and cyclization activities were determined using different substrates (Table 3). SBD_{St1}-TuαGT had 1.3–1.7-fold higher hydrolytic activity on amylose and gelatinised starch and 1.5-fold higher cyclization activity on amylose than the TuαGT parent enzyme. Similarly, SBD_{St2}-TuαGT showed 1.5–1.7-fold increased hydrolysis of gelatinised starch, but more moderate 1.3-fold and 1.2-fold increased hydrolytic and cyclization activities, respectively, on amylose. As a glucanotransferase, it is not expected to show increased hydrolysis by SBD-fusion. However, from an industrial viewpoint, a small increase in hydrolytic activity can help to decrease the viscosity of gelatinised starch, which will also facilitate the TuαGT disproportionation reaction. Notably, for SBD_{GA}-TuαGT containing an SBD that originates from the family GH15 of glucoamylases and not from the family GH77 of 4-α-glucanotransferases, to which TuαGT belongs, the hydrolysis and cyclization activities were both essentially the same as for the parent enzyme, except for a slight increase in hydrolysis of gelatinised waxy maize starch (WMS) (Table 3). We speculate that, perhaps, the domain architecture matters and the naturally N-terminally placed SBDs from the *St*DPE2 of the family GH77, which constitutes glycoside hydrolase clan H together with GH13 and GH70 [1], are able to provide support in the different GH77 4-α-glucanotransferase reactions as opposed to the naturally C-terminally placed SBD_{GA} connected via a long *O*-glycosylated linker to the CD of glucoamylase of the family GH15 that acts in an *exo*-manner on non-reducing ends of malto-oligosaccharides and α-glucans catalysing release of glucose [24].

Table 3. Hydrolysis and cyclization by TuαGT and SBD-TuαGT fusions acting on amylose and gelatinised maize starches at 70 °C and pH 7.0.

Activity	Substrate	TuaGT	SBD_{St1}-TuaGT	SBD_{St2}-TuaGT	SBD_{GA}-TuaGT
Cyclization	Amylose	3.2 ± 0.2	4.8 ± 0.2	3.9 ± 0.3	3.3 ± 0.1
Hydrolysis	Amylose	0.3 ± 0.01	0.4 ± 0.01	0.4 ± 0.02	0.3 ± 0.01
	WMS	0.3 ± 0.02	0.5 ± 0.1	0.5 ± 0.1	0.4 ± 0.02
	NMS	0.2 ± 0.02	0.3 ± 0.03	0.3 ± 0.1	0.2 ± 0.1

2.6. Structure Analysis of Modified NMS

The modification of maize starch both by TuαGT and the SBD-TuαGT fusions significantly affected its structural properties. Chain length distribution (CLD) of NMS and modified NMS (Figure 5A) and the percentage of A-chains as well as of B_1-, B_2-, and B_3-chains (Table 4) showed that all NMS starches treated by TuαGT and its SBD-fusions, to different degrees, contained significantly fewer of the short A-chains and more of the longer B_1-, B_2-, and B_3-chains. Still, only minor differences appeared for the CLD in starches modified by the TuαGT parent compared with SBD-TuαGT fusions (Figure 5A). Previous studies on tapioca starch similarly indicated that exterior chains of amylopectin were elongated by TuαGT [13].

Table 4. Percentage of different chains in normal maize starch (NMS) before and after modification by TuαGT and SBD-TuαGT fusions.

Type of Chain [a]	NMS	TuaGT	SBD_{St1}-TuaGT	SBD_{St2}-TuaGT	SBD_{GA}-TuaGT
A-chain	67.2 ± 0.4	38.3 ± 0.7	35.8 ± 0.9	40.2 ± 2.0	41.6 ± 0.4
B_1-chain	28.0 ± 0.7	46.3 ± 2.0	52.0 ± 1.5	43.8 ± 3.0	45.1 ± 2.0
B_2-chain	4.4 ± 0.2	13.5 ± 0.8	10.2 ± 0.9	11.7 ± 0.9	11.8 ± 1.9
B_3-chain	0.6 ± 0.03	2.5 ± 0.2	2.5 ± 0.3	2.6 ± 0.6	1.9 ± 0.5

[a] A-chain: DP 1–12, B_1-chain: DP 13–24, B_2-chain: DP 25–36, and B_3-chains: DP > 37.

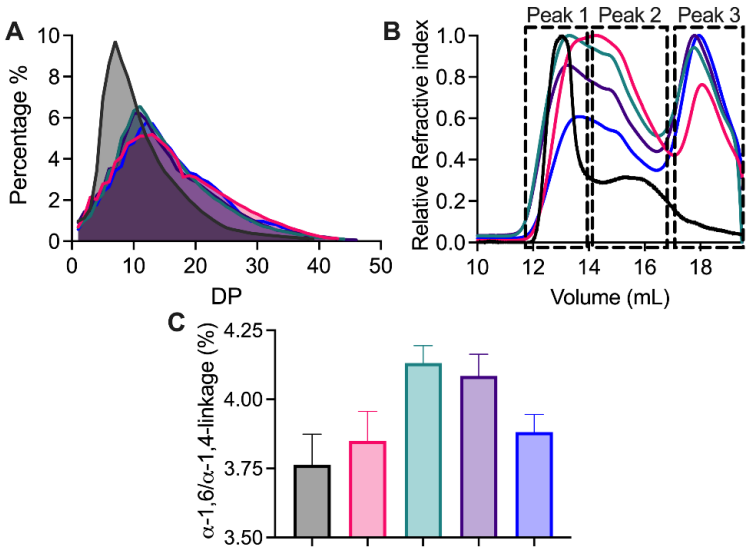

Figure 5. Structural analysis of NMS modified by TuαGT and SBD-TuαGT fusions. (**A**) Chain length distribution; (**B**) Molecular weight distribution; (**C**) ^{1}H-NMR analysis of α-1,6/α-1,4 linkage ratio. Before (black), after modification by TuαGT (red), SBD_{St1}-TuαGT (green), SBD_{St2}-TuαGT (purple), and SBD_{GA}-TuαGT (blue).

The molecular weight distribution of NMS before and after enzyme treatment was analysed by SEC-MALLS-RI (Figure 5B). Before modification, typical amylopectin (peak 1) and amylose (peak 2) molecules were observed in NMS by SEC. However, after the enzyme modification, three peaks were observed, namely the peaks one and two as well as a distinct later eluting peak three of smaller polysaccharide chains. Furthermore, a later elution of peak one from all modified starch samples indicated that amylopectin has a reduced molecular weight and was less well resolved from peak two than found for unmodified NMS. The newly appearing prominent peak three of smaller molecules may contain large-ring cyclodextrins (LR-CDs) produced in cyclization reactions [25] as well as polysaccharide hydrolysis products.

To further understand the reaction of TuαGT and the SBD-TuαGT fusions, the α-1,6/α-1,4-linkage ratio that indicates the degree of branching, was determined for the modified starches by using ^{1}H-NMR (Figure 5C). NMS modified by TuαGT and SBD_{GA}-TuαGT showed a slight increase in the α-1,6/α-1,4-linkage ratio from 3.76 for unmodified to 3.84 and 3.88%, respectively, after modification, whereas treatment by SBD_{St1}-TuαGT and SBD_{St2}-TuαGT increased the ratio to 4.13 and 4.08%, respectively. As TuαGT can catalyze hydrolysis, disproportionation, cyclization, and coupling, which all involve α-1,4-linkages, the increase in the α-1,6/α-1,4-linkage ratio can reflect the level of hydrolysis, in which α-1,4 linkages are lost and not generated, in agreement with the two fusions with SBD_{St1} and SBD_{St2}, i.e., the SBDs from *St*DPE2 belonging to the family GH77, showing an increased degree of hydrolysis of gelatinised NMS compared with TuαGT (Figure 5B; Table 3).

3. Material and Methods

3.1. Materials

Amylose (potato), maltotriose, and protease inhibitor cocktail tablets (cOmplete™, Mini, EDTA-free Protease Inhibitor Cocktail) were purchased from Sigma-Aldrich Co. Ltd. (St. Louis, MO, USA). Pullulanase M2 (from *Bacillus licheniformis*, 900 U/mL) and β-amylase (from barley, 600 U/mg) were purchased from Megazyme Co. Ltd. (Wicklow, Ireland). Waxy maize starch (WMS) was the kind gift of Cargill (USA) and normal maize starch (NMS) of Archer Daniels Midland (ADM, Decatur, IL, USA).

3.2. Bioinformatics Analysis of CBM20

In total, 87 CBM20 domains from 65 different amylolytic and related enzymes were collected (Table 1) based on previous studies focused on GH77 DPE2s and different starch-binding domain CBM families [5,16–19]. All sequences were retrieved from GenBank (https://www.ncbi.nlm.nih.gov/genbank/, accessed on 23 December 2022; [26]) and/or UniProt (https://www.uniprot.org/, accessed on 23 December 2022) [27]) sequence databases. For DPE2s selected from various bacteria and eukaryotes, the number of CBM20 copies and their borders in respective sequences were taken from UniProt [27] and complemented by data available from the literature [5,16–18]; questionable cases were also verified in the InterPro database (https://www.ebi.ac.uk/interpro/, accessed on 23 December 2022 [28]). Although each studied DPE2 could eventually contain two CBM20 copies in tandem at their N-terminus, putative CBM20 copies that lacked most of the functionally important binding site residues were not considered (Table 1). For CAZymes, the appropriate CAZy classification has been checked against the CAZy database (http://www.cazy.org/, accessed on 23 December 2022; [1]) and published data [5,16–19]. Sequences were aligned using the program Clustal Omega (https://www.ebi.ac.uk/Tools/msa/clustalo/, accessed on 23 December 2022; [29]) and the alignment was confirmed by comparison of three-dimensional structures of selected CBM20s: (i) two experimentally determined structures from *Aspergillus niger* GH15 glucoamylase [8,9] and *Bacillus circulans* GH13_2 cyclodextrin glucanotransferase [19] retrieved from Protein Data Bank (PDB; https://www.rcsb.org/, accessed on 23 December 2022; [30]) under their PDB codes 1AC0 and 1CXE, respectively; and (ii) the modelled structure of *Solanum tuberosum* GH77 DPE2 taken from the AlphaFold database (https://alphafold.ebi.ac.uk, accessed on 23 December 2022; [31]) via its UniProt accession No.: Q6R608. The corresponding CBM20 structures were superimposed using the program MultiProt (http://bioinfo3d.cs.tau.ac.il/MultiProt/, accessed on 23 December 2022; [32]). Since the structure superimpositions did not identify any significant discrepancies with the sequence alignment, the Clustal Omega program-produced output was used for calculating the maximum-likelihood evolutionary tree by the bootstrapping procedure with 1000 bootstrap trials [33], implemented in the MEGA-X package [34]. The calculated tree file was displayed with the program iTOL (https://itol.embl.de/, accessed on 23 December 2022; [35]).

3.3. Construction of TuαGT and SBD-TuαGT Fusions

4-α-Glucanotransferase from *Thermoproteus uzoniensis* (TuαGT, GenBank Accession WP_013679179.1) was produced recombinantly essentially as described [13]. Genes codon-optimised for *Escherichia coli* encoding full-length TuαGT connected N-terminally to the indicated SBD (SBD_{St1}, Uniprot Accession Q6R608_2 residues 3–112; SBD_{St2}, Uniprot Accession Q6R608_2 residues 147–259; SBD_{GA}, Uniprot Accession P69328.1, residues 538–639) via an 18-residues linker (TTGESRFVVLSDGLMREM), that naturally connects the SBD_{St1}-SBD_{St2} tandem with the CD in *St*DPE2 [14], were purchased and cloned into the expression vector pET-28a (+) using the restriction sites NheI and XhoI (GenScript, Leiden, The Netherlands) in frame with the N-terminal His-tag.

3.4. Production of TuαGT and SBD-TuαGT Fusions

TuαGT, SBD_{St1}-TuαGT, SBD_{St2}-TuαGT, and SBD_{GA}-TuαGT encoding plasmids were transformed into *E. coli* BL21(DE3)* and screened on Lysogeny broth (LB) agar containing 50 μg/mL kanamycin for selection. Starter cultures (10 mL) made by inoculating LB medium (1% tryptone, 0.5% yeast extract, 0.5% NaCl, 50 μg/mL kanamycin) with a single colony and incubating (37 °C, 170 rpm, overnight) were used to inoculate 800 mL LB medium containing 10 mM glucose and 50 μg/mL kanamycin in shake flasks. Expression was induced at A_{600} = 0.6 by adding isopropyl-β-D-thiogalactopyranoside (IPTG) to 0.2 mM and incubated (18 °C, 160 rpm, 24 h). The cells were harvested (4000× *g*, 4 °C, 30 min) and stored at −20 °C until protein purification.

3.5. Purification of TuαGT and SBD-TuαGT Fusions

Cells (5 g) were thawed and resuspended in 20 mL HisTrap equilibration buffer (20 mM Hepes, 250 mM NaCl, 10% glycerol, pH 7.5), added 1 protease inhibitor cocktail tablet, lysed using a high-pressure homogenizer at 1 bar, added 2 µL Benzonase Nuclease (Sigma-Aldrich, St. Louis, MO, USA), and centrifuged (40,000× *g*, 4 °C, 30 min). The supernatant (~20 mL) was mixed with 2 mL HisPur™ nickel-nitrilotriacetic acid resin (Thermo Fisher Scientific, Waltham, MA, USA) pre-equilibrated with equilibration buffer and washed with 20 column volumes (CV) of equilibration buffer, added 10 mM imidazole. Bound protein was eluted by 10 CV of equilibration buffer, added 300 mM imidazole. Protein-containing fractions were pooled (10 mL) and further purified by gel filtration (Superdex 16/60 200 pre-equilibrated with 20 mM Hepes, 150 mM NaCl, 10% glycerol, pH 7.5) at a flow rate of 1 mL/min. Fractions containing disproportionation activity on maltotriose were pooled and buffer-exchanged to ion exchange chromatography equilibration buffer (20 mM Hepes, 10% glycerol, pH 7.5) using Amicon® Ultra-15 Centrifugal Filter Unit (Ultracel-30 regenerated cellulose membrane, 15 mL sample volume, Merck), concentrated to 2 mL using centrifugal filters (30 kDa MWCO; Amicon® Ultra), filtrated (0.45 µm), and loaded onto a Resource Q column (1 mL, Cytiva), pre-equilibrated with 15 CV equilibration buffer, and eluted by 50 CV of a linear gradient from 0 to 800 mM NaCl in equilibration buffer. Fractions presenting activity were verified by SDS-PAGE to contain TuαGT, SBD_{St1}-TuαGT, SBD_{St2}-TuαGT, and SBD_{GA}-TuαGT with theoretical molecular weights calculated to 55,593, 68,272, 67,068, and 69,562 Da, respectively (https://web.expasy.org/protparam/, accessed on 23 December 2022). Protein concentrations were determined spectrophotometrically at 280 nm (Nanodrop Lite, Thermo Scientific, USA) using theoretical extinction coefficients (ε) for TuαGT, SBD_{St1}-TuαGT, SBD_{St2}-TuαGT and SBD_{GA}-TuαGT of 141,750, 172,690, 160,200, 172,630 $M^{-1}cm^{-1}$, respectively (https://web.expasy.org/protparam/, accessed on 23 December 2022). Recombinant SBD-TuαGT fusion proteins and TuαGT wild type were obtained in yields of 0.05–0.1 and 2.5 mg, respectively, per 5 g *E. coli* cells from 0.8 L culture.

3.6. Enzyme Activity Assays

3.6.1. Total Activity

The total activity of TuαGT and the SBD-TuαGT fusions was determined by incubating amylose (2 mg/mL) in 900 µL assay buffer (50 mM Hepes, pH 7.0, 150 mM NaCl) with 100 µL enzyme (20 nM, final concentration) at 75 °C for 10 min [13]. The reaction was terminated by heating (99 °C, 15 min), and the amylose concentration was determined by mixing 20 µL heated sample with 200 µL iodine reagent (0.2% KI + 0.02% I_2) for 1 min. The absorbance was measured at 620 nm (microplate reader, PowerWave XS, BIO-TEK) [36]. One unit of total activity was defined as the amount of enzyme degrading 0.5 mg/mL amylose per min under the above conditions.

3.6.2. Disproportionation

The disproportionation activity of TuαGT and SBD-TuαGT fusions was determined as reported [13] by incubating 1% (19.8 mM) maltotriose in 900 µL assay buffer (see Section 3.6.1) with 100 µL enzyme (10 nM, final concentration) at 75 °C for 1 h. The reaction was terminated (99 °C, 15 min) and the released glucose was quantified using the GOPOD assay (D-Glucose Assay Kit, Megazyme) with glucose (0–1000 µM) as standard [37]. One unit of disproportionation activity was defined as the amount of enzyme releasing 1 µmol/min glucose under the above conditions.

3.6.3. Hydrolysis

The hydrolytic activity of TuαGT and the SBD-TuαGT fusions was determined by incubating 2 mg/mL amylose in 900 µL assay buffer (see Section 3.6.1) with 100 µL enzyme (20 µM, final concentration) at 70 °C for 1 h [38]. Hydrolytic activity towards 25 mg/mL NMS (gelatinised at 99 °C, 30 min, 1100 rpm, and cooled to 70 °C before the assay) was

determined by addition of enzyme (2 µM, final concentration) and incubated (70 °C, 1 h). The reaction was stopped by the PAHBAH reagent (1:1, *v*:*v*), heating (95 °C, 10 min) [39] and the absorbance was measured at 405 nm after cooling. One unit of activity was defined as the amount of enzyme releasing 1 µmol/min reducing sugar under the above conditions. Glucose (0–1000 µM) was used for the standard curve.

3.6.4. Cyclization

The cyclization activity of TuαGT and SBD-TuαGT fusions was determined by incubating 2 mg/mL amylose in 900 µL assay buffer (see Section 3.6.1) with 100 µL enzyme (20 µM, final concentration) at 70 °C for 1 h [40]. The reaction was terminated (99 °C, 15 min), and 0.24 U β-amylase was added and incubated at 40 °C for 10 h to degrade remaining amylose. The reaction was stopped by adding the PAHBAH reagent (1:1, *v*:*v*) and the absorbance was measured at 405 nm (as in Section 3.6.3). The amount of formed cycloamylose was determined by the difference of maltose released by β-amylase from untreated amylose and from amylose treated with TuαGT and SBD-TuαGT fusions. One unit of cyclization activity was defined as the amount of enzyme leading to release of 1 µmol less maltose per min under the above conditions using maltose (0–1000 µM) for the standard curve.

3.7. Effect of pH and Temperature on Activity

The pH optimum was determined at the optimum temperature 70 °C of TuαGT using the disproportionation activity assay (see Section 3.6.2) in universal buffer (20 mM MES, 20 mM Hepes, 150 mM NaCl, pH 4.0–9.0) [41]. The temperature optimum in the range of 50–90 °C was determined at the optimum pH 7.0 of TuαGT in the above buffer. To assess thermostability, TuαGT and SBD-TuαGT fusions (100 nM) were incubated at 50 °C and pH 7.0 (50 mM Hepes buffer, 150 mM NaCl) and the residual enzyme activity was measured during 8 h with 1 h intervals. The activity before incubation defined 100% stability.

3.8. Kinetic Parameters

Enzyme (10 nM, final concentration) was incubated (70 °C, 300 rpm) with maltotriose (1 mL; six concentrations, 0.5–7.5 µM) in assay buffer (see Section 3.6.1). Aliquots (100 µL) removed at 1, 2, 5, 10, 15 min were mixed with 20 µL 0.2 M NaOH (10 min), neutralized by 20 µL 0.2 M HCl, and the rate of glucose release was determined (see Section 3.6.2). Enzyme (10 nM, final concentration) was incubated (70 °C, 300 rpm) with amylose (1 mL; six concentrations, 0.1–2 mg/mL) in assay buffer (see Section 3.6.1). Aliquots (100 µL) removed at 1, 2, 5, 10, 15 min were mixed with DNS reagent (100 µL) and heated (99 °C, 5 min). After cooling, the absorbance was measured at 520 nm. V_{max}, K_m, and k_{cat} were calculated by fitting the Michaelis–Menten equation using GraphPad Prism 6 (GraphPad Software Inc., San Diego, CA, USA).

3.9. Adsorption to Starch Granules

The binding capacity of TuαGT and SBD-TuαGT fusions on WMS granules at 25 °C was determined under the same conditions as used for the activity assay (see Section 3.6.1) by adding enzyme (200 nM, final concentration) to different WMS concentrations from 0.5 to 75 mg/mL [42]. After 10 min the mixtures were centrifuged (10,000× *g*, 5 min) and 100 µL supernatant was added to 100 µL 2.5-fold diluted protein assay dye reagent (Bio-Rad). The enzyme concentration was determined from the ratio of absorbance values at 590 over 450 nm using TuαGT and SBD-TuαGT (0–1.0 µM) as standards. The Langmuir isotherm (Equation (1)) is a commonly used model for analysis of molecular binding and was fitted to the results using GraphPad Prism 6 (GraphPad Software Inc.), where K_d is the dissociation constant, Γ is the bound protein concentration, and B_{max} is the (apparent) saturation coverage.

$$\Gamma = \frac{B_{max} \cdot E_{free}}{K_d + E_{free}} \quad (1)$$

3.10. Preparation of Modified Maize Starch (MMS)

Enzymatic modification of NMS was performed essentially as reported [13]. Starch (6%, *w*/*v*) was suspended in activity assay buffer (see Section 3.6.1) and gelatinised (99 °C, 30 min, 1100 rpm). The modification was carried out by 1 µmol TuαGT or SBD-TuαGT fusions per 1 g starch at 70 °C for 8 h, and terminated by heating (99 °C, 30 min). The modified starch was precipitated by three volumes of ethanol overnight and isolated by centrifugation (4000× *g*, 10 min). The precipitated starch was kept overnight at −80 °C and freeze-dried for further analysis.

3.11. Molecular Weight Distribution

Size exclusion chromatography with multi-angle laser light scattering-refractive index detector (SEC-MALLS-RI) was used to analyse the molecular weight of starch samples [43]. Dry starch (5 mg/mL) was suspended in a mixture of DMSO and MilliQ water (9:1, *v*/*v*) and gelatinised on a boiling water bath (1 h, shaking every 10 min) until the solution was clear and free of floc. The gelatinised starch was incubated (30 °C, 250 rpm, 48 h) to disrupt remaining starch particles. The samples were re-boiled and filtrated through a 0.45 µm filter. Filtrate (100 µL) was injected on a tandem column (Ohpak SB-804 HQ, Ohpak SB-806 HQ) using 0.1 M $NaNO_3$ (in 0.02% NaN_3) as mobile phase at a flow rate of 0.6 mL/min with the column temperature set at 50 °C. Data obtained from the MALLS and RI detectors were analysed by ASTRA software version 5.3.4 (Wyatt Technologies).

3.12. Chain Length Distribution

High performance anion exchange chromatography with pulsed amperometric detection (HPAEC-PAD) was used to analyse the chain length distribution of NMS before and after enzyme modification. Starch (5 mg/mL, dry solid (*w*/*v*)) was suspended in 50 mM sodium acetate, pH 4.5, followed by gelatinisation (99 °C, 30 min). The gelatinised starch was debranched by incubation with 0.18 U pullulanase per 5 mg starch at 42 °C for 12 h and centrifuged (10,000× *g*, 10 min). The supernatant was analysed by HPAEC-PAD [44].

3.13. 1H-NMR

1D ^{1}H NMR spectra of starch samples were acquired using a 600 MHz NMR spectrometer (Bruker Avance III, Bruker Biospin, Rheinstetten, Germany) [45]. Starch (5 mg/mL, dry solid (*w*/*v*)) was suspended in D_2O, gelatinised (99 °C, 2 h), freeze-dried twice, dissolved in DMSO-d6 (90% DMSO-d6 in 10% D_2O), and heated (99 °C, 30 min) before analysis. The percentage of glucan branch points of starch samples was estimated using the areas of signals representing anomeric protons (δ 5.35–5.45 α-1,4; δ 4.95–5.00 α-1,6).

4. Conclusions

In the present work, three phylogenetically diverse SBDs, two from *St*DPE2 and one from *An*GA, fused one by one via an 18-residues linker to the N-terminus of the thermophilic 4-α-glucotransferase (TuαGT), conferred the TuαGT with altered distinct substrate binding and activity characteristics. The bioinformatics analysis shows the distant relationship between SBD_{St1}, SBD_{St2}, and SBD_{GA} each found in well-separated clusters of the evolutionary tree and sharing this position with close homologues, i.e., copies one and two of GH77 DPE2s and SBDs from various CAZymes. Relative to the parent enzyme TuαGT, the SBD_{St2}-fusion had improved thermostability after 5 h of thermal treatment and also doubled the disproportionation activity on amylose. By contrast, all three SBD-fusions decreased the disproportionation activity using maltotriose as substrate. The SBD_{GA}-fusion resulted in the highest binding affinity and binding capacity on starch granules, presumably reflecting the superior function of the two binding sites in this SBD containing all of the canonical aromatic residues. The structural analysis of starch before and after modification by TuαGT and the three SBD-fusion enzymes indicated that the fusion with SBD_{St1} and SBD_{St2} enhanced hydrolysis the most, along with their highest cyclization activity, and a slightly higher loss of the short A chains and gain of B chains, which is caused by the

disproportionation reaction, compared with fusion by SBD_{GA}. As is known for TuαGT, the starch products may represent nutritional values reminiscent of resistant starch dietary fibres. According to the separation in the evolutionary tree and the different functional improvements, we conclude that SBD_{St1} and SBD_{St2} contribute different effects by fusion with TuαGT and that they probably play different, albeit not yet identified, functional roles in the *St*DPE2. In the longer perspective, the obtained results disclose the potential for utilising insight into the wide diversity of SBDs for enzyme engineering and also to connect individual properties of the two "in tandem" SBDs with structure/function relationships of disproportionating enzymes in plants and bacteria.

Supplementary Materials: The following supporting information can be downloaded at: https://www.mdpi.com/article/10.3390/molecules28031320/s1, Figure S1: Sequence alignment of CBM20s with focus on GH77 DPE2s.

Author Contributions: M.S.M. and B.S. conceived the study and edited the manuscript; Y.W. (Yu Wang) designed and performed the experiments, collected data, and drafted the manuscript; Y.W. (Yazhen Wu) performed molecular weight and ^{1}H-NMR analysis; S.J.C. collected CLD data; Š.J. did the bioinformatics; Y.B. edited the manuscript. All authors contributed to revision and editing of the manuscript. All authors have read and agreed to the published version of the manuscript.

Funding: This work was supported by a China Scholarship Council (CSC) grant #202006790033 (to YW), Technical University of Denmark, National Natural Science Foundation of China (No. 32072268), Fundamental Research Funds for the Central Universities (JUSRP2050205), a travel grant from Otto Mønsteds Fond (22-81-1681),and Slovak Grant Agency VEGA (No. 2/0146/21).

Institutional Review Board Statement: Not applicable.

Informed Consent Statement: Not applicable.

Data Availability Statement: All available data are included in the article.

Acknowledgments: Karina Jansen (Department of Biotechnology and Biomedicine, Technical University of Denmark, Denmark) is gratefully acknowledged for technical assistance. We are thankful to Cargill for providing waxy maize starch and to Archer Daniels Midland for providing normal maize starch.

Conflicts of Interest: The authors declare that they have no competing financial interest or personal relationship influencing the work reported in this paper.

Sample Availability: Samples of the compounds are available from the authors.

Abbreviations

*An*GA: glucoamylase from *Aspergillus niger;* CBM, carbohydrate binding module; CD, catalytic domain; CLD, chain length distribution; CV, column volumes; LR-CD, large-ring cyclodextrin; NMS, normal maize starch; SBD, starch binding domain; *St*DPE2, disproportionating enzyme 2 from *Solanum tuberosum*; TuαGT, 4-α-glucanotransferase from *Thermoproteus uzoniensis*.

References

1. Drula, E.; Garron, M.L.; Dogan, S.; Lombard, V.; Henrissat, B.; Terrapon, N. The carbohydrate-active enzyme database: Functions and literature. *Nucleic Acids Res.* **2022**, *50*, D571–D577. [CrossRef] [PubMed]
2. Park, J.H.; Kim, H.J.; Kim, Y.H.; Cha, H.; Kim, Y.W.; Kim, T.J.; Kim, Y.R.; Park, K.H. The action mode of *Thermus aquaticus* YT-1 4-α-glucanotransferase and its chimeric enzymes introduced with starch-binding domain on amylose and amylopectin. *Carbohydr. Polym.* **2007**, *67*, 164–173. [CrossRef]
3. Suksiri, P.; Ismail, A.; Sirirattanachatchawan, C.; Wangpaiboon, K.; Muangsin, N.; Tananuwong, K.; Krusong, K. Enhancement of large ring cyclodextrin production using pretreated starch by glycogen debranching enzyme from *Corynebacterium glutamicum*. *Int. J. Biol. Macromol.* **2021**, *193*, 81–87. [CrossRef] [PubMed]
4. Li, X.; Wang, Y.; Wu, J.; Jin, Z.; Dijkhuizen, L.; Abou Hachem, M.; Bai, Y. *Thermoproteus uzoniensis* 4- α -glucanotransferase catalyzed production of a thermo-reversible potato starch gel with superior rheological properties and freeze-thaw stability. *Food Hydrocoll.* **2023**, *134*, 108026. [CrossRef]

5. Janecek, S.; Marecek, F.; MacGregor, E.A.; Svensson, B. Starch-binding domains as CBM families—History, occurrence, structure, function and evolution. *Biotechnol. Adv.* **2019**, *37*, 107451. [CrossRef] [PubMed]
6. Williamson, G.; Belshaw, N.J.; Williamson, M.P. O-glycosylation in *Aspergillus* glucoamylase. Conformation and role in binding. *Biochem. J.* **1992**, *282*, 423–428. [CrossRef]
7. Paldi, T.; Levy, I.; Shoseyov, O. Glucoamylase starch-binding domain of *Aspergillus niger* B1: Molecular cloning and functional characterization. *Biochem. J.* **2003**, *372*, 905–910. [CrossRef]
8. Sorimachi, K.; Le Gal-Coëffet, M.-F.; Williamson, G.; Archer, D.B.; Williamson, M.P. Solution structure of the granular starch binding domain of *Aspergillus niger* glucoamylase bound to β-cyclodextrin. *Structure* **1997**, *5*, 647–661. [CrossRef]
9. Giardina, T.; Gunning, A.P.; Juge, N.; Faulds, C.B.; Furniss, C.S.M.; Svensson, B.; Morris, V.J.; Williamson, G. Both binding sites of the starch-binding domain of *Aspergillus niger* glucoamylase are essential for inducing a conformational change in amylose. *J. Mol. Biol.* **2001**, *313*, 1149–1159. [CrossRef]
10. Southall, S.M.; Simpson, P.J.; Gilbert, H.J.; Williamson, G.; Williamson, M.P. The starch-binding domain from glucoamylase disrupts the structure of starch. *FEBS Lett.* **1999**, *447*, 58–60. [CrossRef]
11. Armenta, S.; Moreno-Mendieta, S.; Sánchez-Cuapio, Z.; Sánchez, S.; Rodríguez-Sanoja, R. Advances in molecular engineering of carbohydrate-binding modules. *Proteins* **2017**, *85*, 1602–1617. [CrossRef] [PubMed]
12. Penninga, D.; van der Veen, B.A.; Knegtel, R.M.A.; van Hijum, S.A.F.T.; Rozeboom, H.J.; Kalk, K.H.; Dijkstra, B.W.; Dijkhuizen, L. The raw starch binding domain of cyclodextrin glycosyltransferase from *Bacillus circulans* strain 251. *J. Biol. Chem.* **1996**, *271*, 32777–32784. [CrossRef] [PubMed]
13. Wang, Y.; Li, X.; Ji, H.; Zheng, D.; Jin, Z.; Bai, Y.; Svensson, B. Thermophilic 4-α-glucanotransferase from *Thermoproteus uzoniensis* retards the long-term retrogradation but maintains the short-term gelation strength of tapioca starch. *J. Agric. Food Chem.* **2020**, *68*, 5658–5667. [CrossRef] [PubMed]
14. Lloyd, J.R.; Blennow, A.; Burhenne, K.; Kossmann, J. Repression of a novel isoform of disproportionating enzyme (*St*DPE2) in potato leads to inhibition of starch degradation in leaves but not tubers stored at low temperature. *Plant Physiol.* **2004**, *134*, 1347–1354. [CrossRef]
15. Svensson, B.; Pedersen, T.; Svendsen, I.; Sakai, T.; Ottesen, M. Characterization of two forms of glucoamylase from *Aspergillus niger*. *Carlsb. Res. Commun.* **1982**, *47*, 55–69. [CrossRef]
16. Kuchtova, A.; Janecek, S. In silico analysis of family GH77 with focus on amylomaltases from borreliae and disproportionating enzymes DPE2 from plants and bacteria. *Biochim. Biophys. Acta* **2015**, *1854*, 1260–1268. [CrossRef]
17. Janecek, S.; Svensson, B.; MacGregor, E.A. Structural and evolutionary aspects of two families of non-catalytic domains present in starch and glycogen binding proteins from microbes, plants and animals. *Enzyme Microb. Technol.* **2011**, *49*, 429–440. [CrossRef]
18. Kuchtova, A.; Gentry, M.S.; Janecek, S. The unique evolution of the carbohydrate-binding module CBM20 in laforin. *FEBS Lett.* **2018**, *592*, 586–598. [CrossRef]
19. Knegtel, R.M.A.; Strokopytov, B.; Penninga, D.; Faber, O.G.; Rozeboom, H.J.; Kalk, K.H.; Dijkhuizen, L.; Dijkstra, B.W. Crystallographic studies of the interaction of cyclodextrin glycosyltransferase from *Bacillus circulans* strain 251 with natural substrates and products. *J. Biol. Chem.* **1995**, *270*, 29256–29264. [CrossRef]
20. Janecek, S.; Svensson, B.; MacGregor, E.A. Relation between domain evolution, specificity, and taxonomy of the α-amylase family members containing a C-terminal starch-binding domain. *Eur. J. Biochem.* **2003**, *270*, 635–645. [CrossRef]
21. Tang, C.D.; Li, J.F.; Wei, X.H.; Min, R.; Gao, S.J.; Wang, J.Q.; Yin, X.; Wu, M.C. Fusing a carbohydrate-binding module into the *Aspergillus usamii* β-mannanase to improve its thermostability and cellulose-binding capacity by in silico design. *PLoS ONE* **2013**, *8*, e64766. [CrossRef] [PubMed]
22. Wang, S.; Cui, G.Z.; Song, X.F.; Feng, Y.; Cui, Q. Efficiency and stability enhancement of cis-epoxysuccinic acid hydrolase by fusion with a carbohydrate binding module and immobilization onto cellulose. *Appl. Biochem. Biotechnol.* **2012**, *168*, 708–717. [CrossRef] [PubMed]
23. Juge, N.; Nøhr, J.; Le Gal-Coëffet, M.F.; Kramhøft, B.; Furniss, C.S.M.; Planchot, V.; Archer, D.B.; Williamson, G.; Svensson, B. The activity of barley α-amylase on starch granules is enhanced by fusion of a starch binding domain from *Aspergillus niger* glucoamylase. *Biochim. Biophys. Acta* **2006**, *1764*, 275–284. [CrossRef] [PubMed]
24. Sauer, J.; Sigurskjold, B.W.; Christensen, U.; Frandsen, T.P.; Mirgorodskaya, E.; Harrison, M.; Roepstorff, P.; Svensson, B. Glucoamylase: Structure/function relationships, and protein engineering. *Biochim. Biophys. Acta* **2000**, *1543*, 275–293. [CrossRef]
25. Rho, S.J.; Mun, S.; Hong, J.S.; Kim, Y.L.; Do, H.V.; Kim, Y.W.; Han, S.I.; Kim, Y.R. Physicochemical interactions of cycloamylose with phenolic compounds. *Carbohydr. Polym.* **2017**, *174*, 980–989. [CrossRef]
26. Sayers, E.W.; Cavanaugh, M.; Clark, K.; Pruitt, K.D.; Schoch, C.L.; Sherry, S.T.; Karsch-Mizrachi, I. GenBank. *Nucleic Acids Res.* **2021**, *49*, D92–D96. [CrossRef]
27. UniProt Consortium. UniProt: The universal protein knowledgebase in 2021. *Nucleic Acids Res.* **2021**, *49*, D480–D489. [CrossRef]
28. Blum, M.; Chang, H.-Y.; Chuguransky, S.; Grego, T.; Kandasaamy, S.; Mitchell, A.; Nuka, G.; Paysan-Lafosse, T.; Qureshi, M.; Raj, S.; et al. The InterPro protein families and domains database: 20 years on. *Nucleic Acids Res.* **2021**, *49*, D344–D354. [CrossRef]
29. Sievers, F.; Wilm, A.; Dineen, D.; Gibson, T.J.; Karplus, K.; Li, W.; Lopez, R.; McWilliam, H.; Remmert, M.; Söding, J.; et al. Fast, scalable generation of high-quality protein multiple sequence alignments using Clustal Omega. *Mol. Syst. Biol.* **2011**, *7*, 539. [CrossRef]

30. Burley, S.K.; Bhikadiya, C.; Bi, C.; Bittrich, S.; Chen, L.; Crichlow, G.V.; Christie, C.H.; Dalenberg, K.; Di Costanzo, L.; Duarte, J.M.; et al. RCSB Protein Data Bank: Powerful new tools for exploring 3D structures of biological macromolecules for basic and applied research and education in fundamental biology, biomedicine, biotechnology, bioengineering and energy sciences. *Nucleic Acids Res.* **2021**, *49*, D437–D451. [CrossRef]
31. Varadi, M.; Anyango, S.; Deshpande, M.; Nair, S.; Natassia, C.; Yordanova, G.; Yuan, D.; Stroe, O.; Wood, G.; Laydon, A.; et al. AlphaFold Protein Structure Database: Massively expanding the structural coverage of protein-sequence space with high-accuracy models. *Nucleic Acids Res.* **2022**, *50*, D439–D444. [CrossRef] [PubMed]
32. Shatsky, M.; Nussinov, R.; Wolfson, H.J. A method for simultaneous alignment of multiple protein structures. *Proteins* **2004**, *56*, 143–156. [CrossRef]
33. Felsenstein, J. Confidence limits on phylogenies: An approach using the bootstrap. *Evolution* **1985**, *39*, 783–791. [CrossRef] [PubMed]
34. Kumar, S.; Stecher, G.; Li, M.; Knyaz, C.; Tamura, K. MEGA X: Molecular evolutionary genetics analysis across computing platforms. *Mol. Biol. Evol.* **2018**, *35*, 1547–1549. [CrossRef] [PubMed]
35. Letunic, I.; Bork, P. Interactive Tree Of Life (iTOL) v5: An online tool for phylogenetic tree display and annotation. *Nucleic Acids Res.* **2021**, *49*, W293–W296. [CrossRef]
36. Bai, Y.; van der Kaaij, R.M.; Leemhuis, H.; Pijning, T.; van Leeuwen, S.S.; Jin, Z.; Dijkhuizen, L. Biochemical characterization of the *Lactobacillus reuteri* glycoside hydrolase family 70 GTFB type of 4,6-α-glucanotransferase enzymes that synthesize soluble dietary starch fibers. *Appl. Environ. Microbiol.* **2015**, *81*, 7223–7232. [CrossRef]
37. Huggett, A.S.G.; Nixon, D.A. Enzymic determination of blood glucose. *Biochem. J.* **1957**, *66*, 12.
38. Ballschmiter, M.; Futterer, O.; Liebl, W. Identification and characterization of a novel intracellular alkaline α-amylase from the hyperthermophilic bacterium *Thermotoga maritima* MSB8. *Appl. Environ. Microbiol.* **2006**, *72*, 2206–2211. [CrossRef]
39. Schiano-di-Cola, C.; Røjel, N.; Jensen, K.; Kari, J.; Sørensen, T.H.; Borch, K.; Westh, P. Systematic deletions in the cellobiohydrolase (CBH) Cel7a from the fungus *Trichoderma reesei* reveal flexible loops critical for CBH activity. *J. Biol. Chem.* **2019**, *294*, 1807–1815. [CrossRef]
40. Fujii, K.; Minagawa, H.; Terada, Y.; Takaha, T.; Kuriki, T.; Shimada, J.; Kaneko, H. Use of random and saturation mutageneses to improve the properties of *Thermus aquaticus* amylomaltase for efficient production of cycloamyloses. *Appl. Environ. Microbiol.* **2005**, *71*, 5823–5827. [CrossRef]
41. Brooke, D.; Movahed, N.; Bothner, B. Universal buffers for use in biochemistry and biophysical experiments. *AIMS Biophys.* **2015**, *2*, 336–342. [CrossRef] [PubMed]
42. Møller, M.S.; El Bouaballati, S.; Henrissat, B.; Svensson, B. Functional diversity of three tandem C-terminal carbohydrate-binding modules of a β-mannanase. *J. Biol. Chem.* **2021**, *296*, 100638. [CrossRef] [PubMed]
43. Ji, H.; Bai, Y.; Liu, Y.; Wang, Y.; Zhan, X.; Long, J.; Chen, L.; Qiu, C.; Jin, Z. Deciphering external chain length and cyclodextrin production with starch catalyzed by cyclodextrin glycosyltransferase. *Carbohydr. Polym.* **2022**, *284*, 119156. [CrossRef] [PubMed]
44. Christensen, S.J.; Madsen, M.S.; Zinck, S.S.; Hedberg, C.; Sørensen, O.B.; Svensson, B.; Meyer, A.S. Enzymatic potato starch modification and structure-function analysis of six diverse GH77 4-α-glucanotransferases. *Int. J. Biol. Macromol.* **2023**, *224*, 105–114. [CrossRef] [PubMed]
45. Liu, J.; Bai, Y.; Ji, H.; Wang, Y.; Jin, Z.; Svensson, B. Controlling the fine structure of glycogen-like glucan by rational enzymatic synthesis. *J. Agric. Food Chem.* **2021**, *69*, 14951–14960. [CrossRef] [PubMed]

Supporting Information for

Impact of Starch Binding Domain Fusion on Activities and Starch Product Structure of 4-α-Glucanotransferase

Yu Wang [1], Yazhen Wu [2], Stefan Jarl Christensen [3], Štefan Janeček [4, 5], Yuxiang Bai [2], Marie Sofie Møller [6, *], Birte Svensson [1, *]

1: Enzyme and Protein Chemistry, Department of Biotechnology and Biomedicine, Technical University of Denmark, DK-2800, Kgs. Lyngby, Denmark

2: School of Food Science and Technology, Jiangnan University, Wuxi, Jiangsu, 214122, China

3: Protein Chemistry and Enzyme Technology, Department of Biotechnology and Biomedicine, Technical University of Denmark, DK-2800, Kgs. Lyngby, Denmark

4. Laboratory of Protein Evolution, Institute of Molecular Biology, Slovak Academy of Sciences, SK-84551, Bratislava, Slovakia

5: Department of Biology, Faculty of Natural Sciences, University of SS. Cyril and Methodius, SK-91701, Trnava, Slovakia

6: Applied Molecular Enzyme Chemistry, Department of Biotechnology and Biomedicine, Technical University of Denmark, DK-2800, Kgs. Lyngby, Denmark

* Corresponding authors:

Marie Sofie Møller: msmo@dtu.dk

Birte Svensson: bis@bio.dtu.dk

Figure S1. Sequence alignment of CBM20s with focus on GH77 DPE2s. The alignment of all 87 CBM20 domains from 65 selected enzymes having the CBM20 (Table 1). The most important positions involved in starch-binding sites 1 and 2 – recognized in the CBM20s from *Aspergillus niger* GH15 glucoamylase (site 1: Trp543, Lys578 and Trp590; site 2: Tyr527, Tyr556 and Trp563) [9] and *Bacillus circulans* strain 251 GH13_2 cyclodextrin glucanotransferase (site 1: Trp616, Lys651 and Trp662; site 2: Tyr633 and Trp636) [13] – are indicated, respectively, above and below the alignment by numbers "1" and "2". If conserved, the sites 1 and 2 are highlighted in yellow and blue, respectively; conserved and non-conserved substitutions being coloured red and gray, respectively. The labels of protein sources consist of the name of the organism, letter "A", "B" or "E" for the archaeal, bacterial and eukaryotic origin, respectively, CAZy family affiliation (if any), enzyme abbreviated name (for details, see Table 1) and the UniProt accession number. If there are more CBM20 copies for a single protein, the copies in the order of their appearance in the sequence are also indicated by the relevant number "1", "2" and "3" (at the end of the protein label). The three CBM20 domains studied in the present work – two from GH77 *Solanum tuberosum* DPE2 and one from GH15 *Aspergillus niger* glucoamylase – are marked by an asterisk. The sequence order in the alignment (starting from the top) reflects their order in the tree in the anticlockwise manner (starting from the first sequence in the eukaryotic DPE2 cluster of CBM20 copies 2).

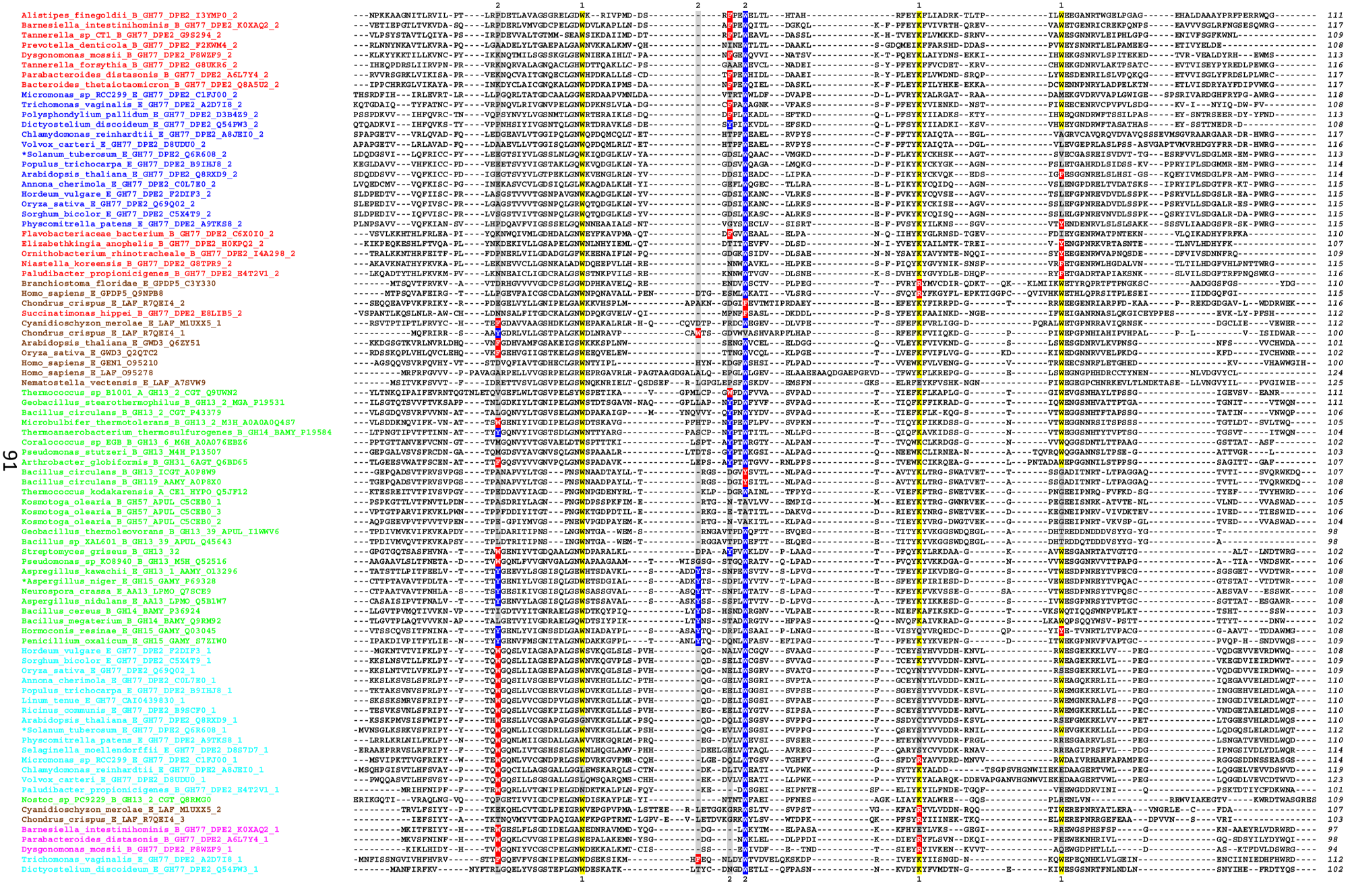
Alistipes_finegoldii_B_GH77_DPE2_I3YMP0_2
Barnesiella_intestinihominis_B_GH77_DPE2_K0XAQ2_2
Tannerella_sp_CT1_B_GH77_DPE2_G9S294_2
Prevotella_denticola_B_GH77_DPE2_F2KWM4_2
Dysgonomonas_mossii_B_GH77_DPE2_F8WZF9_2
Tannerella_forsythia_B_GH77_DPE2_G8UKR6_2
Parabacteroides_distasonis_B_GH77_DPE2_A6L7Y4_2
Bacteroides_thetaiotaomicron_B_GH77_DPE2_Q8A5U2_2
Micromonas_sp_RCC299_E_GH77_DPE2_C1FJ00_2
Trichomonas_vaginalis_E_GH77_DPE2_A2D7I8_2
Polysphondylium_pallidum_E_GH77_DPE2_D3B4Z9_2
Dictyostelium_discoideum_E_GH77_DPE2_Q54PW3_2
Chlamydomonas_reinhardtii_E_GH77_DPE2_A8JEI0_2
Volvox_carteri_E_GH77_DPE2_D8UDU0_2
*Solanum_tuberosum_E_GH77_DPE2_Q6R608_2
Populus_trichocarpa_E_GH77_DPE2_B9IHJ8_2
Arabidopsis_thaliana_E_GH77_DPE2_Q8RXD9_2
Annona_cherimola_E_GH77_DPE2_C0L7E0_2
Hordeum_vulgare_E_GH77_DPE2_F2DIF3_2
Oryza_sativa_E_GH77_DPE2_Q69Q02_2
Sorghum_bicolor_E_GH77_DPE2_C5X4T9_2
Physcomitrella_patens_E_GH77_DPE2_A9TKS8_2
Flavobacteriaceae_bacterium_B_GH77_DPE2_C6X0I0_2
Elizabethkingia_anophelis_B_GH77_DPE2_H0KPQ2_2
Ornithobacterium_rhinotracheale_B_GH77_DPE2_I4A298_2
Niastella_koreensis_B_GH77_DPE2_G8TPR9_2
Paludibacter_propionicigenes_B_GH77_DPE2_E4T2V1_2
Branchiostoma_floridae_E_GPDP5_C3Y330
Homo_sapiens_E_GPDP5_Q9NPB8
Chondrus_crispus_E_LAF_R7QEI4_2
Succinatimonas_hippei_B_GH77_DPE2_E8LIB5_2
Cyanidioschyzon_merolae_E_LAF_M1UXX5_1
Chondrus_crispus_E_LAF_R7QEI4_1
Arabidopsis_thaliana_E_GWD3_Q6ZY51
Oryza_sativa_E_GWD3_Q2QTC2
Homo_sapiens_E_GEN1_O95210
Homo_sapiens_E_LAF_O95278
Nematostella_vectensis_E_LAF_A7SVW9
Thermococcus_sp_B1001_A_GH13_2_CGT_Q9UWN2
Geobacillus_stearothermophilus_B_GH13_2_MGA_P19531
Bacillus_circulans_B_GH13_2_CGT_P43379
Microbulbifer_thermotolerans_B_GH13_2_M3H_A0A0A0Q4S7
Thermoanaerobacterium_thermosulfurogenes_B_GH14_BAMY_P19584
Coraloccoccus_sp_EGB_B_GH13_6_M6H_A0A076EBZ6
Pseudomonas_stutzeri_B_GH13_M4H_P13507
Arthrobacter_globiformis_B_GH31_6AGT_Q6BD65
Bacillus_circulans_B_GH13_ICGT_A0P8W9
Bacillus_circulans_B_GH119_AAMY_A0P8X0
Thermococcus_kodakarensis_A_CE1_HYPO_Q5JF12
Kosmotoga_olearia_B_GH57_APUL_C5CEB0_1
Kosmotoga_olearia_B_GH57_APUL_C5CEB0_3
Kosmotoga_olearia_B_GH57_APUL_C5CEB0_2
Geobacillus_thermoleovorans_B_GH13_39_APUL_I1WWV6
Bacillus_sp_XAL601_B_GH13_39_APUL_Q45643
Streptomyces_griseus_B_GH13_32
Pseudomonas_sp_KO8940_B_GH13_M5H_Q52516
Aspregillus_kawachii_E_GH13_1_AAMY_O13296
*Aspergillus_niger_E_GH15_GAMY_P69328
Neurospora_crassa_E_AA13_LPMO_Q7SCE9
Aspergillus_nidulans_E_AA13_LPMO_Q5B1W7
Bacillus_cereus_B_GH14_BAMY_P36924
Bacillus_megaterium_B_GH14_BAMY_Q9RM92
Hormoconis_resinae_E_GH15_GAMY_Q03045
Penicillium_oxalicum_E_GH15_GAMY_S7ZIW0
Hordeum_vulgare_E_GH77_DPE2_F2DIF3_1
Sorghum_bicolor_E_GH77_DPE2_C5X4T9_1
Oryza_sativa_E_GH77_DPE2_Q69Q02_1
Annona_cherimola_E_GH77_DPE2_C0L7E0_1
Populus_trichocarpa_E_GH77_DPE2_B9IHJ8_1
Linum_tenue_E_GH77_CAI0439830_1
Ricinus_communis_E_GH77_DPE2_B9SCF0_1
Arabidopsis_thaliana_E_GH77_DPE2_Q8RXD9_1
*Solanum_tuberosum_E_GH77_DPE2_Q6R608_1
Physcomitrella_patens_E_GH77_DPE2_A9TKS8_1
Selaginella_moellendorffii_E_GH77_DPE2_D8S7D7_1
Micromonas_sp_RCC299_E_GH77_DPE2_C1FJ00_1
Chlamydomonas_reinhardtii_E_GH77_DPE2_A8JEI0_1
Volvox_carteri_E_GH77_DPE2_D8UDU0_1
Paludibacter_propionicigenes_B_GH77_DPE2_E4T2V1_1
Nostoc_sp_PC9229_B_GH13_2_CGT_Q8RMG0
Cyanidioschyzon_merolae_E_LAF_M1UXX5_2
Chondrus_crispus_E_LAF_R7QEI4_3
Barnesiella_intestinihominis_B_GH77_DPE2_K0XAQ2_1
Parabacteroides_distasonis_B_GH77_DPE2_A6L7Y4_1
Dysgonomonas_mossii_B_GH77_DPE2_F8WZF9_1
Trichomonas_vaginalis_E_GH77_DPE2_A2D7I8_1
Dictyostelium_discoideum_E_GH77_DPE2_Q54PW3_1

2.2 Interfacial Catalysis of Starch Granules by Pullulanase

This chapter is comprised of 1 paper (***Paper 3***) and 2 manuscripts (***Manuscript 1*** and ***Manuscript 2***). All concern interfacial catalysis on granular starches by pullulanase. ***Manuscript 1*** describes the impact of SBDs on enzymatic properties and interfacial catalysis on debranching of granular starch by a *Lactobacillus acidophilus* NCFM pullulanase (*La*Pul). In ***Paper 3***, a commercial pullulanase from *Bacillus licheniformis* (*Bl*Pul) was used as an enzyme probe to quantify branching on the surface of granular starches. ***Manuscript 2*** is a continuation of ***Paper 3***, where we adopt the interfacial kinetic approach to enumerate density of α-1,6-linked branch points hydrolyzed by *Bl*Pul. In ***Manuscript 2***, the Sabatier principle was used to understand enzymatic modification by BE and 4αGT of three types of starches (waxy, normal, and high amylose maize starches), and we concluded that the Sabatier principle can be a useful tool to guide the starch modification.

Starch is a major energy source in diets, animal feed, and industrial applications [296,297]. Its digestibility varies due to factors like origin and processing. Human enzymes efficiently break α-1,4-linkages in starch but struggle with α-1,6-linkages, making α-1,6-linkage rich starch more resistant [298]. In the human digestive tract, microbial PULIs hydrolyze α-1,6-linkages into maltose and maltooligosaccharides [83]. As introduced above in section 1.2.2, PULIs were found in the GH13_12, 13, and 14 subfamilies, and generally adopt a multi-domain architecture of one or several NTDs, including CBMs and some uncharacterized domains, a catalytic domain, and a C-terminal domain. Even though there are many studies on the function of the NTDs, there are still some NTDs with unknown function.

To further explore the diverse functions of NTDs in PUL, *La*Pul was N-terminally truncated CBM41 alone (∆41-*La*Pul) or CBM41 and two DUFs (∆(41+DUFs)-*La*Pul) (***Manuscript 1***). Firstly, truncation of CBM41 and DUFs decreased the optimum temperature from 60 °C for *La*Pul to 40 °C. This loss of thermostability was confirmed by the T_m of *La*Pul and ∆41-*La*Pul being 61.8 and 61.2 °C, while ∆(41+DUFs)-*La*Pul had a T_m of 49.3 °C. The reduced thermostability for ∆(41+DUFs)-*La*Pul indicated that the DUFs serve as a stabilizer and to link CBM41 to the CD. As *La*Pul showed 10.4- and > 20.7-fold higher affinity for starch granules and β-CD, respectively, than ∆41-*La*Pul, CBM41 is found to serve in substrate recognition. Applying the interfacial kinetics methods for hydrolysis of starch granules for by the *La*Pul forms, ∆41-*La*Pul lost 26 and 45% of enzyme attack sites and enzyme binding sites, respectively, than *La*Pul. These results confirmed that CBM41 acts in substrate binding. Interestingly, we found that by truncation of CBM41 and DUFs, ∆(41+DUFs)-*La*Pul showed higher affinity for starch granules than ∆41-*La*Pul. By examining the AlphaFold2 model, we found that four aromatic residues were exposure after truncating the DUFs, which might cause the enhanced substrate affinity for ∆(41+DUFs)-*La*Pul.

Enzymatically modified starch granules play a crucial role in enhancing thermal properties, digestion resistance, and complexation capacity in the food industry [299]. Various techniques, such as HPAEC-PAD, size exclusion chromatography-multi-angle laser light scattering-refractive index detection (SEC-MALLS-RI), and ^{1}H nuclear magnetic resonance (NMR), have been employed to analyze these starch modifications [300]. However, these methods were initially designed for gelatinized starch and are not optimal for directly studying structural alterations on starch granule surfaces. Therefore, there is a growing demand for establishing links between surface-level structural changes of granules and their functional properties relevant to specific applications. Inspired by the attack site density ($^{kin}\Gamma_{max}$) determined by interfacial kinetics on granular starches for *La*Pul, we adopted the interfacial kinetic approach to enumerate density of α-1,6-linked branch points hydrolyzed by *Bl*Pul that is only active on α-1,6-linkages (***Paper 3***).

This novel approach was also verified using starch granules pretreated with BE from *Rhodothermus obamensis* (*Ro*BE) or 4αGT from *Thermoproteus uzoniensis* (TuαGT) (***Paper 3***). Our findings affirmed that *Ro*BE-modified starch granules exhibited 1.9- to 2.3-fold increase in branch point density compared to unmodified starches, indicating the capability of *Ro*BE to foster formation of new α-1,6-linkages on the granule surface. In contrast, as expected, TuαGT-modified starches had similar branch point density to the unmodified starch granules. Our analysis of chain length distribution led us to conclude that TuαGT primarily facilitated hydrolysis and/or cyclization of branch chains on starch granules, while prompting disproportionation of branch chains in gelatinized starches.

Even though there are increasing interest in enzymatic starch modification, the understanding between the process of enzyme modification and starch structure is limited. We applied the Sabatier principle to understand the relationship between enzymatic modification and granular starch structure for native starch granules and starch granules modified by either *Ro*BE or TuαGT, or *Ro*BE+TuαGT (***Manuscript 2***). In ***Manuscript 2***, we firstly introduced the different reaction model for *Ro*BE and TuαGT on granular starches. Subsequentially, the granular structures of these starches were analyzed for gelatinization temperature, crystallinity, surface order degree and chain length distribution of the surface. As a follow up of ***Paper 3***, we also analyzed the parameters from interfacial kinetics on native and modified starch granules. This made it possible to apply the Sabatier principle to understand the mechanism of enzymatic modification, together with the granular structure.

2.2.1 Manuscript 1 – Functional Roles of N-terminal Domains in Pullulanase from Human Gut *Lactobacillus acidophilus*

This manuscript presents results on the effect of NTDs on the enzymatic properties and interfacial catalysis on granular starches of a GH13_14 Type I pullulanase from human gut *Lactobacillus acidophilus*. The supporting information can be found at the end of the manuscript. This manuscript was submitted to *Journal of Agricultural and Food Chemistry* on the 11th of September 2023 and was written in the journal specific format (Under review).

Functional Roles of N-terminal Domains in Pullulanase from Human Gut *Lactobacillus acidophilus*

Yu Wang [a], *Birte Svensson* [a], *Bernard Henrissat* [b], *Marie Sofie Møller* [c,]*

[a] Enzyme and Protein Chemistry, Department of Biotechnology and Biomedicine, Technical University of Denmark, DK-2800, Kgs. Lyngby, Denmark

[b] Enzyme Discovery, Department of Biotechnology and Biomedicine, Technical University of Denmark, DK-2800, Kgs. Lyngby, Denmark

[c] Applied Molecular Enzyme Chemistry, Department of Biotechnology and Biomedicine, Technical University of Denmark, DK-2800, Kgs. Lyngby, Denmark

* Corresponding author:

Marie Sofie Møller: msmo@dtu.dk

ABSTRACT: Pullulanases are multi-domain α-glucan debranching enzymes with one or more N-terminal domains (NTDs) including carbohydrate-binding modules (CBMs) and domains of unknown function (DUFs). To elucidate the roles of NTDs in the *Lactobacillus acidophilus* NCFM pullulanase (*La*Pul), two truncated variants, Δ41-*La*Pul (lacking CBM41) and Δ(41+DUFs)-*La*Pul (lacking CBM41 and two DUFs), were produced recombinantly. *La*Pul recognized 1.3- and 2.2-fold more enzyme attack-sites on starch granules than Δ41-*La*Pul and Δ(41+DUFs)-*La*Pul, respectively, as measured by interfacial kinetics. Δ41-*La*Pul displayed markedly lower affinity for starch granules and β-cyclodextrin (10.4- and >20.7-fold, respectively) than *La*Pul, showing substrate binding mainly stems from CBM41. Δ(41+DUFs)-*La*Pul exhibited 12 °C lower melting temperature than *La*Pul and Δ41-*La*Pul, indicating that the DUFs are critical for *La*Pul stability. Notably, Δ41-*La*Pul exhibited 13.5-fold higher turnover number (k_{cat}) and 9-fold higher Michaelis constant (K_M) than *La*Pul, while Δ(41+DUFs)-*La*Pul's values were close to *La*Pul, possibly due to the exposure of aromatic amino acids by truncation.

KEYWORDS: Pullulanase; Carbohydrate-binding module; N-terminal domains; Granular starch; Interfacial catalysis.

1. INTRODUCTION

Starch serves as a major source of energy in the human diet and animal feed, as well as a constituent in biomaterials and for biorefineries.[1,2] It is synthesized and stored in plants as granules, consisting of two α-glucans; the essentially linear amylose and the branched amylopectin.[3] Starch digestion in the human gastrointestinal tract (GIT) involves oral, duodenal, and small intestinal phases and a series of enzymes including salivary and pancreatic amylases, maltase-glucoamylase, and sucrase-isomaltase.[4] The digestibility of starch varies considerably based on botanical origin, granular crystal packing, and processing.[5] Human digestive enzymes efficiently degrade α-1,4-linkages in starch, but act less readily on α-1,6-linkages. In contrast, pullulanases from the gut microbiota can efficiently degrade α-1,6-linkages in starch.[6] As a result, starch with high content of α-1,6-linkages possess greater enzymatic resistance to human digestive enzymes.[7]

In the GIT, α-1,6-linkages are primarily hydrolyzed by microbial pullulanases into short maltooligosaccharides, which can be taken up by specific transporters and degraded intracellularly by enzymes involved in maltooligosaccharide metabolism.[8] Pullulanases are starch-debranching enzymes (SDBEs) classified in two glycoside hydrolase (GH) families, GH13 and GH57, in the Carbohydrate-active enzymes (CAZy) database.[9] SDBEs are produced by numerous microorganisms, including bacteria, yeast, and fungi. Pullulanases are categorized with two types of linkage specificity: type I (PULI) and type II (PULII), also referred to as amylopullulanase.[10] PULIs only catalyze hydrolysis of α-1,6-linkages in pullulan, starch, and related branched carbohydrates, while PULIIs catalyze hydrolysis of both α-1,4- and α-1,6-linkages. PULIs are organized in three GH13 sequence-based subfamilies, GH13_12, 13, and 14.[9] A previously characterized GH13_14 PULI from the probiotic bacterium *Lactobacillus acidophilus* NCFM (*La*Pul) and homologues from other gut bacteria are suggested to be important in utilization of branched maltooligosaccharides in the GIT.[11]

57 The characteristic structure of GH13 PULIs comprises one or more N-terminal domains
58 (NTDs), a catalytic domain (CD), and a C-terminal domain (CTD) that is typical for most
59 GH13 enzymes. Carbohydrate-binding modules (CBMs) can have important roles for substrate
60 specificity, catalytic efficiency, stability and oligomerization and are commonly present among
61 the NTDs in PULIs.[12] With very few exceptions, GH13 PULIs have a CBM48 located N-
62 terminally to the CD. Although no specific binding function has been identified for CBM48s
63 in PULIs, they might contribute to structural stability and protein production and folding.[13]
64 PULIs often possess at least one additional CBM, such as CBM20, CBM41, or CBM68, which
65 are all starch binding domains.[14] Additionally, they have domains of unknown function (DUFs)
66 not classified as CBMs. A DUF of a sorghum PULI (limit dextrinase) was reported to have an
67 impact on the digestibility of sorghum starch.[15]
68 Despite several attempts to elucidate functions of NTDs in PULI, the specific roles of
69 individual domains remain uncertain due to their interactions with one another and with
70 substrates. In the case of a PULI from *Geobacillus thermocatenulatus*, truncation of a CBM41
71 resulted in a slightly decreased Michaelis constant (K_M) and increased turnover number (k_{cat})
72 on pullulan, possibly due to a more accessible active site.[16] A similar result was found by
73 truncation of the CBM41 from a PULI from *Bacillus deramificans*.[13] In the case of PULI from
74 *Bacillus acidopullulyticus*, truncation of the CBM41 led to 2-fold higher K_M on pullulan,
75 indicating that the CBM41 contributes to the substrate affinity.[17,18] However, to the best of our
76 knowledge, the effect of truncation of non-CBM DUFs on activity and protein stability of PULI
77 has not been investigated. Additionally, the understanding of the activity of PULIs on granular
78 starch is currently very limited.
79 In the present study, two N-terminally truncated variants of *La*Pul were generated, which
80 lack the CBM41 (Δ41-*La*Pul) and the CBM41 as well as the two DUFs situated between the
81 CBM41 and CBM48 (Δ(41+DUFs)-*La*Pul). The result of these truncations was analyzed with

82 regard to thermostability, substrate binding, activity on soluble substrates, and interfacial
83 kinetics on starch granules.

2. MATERIALS AND METHODS

2.1. Materials. β-cyclodextrin, amylopectin from maize and glycogen from oyster were purchased from Sigma-Aldrich Co. Ltd (St. Louis, MO, USA). Pullulan and β-limit dextrin were purchased from Megazyme Co. Ltd (Wicklow, Ireland). Twelve different starches were kind gifts of Andreas Blennow (University of Copenhagen, Denmark, see Supporting Information for details about sources of the starches). Amylose content and crystalline polymorph were previously determined of the starch granules (Table 1).[19–24]

2.2. Construction, Production, and Purification of *La*Pul and N-terminally Truncated Forms. Genes encoding full-length *L. acidophilus* NCFM pullulanase (*La*Pul, GenBank accession: AAV43522.1) and two N-terminally truncated forms (Δ41-*La*Pul and Δ(41+DUFs)-*La*Pul) were produced in *Escherichia coli* Rosetta (DE3) and the recombinant proteins were purified essentially as previously described.[11] See Supporting Information for details on gene construction, including primers for gene amplification (Table S1), production and purification. Protein concentrations were determined spectrophotometrically at 280 nm (Nanodrop Lite, Thermo Scientific, USA) using predicted molar extinction coefficients (ε) for *La*Pul, Δ41-*La*Pul and Δ(41+DUFs)-*La*Pul of 182,900, 164,910, and 103,600 $M^{-1}cm^{-1}$, respectively, and theoretical molecular masses of 132,960, 121,570 and 88,430 Da, respectively (https://web.expasy.org/protparam/). Purity of *La*Pul, Δ41-*La*Pul and Δ(41+DUFs)-*La*Pul was verified by SDS-PAGE.

2.3. Bioinformatics Analysis of GH13_14. Protein sequences for all GH13_14 members in the CAZy database[9] were retrieved from NCBI (4263 sequences). The redundancy was first reduced with CD-HIT[25] using a 90% identity cut-off (resulting in 731 sequences) to compute a phylogenetic tree (Figure S1), and then further reduced using a 55% identity cut-off (109 sequences) for a detailed phylogenetic tree incorporating domain architectures (Figure 1). A multiple sequence alignment of the catalytic domains (CDs) (as predicted by dbCAN3[26])

was generated using the CLC Main Workbench 7 (QIAGEN). Phylogenetic analysis was performed using the maximum likelihood method from the CLC Main Workbench 7. The tree was visualized using the Interactive Tree Of Life (iTOL) online tool (https://itol.embl.de/)[27].

2.4. AlphaFold2 Model. ColabFold (https://colab.research.google.com/github/sokrypton/ColabFold/blob/main/AlphaFold2.ipynb) was used to generate AlphaFold2 models of *La*Pul, Δ41-*La*Pul and Δ(41+DUFs)-LaPul,[28] without the C-terminal surface layer association protein domain (SLAP). For the *La*Pul model, the N-terminal sequence prior to the CBM41 was omitted.

2.5. Oligomer State Analysis. The solution oligomer state was determined for *La*Pul, Δ41-*La*Pul and Δ(41+DUFs)-*La*Pul using size exclusion chromatography loading 100 µL 1 mg/mL protein onto a pre-equilibrated Superdex 200 Increase 10/300 GL column (GE Healthcare), and eluting by 50 mM morpholineethanesulfonic acid (MES), 150 mM NaCl, 1 mM $CaCl_2$, 10% glycerol, pH 6.0. Protein standard mix (69385, Sigma-Aldrich, Germany) of five proteins spanning 15–600 kDa was applied for calibration.

2.6. Determination of Melting Temperature. Melting temperature (T_m) of *La*Pul, Δ41-*La*Pul and Δ(41+DUFs)-*La*Pul was determined by differential scanning fluorimetry using a Prometheus Panta instrument (NanoTemper Technologies, München, Germany).[29] Protein samples (2 µM) were loaded in Prometheus NT.48 High Sensitivity capillaries (NanoTemper Technologies) and fluorescence was measured at 330 and 350 nm upon excitation at 280 nm. The temperature was ramped from 25 to 95 °C at a rate of 1 °C /min to follow the unfolding.

2.7. Enzyme Kinetics on Soluble Substrates. Activity was determined for 0.02–1.0 mg/mL pullulan and 0.11–9.0 mg/mL amylopectin using 0.2–5 nM final enzyme concentrations in assay buffer (20 mM sodium acetate, pH 5.0, 5 mM $CaCl_2$) at 37 °C with shaking (300 rpm). Aliquots (100 µL) were removed at 3, 6, and 10 min, mixed with 100 µL 4-hydroxybenzoic acid hydrazide (PAHBAH) reagent (15 g/L PAHBAH dissolved in 0.177 M potassium sodium

tartrate tetrahydrate and 0.5 M NaOH[30]), heated (95 °C, 10 min), cooled and the absorbance measured at 405 nm using a microplate reader (PowerWave XS, BIO-TEK), as previously described.[31] Glucose (0–1 μM) was used as standard. k_{cat} and K_M were calculated by fitting to initial rates of product formation and substrate concentrations to the Michaelis-Menten (MM) equation using GraphPad Prism 6 (GraphPad Software Inc).

2.8. Activity on Starch Granules. Granules of 12 starches (WMS, NMS, HMS, WWS, NWS, HWS, WBS, NBS, AOBS, WPS, NPS, and HPS) were washed twice with MilliQ water and once with assay buffer. Enzyme (20 μL, 50 nM final concentration) was added to granule samples (180 μL, 50 mg/mL, final concentration) and incubated (25 °C, 1100 rpm). After 1 h, aliquots (100 μL) were transferred to new tubes and mixed with 20 μL 1.8 M Na_2CO_3 to terminate the reaction, followed by centrifugation (4000 *g*, 5 min). Reducing sugar in the supernatant was determined using the PABHAB assay (see section 2.7). One unit of activity was defined as the amount of enzyme releasing 1 nmol reducing sugar per second under the above conditions.

2.9. Interfacial Kinetics Analysis on Granular Starch. Two complementary methods, conventional and inverse MM analyses, were employed to describe the kinetics for hydrolysis of granular starches. For conventional MM analysis starch granules (135 μL, 15–150 mg/mL) were pre-incubated (25 °C, 10 min, 1100 rpm), added enzyme (15 μL, final concentration 50 nM) and incubated (25 °C, 1100 rpm). For inverse MM kinetics analysis, starch granules (135 μL, 20 mg/mL) were mixed with 20 μL of seven enzyme concentrations (50–5000 nM, final concentrations). After 30 min, aliquots (100 μL) were transferred to new tubes, mixed with 20 μL 1.8 M Na_2CO_3 to terminate the reaction,[32] centrifuged (10000 *g*, 5 min), and the concentration of reducing sugar in the supernatant was determined using the PAHBAH (see section 2.7).

158 Conventional MM experiments were analyzed using equation 1 (eq. 1) for non-linear
159 regression analyses where S_0^{mass} is the substrate mass load and $K_{1/2}$ (in g·L^{-1}) the mass load at
160 substrate half-saturation and V_{max} (in M·s^{-1}).

$$v_0 = \frac{V_{max} \cdot S_0^{mass}}{K_{1/2} + S_0^{mass}} \quad (1)$$

161 The inverse experiments we analysed using the inverse MM equation (eq. 2) by nonlinear
162 regression analysis of the data to give the parameters $^{inv}V_{max}$ (in g·L^{-1}·s^{-1}) and $^{inv}K_M$ (in M).[33]

$$v_0 = \frac{^{inv}V_{max} \cdot E_0}{^{inv}K_M + E_0} \quad (2)$$

163 The attack site density ($^{kin}\Gamma_{max}$) was calculated by eq. 3 using V_{max} (eq. 1) and $^{inv}V_{max}$ (eq.
164 2).[33]

$$\frac{\frac{^{inv}V_{max}}{S_0^{mass}}}{\frac{V_{max}}{E_0}} = {}^{kin}\Gamma_{max} \quad (3)$$

165 **2.10. Adsorption to Starch Granules.** The binding capacity of starch granules (135 µL, 25
166 mg/mL) was determined under the same conditions as used for activity assay by adding 15 µL
167 of seven different enzyme concentrations (final concentrations: *La*Pul, 50–1500 nM; Δ41-
168 *La*Pul, 50–4000 nM; Δ(41+DUFs)-*La*Pul, 50–2000 nM). After 30 min incubation (4 °C, 1100
169 rpm), the mixtures were centrifuged (10,000 *g*, 5 min) and 100 µL supernatant was transferred
170 to 100 µL 2.5-fold diluted Protein assay dye reagent (#5000006, Bio-Rad Laboratories, Inc.
171 California, USA). Protein in the supernatant was quantified from the ratio of absorbance at 590
172 over 450 nm using *La*Pul, Δ41-*La*Pul and Δ(41+DUFs)-*La*Pul (0–2000 nM) as standards.[34]
173 The data were fitted with the Langmuir isotherm (eq. 4) using GraphPad Prism 6, where K_d is
174 the dissociation constant and $^{ads}\Gamma_{max}$ is the (apparent) saturation coverage.[33]

$$\Gamma = \frac{^{ads}\Gamma_{max} \cdot E_{free}}{K_d + E_{free}} \quad (4)$$

2.11. Surface Plasmon Resonance Analysis of β-cyclodextrin Binding. The affinity of *La*Pul, Δ41-*La*Pul and Δ(41+DUFs)-*La*Pul for β-cyclodextrin was determined by surface plasmon resonance analysis (SPR) using Biacore T100 (GE Healthcare). The enzymes (100 μg/mL) in immobilization buffer (10 mM sodium acetate, pH 4.0, 0.5 mM $CaCl_2$, and 1 mM β-cyclodextrin) were immobilized on a CM5 sensor chip using random amine coupling adopting the manufacturer's protocol to a final chip density of 4998 response units (RU) for *La*Pul, 4310 RU for Δ41-*La*Pul and 3459 RU for Δ(41+DUFs)-*La*Pul. Binding analysis comprised 100 s of association followed by 90 s of dissociation at a flow rate of 30 μL/min and 25°C for 17 β-cyclodextrin concentrations (0.25–1024 μM) in running buffer (10 mM sodium acetate, pH 5.5, 150 mM NaCl, and 0.005% (v/v) P20 surfactant). A one-site binding model was fitted to the steady-state response blank and reference cell-corrected sensograms using the BIA evaluation software supplied with the instrument to obtain the dissociation constant (K_d).

2.12. Statistical Analysis. Interfacial kinetics were analyzed in duplicate, while all other experiments were conducted in triplicate. The statistical significance was assessed with two-way ANOVA using GraphPad Prism 6 (GraphPad Software Inc). p-values<0.05 were considered statistically significant.

3. RESULTS

3.1. Bioinformatic Analysis of GH13_14. More than 4260 protein sequences are classified into subfamily GH13_14.[9] They mainly belong to the *Bacillota* phylum of bacteria, and the phylogenetic analysis including only CDs reveals a distinct clustering pattern that is primarily associated with the origin of the proteins, as depicted in Figure S1. To gain further insights into differences and similarities in the domain architecture, the sequence redundancy was reduced using a 55% identity cut-off and domains were identified (Figure 1).

The analysis of the domain architecture (Figure 1) showed that all members of subfamily GH13_14 possess a multi-domain architecture with characteristic domains appended to the N-terminal region. In rare cases, a CBM20 or CBM26 is found at the C-terminus. Notable NTDs identified in GH13_14 members, include CBM41, CBM48, CBM68, and DUFs. CBM48, known to play a crucial role in the stability of PULI, consistently appears adjacent to the CDs. CBM68, which is common in GH13_14 from the *Bacillota* group, is positioned immediately upstream of CBM48. By contrast, in the majority of sequences containing CBM41, the latter is separated from CBM48 via one or several DUFs. *La*Pul represents this domain architecture: CBM41-DUF1-DUF2-CBM48-CD (Figures 1 and 2). Conversely, PULIs from *Lactobacillus iners* have either a CBM41-CBM41-DUF-CBM48-CD or a simple CBM48-CD domain organization.

To explore the functional significance of CBM41 and the DUFs in *La*Pul, two truncated forms were designed: Δ41-*La*Pul and Δ(41+DUFs)-*La*Pul (Figure 2A).

3.2. Effect of NTDs on Biochemical Properties of *La*Puls. Following a two-step purification process, SDS-PAGE analysis revealed single protein bands of molecular mass of about 133, 123 and 88 kDa for *La*Pul, Δ41-*La*Pul and Δ(41+DUFs)-*La*Pul, respectively (Figure 3A) in agreement with the theoretical values. *La*Pul, Δ41-*La*Pul and Δ(41+DUFs)-*La*Pul were obtained in yields of 0.5–2 mg/g cells after purification. Size exclusion chromatography

indicated that Δ41-*La*Pul is a monomer in solution, while *La*Pul and Δ(41+DUFs)-*La*Pul are dimers (Figure 3B). All three *La*Pul forms showed maximum activity at pH 5.5 (Figure 3C), but *La*Pul and Δ41-*La*Pul showed higher pH resistance than Δ(41+DUFs)-*La*Pul at pH < 4.5 and pH > 5.5. The temperature optimum for the activity of *La*Pul and Δ41-*La*Pul was 60 °C (Figure 3D), indicating that *La*Pul is a thermophilic enzyme, as also shown previously.[11] Truncation of both CBM41 and the DUFs decreased the optimum temperature to 40 °C (Figure 3D) and the rate of inactivation at 37 °C was much faster than for *La*Pul and Δ41-*La*Pul (Figure 3E), in accordance with their T_m of 61.8 and 61.2 °C, respectively, and T_m of Δ(41+DUFs)-*La*Pul of 49.3 °C (Figure 3F).

3.3. Effect of NTDs on Activity and Binding of Soluble Substrates. Pullulan and amylopectin were used as substrates to compare the effects of NTDs on *La*Pul activity. The K_M and k_{cat} of *La*Pul on pullulan determined in this work was consisted with that from our previous work (Table 2).[11] Remarkably, removal of CBM41 resulted in 13.6- and 2.9-fold higher k_{cat}, but also 11.3- and 2.5-fold higher K_M on pullulan and amylopectin, respectively, compared to *La*Pul (Table 2), resulting in only a modest change to a higher catalytic efficiency (k_{cat}/K_M) (1.2–1.3-fold). The increased K_M for Δ41-*La*Pul compared with *La*Pul also demonstrated that Δ41-*La*Pul showed lower affinity for the soluble substrate. However, the K_M and k_{cat} values for Δ(41+DUFs)-*La*Pul are quite similar to those of full-length *La*Pul (Table 2).

To study the effects of NTDs on the binding to soluble oligosaccharides and understand the observed differences in K_M to pullulan and amylopectin, the affinity of the three *La*Pul forms for β-cyclodextrin, a well-known starch mimic, was determined using SPR. The full-length enzyme bound β-cyclodextrin strongly with K_d of 48.3 μM, whereas, as expected, removal of the CBM41 resulted in almost complete loss of binding yielding K_d >1 mM (exact determination was not possible due to limited water solubility of β-cyclodextrin). The affinity for Δ(41+DUFs)-*La*Pul to β-cyclodextrin could not be determined using SPR, due to instability

of protein during the immobilization process at pH 4.0, where Δ(41+DUFs)-*La*Pul maintained less than 20% activity (Figure 3C).

3.4. Effect of NTDs on Activity on Starch Granules. Enzymatic hydrolysis of α-1,6-linkages on granular starches is vital for digestion of starch granules in the human GIT. The activity of *La*Pul was determined towards granular starches (Figure 4). Depending on the starch type, *La*Pul showed 1.3–4.5- and 1.8–7.2-fold higher activity than Δ41-*La*Pul and Δ(41+DUFs)-*La*Pul, respectively. This indicates that both the CBM41 and the DUFs played an important role in hydrolysis of starch granules. Besides, all three *La*Pul forms had highest activity on barley, followed by wheat, maize, and potato starches. Using maize starches as an example, amylopectin-rich (waxy) starch granules had more branch points on the surface hydrolyzed by *La*Pul leading to higher activity on WMS and NMS than HMS granules in agreement with our previous work.[35]

3.5. Effect of NTDs on Interfacial Catalysis of Starch Granules. The heterogeneous catalysis of granular WMS and NMS was analyzed at 25 °C, where $K_{1/2}$ and ${}^{inv}K_M$ were consistently lower than the highest starch concentration used and in practice this meant that we could get data to support linear regression of eqs. (1) and (3) (see section 2.9. Interfacial Kinetics Analysis on Granular Starch). $K_{1/2}$ and ${}^{inv}K_M$ are the substrate mass load at substrate half-saturation in conventional MM and the molar concentration of enzyme that gives half-saturation in inverse MM analysis, respectively. The conventional MM kinetics analysis of the three *La*Pul forms gave highest $k_{cat}/K_{1/2}$ for the pure amylopectin WMS granules (Figure 5G), while it was reduced by 5–10-fold for NMS (Figure 5K), consistent with the higher specific activity on WMS (Figure 4). Compared with Δ41-*La*Pul, *La*Pul showed 6.5- and 4.5-fold lower $K_{1/2}$ and 2.2- and 2.3-fold higher k_{cat}, resulting in 17- and 12.5-fold higher $k_{cat}/K_{1/2}$ for WMS and NMS, respectively. Interestingly, Δ(41+DUFs)-LaPul demonstrated higher affinity to starch granules by showing 4.7- and 2.9-fold lower $K_{1/2}$ than Δ41-*La*Pul (Table S2).

Inverse kinetics analysis was conducted to determine and compare the density of attack sites ($^{kin}\Gamma_{max}$) on the granules (Figure 5H,L). *La*Pul had $^{kin}\Gamma_{max}$ of 3.86 nmol/g for WMS and 1.82 nmol/g for NMS (Figure 5H,L). In comparison, Δ41-*La*Pul and Δ(41+DUFs)-*La*Pul recognized 1.3–1.7-fold and 2.2–2.2-fold, respectively, fewer attack sites than *La*Pul. Different, albeit consistent, trends were observed both regarding the influence of the NTDs and the type of substrate. For the effects of the different substrates, all three *La*Pul forms showed higher $^{kin}\Gamma_{max}$ for WMS than NMS. The higher attack site density of WMS, stemmed from the higher content of α-1,6-linkages in WMS, supposedly explaining the faster degradation of this substrate.

3.6. Effect of NTDs on Binding to Starch Granules. Compared to *La*Pul, the two N-terminally truncated forms had decreased affinity for granular maize starches, illustrated by 1.7–2.9-fold lower binding site density ($^{ads}\Gamma_{max}$), depending on the starch type (Figure 6C,F). For example, Δ41-*La*Pul showed 1.9- and 1.7-fold lower $^{ads}\Gamma_{max}$ on WMS and NMS, respectively, than *La*Pul (Figure 6C,F) and decreased the affinity ($1/K_d$) for WMS and NMS decreased by 10.4- and 5.0-fold (Figure 6D,G). Interestingly, the removal of both CBM41 and the two DUFs only resulted in 3.4- and 1.2-fold decrease in affinity for WMS and NMS, respectively, compared to *La*Pul. However, it led to a 3.0- and 4.1-fold increased affinity for WMS and NMS, respectively, compared to Δ41-*La*Pul (Figure 6D,G). This indicates that further truncation of the DUFs from Δ41-*La*Pul in part recovered the affinity. Similar to the trend observed for $^{kin}\Gamma_{max}$, a decrease in $^{ads}\Gamma_{max}$ was seen, suggesting that the accessibility of branch points is much higher in WMS composed purely of amylopectin compared to NMS (see also section 3.4.).

4. DISCUSSION

4.1. Effect of CBM41 on *La*Pul. The truncation of CBM41 changed *La*Pul from a dimer to a monomer in solution (Figure 3B). Similarly, in a *Thermus* maltogenic amylase, its N-terminal CBM34 has been demonstrated to play a crucial role in dimer formation. Specifically, the full-length enzyme is a dimer, but a monomer when the CBM34 is removed.[36]

It is well known that CBM41, as other starch binding domains, can interact with α-glucans and be important for the stability of enzymes.[37,38] Recombinant CBM41 from *Thermotoga maritima* binds β-cyclodextrin with high affinity (K_d = 2.9 μM) determined using isothermal titration calorimetry.[39] Moreover removal of the N-terminal CBM41 from two different pullulanases of GH13_14 led to 1.6- and 2.4-fold increase in K_M for pullulan (Table S3).[13,18] Based on the present results, the N-terminal CBM41 of *La*Pul is proposed to anchor the enzyme to soluble substrates as removal of the CBM41 resulted in a higher K_M on soluble substrates (Table 2) in agreement with more than 20-fold reduced affinity for β-cyclodextrin of Δ41-*La*Pul compared to *La*Pul (Table 4). However, it should be noted that Δ41-*La*Pul also showed 13.6-fold increased k_{cat} compared with *La*Pul (Table 2). The behavior of Δ41-*La*Pul, which loses affinity for the substrate, while it gains activity can be described as desorption-limited reactions according to the Sabatier principle.[40] The Sabatier principle can be applied to two scenarios: desorption-limited and adsorption-limited reactions.[41] In adsorption-limited reactions, higher affinity between catalyst and substrate leads to higher activity. Conversely, in desorption-limited reactions higher affinity between catalyst and substrate results in lower activity.[42] The presence of CBM41 in *La*Pul makes the enzyme bind too tightly to the substrate, leading to slower dissociation from substrate and therefore a lower k_{cat}.

Δ41-*La*Pul has higher $K_{1/2}$ and lower k_{cat} thus a decreased $k_{cat}/K_{1/2}$ for granular starches compared to *La*Pul. The removal of CBM41 significantly reduced affinity for starch granules (Figure 6D). In contrast to the desorption-limited situation observed for *La*Pul and Δ41-*La*Pul

on soluble substrate (pullulan and amylopectin in this work), the reaction of *La*Pul and Δ41-*La*Pul on granular starches showed an adsorption-limited situation according to the Sabatier principle.[40] To better understand the observed differences between soluble α-glucan substrates and starch granules, it is important to consider the substrate variation. Glucan chains in solution are very flexible, allowing for easy binding to CBM41 and CD. Hence, the soluble product may still occupy the binding site in CBM41 after catalysis is completed, preventing new substrate molecules to bind and finally leads to the desorption-limited situation. By comparison, glucan chains on the surface of starch granules are less flexible, and do not readily bind productively to the active site in the presence of CBM41, resulting in the adsorption-limited situation.[43]

4.2. Effect of DUFs on *La*Pul. The function of DUFs has not been explored experimentally, although some share fold similarity with functionally characterized CBMs.[44] The phylogenetic analysis (Figure 1) shows that CBM41 is frequently connected to the CBM48-CD ensemble via one or more DUFs. For multi-modular enzymes, such non-catalytic modules may act as binding domains, while others can serve as linkers or spacers not engaged in direct substrate binding.[45] In the case of *La*Pul, the loss of binding after truncation of CBM41 showed that CBM41 acts as a binder. However, when also the two DUFs were removed, a significant decrease in thermostability was observed, providing clear evidence that these DUFs contribute to the overall stability. Notably, Δ(41+DUFs)-*La*Pul exhibits the same K_M on pullulan and amylopectin as *La*Pul, which is significantly lower than that of Δ41-*La*Pul. This indicates a regained substrate affinity resulting from the larger N-terminal truncation. Similarly, the gain in affinity was seen by a decreased K_d for WMS and NMS granules of Δ(41+DUFs)-*La*Pul compared to Δ41-*La*Pul (Table S2, Figure 6D,G). In the AlphaFold2 models of Δ41-*La*Pul and Δ(41+DUFs)-*La*Pul four aromatic residues, Trp420, Tyr 661, Tyr 662, and Tyr 666, on the surface of CBM48 and CD are blocked by the α-helix at the C-terminus of DUF2 (Figure 7B,C),

but become exposed by removal of the DUFs (Figure 7D,E). Therefore, the exposure of the four aromatic residues may provide Δ(41+DUFs)-*La*Pul with higher substrate affinity than Δ41-*La*Pul. Similarly, a CBM98 isolated from a *Bacteroides ovatus* α-amylase showed 13.7-fold higher affinity to potato amylopectin than the CBM98 together with CBM48 (CBM98-CBM48), suggesting that CBM48 may somehow restrict the CBM98 binding site or impose steric restraints on CBM98 itself.[46]

In conclusion, the CBM41 and DUFs play a crucial role in maintaining substrate affinity and stability of *La*Pul as demonstrated by domain truncation. Firstly, interfacial catalysis and adsorption to starch granules indicated that substrate recognition is harbored primarily by CBM41. Moreover, the loss in substrate affinity by truncation of CBM41 along with loss of thermostability by additional truncation of the DUFs (Δ(41+DUFs)-*La*Pul) showed that the DUFs serve as stabilizers and link the CBM41 to the CBM48-CD. Additionally, exposure of the DUFs by CBM41 truncation in Δ41*La*Pul led to monomer formation, whereas both *La*Pul and Δ(41+DUFs)-*La*Pul are dimers in solution. Notably, the enhanced affinity for starch granules resulting from the truncation of both CBM41 and the DUFs could potentially arrise from interactions with aromatic residues exposed on the surface of CBM48 and the CD.

ABBREVIATIONS

AOBS, amylose only barley starch; CAZy, carbohydrate active enzymes; CBM, carbohydrate-binding module; CD, catalytic domain; CTD, C-terminal domain; DBE, debranching enzyme; DP, degree of polymerization; DUF, domain of unknown function; GH, glycoside hydrolase; GIT, gastrointestinal tract; HMS, high-amylose maize starch; HPS, high-amylose potato starch; HWS, high-amylose wheat starch; *La*Pul, pullulanase from *Lactobacillus acidophilus* NCFM; MM, Michaelis–Menten; NBS, normal barley starch; NMS, normal maize starch; NPS, normal potato starch; NTD, N-terminal domain; NWS, normal wheat starch; PULI, pullulanase type I; PULII, pullulanase type II; RS, resistant starch; SDBE, starch-debranching enzyme; SLAP, surface layer association protein; SPR, surface plasmon resonance; T_m, melting temperature; WBS, waxy barley starch; WMS, waxy maize starch; WPS, waxy potato starch; WWS, waxy wheat starch.

ACKNOWLEDGMENTS

Karina Jansen (Technical University of Denmark, Denmark) is gratefully thanked for technical assistance. We also thank Andreas Blennow (University of Copenhagen, Denmark), Archer Daniels Midland (ADM, Decatur, IL), Cargill (USA), Chinese Academy of Sciences (China), Lantmännen (Sweden), Lyckeby Stärkelsen (Sweden), and Northwest A&F University (China) for providing starches. The Danish Council for Independent Research | Natural Sciences is thanked for an instrument grant for the SPR. We thank Professor Alexander Büll for allowing us to use the Prometheus Panta for nano differential scanning fluorimetry experiments.

ASSOCIATED CONTENT

Supporting Information

The Supporting Information is available free of charge:

Gene construction, protein production and purification for *La*Pul, Δ41-*La*Pul and Δ(41+DUFs)-*La*Pul; Primers for gene amplification. The restriction sites (forward, NheI; reverse, XhoI) are underlined (Table S1); Summary of characteristics of N-terminal domain truncations in PULIs (Table S2); Conventional and inverse kinetic parameters of *La*Pul, Δ41-*La*Pul and Δ(41+DUFs)-*La*Pul acting on different granular starches at 25 °C and pH 5.5 (Table S3); Phylogenetic tree of pullulanase in GH13_14 (Figure S1).

AUTHOR INFORMATION

Corresponding Author

Marie Sofie Møller—*Applied Molecular Enzyme Chemistry, Department of Biotechnology and Biomedicine, Technical University of Denmark, DK-2800, Kgs. Lyngby, Denmark*; orcid.org/0000-0001-9017-3367; E-mail: msmo@dtu.dk; phone: +45 45252741

Author

Yu Wang—*Enzyme and Protein Chemistry, Department of Biotechnology and Biomedicine, Technical University of Denmark, DK-2800, Kgs. Lyngby, Denmark*; orcid.org/0000-0002-0019-6889; E-mail: yuawa@dtu.dk

Birte Svensson—*Enzyme and Protein Chemistry, Department of Biotechnology and Biomedicine, Technical University of Denmark, DK-2800, Kgs. Lyngby, Denmark*; orcid.org/0000-0002-2993-8196; E-mail: bis@bio.dtu.dk; phone: +45 45252740

Bernard Henrissat— *Enzyme Discovery, Department of Biotechnology and Biomedicine, Technical University of Denmark, DK-2800, Kgs. Lyngby, Denmark*; orcid.org/0000-0002-3434-8588; E-mail: behen@dtu.dk

Author Contributions

Y.W. designed and performed experiments, collected data, and drafted the manuscript; B.S. developed the theoretical framework and edited the manuscript. B.H. collected the family information for GH13_14. M.S.M. performed experiments, developed the theoretical framework and edited the manuscript.

Funding

This work was supported by a China Scholarship Council (CSC) #202006790033 (YW) and Technical University of Denmark.

409 **Notes**

410 The authors declare no competing financial interests or personal relationships that influenced

411 the work reported in this paper.

REFERENCES

(1) Kaimal, A. M.; Mujumdar, A. S.; Thorat, B. N. Resistant starch from millets: Recent developments and applications in food industries. *Trends Food Sci. Technol.* **2021**, *111*, 563–580.

(2) Ståhl, M.; Berghel, J.; Frodeson, S.; Granström, K.; Renström, R. Effects on pellet properties and energy use when starch is added in the wood-fuel pelletizing process. *Energy and Fuels* **2012**, *26*, 1937–1945.

(3) Chi, C.; Li, X.; Huang, S.; Chen, L.; Zhang, Y.; Li, L.; Miao, S. Basic principles in starch multi-scale structuration to mitigate digestibility: A review. *Trends Food Sci. Technol.* **2021**, *109*, 154–168.

(4) Diaz-Sotomayor, M.; Quezada-Calvillo, R.; Avery, S. E.; Chacko, S. K.; Yan, L. K.; Lin, A. H. M.; Ao, Z. H.; Hamaker, B. R.; Nichols, B. L. Maltase-glucoamylase modulates gluconeogenesis and sucrase-isomaltase dominates starch digestion glucogenesis. *J. Pediatr. Gastroenterol. Nutr.* **2013**, *57*, 704–712.

(5) Tian, Y.; Wang, Y.; Zhong, Y.; Møller, M. S.; Westh, P.; Svensson, B.; Blennow, A. Interfacial catalysis during amylolytic degradation of starch granules : Current understanding and kinetic approaches. *Molecules* **2023**, *28*, 3799.

(6) Cockburn, D. W.; Koropatkin, N. M. Polysaccharide degradation by the intestinal microbiota and its influence on human health and disease. *J. Mol. Biol.* **2016**, *428*, 3230–3252.

(7) Tian, Y.; Wang, Y.; Liu, X.; Herburger, K.; Westh, P.; Møller, M. S.; Svensson, B.; Zhong, Y.; Blennow, A. Interfacial enzyme kinetics reveals degradation mechanisms behind resistant starch. *Food Hydrocoll.* **2023**, *28*, 108621.

(8) Cockburn, D. W.; Kibler, R.; Brown, H. A.; Duvall, R.; Moraïs, S.; Bayer, E.; Koropatkin, N. M. Structure and substrate recognition by the *Ruminococcus bromii* amylosome pullulanases. *J. Struct. Biol.* **2021**, *213*, 107765.

(9) Drula, E.; Garron, M.-L.; Dogan, S.; Lombard, V.; Henrissat, B.; Terrapon, N. The carbohydrate-active enzyme database: Functions and literature. *Nucleic Acids Res.* **2022**, *50*, D571–D577.

(10) Saha, B. C.; Zeikus, J. G. Novel highly thermostable pullulanase from thermophiles. *Trends Biotechnol.* **1989**, *7*, 234–239.

(11) Møller, M. S.; Goh, Y. J.; Rasmussen, K. B.; Cypryk, W.; Celebioglu, H. U.; Klaenhammer, T. R.; Svensson, B.; Abou Hachem, M. An extracellular cell-attached

pullulanase confers branched α-glucan utilization in human gut *Lactobacillus acidophilus*. *Appl. Environ. Microbiol.* **2017**, *83*, 1–13.

(12) Shoseyov, O.; Shani, Z.; Levy, I. Carbohydrate binding modules: Biochemical properties and novel applications. *Microbiol. Mol. Biol. Rev.* **2006**, *70*, 283–295.

(13) Duan, X.; Wu, J. Enhancing the secretion efficiency and thermostability of a *Bacillus deramificans* pullulanase mutant (D437H/D503Y) by N-terminal domain truncation. *Appl. Environ. Microbiol.* **2015**, *81*, 1926–1931.

(14) Janeček, Š.; Mareček, F.; MacGregor, E. A.; Svensson, B. Starch-binding domains as CBM families–history, occurrence, structure, function and evolution. *Biotechnol. Adv.* **2019**, *37*, 107451.

(15) Gilding, E. K.; Frere, C. H.; Cruickshank, A.; Rada, A. K.; Prentis, P. J.; Mudge, A. M.; Mace, E. S.; Jordan, D. R.; Godwin, I. D. Allelic variation at a single gene increases food value in a drought-tolerant staple cereal. *Nat. Commun.* **2013**, *4*, 1483.

(16) Li, L.; Dong, F.; Lin, L.; He, D.; Wei, W.; Wei, D. N-terminal domain truncation and domain insertion-based engineering of a novel thermostable type I pullulanase from *Geobacillus thermocatenulatus*. *J. Agric. Food Chem.* **2018**, *66*, 10788–10798.

(17) Chen, A.; Sun, Y.; Zhang, W.; Peng, F.; Zhan, C.; Liu, M.; Yang, Y.; Bai, Z. Downsizing a pullulanase to a small molecule with improved soluble expression and secretion efficiency in *Escherichia coli*. *Microb. Cell Fact.* **2016**, *15*, 1–10.

(18) Chen, A.; Liu, X.; Dai, X.; Zhan, J.; Peng, F.; Li, L.; Wang, F.; Li, S.; Yang, Y.; Bai, Z. Effect of N-terminal truncation of *Bacillus acidopullulyticus* pullulanase on enzyme properties and functions. *Shengwu Gongcheng Xuebao/Chinese J. Biotechnol.* **2016**, *32*, 355–364.

(19) Blennow, A.; Wischmann, B.; Houborg, K.; Ahmt, T.; Jørgensen, K.; Engelsen, S. B.; Bandsholm, O.; Poulsen, P. Structure function relationships of transgenic starches with engineered phosphate substitution and starch branching. *Int. J. Biol. Macromol.* **2005**, *36*, 159–168.

(20) Kozlov, S. S.; Blennow, A.; Krivandin, A. V; Yuryev, V. P. Structural and thermodynamic properties of starches extracted from GBSS and GWD suppressed potato lines. *Int. J. Biol. Macromol.* **2007**, *40*, 449–460.

(21) Htoon, A.; Shrestha, A. K.; Flanagan, B. M.; Lopez-Rubio, A.; Bird, A. R.; Gilbert, E. P.; Gidley, M. J. Effects of processing high amylose maize starches under controlled conditions on structural organisation and amylase digestibility. *Carbohydr. Polym.* **2009**, *75*, 236–245.

(22) Tian, Y.; Qu, J.; Zhou, Q.; Ding, L.; Cui, Y.; Blennow, A.; Zhong, Y.; Liu, X. High pressure/temperature pasting and gelling of starch related to multilevel structure-analyzed with RVA 4800. *Carbohydr. Polym.* **2022**, *295*, 119858.

(23) Carciofi, M.; Blennow, A.; Jensen, S. L.; Shaik, S. S.; Henriksen, A.; Buléon, A.; Holm, P. B.; Hebelstrup, K. H. Concerted suppression of all starch branching enzyme genes in barley produces amylose-only starch granules. *BMC Plant Biol.* **2012**, *12*, 1–16.

(24) Zhong, Y.; Bertoft, E.; Li, Z.; Blennow, A.; Liu, X. Amylopectin starch granule lamellar structure as deduced from unit chain length data. *Food Hydrocoll.* **2020**, *108*, 106053.

(25) Huang, Y.; Niu, B.; Gao, Y.; Fu, L.; Li, W. CD-HIT Suite: A web server for clustering and comparing biological sequences. *Bioinformatics* **2010**, *26*, 680–682.

(26) Huang, L.; Zhang, H.; Wu, P.; Entwistle, S.; Li, X.; Yohe, T.; Yi, H.; Yang, Z.; Yin, Y. DbCAN-seq: A database of carbohydrate-active enzyme (CAZyme) sequence and annotation. *Nucleic Acids Res.* **2018**, *46*, D516–D521.

(27) Letunic, I.; Bork, P. Interactive Tree Of Life (iTOL) v5: An online tool for phylogenetic tree display and annotation. *Nucleic Acids Res.* **2021**, *49*, W293–W296.

(28) Jumper, J.; Evans, R.; Pritzel, A.; Green, T.; Figurnov, M.; Ronneberger, O.; Tunyasuvunakool, K.; Bates, R.; Žídek, A.; Potapenko, A.; Bridgland, A.; Meyer, C.; Kohl, S. A. A.; Ballard, A. J.; Cowie, A.; Romera-Paredes, B.; Nikolov, S.; Jain, R.; Adler, J.; Back, T.; Petersen, S.; Reiman, D.; Clancy, E.; Zielinski, M.; Steinegger, M.; Pacholska, M.; Berghammer, T.; Bodenstein, S.; Silver, D.; Vinyals, O.; Senior, A. W.; Kavukcuoglu, K.; Kohli, P.; Hassabis, D. Highly accurate protein structure prediction with AlphaFold. *Nature* **2021**, *596*, 583–589.

(29) Møller, M. S. Impact of modular architecture on activity of glycoside hydrolase family 5 subfamily 8 mannanases. *Molecules* **2022**, *27*, 1915.

(30) Schiano-di-Cola, C.; Røjel, N.; Jensen, K.; Kari, J.; Sørensen, T. H.; Borch, K.; Westh, P. Systematic deletions in the cellobiohydrolase (CBH) Cel7A from the fungus *Trichoderma reesei* reveal flexible loops critical for CBH activity. *J. Biol. Chem.* **2019**, *294*, 1807–1815.

(31) Wang, Y.; Wu, Y.; Christensen, S. J.; Janeček, Š.; Bai, Y.; Møller, M. S.; Svensson, B. Impact of starch binding domain fusion on activities and starch product structure of 4-α-glucanotransferase. *Molecules* **2023**, *23*, 1320.

(32) Wang, Y.; Tian, Y.; Zhong, Y.; Suleiman, M. A.; Feller, G.; Westh, P.; Blennow, A.;

513 Møller, M. S.; Svensson, B. Improved hydrolysis of granular starches by a
514 psychrophilic α-amylase starch binding domain-fusion. *J. Agric. Food Chem.* **2023**,
515 *71*, 9040–9050.
516 (33) Kari, J.; Andersen, M.; Borch, K.; Westh, P. An inverse Michaelis-Menten approach
517 for interfacial enzyme kinetics. *ACS Catal.* **2017**, *7*, 4904–4914.
518 (34) Ernst, O.; Zor, T. Linearization of the Bradford protein assay. *J. Vis. Exp.* **2010**, No.
519 38, e1918.
520 (35) Wang, Y.; Tian, Y.; Christensen, S. J.; Blennow, A.; Svensson, B.; Møller, M. S. An
521 enzymatic approach to quantify branching on the surface of starch granules by
522 interfacial catalysis. *Food Hydrocoll.* **2024**, *146*.
523 (36) Kim, T. J.; Nguyen, V. D.; Lee, H. S.; Kim, M. J.; Cho, H. Y.; Kim, Y. W.; Moon, T.
524 W.; Park, C. S.; Kim, J. W.; Oh, B. H.; Lee, S. B.; Svensson, B.; Park, K. H.
525 Modulation of the multisubstrate specificity of *Thermus* maltogenic amylase by
526 truncation of the N-terminal domain and by a salt-induced shift of the monomer/dimer
527 equilibrium. *Biochemistry* **2001**, *40*, 14182–14190.
528 (37) Janeček, Š.; Majzlová, K.; Svensson, B.; MacGregor, E. A. The starch-binding domain
529 family CBM41—An in silico analysis of evolutionary relationships. *Proteins Struct.*
530 *Funct. Bioinforma.* **2017**, *85*, 1480–1492.
531 (38) Møller, M. S.; Henriksen, A.; Svensson, B. Structure and function of α-glucan
532 debranching enzymes. *Cell. Mol. Life Sci.* **2016**, *73*, 2619–2641.
533 (39) Lammerts Van Bueren, A.; Finn, R.; Ausió, J.; Boraston, A. B. α-Glucan recognition
534 by a new family of carbohydrate-binding modules found primarily in bacterial
535 pathogens. *Biochemistry* **2004**, *43*, 15633–15642.
536 (40) Kari, J.; Schaller, K.; Molina, G. A.; Borch, K.; Westh, P. The Sabatier principle as a
537 tool for discovery and engineering of industrial enzymes. *Curr. Opin. Biotechnol.*
538 **2022**, *78*, 102843.
539 (41) Ooka, H.; Huang, J.; Exner, K. S. The Sabatier principle in electrocatalysis: basics,
540 limitations, and extensions. *Front. Energy Res.* **2021**, *9*, 155.
541 (42) Kari, J.; Olsen, J. P.; Jensen, K.; Badino, S. F.; Krogh, K. B. R. M.; Borch, K.; Westh,
542 P. Sabatier principle for interfacial (heterogeneous) enzyme catalysis. *ACS Catal.*
543 **2018**, *8*, 11966–11972.
544 (43) Bertoft, E. Understanding starch structure: Recent progress. *Agronomy* **2017**, *7*, 56.
545 (44) Møller, M. S.; Abou Hachem, M.; Svensson, B.; Henriksen, A. Structure of the starch-
546 debranching enzyme barley limit dextrinase reveals homology of the N-terminal

547 domain to CBM21. *Acta Crystallogr. Sect. F Struct. Biol. Cryst. Commun.* **2012**, *68*,
548 1008–1012.
549 (45) Møller, M. S.; Bouaballati, S. El; Henrissat, B.; Svensson, B. Functional diversity of
550 three tandem C-terminal carbohydrate-binding modules of a β-mannanase. *J. Biol.*
551 *Chem.* **2021**, *296*, 100638.
552 (46) Brown, H. A.; Deveaux, A. L.; Juliano, B. R.; Photenhauer, A. L.; Boulinguiez, M.;
553 Bornschein, R. E.; Wawrzak, Z.; Ruotolo, B. T.; Terrapon, N.; Koropatkin, N. M.
554 BoGH13A Sus from Bacteroides ovatus represents a novel α-amylase used for
555 *Bacteroides* starch breakdown in the human gut. *Cell. Mol. Life Sci.* **2023**.

Figure 1. Phylogenetic tree of pullulanase in glycoside hydrolase (GH) subfamily 13_14. The tree was constructed based on the multiple alignment including CDs of 110 representative GH13_14 sequences. Black star, PULI from *Lactobacilli*; red arrow, *La*Pul from *L. acidophilus* NCFM; green arrow, characterized PULIs with crystal structures; blue arrow, characterized PULIs from *B. deramificans* (Accession: CAC60157.1)[13] and *Thermotoga maritima* (Accession: NP_229641.1).[39] The domain architectures of the full-length proteins are shown in the outer ring for CBM20 (light pink circle), CBM26 (brown circle), CBM41 (green circle), CBM48 (magenta circle), CBM68 (dark red circle), DUF (gray circle), GH13_14 CD (cyan square), and other GH13 CDs (dark pink square). The branches are colored according to taxonomy (red, *Bacillota*; green, *Pseudomonadota*; blue, *Bacteroidota*; yellow, *Actinomycetota*; purple, *Thermotogota*; gray, others). Protein sequences were retrieved from the NCBI database (https://www.ncbi.nlm.nih.gov/).

Figure 2. Domain architecture of *La*Pul, Δ41-*La*Pul and Δ(41+DUFs)-*La*Pul. (A) Schematic overview of the domain architecture of the three enzymes included in the study. *La*Pul were truncated at Thr105 and Gly403 to get Δ41-*La*Pul and Δ(41+DUFs)-*La*Pul, respectively. (B) AlphaFold2 model of *La*Pul excluding the surface layer association protein domain (SLAP): CBM41 (green), DUF1 (blue), DUF2 (yellow), CBM48 (magenta), CD (cyan), CTD (orange), two α-helical linker regions (gray) and the three catalytic residues (red sticks): Asp712, Glu741 and Asp838.

Figure 3. Characterization of *La*Pul and N-terminal truncated forms. (A) SDS-PAGE of purified enzymes: *La*Pul (lane 1), Δ41-*La*Pul (lane 2), Δ(41+DUFs)-*La*Pul (lane 3), and protein marker (lane 4). (B) Size exclusion chromatography of *La*Pul forms and protein standards (purple). (C) pH and (D) temperature dependence of activity on pullulan using standard assay.

(E) Temperature stability at 37 °C and pH 5.0. (F) Melting temperature. *La*Pul (black), Δ41-*La*Pul (red), and Δ(41+DUFs)-*La*Pul (green).

Figure 4. Activity of *La*Pul, Δ41-*La*Pul and Δ(41+DUFs)-*La*Pul towards different starch granules at 25 °C and pH 5.0. [a]Specific activity (nmol/s)/nmol protein; [b]Specific activity relative to *La*Pul on WMS (100%) is given in parenthesis.

Figure 5. Interfacial catalysis of granular starches by *La*Pul (black), Δ41-*La*Pul (red) and Δ(41+DUFs)-*La*Pul (green) at 25 °C and pH 5.0. (A) Conventional and (B) inverse kinetics on WMS. (C) Conventional and (D) inverse kinetics on NMS. Lines represent best fits of the Michaelis-Menten kinetics. (E) $K_{1/2}$, (F) k_{cat}, (G) $k_{cat}/K_{1/2}$, and (H) $^{kin}\Gamma_{max}$ for WMS, and (I) $K_{1/2}$, (J) k_{cat}, (K) $k_{cat}/K_{1/2}$, and (L) $^{kin}\Gamma_{max}$ for NMS. ****, ***, **, and * represent statistical significance with p value < 0.0001, 0.0001–0001, 0.001–0.01, and 0.01–0.05, respectively.

Figure 6. Adsorption to maize starches granules by *La*Pul (black), Δ41-*La*Pul (red) and Δ(41+DUFs)-*La*Pul (green) at 25 °C and pH 5.0. Binding isotherms on (A) WMS and (B) NMS. Lines represent best fits of the Langmuir eq. 4 (see section 2.10). (C) $^{ads}\Gamma_{max}$ (binding site density), (D) K_d and (E) Attack site density / binding density site (A/B ratio) for WMS and (F) $^{ads}\Gamma_{max}$, (G) K_d and (H) A/B ratio for NMS. ***, **, and * represent statistical significance with p value 0.0001–0001, 0.001–0.01, and 0.01–0.05, respectively.

Figure 7. AlphaFold2 models of Δ41-*La*Pul and Δ(41+DUFs)-*La*Pul. (A) Surface representation of Δ(41+DUFs)-*La*Pul (gray) and cartoon representation of Δ41-*La*Pul (deepteal) including the possible binding site (black dotted square): Trp420 from CBM48 (green), and Tyr 661, Tyr 662 and Tyr 666 from CD (magenta). Comparison of the exposure

605 of the possible binding site with DUF2 (B and C) and without DUF2 (D and E). (F) Close-up
606 of the possible binding aromatic residues.

607 **Table 1. Characteristics of Starch Granules**

Name of starch type	Abbreviation	Amylose content (%)	Crystalline polymorph
Waxy maize starch	WMS	0.7	A-type
Normal maize starch	NMS	20.7	A-type
High-amylose maize starch	HMS	72.2	B-type
Waxy wheat starch	WWS	0.2	A-type
Normal wheat starch	NWS	33.1	A-type
High-amylose wheat starch	HWS	67.4	B-type
Waxy barley starch	WBS	0.3	A-type
Normal barley starch	NBS	27.9	A-type
Amylose-only barley starch	AOBS	97.5	B-type
Waxy potato starch	WPS	1.9	B-type
Normal potato starch	NPS	26.3	B-type
High-amylose potato starch	HPS	35.2	B-type

608

609 **Table 2. Michaelis-Menten Kinetic Parameters of *La*Pul, Δ41-*La*Pul and Δ(41+DUFs)-**

610 ***La*Pul towards Pullulan and Amylopectin at 37 °C and pH 5.0**

Substrate	Enzyme	K_M (mg/mL)	k_{cat} (s^{-1})	k_{cat}/K_M ($mL \cdot s^{-1} \cdot mg^{-1}$)
Pullulan	*La*Pul	0.04 ± 0.01	484 ± 32	11950 (100[a])
	*La*Pul[b]	0.05 ± 0.004	518 ± 10.5	10368 (87)
	Δ41-*La*Pul	0.45 ± 0.14	6575 ± 866	14490 (131)
	Δ(41+DUFs)-*La*Pul	0.05 ± 0.01	391 ± 9	8296 (69)
Amylopectin (potato)	*La*Pul	0.18 ± 0.04	11 ± 2	61 (100[c])
	*La*Pul[b]	0.37 ± 0.041	25 ± 0.7	67 (110)
	Δ41-*La*Pul	0.45 ± 0.19	32 ± 1	71 (116)
	Δ(41+DUFs)-*La*Pul	0.18 ± 0.06	8 ± 1	49 (80)

611 [a] Percentage of the k_{cat}/K_M of *La*Pul on pullulan (100%) is given in parenthesis.
612 [b] Data from Møller et al.[11]
613 [c] Percentage of the k_{cat}/K_M of *La*Pul on amylopectin (100%) is given in parenthesis.

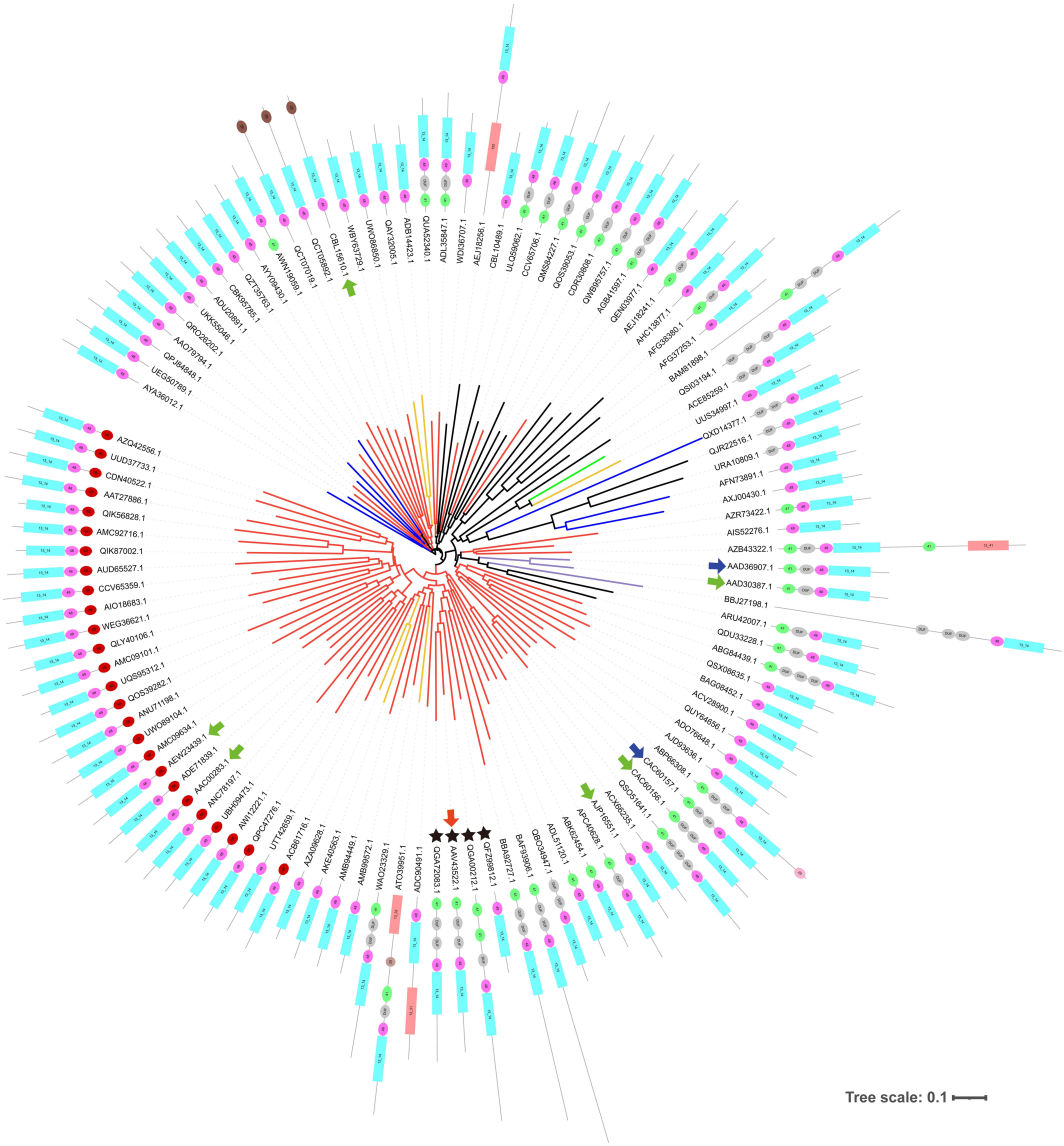

614

615 **Figure 1**

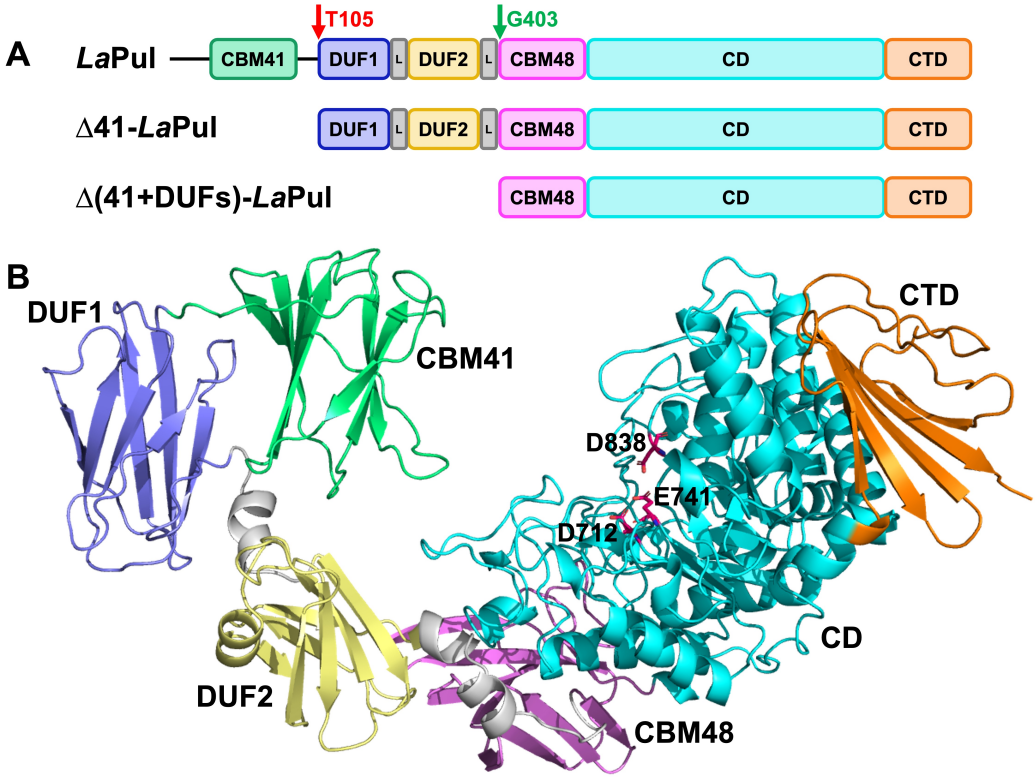

616

617 **Figure 2**

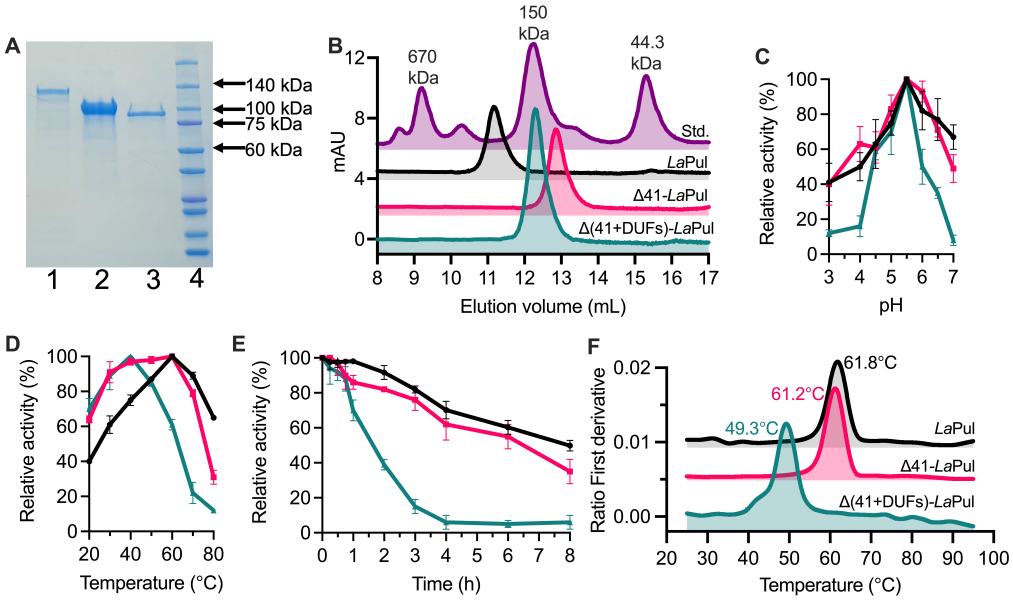

618

619 **Figure 3**

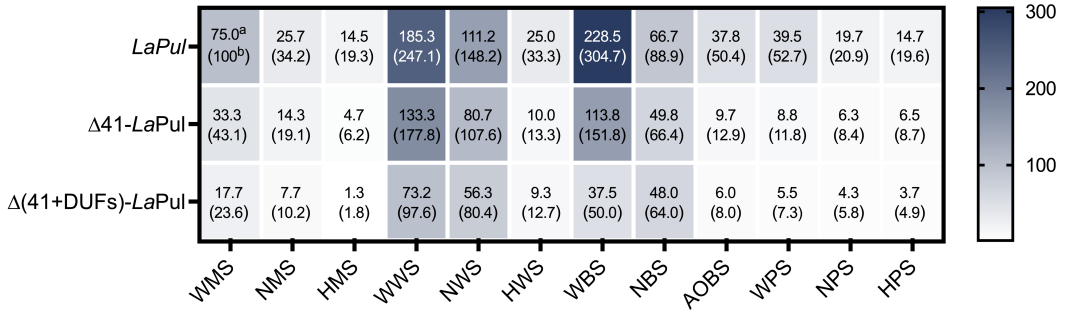

620

621 **Figure 4**

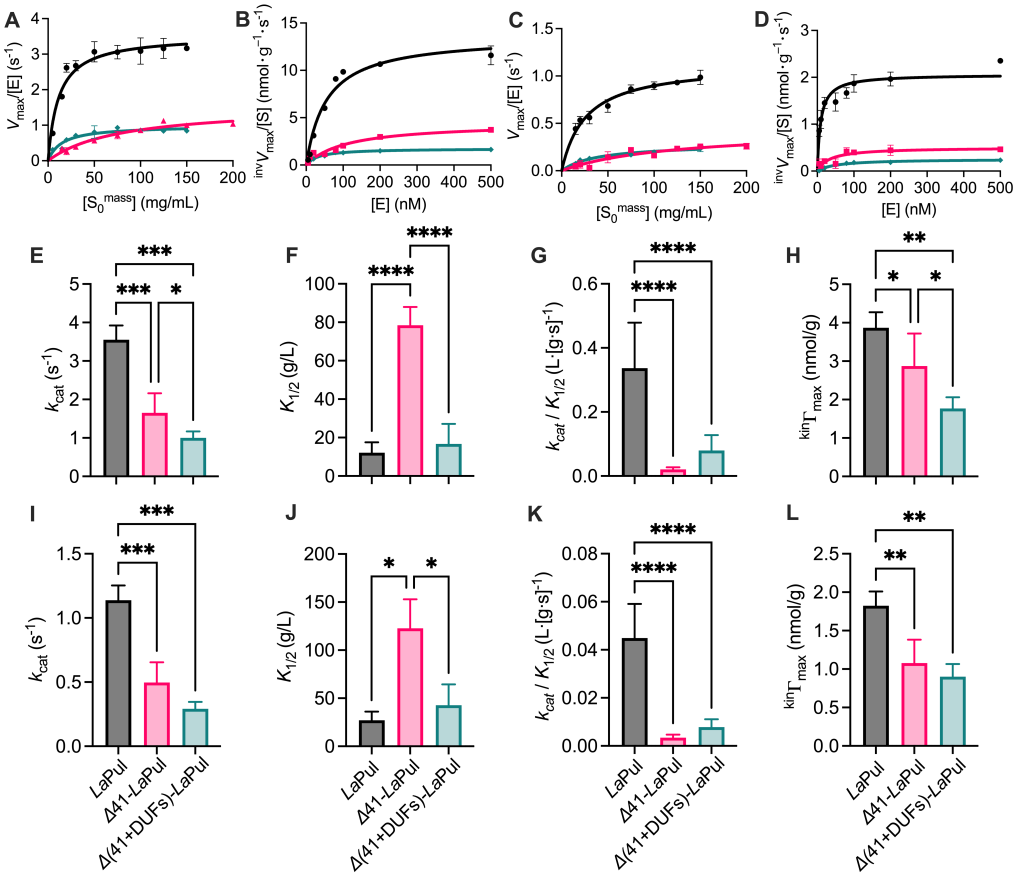

622

623 **Figure 5**

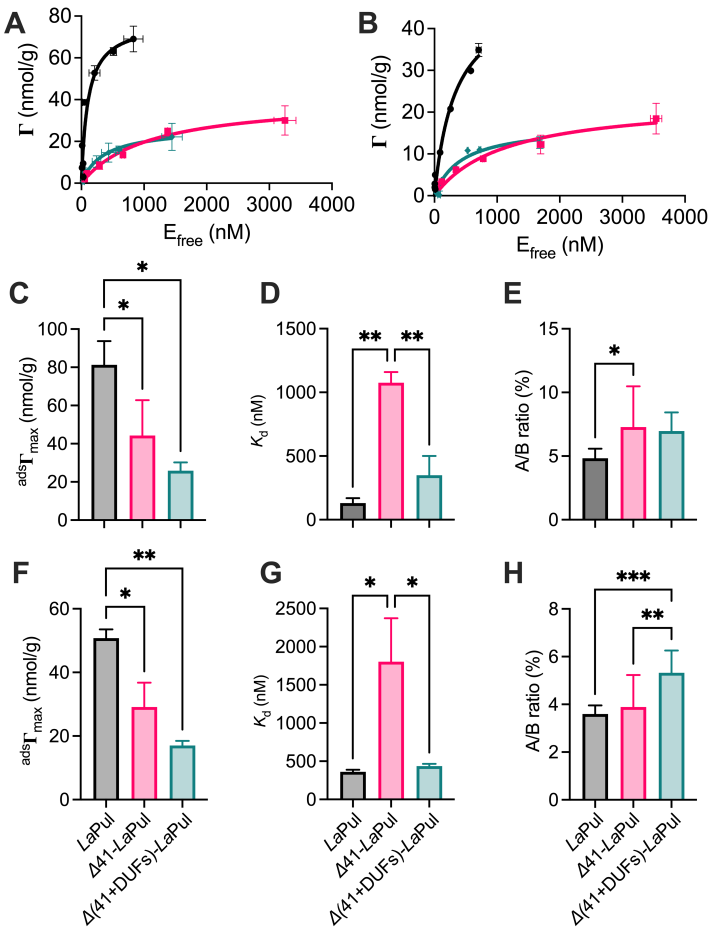

624

625 **Figure 6**

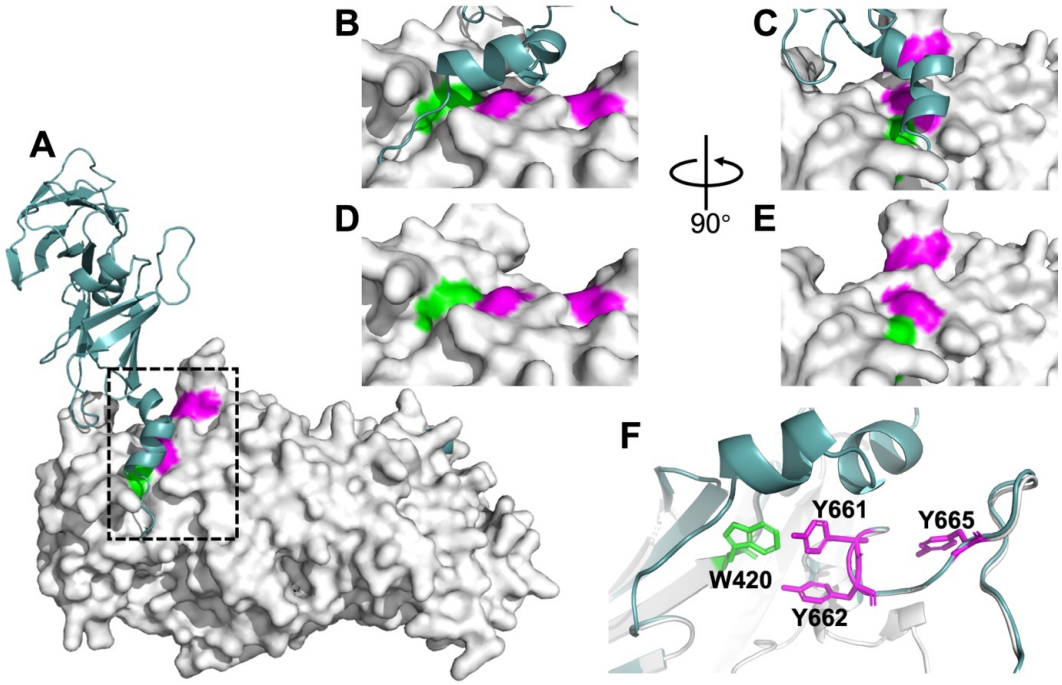

626

627 **Figure 7**

628 **TOC graphic:**

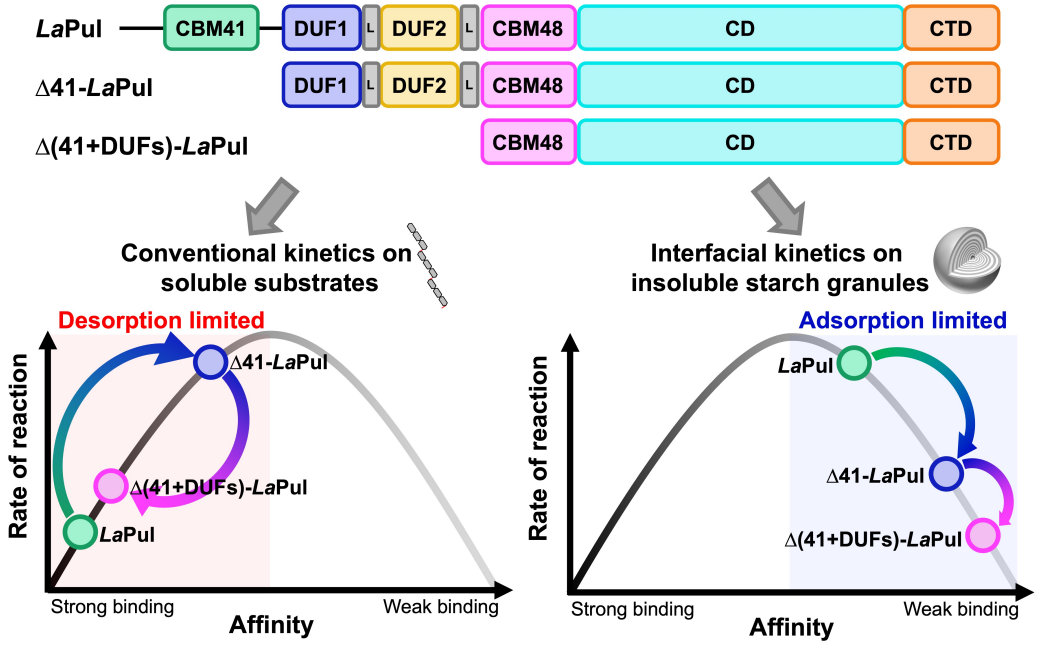

629

Supporting Information for

Functional Roles of N-terminal Domains in Pullulanase from Human Gut *Lactobacillus acidophilus*

Yu Wang [a], *Birte Svensson* [a], *Bernard Henrissat* [b], *Marie Sofie Møller* [c,] *

[a] Enzyme and Protein Chemistry, Department of Biotechnology and Biomedicine, Technical University of Denmark, DK-2800, Kgs. Lyngby, Denmark

[b] Enzyme Discovery, Department of Biotechnology and Biomedicine, Technical University of Denmark, DK-2800, Kgs. Lyngby, Denmark

[c] Applied Molecular Enzyme Chemistry, Department of Biotechnology and Biomedicine, Technical University of Denmark, DK-2800, Kgs. Lyngby, Denmark

* Corresponding author:

Marie S. Møller: msmo@dtu.dk

EXPERIMENTAL SECTION

Starches. Waxy maize starch (WMS) was a kind gift of Cargill, USA and normal maize starch (NMS) of Archer Daniels Midland (ADM, Decatur, IL). High-amylose maize starch (HMS) and high-amylose wheat starch (HWS) were obtained from experimental fields of Northwest A&F University, Yangling, China. Waxy wheat starch (WWS) was generously provided by the Chinese Academy of Sciences, China.[1] Normal wheat starch (NWS) was a kind gift of Lantmännen, Sweden. Normal potato starch (NPS) and high-amylose/high-phosphate potato starch (HPS) were extracted from the cultivar Dianella respectively a dual RNA interference starch branching enzyme I and II line in the Dianella genetic background, as previously described.[2,3] Starch from an RNA interference GBSS line (waxy potato starch, WPS) was a kind gift of Lyckeby Stärkelsen, Sweden. Two varieties of barley, Cinnamon (waxy barley starch; WBS) and Golden Promise (normal barley starch; NBS), were cultivated under normal diurnal (16 h light) or constant light growing conditions in a greenhouse at the University of Copenhagen (Copenhagen, Denmark). Amylose-only barley starch (AOBS) was obtained as described.[4]

Gene construction. The genes encoding the full-length *L. acidophilus* NCFM pullulanase (*La*Pul, GenBank accession: AAV43522.1) was cloned within the NheI and XhoI restriction sites in pET21a(+) (Novagen, Darmstadt, Germany) as reported.[5] *La*Pul were truncated at T105 and G403 to get Δ41-*La*Pul and Δ(41+DUFs)-*La*Pul, respectively. Plasmids for production of Δ41-*La*Pul and Δ(41+DUFs)-*La*Pul were constructed by first amplifying the gene parts from the full-length gene using the *La*Pul-pET21a(+) plasmid as template (see Table S1 for information about primers), followed by restriction digestion (NheI and XhoI) and ligation into pET21a(+). The resulting plasmids were cloned into *Escherichia coli* XL10-Gold Ultracompetent cells (Stratagene, California, USA) according to the manufacturer's protocols. Transformants were selected on LB agar plates with 100 μg/mL ampicillin and verified by

restriction analysis and full sequencing. *E. coli* Rosetta (DE3) cells (Invitrogen, USA) transformed with the sequence verified-plasmids were used for production of the enzyme.

Table S1. Primers for gene amplification. The restriction sites (forward, NheI; reverse, XhoI) are underlined.

Construct	Forward primer	Reverse primer
Δ41-*La*Pul	5'-ACT TAA GCT AGC GAT GAC GTA ACA TCT ATT AGT TAT TGG-3'	5'-TTA CCG CTC GAG AGC TTT TAC TTC AAT AAC AAC ATT C-3'
Δ(41+DUF)-*La*Pul	5'-ACT TTT GCT AGC GAT GAT TTA GGT GCT ACT TAC AC-3'	

Protein production. The enzymes were produced in a 5-liter bioreactor (Biostat B Plus; Sartorius Stedim, Germany) as described elsewhere.[5] Briefly, an overnight culture grown in LB medium described above was used to inoculate 3.7 L defined medium to an OD600 of approx. 0.75–1.5. The fermentation was conducted at 37 °C until the OD600 reached 8–12, followed by a temperature decrease to 15 °C and induction of expression using isopropyl-β-D-thiogalactopyranoside (100 µM, final concentration). Cells were harvested (6,000 *g*, 20 min, 4°C) at an OD600 of 26–37 after 70 h of induction and stored at –20 °C until protein purification.

Protein purification. The full-length (*La*Pul) was purified as described with minor modification.[5] Briefly, cells (5 g) were resuspended in 20 mL HisTrap equilibration buffer (10 mM Hepes, 500 mM NaCl, 25 mM imidazole, 1 mM $CaCl_2$, 10% glycerol, pH 7.5), lysed by high-pressure homogenization at 1 bar, added 2 µL Benzonase Nuclease (Sigma-Aldrich) and centrifuged (40,000 *g*, 4 °C, 30 min). The supernatant (20 mL) was mixed with 2 mL HisPur™ nickel-nitrilotriacetic acid resin (Thermo Fisher Scientific), pre-equilibrated with equilibration buffer, and washed with 20 mL washing buffer (50 mM imidazole in equilibration buffer). Bound protein was eluted by 10 mL elution buffer (300 mM imidazole in equilibration buffer), loaded onto a pre-equilibrated HiLoad 26/60 Superdex G200 column (GE Healthcare),

and eluted with gel-filtration buffer (50 mM morpholineethanesulfonic acid (MES), 150 mM NaCl, 1 mM $CaCl_2$, 10% glycerol, pH 6.0).

The N-terminally truncated forms Δ41-*La*Pul and Δ(41+DUFs)-*La*Pul were purified using β-CD-Sepharose,[6] followed by gel-filtration. Cells (5 g) were resuspended in 20 mL β-CD-Sepharose equilibration buffer (20 mM sodium-acetate, 500 mM NaCl, pH 5.5), lysed by high-pressure homogenization at 1 bar, added 2 µL Benzonase Nuclease (Sigma-Aldrich) and centrifuged (40,000 *g*, 4 °C, 30 min). The supernatant (20 mL) was loaded onto β-CD-Sepharose (20 mL bed volume in XK 16/10 column; GE Healthcare, Sweden), pre-equilibrated with equilibration buffer, at 0.5 mL/min and washed with 3 column volumes (CV) of equilibration buffer. Bound protein was eluted by 3 CV of elution buffer (20 mM sodium-acetate, 7 mM β-cyclodextrin, pH 5.5). Fractions containing protein were pooled and concentrated (30-kDa Amicon Ultra spin filters; Millipore) to 5 mL, loaded onto a pre-equilibrated HiLoad 26/60 Superdex G200 column (GE Healthcare), and eluted with gel-filtration buffer.

Protein concentrations were determined spectrophotometrically at 280 nm (Nanodrop Lite, Thermo Scientific, USA) using predicted molar extinction coefficients (ε) for *La*Pul, Δ41-*La*Pul and Δ(41+DUFs)-*La*Pul of 182,900, 164,910 and 103,600 $M^{-1}cm^{-1}$ and theoretical molecular masses of 132,960, 121,570 and 88,430 Da, respectively (https://web.expasy.org/protparam/). The purity of *La*Pul, Δ41-*La*Pul and Δ(41+DUFs)-*La*Pul was verified by SDS-PAGE.

Table S2. Conventional and Inverse Kinetic Parameters of *La*Pul, Δ41-*La*Pul and Δ(41+DUFs)-*La*Pul Acting on Different Granular Starches at 25 °C and pH 5.5

Enzyme	Substrate	WMS	NMS
*La*Pul	k_{cat} (s^{-1})	3.55 ± 0.30	1.14 ± 0.09
	$K_{1/2}$ (g/L)	12.10 ± 4.46	27.10 ± 7.37
	$k_{cat}/K_{1/2}$ ($L\cdot[g\cdot s]^{-1}$)	0.34 ± 0.13	0.05 ± 0.01
	$^{kin}\Gamma_{max}$ (nmol/g)	3.87 ± 0.33	1.82 ± 0.15
	$^{ads}\Gamma_{max}$ (nmol/g)	82.60 ± 9.81	51.22 ± 2.05
	A/B ratio (%)[b]	4.83 ± 0.67	3.60 ± 0.32
	K_d (nM)	103.6 ± 13.4	360.8 ± 22.1
Δ41-*La*Pul	k_{cat} (s^{-1})	1.65 ± 0.42	0.50 ± 0.13
	$K_{1/2}$ (g/L)	78.43 ± 7.76	122.80 ± 24.62
	$k_{cat}/K_{1/2}$ ($L\cdot[g\cdot s]^{-1}$)	0.02 ± 0.01	0.004 ± 0.001
	$^{kin}\Gamma_{max}$ (nmol/g)	2.87 ± 0.69	1.08 ± 0.25
	$^{ads}\Gamma_{max}$ (nmol/g)	45.47 ± 14.88	26.57 ± 3.64
	A/B ratio (%)	7.28 ± 2.86	3.89 ± 1.20
	K_d (nM)	1075 ± 84.2	1803 ± 464.6
Δ(41+DUFs)-*La*Pul	k_{cat} (s^{-1})	1.00 ± 0.13	0.29 ± 0.04
	$K_{1/2}$ (g/L)	16.68 ± 8.51	42.80 ± 17.65
	$k_{cat}/K_{1/2}$ ($L\cdot[g\cdot s]^{-1}$)	0.08 ± 0.05	0.008 ± 0.003
	$^{kin}\Gamma_{max}$ (nmol/g)	1.77 ± 0.24	0.90 ± 0.14
	$^{ads}\Gamma_{max}$ (nmol/g)	24.62 ± 2.43	16.61 ± 0.62
	A/B ratio (%)	6.97 ± 1.31	5.32 ± 0.84
	K_d (nM)	354.1 ± 24.5	437.4 ± 22.8

[a] ND: Not determined.

[b] A/B ratio: Density of attack sites/density of binding sites.

Table S3. Summary of characteristics of N-terminal domain truncations in PULIs

Organism	GenBank accession no.	Modular organization of wild type & truncated variants	Enzymatic properties		Kinetic parameters [a]		Relative activity (%) [b]	Ref.
			Temperature optimum (°C)	pH optimum	K_M (mg/mL)	k_{cat} (s^{-1})		
Lactobacillus acidophilus	AAV43522.1	CBM41-DUF1- DUF2-CBM48-GH13	60	5.5	0.04	484	100	5, and this study
		DUF1- DUF2-CBM48-GH13	60	5.5	0.45	6575	131	
		CBM48-GH13	40	5.5	0.05	391	69	
B. deramificans	CAC60157.1	CBM41-X45a-X25-X45b-CBM48-GH13	60	4.5	0.34	2031	100	7
		X45a-X25-X45b-CBM48-GH13	60	4.5	0.56	2685	93.9	
		X45a-X45b-CBM48-GH13	60	4.5	1.05	2851	111.0	
B. acidopullulyticus	AX203843.1	CBM41-X45a-X25-X45b-CBM48-GH13	60	5.0	0.60	884	100	8,9
		CBM41-X45a-X45b-CBM48-GH13	60	5.0	0.69	947	102.5	
		X45a-X25-X45b-CBM48-GH13	60	5.0	1.42	1864	106.5	
		X45a-X45b-CBM48-GH13	60	5.0	1.85	1751	115.9	
Bacillus megaterium	MH229770	CBM41a-CBM41b-X-CBM48-GH13	45	6.5	2.4	ND[c]	100	10
		CBM48-GH13	50	7.0	3.1	ND	28.3	
Bacillus methanolicus PB1	WP_004439017.1	CBM68-CBM48-GH13	50	5.5	ND	ND	100	11
		CBM48-GH13	45	6.0	ND	ND	48.3	
Anoxybacillus sp. LM18-11	AEW23439.1	CBM68-N2-GH13	60	6.0	16.4[d]	ND	100	12
		N2-GH13	50	6.0	21.8[d]	ND	43.2	
Anoxybacillus sp. WB42	KX576675	CBM68-CBM48-GH13	60	ND	5.7	128	100	13
		CBM48-GH13	60	ND	7.4	45	22	

[a] Kinetic parameter using pullulan as substrate.

[b] Specific activity relative to wild type enzyme on pullulan.

[c] ND: not determined.

[d] K_M calculated in μmol/L.

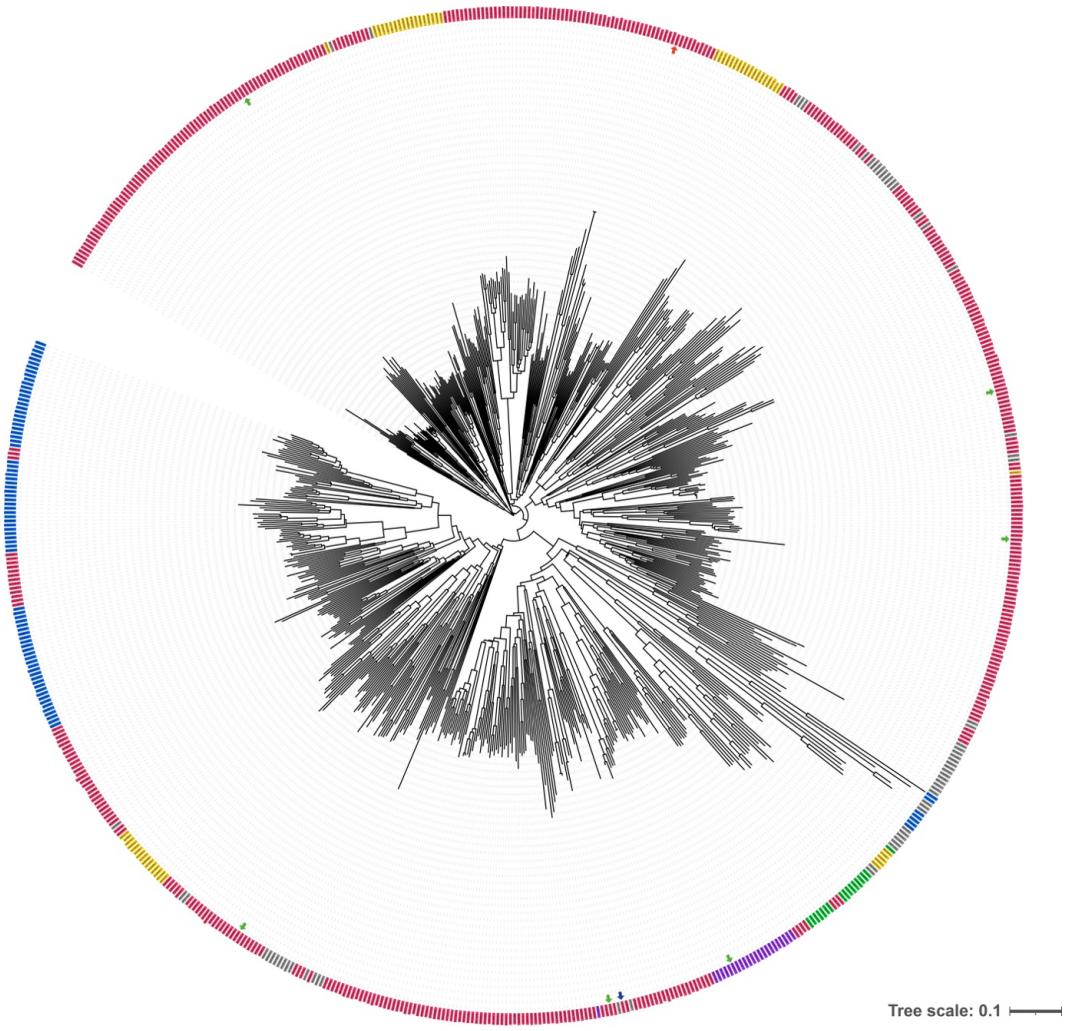

Figure S1. Phylogenetic tree of pullulanase in GH 13_14. The tree was constructed according to the multiple alignment including the CDs of 731 representative GH13_14 sequences (redundancy was reduced using CD-HIT[14] with a 90% sequence identity cut-off). PULI from *Lactobacillus acidophilus* NCFM (red arrow), characterized PULIs with crystal structure (green arrow), and PULI from *Bacillus deramifican* (blue arrow) are marked. The origin of the full-length proteins is show in the ring: *Bacillota* (red), *Pseudomonadota* (green), *Bacteroidota* (blue), *Actinomycetota* (yellow), *Thermotogota* (purple), and others (gray). Gene sequences were obtained from the NCBI database (https://www.ncbi.nlm.nih.gov/).

REFERENCES

(1) Zhong, Y.; Bertoft, E.; Li, Z.; Blennow, A.; Liu, X. Amylopectin starch granule lamellar structure as deduced from unit chain length data. *Food Hydrocoll.* **2020**, *108*, 106053.

(2) Blennow, A.; Wischmann, B.; Houborg, K.; Ahmt, T.; Jørgensen, K.; Engelsen, S. B.; Bandsholm, O.; Poulsen, P. Structure function relationships of transgenic starches with engineered phosphate substitution and starch branching. *Int. J. Biol. Macromol.* **2005**, *36*, 159–168.

(3) Kozlov, S. S.; Blennow, A.; Krivandin, A. V; Yuryev, V. P. Structural and thermodynamic properties of starches extracted from GBSS and GWD suppressed potato lines. *Int. J. Biol. Macromol.* **2007**, *40*, 449–460.

(4) Carciofi, M.; Blennow, A.; Jensen, S. L.; Shaik, S. S.; Henriksen, A.; Buléon, A.; Holm, P. B.; Hebelstrup, K. H. Concerted suppression of all starch branching enzyme genes in barley produces amylose-only starch granules. *BMC Plant Biol.* **2012**, *12*, 1–16.

(5) Møller, M. S.; Goh, Y. J.; Rasmussen, K. B.; Cypryk, W.; Celebioglu, H. U.; Klaenhammer, T. R.; Svensson, B.; Abou Hachem, M. An extracellular cell-attached pullulanase confers branched α-glucan utilization in human gut *Lactobacillus acidophilus*. *Appl. Environ. Microbiol.* **2017**, *83*, 1–13.

(6) Vester-Christensen, M. B.; Abou Hachem, M.; Naested, H.; Svensson, B. Secretory expression of functional barley limit dextrinase by *Pichia pastoris* using high cell-density fermentation. *Protein Expr. Purif.* **2010**, *69*, 112–119.

(7) Duan, X.; Wu, J. Enhancing the secretion efficiency and thermostability of a *Bacillus deramificans* pullulanase mutant (D437H/D503Y) by N-terminal domain truncation. *Appl. Environ. Microbiol.* **2015**, *81*, 1926–1931.

(8) Chen, A.; Sun, Y.; Zhang, W.; Peng, F.; Zhan, C.; Liu, M.; Yang, Y.; Bai, Z. Downsizing a pullulanase to a small molecule with improved soluble expression and secretion efficiency in *Escherichia coli*. *Microb. Cell Fact.* **2016**, *15*, 1–10.

(9) Chen, A.; Liu, X.; Dai, X.; Zhan, J.; Peng, F.; Li, L.; Wang, F.; Li, S.; Yang, Y.; Bai, Z. Effect of N-terminal truncation of *Bacillus acidopullulyticus* pullulanase on enzyme properties and functions. *Shengwu Gongcheng Xuebao/Chinese J. Biotechnol.* **2016**, *32*, 355–364.

(10) Jiao, Y. L.; Wu, Y.; Chen, H. X.; Wang, S. J.; Chen, L.; Lv, M. S.; Fang, Y. W.; Liu,

S. The impact of N-terminal nonessential domains on the enzymological properties of the pullulanase from a marine *Bacillus megaterium*. *Biotechnol. Lett.* **2019**, *41*, 849–857.

(11) Zhang, S. Y.; Guo, Z. W.; Wu, X. L.; Ou, X. Y.; Zong, M. H.; Lou, W. Y. Recombinant expression and characterization of a novel cold-adapted type I pullulanase for efficient amylopectin hydrolysis. *J. Biotechnol.* **2020**, *313*, 39–47.

(12) Xu, J.; Ren, F.; Huang, C.; Zheng, Y.; Zhen, J.; Sun, H.; Ko, T.; He, M.; Chen, C.; Chan, H. Functional and structural studies of pullulanase from *Anoxybacillus* sp. LM18-11. *Proteins Struct. Funct. Bioinforma.* **2014**, *82*, 1685–1693.

(13) Wang, J.; Liu, Z.; Zhou, Z. The N-terminal domain of the pullulanase from *Anoxybacillus* sp. WB42 modulates enzyme specificity and thermostability. *ChemBioChem* **2018**, *19*, 949–955.

(14) Huang, Y.; Niu, B.; Gao, Y.; Fu, L.; Li, W. CD-HIT Suite: A web server for clustering and comparing biological sequences. *Bioinformatics* **2010**, *26*, 680–682.

2.2.2 Paper 3 – An Enzymatic Approach to Quantify Branching on the Surface of Starch Granules by Interfacial Catalysis

This paper (Short Communication) was accepted for publication in *Food Hydrocolloids* on the 12th of August 2023. The paper presents results on a novel approach to quantify branch points on the surface of starch granules by interfacial kinetics using a commercial pullulanase as a probe. The supporting information can be found at the end of the paper. The permission to reuse this article in this PhD thesis was obtained from the publisher.

Food Hydrocolloids 146 (2024) 109162

Contents lists available at ScienceDirect

Food Hydrocolloids

journal homepage: www.elsevier.com/locate/foodhyd

An enzymatic approach to quantify branching on the surface of starch granules by interfacial catalysis

Yu Wang [a], Yu Tian [b], Stefan Jarl Christensen [c], Andreas Blennow [b], Birte Svensson [a,*], Marie Sofie Møller [d,**]

[a] Enzyme and Protein Chemistry, Department of Biotechnology and Biomedicine, Technical University of Denmark, DK-2800, Kgs. Lyngby, Denmark
[b] Department of Plant and Environmental Sciences, University of Copenhagen, DK-1871, Frederiksberg C, Denmark
[c] Protein Chemistry and Enzyme Technology, Department of Biotechnology and Biomedicine, Technical University of Denmark, DK-2800, Kgs. Lyngby, Denmark
[d] Applied Molecular Enzyme Chemistry, Department of Biotechnology and Biomedicine, Technical University of Denmark, DK-2800, Kgs. Lyngby, Denmark

ARTICLE INFO

Keywords:
Starch granules
Interfacial catalysis
Surface branch points
Attack site density
Glucotransferase
Chain length distribution

ABSTRACT

Enzymatically modified starch granules are useful in the food industry by endowing improved thermal properties, resistance to digestion and complexation capacity. However, it is of interest to correlate structural features on the granular surface with functional characteristics relevant to given applications. To meet this requirement, a method was developed to quantify the density of α-1,6 branch points on differently structured starch granules as based on interfacial enzyme catalysis. The branch points are attacked by pullulanase, a debranching enzyme, and the branch point density, as calculated from the kinetic attack site density ($^{kin}\Gamma_{max}$), was linked to the chain length distribution (CLD) of the released segments. The procedure involved a combination of conventional and inverse Michaelis–Menten (MM) kinetics for pullulanase degradation of native, branching enzyme- or 4-α-glucanotransferase-modified granular waxy and normal maize starch (WMS and NMS). The treatment by branching enzyme increased the branch point density for WMS from 1.7 to 3.3 nmol/g starch granules. CLD analysis indicated that 4-α-glucanotransferase catalyzed hydrolysis and/or cyclization on the surface of the granules, rather than disproportionation. The CLD data reflected the different spatial organization of amylopectin chains within WMS and NMS granules related to their different amylose contents of 0.7 and 20.7%, respectively. Scanning electron microscopy confirmed that the starch granules retained the morphology without prominent cracks or pores after pullulanase hydrolysis for the analysis of interfacial kinetics. Comparison with the corresponding gelatinized starches gave new insights into the connection between substrate structure and specificity of the two glucotransferases acting on the different starches.

1. Introduction

Starch is a widely occurring renewable plant polysaccharide that plays a major role in the food industry (Chi et al., 2021). For most applications, starch is gelatinized in heat-moisture processes (Liu et al., 2020; Zhong et al., 2022). However, focus on sustainability and energy-saving motivates use of the raw starch granules and their applications are emerging (Liu et al., 2020; Zhong et al., 2022). To confer novel functionalities and enhance its positive attributes, starch is generally subjected to functional improvements by structural engineering using enzymatic, chemical or physical treatments (Li et al., 2023; Miao & Bemiller, 2023). Clearly enzyme treatment of native starch granules represents an environmentally friendly strategy. Moreover, it is attractive because it avoids high viscosity and instability caused by retrogradation as compared to treatment of gelatinized starch (Wang, Li, Copeland, Niu, & Wang, 2015). Overall, there is currently a growing interest in the application of various transglycosylases or hydrolytic enzymes for modifying granular starches (Guo, Deng, Lu, Zou, & Cui, 2019; Miao & Bemiller, 2023; Zhong et al., 2022). Notably, maize starch granules modified by branching enzyme (Ren et al., 2020; Zhong et al., 2021) or cyclodextrin glycosyltransferase (Dura & Rosell, 2016) have shown higher resistance to digestion.

Several techniques have been used to analyze enzyme-modified starches, including high performance anion exchange chromatography

* Corresponding author.
** Corresponding author.
E-mail addresses: bis@bio.dtu.dk (B. Svensson), msmo@dtu.dk (M.S. Møller).

https://doi.org/10.1016/j.foodhyd.2023.109162
Received 6 June 2023; Received in revised form 9 August 2023; Accepted 12 August 2023
Available online 12 August 2023

with pulsed amperometric detection (HPAEC-PAD), size exclusion chromatography-multi-angle laser light scattering-refractive index detection (SEC-MALLS-RI) and ^{1}H NMR (Zhai, Li, Bai, Jin, & Svensson, 2022). However, these methods were developed for solubilized starch and are not suitable for direct analysis of structural changes on starch granule surfaces. Recently we introduced a procedure for kinetics analysis of the interfacial hydrolysis of α-1,4-linkages on the surface of different granular starches using the *exo*-acting glucoamylase and *endo*-acting α-amylase (Tian, Wang, Liu, et al., 2023; Tian, Wang, Zhong, et al., 2023; Wang, Tian, et al., 2023). This involved combining conventional and inverted Michaelis-Menten (MM) kinetics having substrate and enzyme, respectively, in excess, which lead to values of the density of enzyme attack sites, $^{kin}\Gamma_{max}$ (in units of mol/g), on the granules (Tian, Wang, Liu, et al., 2023; Wang, Tian, et al., 2023). The used approach was inspired by kinetics analysis of the heterogenous catalysis of cellulase depolymerization of crystalline cellulose (Kari, Andersen, Borch, & Westh, 2017).

Here, we adopt the kinetics analysis of heterogenous catalysis to enumerate α-1,6-linked branch points hydrolyzed by *Bacillus licheniformis* pullulanase (*Bl*Pul) (Abdel-Naby, Osman, & Abdel-Fattah, 2011) on the surface of granules of waxy and normal maize starch (WMS and NMS). This new method was validated using the same WMS and NWS granular starches, which were pretreated by either branching enzyme from *Rhodothermus obamensis* (*Ro*BE; EC 2.4.1.18; glucoside hydrolase family 13, GH13) that catalyzes the introduction of new α-1,6 linked branch chains (Tetlow & Emes, 2014) or by 4-α-glucanotransferase from *Thermoproteus uzoniensis* (TuαGT; EC 2.4.1.25; GH77), which is able to catalyze four reactions on starch, namely hydrolysis, coupling, cyclization and disproportionation (Wang et al., 2020). The disproportionation reaction is particularly attractive as it delivers elongated exterior branch chains in amylopectin by transfer of short fragments from amylose to non-reducing chain ends via new α-1,4-linkages (Wang et al., 2020). In the current study, surprisingly it was found that TuαGT did not elongate the chains on the surface of granular starches, but rather catalyzed hydrolysis and/or cyclization. Despite this, the contrasting effects of *Ro*BE and TuαGT on solubilized and granular starches provide novel insights into modification of starch granules using glucanotransferases.

2. Material and methods

2.1. Materials

Waxy maize starch (WMS) was a kind gift of Cargill, USA, and normal maize starch (NMS) of Archer Daniels Midland (ADM, Decatur, IL). Pullulanase M2 from *Bacillus licheniformis* (*Bl*Pul, E-PULBL, 900 U/mL) was purchased from Megazyme Co. Ltd (Wicklow, Ireland). Branching enzyme from *Rhodothermus obamensis* (*Ro*BE, 5.98 U/mg) was a kind gift of Novozymes, Denmark. *Thermoproteus uzoniensis* 4-α-glucanotransferase (TuαGT, 542 U/mg) was produced as described (Wang et al., 2020).

2.2. Modification of granular starch

Starch (6%, w/v), washed twice with MilliQ water and once with reaction buffer (20 mM sodium citrate, pH 6.0), was suspended in reaction buffer and modified by either 1.0 U *Ro*BE or 32.5 U TuαGT per 1 g starch (50 °C, 20 h). As a control, starch was incubated with reaction buffer (50 °C, 20 h). Reactions were terminated by addition of Na_2CO_3 (final concentration: 0.3 M) followed by centrifugation (10,000 *g*, 5 min) after 10 min of incubation. The unmodified (control) and modified starch granules were washed with MilliQ water and freeze-dried.

2.3. Modification of gelatinized starch

Starch (6%, w/v) was washed as above and suspended in reaction buffer, gelatinized (99 °C, 30 min), cooled and modified by either 1.0 U *Ro*BE (60 °C, 20 h) or 32.5 U TuαGT (70 °C, 20 h) per 1 g starch. As a control, gelatinized starch was incubated with reaction buffer (60 °C, 20 h). Reactions were terminated by heating (100 °C, 30 min). The unmodified and modified starch were precipitated by three volumes of ethanol, centrifuged (10,000 *g*, 5 min), kept overnight at −80 °C, and freeze-dried.

2.4. Chain length distribution (CLD)

Granular starch (50 mg/mL, w/v), resuspended in 50 mM sodium acetate pH 5.5, was debranched by 50 nM (final concentration) *Bl*Pul (25 °C, 30 min), followed by centrifugation (10000 *g*, 5 min). Gelatinized starch (5 mg/mL, w/v) was suspended in 50 mM sodium acetate pH 5.5, gelatinized again (99 °C, 30 min), debranched by 50 nM (final concentration) *Bl*Pul (42 °C, 2 h) and centrifuged (10000 *g*, 5 min). The supernatants were analyzed by HPAEC-PAD to determine the CLD as described (Christensen et al., 2022).

2.5. Determination of attack site density ($^{kin}\Gamma_{max}$) on the starch granule surface

The attack site density, $^{kin}\Gamma_{max}$, was determined for *Bl*Pul by a combination of conventional and inverse MM kinetics, adopting procedures applied for enzymatic hydrolysis of solid polysaccharide substrates as discussed in more detail elsewhere (Andersen, Kari, Borch, & Westh, 2018; Kari et al., 2017, 2018; Tian, Wang, Liu, et al., 2023; Tian, Wang, Zhong, et al., 2023; Wang, Tian, et al., 2023). Briefly, in conventional MM analysis starch granules (15–150 mg/mL, 135 μL) were pre-incubated (25 °C, 15 min, 1100 rpm), added *Bl*Pul (15 μL, final 62.5 nM) and incubated (25 °C, 1100 rpm). For inverse MM analysis, *Bl*Pul (0.3–625 nM) was added to starch granules (20 mg/mL) and after 30 min, which is within the linear range of hydrolysis (data not shown), aliquots (100 μL) were transferred to new tubes, mixed with 20 μL 1.8 M Na_2CO_3 to terminate the reaction, and centrifuged (10000 *g*, 5 min). The concentration of reducing sugar in the supernatants was determined using the PAHBAH assay with glucose as standard (Lever, Powell, Killip, & Small, 1973).

Conventional MM kinetics (substrate in excess) were analyzed according to eq. (1), where S_0^{mass} is substrate mass load and $K_{1/2}$ the mass load at substrate half-saturation. Non-linear regression analyses of the data returned values of V_{max} (in M·s^{-1}) and $K_{1/2}$ (in g·L^{-1}).

$$v_0 = \frac{V_{max} \cdot S_0^{mass}}{K_{1/2} + S_0^{mass}} \quad (1)$$

Inverse MM kinetics (enzyme in excess) were analyzed according to eq. (2), where E_0 is enzyme concentration and K_M the enzyme concentration at enzyme half-saturation. Nonlinear regression analysis of data led to $^{inv}V_{max}$ (in g·L^{-1}·s^{-1}) and K_M (in M).

$$v_0 = \frac{^{inv}V_{max} \cdot E_0}{K_M + E_0} \quad (2)$$

The $^{kin}\Gamma_{max}$ was determined from V_{max} (eq. (1)) and $^{inv}V_{max}$ (eq. (2)) using eq. (3) as previously described (Kari et al., 2017).

$$\frac{\frac{^{inv}V_{max}}{S_0^{mass}}}{\frac{V_{max}}{E_0}} = {}^{kin}\Gamma_{max} \quad (3)$$

For validation of quasi-steady state assumption (QSSA) (Kari et al., 2017) see Supplementary material.

2.6. Scanning electron microscopy (SEM)

Starch granules (20 mg/mL) were suspended in reaction buffer, treated with 625 nM *Bl*Pul (25 °C, 30 min, 1100 rpm) and the reactions were terminated by addition of Na_2CO_3 (final concentration: 0.3 M) and centrifuged (10,000 *g*, 5 min) after 10 min. The starch granules were washed with MilliQ water and freeze-dried. For imaging, all starch

granules were mounted on carbon tapes on aluminum SEM stubs and sputter-coated with 6 nm gold under a Leica EM ACE200 gold coater (Leica Microsystems, Wetzlar, Germany). Both overall and detailed morphology of granular starch samples were visualized using field emission scanning electron microscopy (FE-SEM) using an FEI Quanta 200 microscope at 3500 × and 15,000 × magnification, respectively, as previously described (Tian, Wang, Liu, et al., 2023).

3. Results and discussion

3.1. CLD of starches before and after enzymatic modification

Treatment of starch by either *Ro*BE or TuαGT led to an increase in the number of branch chains and longer branch chains, respectively (Table 1). It is noteworthy that the enzyme modifications of both granular and gelatinized starches were carried out using the same enzyme concentration and starch loads. Importantly, the precise substrate concentration represented by accessible branch points (α-1,6 glucosidic bonds) on the starch granule surface was not accurately known.

The *Ro*BE-modified granular WMS exhibited 2.5-fold higher and 9.5-fold lower proportion of A-chains (DP < 12) and B_1-chains, respectively, compared to native WMS granules (Table 1, Fig. 1A). On the other hand, in *Ro*BE-modified granular NMS A-chains only increased 1.9-fold while B_1-chains decreased 10.7-fold compared to the native NMS (Table 1, Fig. 1B). Thus *Ro*BE-catalyzed transfer of maltooligosaccharide chains yielded new branches in amylopectin, leading to a shorter average length of the branch chains released from the granules by *Bl*Pul. By contrast, modification of gelatinized WMS using *Ro*BE increased the proportion of A-chains by only 1.3-fold, and reduced the proportion of B_1-(DP 13–24) and B_3-chains (DP > 37) by 1.1-fold (Table 1, Fig. 1C). Similarly, *Ro*BE-modified gelatinized NMS exhibited 1.2-fold increase in A-chains and 1.1−1.2-fold decrease in B_1- and B_3-chains compared to gelatinized unmodified NMS (Table 1, Fig. 1D). Consequently, *Ro*BE demonstrated highly efficient catalytic activity in introducing new branch chains onto the surface of starch granules as shown by the *Bl*Pul CLD analysis confirming the *Ro*BE-mediated enrichment of short chains on the granular surface.

The TuαGT modification of granular WMS (Fig. 1A) resulted in a 1.2-fold increase in A-chains and decreased B_1, B_2- and B_3-chains by 1.1-, 1.1- and 1.8-fold, respectively, compared to native WMS. This resulted in a slight overall decrease in DP_{Ave} (Table 1). A similar trend was seen by TuαGT modification of NMS granules, where 1.3-fold higher and 1.2-fold lower proportions, respectively of A- and B_1-chains were obtained relative to native NMS granules (Fig. 1B; Table 1). The CLD patterns for the corresponding native and modified gelatinized starches differed, as in case of WMS, both A- and B_1-chains slightly decreased by 1.1-fold, while B_2- and B_3-chains increased by 1.2- and 1.1-fold, respectively. NMS exhibited a similar pattern, although its B_1-chain content remained unchanged (Table 1). The CLD data supported the role of TuαGT catalyzing disproportionation between glucan chains, resulting in less short and more long chains. Notably, among the four different reactions catalyzed by TuαGT, only hydrolysis and cyclization will lead to an overall decrease in average chain length as found for the surface of modified granular starches (Table 1). Therefore, TuαGT apparently mainly catalyzed hydrolysis and/or cyclization of branch chains on the starch granules, but catalyzed disproportionation of the branch chains in gelatinized starches (Table 1).

3.2. Density of BlPul attack sites ($^{kin}\Gamma_{max}$) on granular starches before and after enzymatic modification

Normally the α-1,6-/α-1,4-linkage ratio of starch is determined by ^{1}H NMR spectroscopy after complete gelatinization. However, this method is not suitable for the analysis of starch granule surfaces since these only constitute a fraction of the entire starch granule.

Table 1
Relative content of different branch chains released by *Bl*Pul from granular and gelatinized WMS and NMS before and after modification by either *Ro*BE or TuαGT.

Starch	Type of chain[a]	Native starch	*Ro*BE modified starch	TuαGT modified starch
Granular WMS	A-chain	37.4 ± 0.9[b] (100[c])	94.3 ± 3.1 (252)	44.0 ± 0.9 (118)
	B_1-chain	54.1 ± 1.1 (100)	5.7 ± 0.4 (11)	48.5 ± 1.1 (90)
	B_2-chain	7.7 ± 0.3 (100)	ND[d]	7.1 ± 0.5 (92)
	B_3-chain	0.7 ± 0.0 (100)	ND	0.4 ± 0.1 (57)
	DP_{Ave}[e]	14.9 ± 0.8 (100[f])	5.7 ± 0.4 (38)	13.1 ± 1.1 (88)
	α-1,6-/α-1,4-linkage ratio	7.2	21.1	8.3
Granular NMS	A-chain	51.0 ± 1.3 (100)	96.0 ± 2.9 (188)	65.5 ± 1.5 (128)
	B_1-chain	42.9 ± 1.1 (100)	4.0 ± 0.3 (9)	34.5 ± 0.7 (80)
	B_2-chain	5.9 ± 0.4 (100)	ND	ND
	B_3-chain	0.2 ± 0.0 (100)	ND	ND
	DP_{Ave}	12.6 ± 1.2 (100)	6.6 ± 0.5 (52)	9.5 ± 0.7 (75)
	α-1,6-/α-1,4-linkage ratio	8.7	18.0	11.8
Gelatinized WMS	A-chain	18.7 ± 0.3 (100)	25.0 ± 0.7 (134)	16.8 ± 0.4 (90)
	B_1-chain	39.0 ± 0.8 (100)	35.0 ± 0.3 (90)	35.2 ± 1.3 (90)
	B_2-chain	20.6 ± 0.6 (100)	20.6 ± 1.0 (100)	23.8 ± 1.5 (116)
	B_3-chain	21.7 ± 2.2 (100)	19.4 ± 1.0 (89)	24.2 ± 1.1 (112)
	DP_{Ave}	25.2 ± 1.8 (100)	23.9 ± 2.1 (95)	26.9 ± 1.9 (107)
Gelatinized NMS	A-chain	32.0 ± 0.2 (100)	38.7 ± 1.0 (121)	28.9 ± 1.1 (90)
	B_1-chain	41.9 ± 0.7 (100)	36.9 ± 1.1 (88)	41.3 ± 1.9 (99)
	B_2-chain	16.8 ± 0.3 (100)	16.4 ± 0.8 (98)	19.6 ± 0.5 (117)
	B_3-chain	9.2 ± 0.5 (100)	8.0 ± 0.2 (87)	10.2 ± 0.3 (111)
	DP_{Ave}	19.0 ± 0.9 (100)	17.9 ± 1.1 (94)	20.1 ± 1.4 (106)

[a] A-chain: DP 1–12, B_1-chain: DP 13–24, B_2-chain: DP 25−36, and B_3-chains: DP > 37 (Bertoft, 2017).
[b] Values are means ± standard deviation.
[c] Percentage of the relative content of chains for unmodified starch (100%) are given in parentheses.
[d] ND: not determined.
[e] Average DP.
[f] Percentage of the DP_{Ave} of chains for unmodified starch (100%) are given in parentheses.

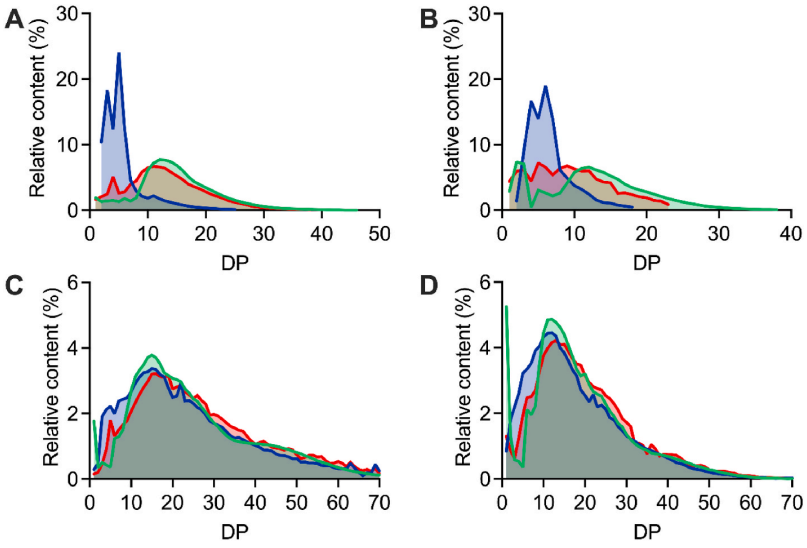

Fig. 1. Chain length distribution (CLD) of products released by *Bl*Pul from granular and gelatinized starches. (A) Granular WMS, (B) granular NMS, (C) gelatinized WMS, (D) gelatinized NMS. The granules were native (green), modified by *Ro*BE (blue) or TuαGT (red).

The cornerstone of the presented new method is the specific hydrolysis of α-1,6-linkages (branch points) on the starch granule surface by *Bl*Pul (Jung et al., 2013). This hydrolysis enables quantification of the density of branch points ($^{kin}\Gamma_{max}$) by using a combination of conventional and inverse MM kinetics implemented for heterogenous catalysis (Tian, Wang, Liu, et al., 2023; Wang, Tian, et al., 2023). The two MM equations (Section 2.5, eqs. (1) and (2)) were firstly validated under the quasi-steady-state assumption (QSSA) (Fig. S1 and Supplementary material "Validation of Quasi-Steady State Assumption (QSSA)") (Kari et al., 2017). The validity ranges of the conventional and inverse MM equations were calculated according to eqs. S1 and S2 and illustrated in Fig. S1. This confirmed that interfacial kinetics analysis for all six starch samples provided sufficient data to estimate the desired parameters (E_0, S_0^{mass}, $K_{1/2}$, K_M, $^{kin}\Gamma_{max}$). In the conventional MM approach starch in the range 20–150 mg/mL and 62.5 nM *Bl*Pul fell within the region of conventional MM, ensuring that the substrate was in excess, thus the QSSA was valid for conventional MM analysis (Kari et al., 2017; Schnell, 2014). Furthermore, for the inverse approach *Bl*Pul of 0.3–625 nM and 20 mg/mL starch were within the range of inverse MM, hence the enzyme was in excess and the QSSA was valid under inverse MM.

The attack site density, $^{kin}\Gamma_{max}$, varied significantly between the two types of starch granules. Specifically, WMS contained 1.7 nmol and NMS 0.9 nmol of α-1,6-linkages cleaved by *Bl*Pul per g of starch. This variation in $^{kin}\Gamma_{max}$ can be attributed primarily to the different amylopectin contents. Moreover, it may reflect the differences between WMS and NMS in CLD patterns and thus branch point environments, crystallinity and double helical chain contents. Notably, the $^{kin}\Gamma_{max}$ values for α-amylase acting on WMS was 0.28 nmol/g, which was 1.6-fold higher than 0.17 nmol/g observed for NMS granules (Tian, Wang, Liu, et al., 2023; Wang, Tian, et al., 2023). These previous findings are comparable with the present 1.9-fold higher attack site density for *Bl*Pul on WMS compared to NMS. Besides, kinetics analysis of glucoamylase, which removes glucose from non-reducing ends (Sauer et al., 2000), acting on six starch types showed 14.6-fold higher k_0 (molecular activity of the enzyme) on granular rice starch than on potato starch (Tatsumi & Katano, 2005). The different k_0 for different starches might stem from the density of non-reducing ends on the surface of starch granules. This suggests k_0 as an indicator for the non-reducing ends in starch, similar to the $^{kin}\Gamma_{max}$ values obtained in the present work for *Bl*Pul.

The α-1,6-/α-1,4-linkage ratio can be calculated from the $^{kin}\Gamma_{max}$ and the values of DP_{Ave} of branch chains released by *Bl*Pul from the granular surface (Table 1) according to eq. (4).

$$\alpha\text{-}1,6\text{-}\Big/\alpha\text{-}1,4\text{-linkage ratio} = \frac{^{kin}\Gamma_{max}}{(DP_{Ave}-1)\times {}^{kin}\Gamma_{max}} \times 100 \quad (4)$$

Remarkably, the α-1,6-/α-1,4-ratio of 7.2% for the WMS granule surface was very similar to 7.0% determined for gelatinized WMS by using ^{1}H NMR spectroscopy (Chen et al., 2017). Surprisingly, the granular NMS showed an α-1,6-/α-1,4-ratio of 8.2%, which is 1.1-fold higher than of WMS, whereas a 1.4-fold lower α-1,6-/α-1,4-ratio was reported for gelatinized NMS than for WMS as determined by ^{1}H NMR (Chen et al., 2017). This discrepancy relates to NMS containing 20.7% amylose as opposed to 0.7% in WMS (Htoon et al., 2009; Tian et al., 2022). The presence of the mainly linear amylose, interspersed among amylopectin molecules in starch granules, influences the distribution of amylopectin (Bertoft, 2017). Thus, due to the very low amylose content, amylopectin is relatively evenly distributed in WMS, and a similar α-1,6-/α-1,4-ratio may be expected for the amylopectin exposed on the surface of the WMS granules as determined in the corresponding gelatinized WMS. However, in NMS granules the presence of amylose results in an uneven distribution of amylopectin on the granular surface, leading to a higher α-1,6-/α-1,4-ratio compared to in the corresponding gelatinized NMS representing the entire granule.

WMS and NMS granules modified by *Ro*BE exhibited 1.9- and 2.3-fold higher $^{kin}\Gamma_{max}$, respectively, compared to the corresponding unmodified granules (Fig. 2C, F). This increase in $^{kin}\Gamma_{max}$ aligns with *Ro*BE-catalyzed formation of new α-1,6-linkages on the granular surface, as observed for the *Ro*BE-treatment of gelatinized WMS and NMS (Table 1) and in a previous study (Ban et al., 2020). A similar effect of *Ro*BE on NMS was recently reported by using NMR for the α-1,6-/α-1,4-linkage ratio analysis on gelatinized starch after *Ro*BE-modification of NMS granules (Zhong et al., 2021). However, the NMR analysis conducted on gelatinized starch, was not suitable for direct quantification of changes in α-1,6-linkage contents resulting from surface modification.

Notably, the CLD of TuαGT-treated granular starches (Fig. 1C and D) indicated that TuαGT preferably catalyzed hydrolysis or cyclization on the granule surface, which resulted in the shortening of branch chains. Moreover, as expected, $^{kin}\Gamma_{max}$ for *Bl*Pul of TuαGT-treated WMS and NMS granules was essentially the same as for the corresponding unmodified starch granules. This indicates that shortening of branch chains

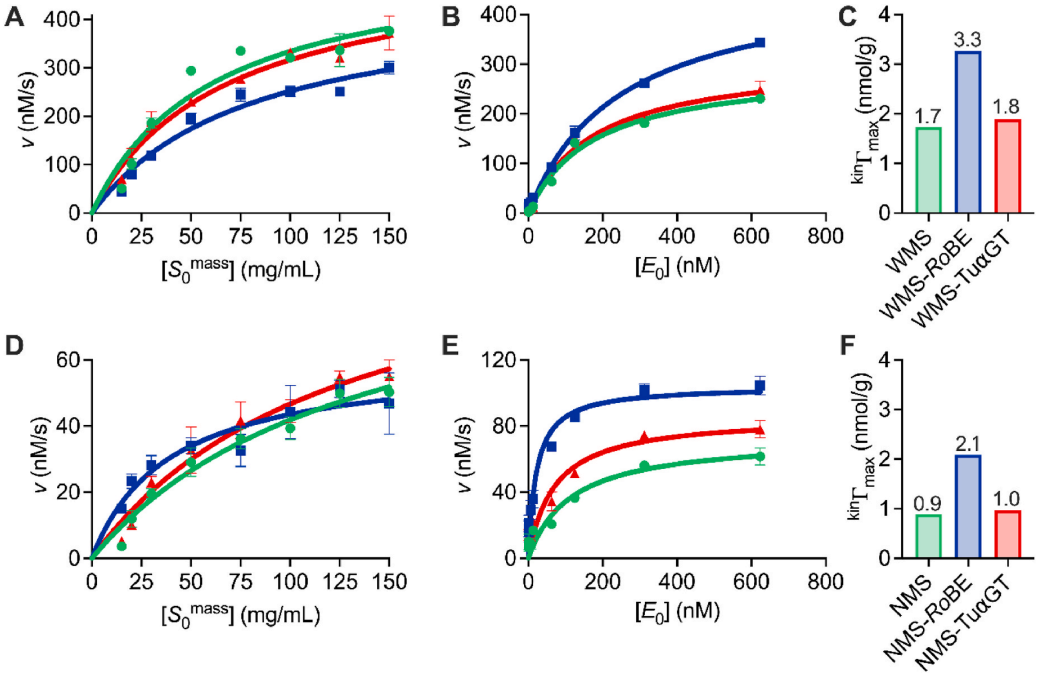

Fig. 2. Interfacial catalysis of *Bl*Pul debranching starches granules at 25 °C and pH 5.5. (A) Conventional, (B) inverse MM kinetics, and (C) $^{kin}\Gamma_{max}$ for WMS (green), WMS-*Ro*BE (blue), and WMS-TuαGT (red). (D) Conventional, (E) inverse MM kinetics, and (F) $^{kin}\Gamma_{max}$ for NMS (green), NMS-*Ro*BE (blue), and NMS-TuαGT (red).

by TuαGT did not affect the recognition of branch points by *Bl*Pul, underscoring that $^{kin}\Gamma_{max}$ is a valid parameter for determining the density of *Bl*Pul-accessible branch points on starch granule surfaces.

3.3. Appearance of starch granule surfaces after BlPul treatment

To assess the impact of *Bl*Pul treatment on the surface of different starch granules, samples subjected to 30 min of reaction in inverse MM kinetics analysis at high E_0/S_0^{mass} were examined using SEM. Prior to debranching, SEM imaging showed overall morphology (Fig. S2) and detailed surface morphology (Fig. 3) as round or irregular shaped granules with smooth surface without significant pores of native, *Ro*BE-, and TuaGT-modified granular starches (Fig. S2, Fig. 3 A–C, G–I). These results align with our previous study, indicating that the modifications caused by *Ro*BE and TuαGT did not affect the surface of the granules (Zhong et al., 2021). Importantly after *Bl*Pul hydrolysis for 30 min, the surface of the granules remained smooth without appearance of more pores or cracks (Fig. 3 D–F, J–L), supporting that the hydrolysis during the kinetic analysis primarily occurs on the starch granule surface (Fig. 3). For enzyme kinetics analysis it is assumed that $^{kin}\Gamma_{max}$ is constant throughout the reaction. While this in principle may not hold true as some substrate conversion occurs, the current set of results from interfacial kinetic analysis indicate that, the extent of substrate conversion was <0.3% in most cases although amounting to 0.5% for the highest E_0 (625 nM) and lowest S_0^{mass} (20 mg/mL). This low degree of substrate consumption indicates that the surface does not undergo significant destruction, supporting the assumption of constant $^{kin}\Gamma_{max}$ during the kinetics analysis.

4. Conclusions

In the present work, we implemented a novel approach to quantify branch points on the surfaces of WMS and NMS granules by measuring the attack site density ($^{kin}\Gamma_{max}$) for *Bl*Pul using heterogenous catalysis. This procedure involved a combination of conventional and inverse MM kinetics and was validated for *Ro*BE- and TuαGT-modified starch granules. Our results demonstrate that *Ro*BE-treatment led to the formation of shorter chains and a reduction in longer chains, as evidenced by the increased attack site density ($^{kin}\Gamma_{max}$) for *Bl*Pul and CLD analysis of the released chains. SEM confirmed that the morphology and surface appearance of the starch granules were essentially unchanged by the enzyme modifications and the pullulanase catalyzed debranching. This method serves as a valuable tool for analyzing branch structures resulting from *Ro*BE- and TuαGT-modifications of the surface of starch granules, and it can be adapted to quantify other modifications of granular starches. Additionally, the method may be applied as a tool to analyze pretreated less compact porous or cold water swollen starch granules, which are physical modifications introduced to minimize need for starch processing.

Author statement

Yu Wang designed and performed the experiments, collected the data, and drafted the manuscript.

Marie Sofie Møller and Birte Svensson developed the theoretical framework and edited the manuscript.

Yu Tian and Andreas Blennow collected the data for chain length distribution of gelatinized starches and scanning electron microscopy images.

Stefan Jarl Christensen collected the data for chain length distribution of ungelatinized starch.

All other authors contributed to the revision and editing.

Declaration of competing interest

The authors declare that they have no known competing financial interests or personal relationships that could have appeared to influence the work reported in this paper.

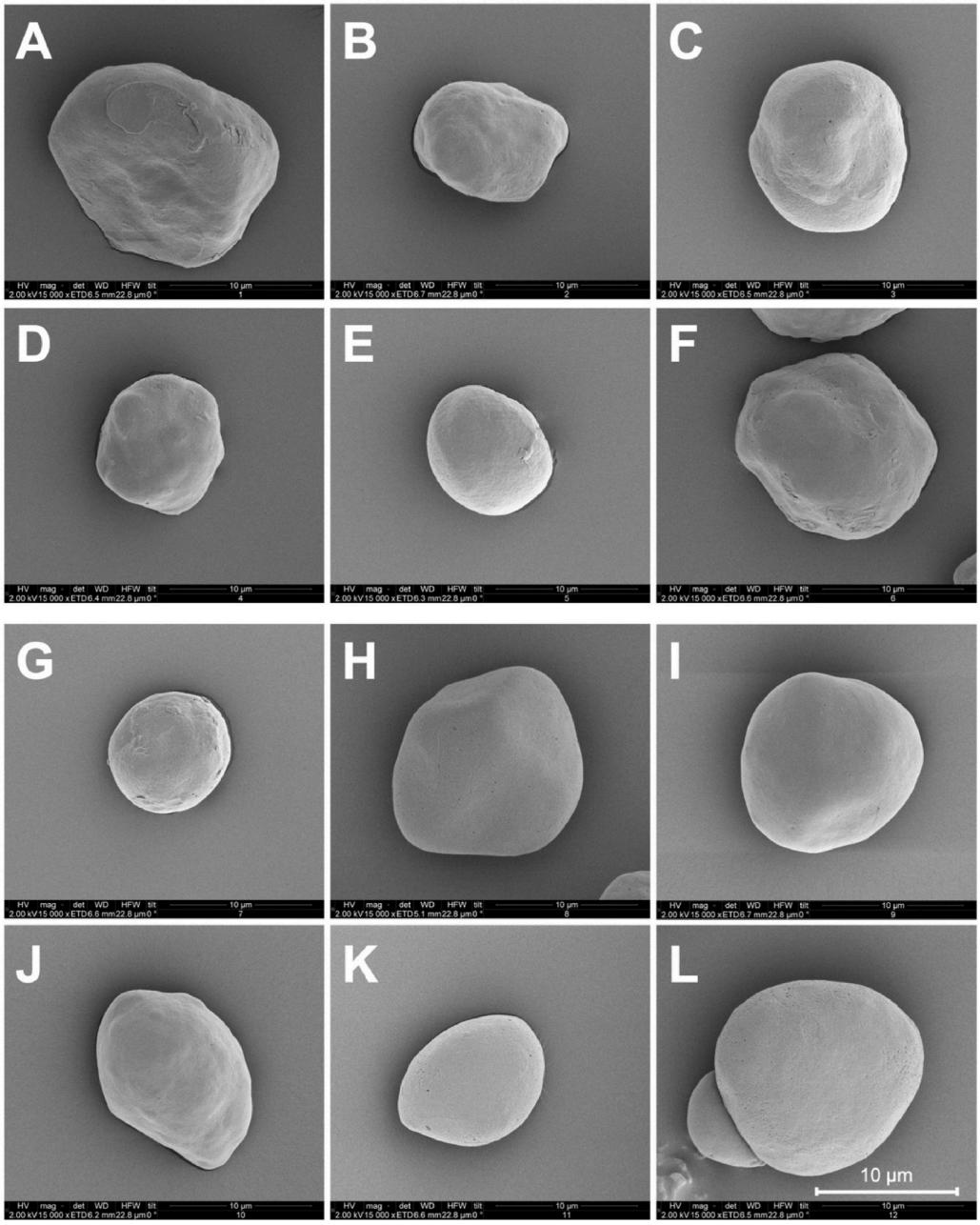

Fig. 3. SEM images of unmodified and modified starch granules before and after 30 min hydrolysis by 625 nM *Bl*Pul. Before hydrolysis (A) WMS, (B) WMS-*Ro*BE, and (C) WMS-TuαGT; after hydrolysis (D) WMS, (E) WMS-*Ro*BE, and (F) WMS-TuαGT. Before hydrolysis (G) NMS, (H) NMS-*Ro*BE, and (I) NMS-TuαGT; after hydrolysis (J) WMS (K) WMS-*Ro*BE, and (L) WMS-TuαGT. Magnification is 15,000 × .

Data availability

Data will be made available on request.

Acknowledgements

Karina Jansen (Department of Biotechnology and Biomedicine, Technical University of Denmark) is gratefully thanked for technical assistance. This work was supported by a China Scholarship Council, China (CSC) grant #202006790033 and the Technical University of Denmark, Denmark (YW), and by a China Scholarship Council, China (CSC) grant #202003250068 (YT). We are thankful to Cargill for providing waxy maize starch and to Archer Daniels Midland for providing normal maize starch.

Appendix A. Supplementary data

Supplementary data to this article can be found online at https://doi.org/10.1016/j.foodhyd.2023.109162.

Abbreviations

4αGT	4-α-glucanotransferase
BE	branching enzyme
*Bl*Pul	pullulanase from *Bacillus licheniformis*
CLD	chain length distribution
DP	degree of polymerization
MM	Michaelis–Menten
NMS	normal maize starch
*Ro*BE	branching enzyme from *Rhodothermus obamensis*
TuαGT	4-α-glucanotransferase from *Thermoproteus uzoniensis*
WMS	waxy maize starch

References

Abdel-Naby, M. A., Osman, M. Y., & Abdel-Fattah, A. F. (2011). Production of pullulanase by free and immobilized cells of *Bacillus licheniformis* NRC22 in batch and continuous cultures. *World Journal of Microbiology and Biotechnology, 27*(12), 2903–2911. https://doi.org/10.1007/s11274-011-0773-8

Andersen, M., Kari, J., Borch, K., & Westh, P. (2018). Michaelis–Menten equation for degradation of insoluble substrate. *Mathematical Biosciences, 296*, 93–97. https://doi.org/10.1016/J.MBS.2017.11.011

Ban, X., Dhoble, A. S., Li, C., Gu, Z., Hong, Y., Cheng, L., et al. (2020). Bacterial 1,4-α-glucan branching enzymes: Characteristics, preparation and commercial applications. *Critical Reviews in Biotechnology, 40*(3), 380–396. https://doi.org/10.1080/07388551.2020.1713720

Bertoft, E. (2017). Understanding starch structure: Recent progress. *Agronomy, 7*(3), 56. https://doi.org/10.3390/agronomy7030056

Chen, Y., Yang, Q., Xu, X., Qi, L., Dong, Z., Luo, Z., et al. (2017). Structural changes of waxy and normal maize starches modified by heat moisture treatment and their relationship with starch digestibility. *Carbohydrate Polymers, 177*, 232–240. https://doi.org/10.1016/j.carbpol.2017.08.121

Chi, C., Li, X., Huang, S., Chen, L., Zhang, Y., Li, L., et al. (2021). Basic principles in starch multi-scale structuration to mitigate digestibility: A review. *Trends in Food Science & Technology, 109*, 154–168. https://doi.org/10.1016/J.TIFS.2021.01.024

Christensen, S. J., Madsen, M. S., Zinck, S. S., Hedberg, C., Sørensen, O. B., Svensson, B., et al. (2022). Enzymatic potato starch modification and structure-function analysis of six diverse GH77 4-alpha-glucanotransferases. *International Journal of Biological Macromolecules, 224*, 105–1149. https://doi.org/10.1016/j.ijbiomac.2022.10.107

Dura, A., & Rosell, C. M. (2016). Physico-chemical properties of corn starch modified with cyclodextrin glycosyltransferase. *International Journal of Biological Macromolecules, 87*, 466–472. https://doi.org/10.1016/j.ijbiomac.2016.03.012

Guo, L., Deng, Y., Lu, L., Zou, F., & Cui, B. (2019). Synergistic effects of branching enzyme and transglucosidase on the modification of potato starch granules. *International Journal of Biological Macromolecules, 130*, 499–507. https://doi.org/10.1016/j.ijbiomac.2019.02.160

Htoon, A., Shrestha, A. K., Flanagan, B. M., Lopez-Rubio, A., Bird, A. R., Gilbert, E. P., et al. (2009). Effects of processing high amylose maize starches under controlled conditions on structural organisation and amylase digestibility. *Carbohydrate Polymers, 75*(2), 236–245. https://doi.org/10.1016/J.CARBPOL.2008.06.016

Jung, K. H., Kim, M. J., Park, S. H., Hwang, H. S., Lee, S., Shim, J. H., et al. (2013). The effect of granule surface area on hydrolysis of native starches by pullulanase. *Starch/Staerke, 65*(9–10), 848–853. https://doi.org/10.1002/star.201200226

Kari, J., Andersen, M., Borch, K., & Westh, P. (2017). An inverse Michaelis-Menten approach for interfacial enzyme kinetics. *ACS Catalysis, 7*(7), 4904–4914. https://doi.org/10.1021/ACSCATAL.7B00838

Kari, J., Olsen, J. P., Jensen, K., Badino, S. F., Krogh, K. B. R. M., Borch, K., et al. (2018). Sabatier principle for interfacial (heterogeneous) enzyme catalysis. *ACS Catalysis, 8*(12), 11966–11972. https://doi.org/10.1021/acscatal.8b03547

Lever, M., Powell, J. C., Killip, M., & Small, C. W. (1973). A comparison of 4-hydroxybenzoic acid hydrazide (PAHBAH) with other reagents for the determination of glucose. *The Journal of Laboratory and Clinical Medicine, 82*(4), 649–655.

Liu, X., Luan, H., Jinglin, Y., Wang, S., Wang, S., & Copeland, L. (2020). A method for characterizing short-range molecular order in amorphous starch. *Carbohydrate Polymers, 242*, Article 116405.

Li, X., Wang, Y., Wu, J., Jin, Z., Dijkhuizen, L., Svensson, B., et al. (2023). Designing starch derivatives with desired structures and functional properties via rearrangements of glycosidic linkages by starch-active transglycosylases. *Critical Reviews in Food Science and Nutrition*, 1–14. https://doi.org/10.1080/10408398.2023.2198604

Miao, M., & Bemiller, J. N. (2023). Enzymatic approaches for structuring starch to improve functionality. *Annual Review of Food Science and Technology, 14*, 1–25. https://doi.org/10.1146/annurev-food-072122-023510

Ren, J., Chen, S., Li, C., Gu, Z., Cheng, L., Hong, Y., et al. (2020). A two-stage modification method using 1, 4-α-glucan branching enzyme lowers the *in vitro* digestibility of corn starch. *Food Chemistry, 305*, Article 125441. https://doi.org/10.1016/j.foodchem.2019.125441

Sauer, J., Sigurskjold, B. W., Christensen, U., Frandsen, T. P., Mirgorodskaya, E., Harrison, M., et al. (2000). Glucoamylase: Structure/function relationships, and protein engineering. *Biochimica et Biophysica Acta (BBA) - Protein Structure and Molecular Enzymology, 1543*(2), 275–293. https://doi.org/10.1016/S0167-4838(00)00232-6

Schnell, S. (2014). Validity of the michaelis–menten equation–steady-state or reactant stationary assumption: That is the question. *FEBS Journal, 281*(2), 464–472.

Tatsumi, H., & Katano, H. (2005). Kinetics of the surface hydrolysis of raw starch by glucoamylase. *Journal of Agricultural and Food Chemistry, 53*(21), 8123–8127. https://doi.org/10.1021/jf050934c

Tetlow, I. J., & Emes, M. J. (2014). A review of starch-branching enzymes and their role in amylopectin biosynthesis. *IUBMB Life, 66*(8), 546–558. https://doi.org/10.1002/iub.1297

Tian, Y., Qu, J., Zhou, Q., Ding, L., Cui, Y., Blennow, A., et al. (2022). High pressure/temperature pasting and gelling of starch related to multilevel structure-analyzed with RVA 4800. *Carbohydrate Polymers, 295*, Article 119858. https://doi.org/10.1016/j.carbpol.2022.119858

Tian, Y., Wang, Y., Liu, X., Herburger, K., Westh, P., Møller, M. S., et al. (2023a). Interfacial enzyme kinetics reveals degradation mechanisms behind resistant starch. *Food Hydrocolloids, 28*, Article 108621. https://doi.org/10.1016/j.foodhyd.2023.108621

Tian, Y., Wang, Y., Zhong, Y., Møller, M. S., Westh, P., Svensson, B., et al. (2023b). Interfacial catalysis during amylolytic degradation of starch granules : Current understanding and kinetic approaches. *Molecules, 28*(9), 3799. https://doi.org/10.3390/molecules28093799%0A

Wang, S., Li, C., Copeland, L., Niu, Q., & Wang, S. (2015). Starch retrogradation: A comprehensive review. *Comprehensive Reviews in Food Science and Food Safety, 14*(5), 568–585. https://doi.org/10.1111/1541-4337.12143

Wang, Y., Li, X., Ji, H., Zheng, D., Jin, Z., Bai, Y., et al. (2020). Thermophilic 4-α-glucanotransferase from *Thermoproteus uzoniensis* retards the long-term retrogradation but maintains the short-term gelation strength of tapioca starch. *Journal of Agricultural and Food Chemistry, 68*(20), 5658–5667. https://doi.org/10.1021/acs.jafc.0c00927

Wang, Y., Tian, Y., Zhong, Y., Suleiman, M. A., Feller, G., Westh, P., et al. (2023a). Improved hydrolysis of granular starches by a psychrophilic α-amylase starch binding domain-fusion. *Journal of Agricultural and Food Chemistry, 71*(23), 9040–9050. https://doi.org/10.1021/acs.jafc.3c01898

Wang, Y., Wu, Y., Christensen, S. J., Janeček, Š., Bai, Y., Møller, M. S., et al. (2023b). Impact of starch binding domain fusion on activities and starch product structure of 4-α-glucanotransferase. *Molecules, 23*, 1320. https://doi.org/10.3390/molecules28031320

Zhai, Y., Li, X., Bai, Y., Jin, Z., & Svensson, B. (2022). Maltogenic α-amylase hydrolysis of wheat starch granules: Mechanism and relation to starch retrogradation. *Food Hydrocolloids, 124*, Article 107256. https://doi.org/10.1016/j.foodhyd.2021.107256

Zhong, Y., Herburger, K., Kirkensgaard, J. J. K., Khakimov, B., Hansen, A. R., & Blennow, A. (2021). Sequential maltogenic α-amylase and branching enzyme treatment to modify granular corn starch. *Food Hydrocolloids, 120*, Article 106904. https://doi.org/10.1016/J.FOODHYD.2021.106904

Zhong, Y., Xu, J., Liu, X., Ding, L., Svensson, B., Herburger, K., et al. (2022). Recent advances in enzyme biotechnology on modifying gelatinized and granular starch. *Trends in Food Science & Technology, 123*(March), 343–354. https://doi.org/10.1016/j.tifs.2022.03.019

Supplementary material

An enzymatic approach to quantify branching on the surface of starch granules by interfacial catalysis

Yu Wang [a], *Yu Tian* [b], *Stefan Jarl Christensen* [c], *Andreas Blennow* [b],

Birte Svensson [a,] *, *Marie Sofie Møller* [d,] *

[a] Enzyme and Protein Chemistry, Department of Biotechnology and Biomedicine, Technical University of Denmark, DK-2800, Kgs. Lyngby, Denmark

[b] Department of Plant and Environmental Sciences, University of Copenhagen, DK-1871, Frederiksberg C, Denmark

[c] Protein Chemistry and Enzyme Technology, Department of Biotechnology and Biomedicine, Technical University of Denmark, DK-2800, Kgs. Lyngby, Denmark

[d] Applied Molecular Enzyme Chemistry, Department of Biotechnology and Biomedicine, Technical University of Denmark, DK-2800, Kgs. Lyngby, Denmark

* Corresponding authors:

Birte Svensson: bis@bio.dtu.dk; phone: +45 45252740

Marie Sofie Møller: msmo@dtu.dk; phone: +45 45252741

Validation of Quasi-Steady State Assumption (QSSA)

To investigate whether the interfacial kinetics analysis fulfill criteria for obeying the Quasi-Steady State Assumption (QSSA), we examined the experimental system used for the conventional and inverse MM, for the relations $E_0 \ll K_{1/2} + S_0$ and $S_0 \ll K_M + E_{0,}$ respectively. Applying the parameters for ${}^{kin}\Gamma_{max}$ (see eq. 3 below), these criteria are given as eqs. S1 and S2 (Kari et al., 2017) and expressed as follows:

$$E_0 \ll {}^{kin}\Gamma_{max}(S_0^{mass} + K_{1/2}) \tag{S1}$$

$$S_0^{mass} \ll \frac{E_0 + K_M}{{}^{kin}\Gamma_{max}} \tag{S2}$$

$$\frac{\frac{{}^{inv}V_{max}}{S_0^{mass}}}{\frac{V_{max}}{E_0}} = {}^{kin}\Gamma_{max} \tag{3}$$

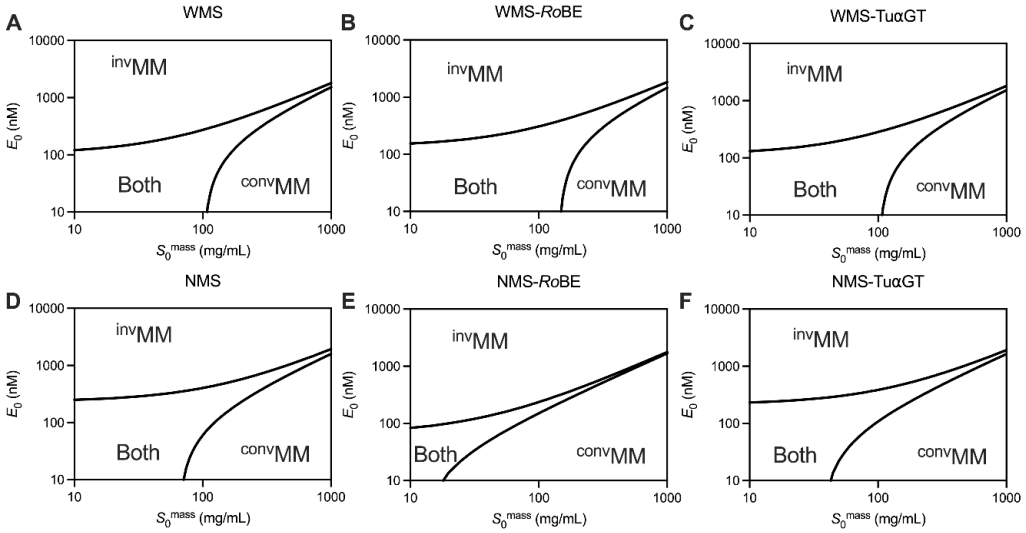

Fig. S1. Validity ranges of the conventional and inverse MM equations for (A) WMS, (B) WMS-*Ro*BE, (C) WMS-TuαGT, (D) NMS, (E) NMS-*Ro*BE, and (F) NMS-TuαGT. The lower left area represents conditions where both approaches are valid. At higher enzyme concentrations, the inverse approach (^{inv}MM) is valid, and at higher substrate loads, the conventional (^{conv}MM) equation can be used (Kari et al., 2017).

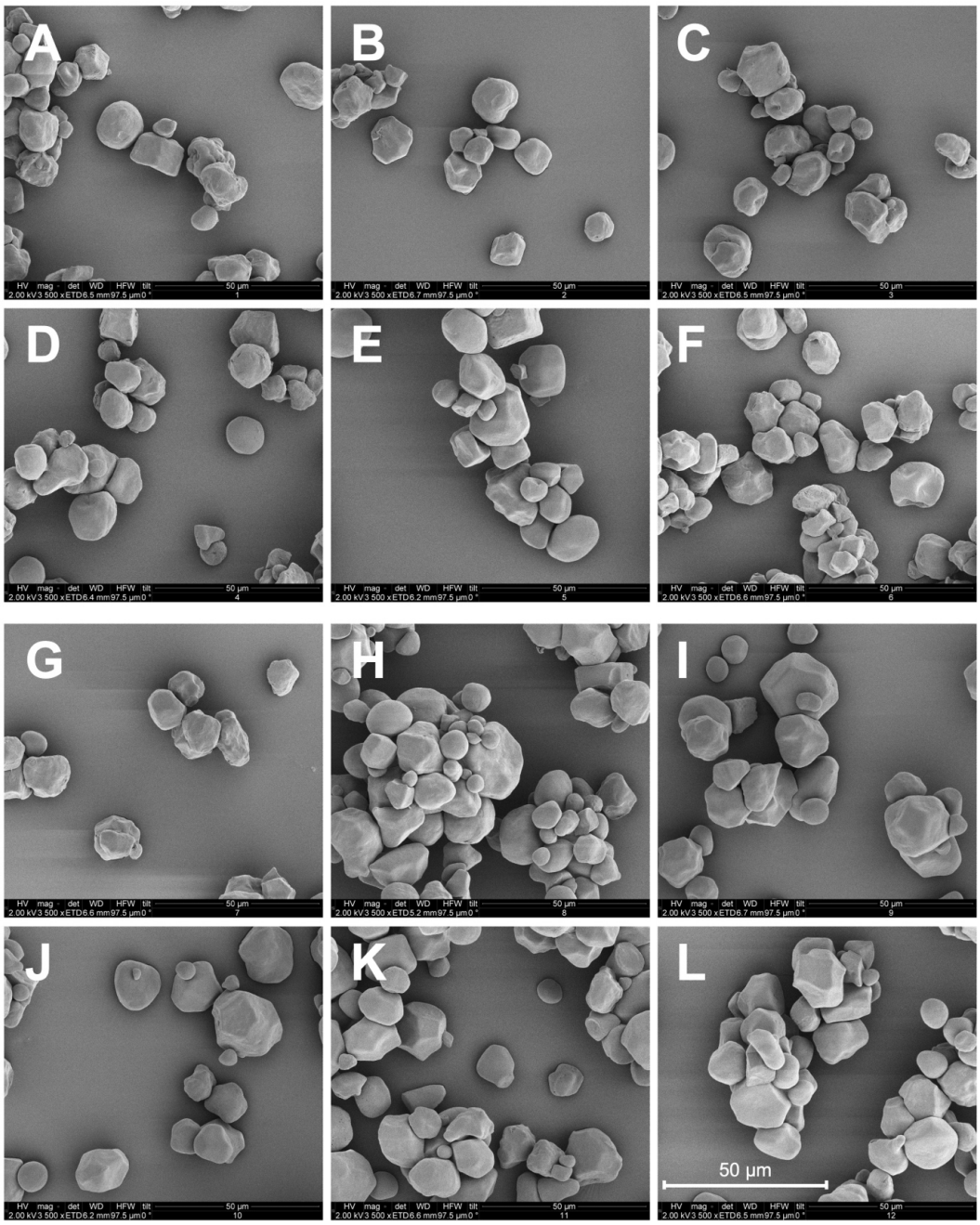

Fig. S2. SEM images of unmodified and modified starch granules before and after 30 min hydrolysis by 625 nM *Bl*Pul. Before hydrolysis (A) WMS, (B) WMS-*Ro*BE, and (C) WMS-TuαGT; after hydrolysis (D) WMS, (E) WMS-*Ro*BE, and (F) WMS-TuαGT. Before hydrolysis (G) NMS, (H) NMS-*Ro*BE, and (I) NMS-TuαGT; after hydrolysis (J) WMS (K) WMS-*Ro*BE, and (L) WMS-TuαGT. Magnification is 3,500×.

References

Kari, J., Andersen, M., Borch, K., & Westh, P. (2017). An inverse Michaelis-Menten approach for interfacial enzyme kinetics. *ACS Catalysis*, *7*(7), 4904–4914. https://doi.org/10.1021/ACSCATAL.7B00838

2.2.3 Manuscript 2 – Sabatier Principle for Understanding the Effect of Enzyme Modification of Granular Starch

This manuscript presents results on the interfacial kinetics on BE and 4αGT modified starch granules using *Bl*Pul, including the structure analysis of these modified starches. Notably, we emphasized the application of the Sabatier principle in guiding the starch modification process. This manuscript is in preparation and is aimed for submission to *Carbohydrate Polymers* and is written in the journal specific format.

Sabatier Principle for Understanding the Effect of Enzyme Modification of Granular Starch

Yu Wang [a, 1], *Yu Tian* [b, 1], *Andreas Blennow* [b], *Peter Westh* [c], *Birte Svensson* [a, *], *Marie Sofie Møller* [d, *]

[a] Enzyme and Protein Chemistry, Department of Biotechnology and Biomedicine, Technical University of Denmark, DK-2800, Kgs. Lyngby, Denmark

[b] Department of Plant and Environmental Sciences, University of Copenhagen, DK-1871, Frederiksberg C, Denmark

[c] Interfacial Enzymology, Department of Biotechnology and Biomedicine, Technical University of Denmark, DK-2800, Kgs. Lyngby, Denmark

[d] Applied Molecular Enzyme Chemistry, Department of Biotechnology and Biomedicine, Technical University of Denmark, DK-2800, Kgs. Lyngby, Denmark

[1] These authors contributed equally to this work.

* Corresponding authors:

Birte Svensson: bis@bio.dtu.dk;

Marie Sofie Møller: msmo@dtu.dk.

Abstract

Interfacial enzyme reactions are a common occurrence in both natural biological processes and industrial applications, including enzymatic degradation during starch synthesis and utilization. To establish a correlation between catalytic processes and the structural changes occurring on the surface of granular starches. We employed the Sabatier principle on enzyme degradation of maize starch granules with different amylose content (waxy, normal, and high amylose maize starch). Initially, the granular starches were modified using either branching enzyme (BE), 4-α-glucanotransferase (4αGT), or BE followed by 4αGT, resulting in modified starches (MSs) named MS-B, MS-T, and MS-BT, respectively. Structural analyses of the starches and molecular docking revealed that BE could catalyze transglycosylation on the surface of starch granules, whereas 4αGT catalyzed disproportionation on MS-B, but exhibited hydrolysis and/or cyclization activity on the unmodified starch granules. Distinct differences in the architecture of active sites of BE and 4αGT most likely account for these outcomes. BE has an open active site and is able to bind chains on the surface of granular starch, whereas the partially closed active site of 4αGT restricts its transglycosylation of starch granules. Applying the Sabatier principle demonstrated that modifying starches using BE or 4αGT controls the binding affinity between the enzyme and starch, thereby influencing the catalytic rate of a pullulanase. This research introduces a novel strategy for comprehending the enzymatic modification of starches by regulating binding affinity.

Keywords: Starch granules; Enzymatic modification; Glucanotransferase; Pullulanase; Interfacial catalysis; Sabatier Principle.

1. Introduction

Starch is a widely occurring renewable plant polysaccharide that plays a major role in the food industry [299]. For most applications, starch is gelatinized in heat-moisture processes [301,302]. However, focus on sustainability and energy-saving motivates use of the raw starch granules, and their applications are emerging [301,302]. To confer novel functionalities and enhance its positive attributes, starch is generally subjected to functional improvements by structural engineering using enzymatic, chemical or physical treatments [142,303]. Enzyme treatment of native starch granules represents an environmentally friendly strategy and an attractive alternative to gelatinized starch because it avoids high viscosity and instability caused by retrogradation.

Interest is growing in the use of transglycosylases or hydrolytic enzymes for modifying granular starches [142,301,304]. In general, hydrolases break down the granular structure into products of varying composition depending on reaction conditions and enzymes. α-amylase, β-amylase, glucoamylase, and pullulanase have been applied for modification of starch granules, generating pores, or rough surfaces [300,305]. Moreover, glucanotransferases are used to transglycosylate starch granules and further imparts improved properties. For example, treating pea starch with 4-α-glucanotransferase (4αGT) enhances its thermal resistance, but has the opposite effect on cassava starch [146]. Maize starch granules modified by branching enzyme (BE) exhibit increased resistance to digestion [306]. However, granular rice starch pretreated with maltogenic α-amylase, does not change crystallinity and pores by BE treatment, whereas BE boosts both crystallinity and the number of pores in rice starch granules with hot ethanol [147,148]. Similarly, like the creation of surface pores on granular starch by hydrolases, maize starch granules modified by cyclodextrin glycosyltransferase (CGTase) obtained irregular surfaces and small pores [150] and were less susceptible to hydrolysis by α-amylase [150].

Despite the increased use of enzymatic starch modification, the understanding of the relationship between the enzymatic process and the starch structure is limited. Recently, we applied an interfacial kinetics approach combined with enzyme-starch granule adsorption isotherms to describe the mechanism of enzyme-resistance of resistant starches (RS) using the glucoamylase from *Aspergillus niger*, serving as a model for degradation of nutritionally important resistant starch in the gut [298].

The enzymatic reaction on starch granules can be divided into four process: diffusion, adsorption, catalysis, and desorption [5]. Hence, the enzyme affinity for starch granules is crucial for the degradation. A trade-off between affinity and reaction rate is a well-known phenomenon in inorganic heterogeneous catalysis, referred to as the Sabatier principle

[264,307,308]. According to the Sabatier principle, optimal catalysis occurs when the interactions between catalyst and substrate are of intermediary strength [264,308]. The Sabatier principle has been applied to design catalysts and to understand the relationship between catalyst structure and efficiency [264,309,310]. The Sabatier principle has been extended to biological catalysts. For instance, Kari et al. explained the relationship between affinity of different cellulases and their catalytic activity on crystalline cellulose [264]. Besides, Bååth et al controlled the affinity of a poly(ethylene terephthalate) (PET) hydrolase by addition of different concentrations of surfactant to improve the catalytic activity of these enzymes according to the Sabatier principle [271]. Nevertheless, the investigation into modifying the substrate, such as granular starch in the present study, to enhance enzymatic catalysis by altering the enzyme-substrate affinity based on the Sabatier principle is limited.

In the current work, the starch granules were modified using either BE, 4αGT, or BE followed by 4αGT. Subsequently, the interfacial kinetics, combining conventional and inverse Michaelis-Menten (MM) kinetics having substrate and enzyme, respectively, in excess, for unmodified and modified starch granules were analyzed using a pullulanase to understand the relationship between affinity and reaction rates [6,274]. Additionally, the granular structure of these starches was analyzed to a comprehensive examination, including gelatinization temperature, crystallinity, surface order degree, and chain length distribution on the surface. The findings indicated that altering the structure of starch granules through modification with both BE and/or 4αGT resulted in pullulanase exhibiting varying affinity toward distinct starch granules. Consequently, this led to markedly different catalytic behaviors, namely adsorption-limited or desorption-limited situations according to the Sabatier principle. We concluded that the Sabatier principle can be served as a tool to understand enzyme reactions on starch granules, and guide modification of starch granules.

2. Materials and methods

2.1. Materials

Waxy maize starch (WMS) was a kind gift of Cargill, USA, and normal maize starch (NMS) of Archer Daniels Midland (ADM, Decatur, IL). High-amylose maize starch AE 35 (AE) was obtained from experimental fields of Northwest A&F University, Yangling, China. Pullulanase M2 from *Bacillus licheniformis* (*Bl*Pul, E-PULBL, 900 U/mL) was purchased from Megazyme Co. Ltd (Wicklow, Ireland). Branching enzyme from *Rhodothermus obamensis* (*Ro*BE, 5.98 U/mg) was a kind gift of Novozymes, Denmark. One unit of enzyme activity was defined as the amount of BE that decreased A530 by 1% per min [311]. *Thermoproteus uzoniensis* 4-α-glucanotransferase (TuαGT, 542 U/mg) was prepared as described. One unit of disproportionation activity was defined as the amount of 4aGT releasing 1 μmol of glucose per min under the above conditions [312].

2.2 Modification of granular starch by BE and TuαGT

For preparation of MS-Bs and MS-Ts, NSs (6%, w/v) was washed twice with MilliQ water and once with reaction buffer (20 mM sodium citrate, pH 6.0), suspended in reaction buffer and modified by either 1.0 U RoBE or 32.5 U TuαGT per 1 g starch (50 °C, 20 h). NSs was incubated with reaction buffer (50 °C, 20 h) to obtain control starch. Reactions were terminated by addition of Na_2CO_3 (final concentration: 0.3 M) for 10 min and centrifugation (10,000 *g*, 5 min) [274]. To obtain MS-BT, MS-Bs was further modified by addition of 32.5 U TuαGT/g starch and incubated (50 °C, 20 h). Reactions were terminated as described. The unmodified (control) and modified starch granules were washed with MilliQ water and freeze-dried.

2.3 Interfacial kinetics analysis on granular starch

The kinetics of *Bl*Pul acting on starch granules were determined byusing two complementary methods denoted conventional and inverse Michaelis-Menten (MM) analyses applied for enzyme hydrolysis of solid polysaccharides as described in more detail elsewhere [5,6,273,298]. Briefly, in conventional MM analysis starch granules (15–150 mg/mL, 135 μL) were pre-incubated (25 °C, 15 min, 1100 rpm), added *Bl*Pul (15 μL, final 62.5 nM) and incubated (25 °C, 1100 rpm, 30 min). For inverse MM analysis, *Bl*Pul (0.3–625 nM) was added to starch granules (20 mg/mL) and after 30 min, which is within the linear range of hydrolysis (data not shown), aliquots (100 μL) were transferred to new tubes, mixed with 20 μL 1.8 M Na_2CO_3 to terminate the reaction, and centrifuged (10000 *g*, 5 min). The concentration of reducing sugar in the supernatants was determined using the PAHBAH assay and glucose as standard [293].

Data from conventional MM kinetics (substrate in excess) were analyzed according to eq. 1, where S_0^{mass} is substrate mass load, $K_{1/2}$ the mass load at substrate half-saturation, and V_{max} the maxiumum velocity. Non-linear regression analyses of the data returned values of V_{max} (in $M \cdot s^{-1}$) and $K_{1/2}$ (in $g \cdot L^{-1}$).

$$v_0 = \frac{V_{max} \cdot S_0^{mass}}{K_{1/2} + S_0^{mass}} \quad (1)$$

Inverse MM kinetics (enzyme in excess) were analyzed according to eq. 2, where E_0 is enzyme load and K_M the enzyme load at enzyme half-saturation. Nonlinear regression analysis of data led to ${}^{inv}V_{max}$ (in $g \cdot L^{-1} \cdot s^{-1}$) and K_M (in M).

$$v_0 = \frac{{}^{inv}V_{max} \cdot E_0}{K_M + E_0} \quad (2)$$

The density of attack site (${}^{kin}\Gamma_{max}$) was determined from V_{max} (eq. 1) and ${}^{inv}V_{max}$ (eq. 2) using eq. 3 as previously described [6].

$$\frac{\frac{{}^{inv}V_{max}}{S_0^{mass}}}{\frac{V_{max}}{E_0}} = {}^{kin}\Gamma_{max} \quad (3)$$

The relationship between binding strength and turnover number were described by a relative standard free energy of enzyme-substrate binding ($\Delta\Delta G°$) calculated according to eq. (4), where $K_{1/2,i}$ is the Michaelis constant for the enzyme in question and $K_{1/2,ref}$ is the value for a reference enzyme [264], here chosen as the $K_{1/2}$ for *Bl*Pul acting on WMS.

$$\Delta\Delta G° = RT \ln\left(\frac{K_{1/2,i}}{K_{1/2,ref}}\right) \quad (4)$$

2.4 Chain length distribution (CLD)

Native and modified starch granules (50 mg/mL, w/v), suspended in 50 mM sodium acetate pH 5.5 were debranched by 50 nM *Bl*Pul (final concentration, 25 °C, 30 min), centrifuged (10000 *g*, 5 min) and supernatants were analyzed by HPAEC-PAD to determine the CLD [274].

2.5 Differential scanning calorimetry (DSC)

The gelatinization/melting temperatures of native and modified starch granules were assessed in excess distilled water, with the weight of water being three times that of starch. The measurements were conducted using DSC1 (Mettler Toledo, Switzerland). The temperature ranges from 20 to 100 °C (WMS and NMS), and 20 to 180 °C (AE) were scanned at a rate of 5 °C/min. The DSC measurements provided several thermal transition parameters for the

starches, including onset temperature (T_o), peak temperature (T_p), conclusion temperature (T_c), and enthalpy change (ΔH) in J/g. The Stare Software version 9.1 (Mettler Toledo) was employed for the calculation of these values.

2.6 Wide angle X-ray scattering (WAXS)

The measurement of crystalline allomorphs and crystallinity involved subjecting starch granular samples to a controlled relative humidity of 90% within a chamber for a duration of 48 h. Subsequently, analysis was conducted using a SAXSLab instrument (JJ-X-ray, Copenhagen, Denmark) equipped with a 100 XL+ microfocus sealed X-ray tube (Cu-Kα radiation, Rigaku, The Woodlands, Texas, USA) and a 2D 300 K Pilatus detector (Dectris Ltd, Baden, Switzerland). To prepare hydrated samples, they were securely sealed between 5 and 7 µm mica films under vacuum. The two-dimensional scattering data obtained was processed using standard reduction software (SAXSGUI) to perform averaging and correction. The resulting radially averaged intensity (I) was plotted as a function of the scattering angle (2θ) within the angular range of 5°–30°, utilizing a wavelength of 0.1542 nm. The relative crystallinity was subsequently calculated as described, employing established methods [313].

2.7 Fourier transform infrared - Attenuated total reflectance spectroscopy (FTIR–ATR)

The spectral data were acquired using a PerkinElmer Spectrum One FTIR spectrometer equipped with a PerkinElmer UATR single bounce ATR accessory featuring a diamond crystal. Data acquisition was performed using PerkinElmer Spectrum 6 software on a connected computer. Prior to analysis, the starch samples were allowed to reach the laboratory humidity level of 50% RH. Spectra for each sample were collected and combined by co-adding at a resolution of 4 cm^{-1}. To obtain the background spectrum, the crystal was cleaned with a mixture of ethanol and water, followed by collecting 128 co-added scans. A Lorentzian line shape was assumed with a half-width of 19 cm^{-1} and a resolution enhancement factor of 1.9. After baseline correction and deconvolution, IR absorbance values at 1022 cm^{-1} and 1045 cm^{-1} were extracted from the spectra using OMNIC software.

2.8 Molecular Docking

A 3D model of TuαGT was built using AlphaFold2 [314]. Since the *Ro*BE is a commercial enzyme the exact sequence is unknown and AlphaFold2 model cannot be ontained. Therefore, crystal structure of BE from *Rhodothermus obamensis* STB05 (PDB: 6JOY) [315] from pdb database (https://www.rcsb.org/) was used to repersent *Ro*BE. A part (17 glucose units) of 34-meric cycloamylose was extracted from a complex structure of *Thermus aquaticus* amylomaltase (PDB: 5JIW). The 3D structure of maltododecaose was obtained from ChemSpider (http://www.chemspider.com/). AutoDock version 1.5.7 (La Jolla, CA, USA) was used to add missing hydrogens and to calculate Gasteiger charges and generate PDBQT files.

The molecular docking between BE from *Rhodothermus obamensis* STB05 (PDB: 6JOY) and maltododecaose, and between TuαGT and cycloamylose were performed with Auto Dock tools (ADT) version1.5.7 (www.autodock. scrips.edu) and the interaction were performed by using PyMol (New York, USA).

2.9 Statistical analysis

Experiments were performed in triplicate. The statistical significance was assessed with two-way ANOVA using GraphPad Prism 6 (GraphPad Software Inc). *p*-values <0.05 were considered statistically significant throughout the study.

3. Results

3.1 Interfacial kinetics of granular starch hydrolysis

The degradation of different starch granules by *Bl*Pul was analyzed using interfacial kinetics approach by using a combination of conventional and inverse MM kinetics [6,274]. The conventional MM kinetics gave the highest k_{cat} and lowest $K_{1/2}$, and therefore highest $k_{cat}/K_{1/2}$ towards unmodified WMS, showing that WMS is a better substrate for *Bl*Pul in the conventional perspective. However, the interfacial kinetics by combining conventional and inverse MM kinetics showed that *Bl*Pul recognized 1.9- and 4.5-fold more attack site ($^{kin}\Gamma_{max}$) on WMS than NMS and AE, respectively (Table 6). The faster degradation of WMS is attributed to the higher attack site density, due to a higher content of amylopectin and α-1,6-linkages.

Furthermore, *Ro*BE-modified WMS, NMS, and AE granules exhibited a respective 1.9-, 2.3-, and 5-fold higher $^{kin}\Gamma_{max}$ than the corresponding unmodified granules (Table 6). This increases in $^{kin}\Gamma_{max}$ aligns with the *Ro*BE-catalyzed formation of new α-1,6-linkages on the starch granule surfaces. By contrast, TuαGT-modified starch granules exhibited nearly the same $^{kin}\Gamma_{max}$ as unmodified starch granules (Table 6), indicating that TuαGT modification did not change the number of branches on the surface of starch granules. Accordingly, MS-BT had $^{kin}\Gamma_{max}$ values similar to those of MS-B.

According to the relative standard free energy of enzyme-substrate binding ($\Delta\Delta G°$), it can be seen that *Bl*Pul had significantly enhanced affinity for NMS-B and AE-B, whereas decreased affinity for WMS-B. In contrast, *Bl*Pul showed similar affinity between MS-Ts and the relative MSs. Notably, the $\Delta\Delta G°$ between MS-BTs and NS-Bs are different for different starches. *Bl*Pul displayed improved affinity to WMS-BT than WMS-B, while reduced affinity to NMS-BT and AE-BT in comparison to NMS-B and AE-B, respectively.

Table 6. Conventional and inverse kinetic parameters of *Bl*Pul acting on native, *Ro*BE- and TuαGT-modified starch granules

Starch	k_{cat} (s^{-1})	$K_{1/2}$ (g/L)	$k_{cat}/K_{1/2}$ ($L\cdot[g\cdot s]^{-1}$)	$^{kin}\Gamma_{max}$ (nmol/g)	$\Delta\Delta G°$ (kJ/mol)
WMS	8.6 ± 0.5	60.9 ± 8.6	0.14	1.7	0.00
WMS-B	7.3 ± 0.6	80.7 ± 17.7	0.091	3.3	0.66
WMS-T	8.5 ± 0.4	66.7 ± 3.4	0.13	1.8	0.22
WMS-BT	2.2 ± 0.2	42.3 ± 5.2	0.051	2.8	-0.81
NMS	1.6 ± 0.01	137.3 ± 2.3	0.012	0.92	1.91
NMS-B	1.0 ± 0.2	39.0 ± 10.9	0.025	2.1	-1.05
NMS-T	1.7 ± 0.1	126.9 ± 25.1	0.013	1.0	1.73
NMS-BT	1.9 ± 0.3	99.5 ± 10.0	0.019	2.1	1.16
AE	1.0 ± 0.2	123.1 ± 21.4	0.008	0.38	1.66
AE-B	0.6 ± 0.2	28.2 ± 4.6	0.022	1.9	-1.81
AE-T	1.1 ± 0.2	172.3 ± 16.9	0.006	0.34	2.45
AE-BT	4.0 ± 0.8	101.0 ± 19.7	0.039	1.5	1.19

3.2 Apparent CLD on the surface of NSs and MSs

The modification of starch by *Ro*BE resulted to varying degrees in an increase in the number of short chains and a decrease in longer branch chains (Table 7). *Ro*BE-modified WMS and NMS exhibited 2.8- and 1.9-fold higher proportion of A-chains (DP 1–12) and 8.4- and 7.3-fold decrease in B_1-chains (DP 12–24). Together with the $^{kin}\Gamma_{max}$ value for *Bl*Pul, defining the density of branch points, *Ro*BE indicated capability to form new α-1,6-linked branch chains on the surface of WMS and NMS [274]. However, AE-B exhibited the same content of A-chains as AE and examining the branch pattern (Figure 15C) made it clear that *Ro*BE-modified AE had notably higher proportion of chains with DP 1–4 and reduced content of chains with DP 5–12. This observation, coupled with the 5-fold higher $^{kin}\Gamma_{max}$ value for AE-B compared to AE, indicates that catalyzes formation of new α-1,6-branches on the surface of AE.

TuαGT-modification to WMS and NMS (WMS-T and NMS-T) resulted in a slight increase (1.4-–1.5-fold) in A-chains and decrease (1.3- –1.5-fold) in B_1-chains compared to native WMS and NMS (Table 7). We previously noted that TuαGT predominantly catalyzes hydrolysis and/or cyclization of branch chains on starch granules, but catalyzes disproportionation of branch chains in gelatinized starches [274]. The hydrolysis and/or cyclization led to shortening of the chain length on the surface of granular starches. TuαGT-modified AE exhibited a slightly higher proportion of chains with DP 1–3 and a lower content of chains with DP 4–12. Compared with WMS-B and NMS-B, WMS-BT and NMS-BT showed decreased content of A-chains by 1.8- and 1.6-fold, while increases in B_1-chains by 5.7- and 6.3-fold, respectively.

Table 7. Relative content of different branch chains released by *Bl*Pul from starch granules before and after modification with *Ro*BE and TuαGT

Granular starch	Type of chain[a]			
	A-chain	B_1-chain	B_2-chain	B_3-chain
WMS	32.9 ± 0.9	58.6 ± 0.3	8.5 ± 0.3	ND[b]
WMS-B	92.8 ± 0.3	7.0 ± 0.1	0.2 ± 0.0	ND
WMS-T	48.0 ± 1.1	46.1 ± 0.3	5.7 ± 0.1	0.3 ± 0.0
WMS-BT	52.8 ± 1.4	39.7 ± 0.4	4.5 ± 0.2	0.2 ± 0.1
NMS	48.8 ± 2.1	45.0 ± 0.5	6.0 ± 0.1	0.2 ± 0.1
NMS-B	93.9 ± 0.5	6.1 ± 0.1	ND	ND
NMS-T	69.3 ± 0.7	30.7 ± 0.3	ND	ND
NMS-BT	58.3 ± 0.8	38.6 ± 0.1	3.2 ± 0.1	ND
AE	100	ND	ND	ND
AE-B	99.3 ± 0.3	0.7 ± 0.1	ND	ND
AE-T	100	ND	ND	ND
AE-BT	98.0 ± 0.5	2.0 ± 0.2	ND	ND

[a] A-chain: DP 1–12, B_1-chain: DP 13–24, B_2-chain: DP 25− 36, and B_3-chains: DP > 37 [8]

[b] ND: not determined.

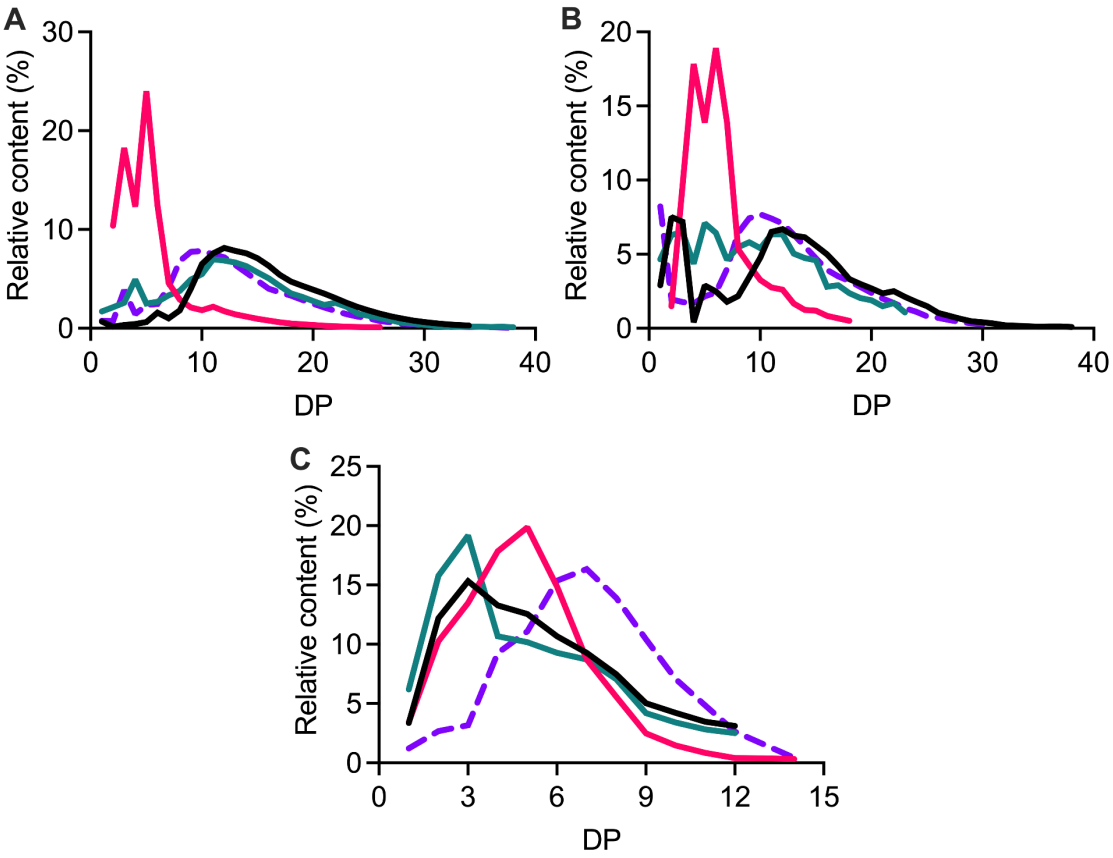

Figure 15. Chain length distribution (CLD) as released by *Bl*Pul from starch granules. (A) WMS, (B) NMS, (C) AE. The granules were native (black solid line), modified by *Ro*BE (red solid line), TuαGT (blue solid line), or *Ro*BE+TuαGT (purple dashed line).

3.3 Gelatinization Properties of NSs and MSs

The gelatinization showed that WMS, NMS and AE granules exhibited one major endotherm transition between 64.8–83.2 °C, 66.3–76.5 °C, and 80.4–109.7 °C, respectively (Figure 16), attributed to the melting of the crystalline content [316]. WMS had lowest onset gelatinization temperature (T_o) of 64.8 °C, demonstrating low crystalline and low thermal resistance [317]. All modified WMSs had narrower gelatinization temperature range (the gap between conclusion temperature T_c and onset temperature T_o), reflecting heterogeneity of crystalline structures in the granules [302], which decreased in the order WMS>WMS-B>WMS-BT>WMS-T. Besides, the gelatinization enthalpy (ΔH) is considered to be associated with the thermal energy required to mainly disrupt the granular crystalline structure [318]. ΔH of melting was decreasing in the order: WMS>WMS-B>WMS-T>WMS-BT. Unmodified NMS and modified NMSs showed similar T_o (66.3–66.7 °C) and T_c (75.5–76.5 °C). However, the ΔH of NMS showed the similar tendency with WMS by showing the order: NMS>NMS-B>NMS-

T>NMS-BT. As for AE, unmodified AE and modified AEs showed close T_o (80.3–80.8 °C) and T_c (109.7–109.5 °C), while significantly different T_p (93.1 °C for unmodified AE and 96.4–97.8 °C for modified AEs). Besides, the Δ*H* of AEs showed different tendency as compared with WMS and NMS: AE-BT>AE-T>AE>AE-B.

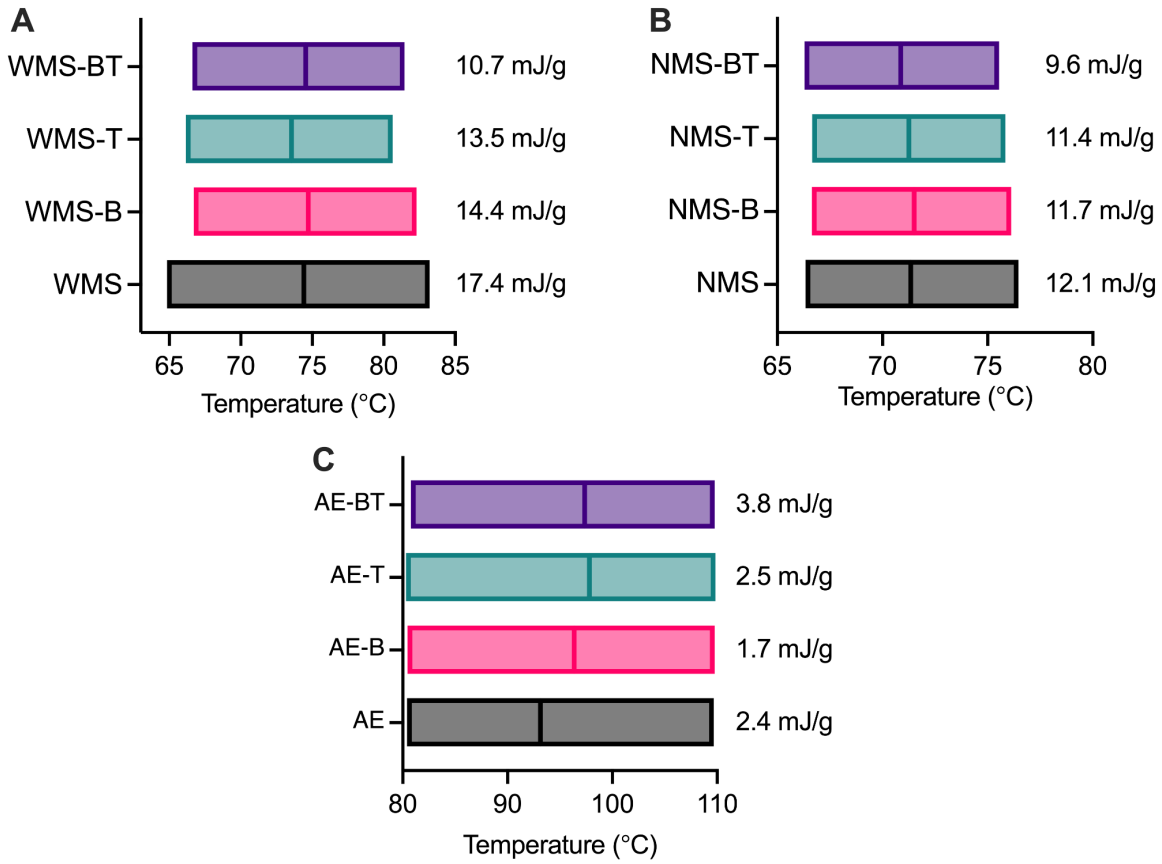

Figure 16. Gelatinization properties of NSs (black), MS-Bs (red), MS-Ts (green), and MS-BTs (purple). (A) WMS, (B) NMS, and (C) AE. Vertical line from left to right in each panel represents onset temperature (T_o), peak temperature (T_p), and conclusion temperature (T_c), respectively. Δ*H* in mJ/g was shown next to each panel.

3.4 Crystallinity of NSs and MSs

X-ray diffraction (XRD) analysis was conducted to investigate the crystalline structure and crystallinity of the unmodified and modified starches. In the case of WMS and NMS, distinct diffraction peaks were observed at 15° and 23° 2θ angles, along with an unresolved doublet at 17° and 18° 2θ angles, indicating the presence of an A-type crystalline allomorph [16,17]. In contrast, AE exhibited the strongest diffraction peak at around 17° 2θ, accompanied by smaller peaks at 20°, 22°, and 23° 2θ angles. Additionally, a new peak appeared at approximately 5° 2θ, characteristic of a B-type crystalline allomorph (Figure 17C).

Comparing WMS with WMS-B, the *Ro*BE modification showed no impact on the crystallinity. However, NMS-B and AE-B displayed significantly reduced crystallinity compared to NMS and AE. In comparison to NSs and MS-Bs, both MS-Ts and MS-BTs exhibited an important increase in crystallinity.

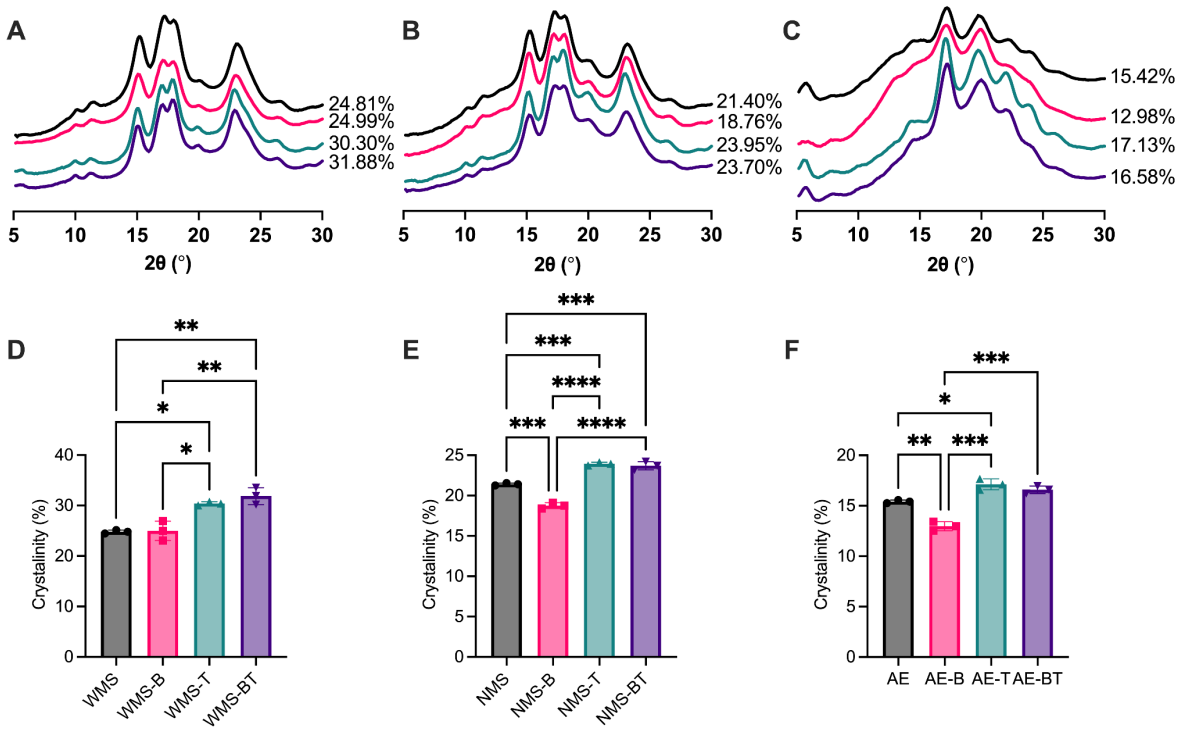

Figure 17. Wide-angle X-ray diffraction (XRD) patterns and crystallinity of NSs (black), MS-Bs (red), MS-Ts (green), and MS-BTs (purple). XRD patterns of (A) WMSs, (B) NMSs, and (C) AEs. Crystallinity of (D) WMSs, (E) NMSs, and (F) AEs.

3.5 Surface Order Degree Analysis of NSs and MSs

Fourier transform infrared - Attenuated total reflectance spectroscopy (FTIR–ATR) analysis was conducted to investigate the surface order degree of NSs and MSs (Figure 18). The FTIR-ATR spectra of the starches in the range of 800–1300 cm^{-1}, corresponding to C-O and C-C stretching vibrations, provide insights into polymer conformation at the surface (~2 μm) of starch granules [319]. The presence of ordered and amorphous regions is indicated by bands observed at 1045 cm^{-1} and 1022 cm^{-1}, respectively. The ratio of 1045/1022 cm^{-1} is commonly employed to evaluate the degree of surface order (short-range order) in starch [320]. Among the various native starches, WMS exhibited the highest degree of surface order (0.58), followed by NMS (0.51) and AE (0.42), as shown in our pervious study [298]. Compared with NSs, MS-B gave the same range of 1045/1022 cm^{-1} ratio, indicating that the short branch chains introduced by *Ro*BE had no effect on the degree of order on the surface of the starch

granules. MS-Ts and MS-BTs showed significantly higher short-range order than NSs and NS-B, respectively, consistent with the XRD analysis.

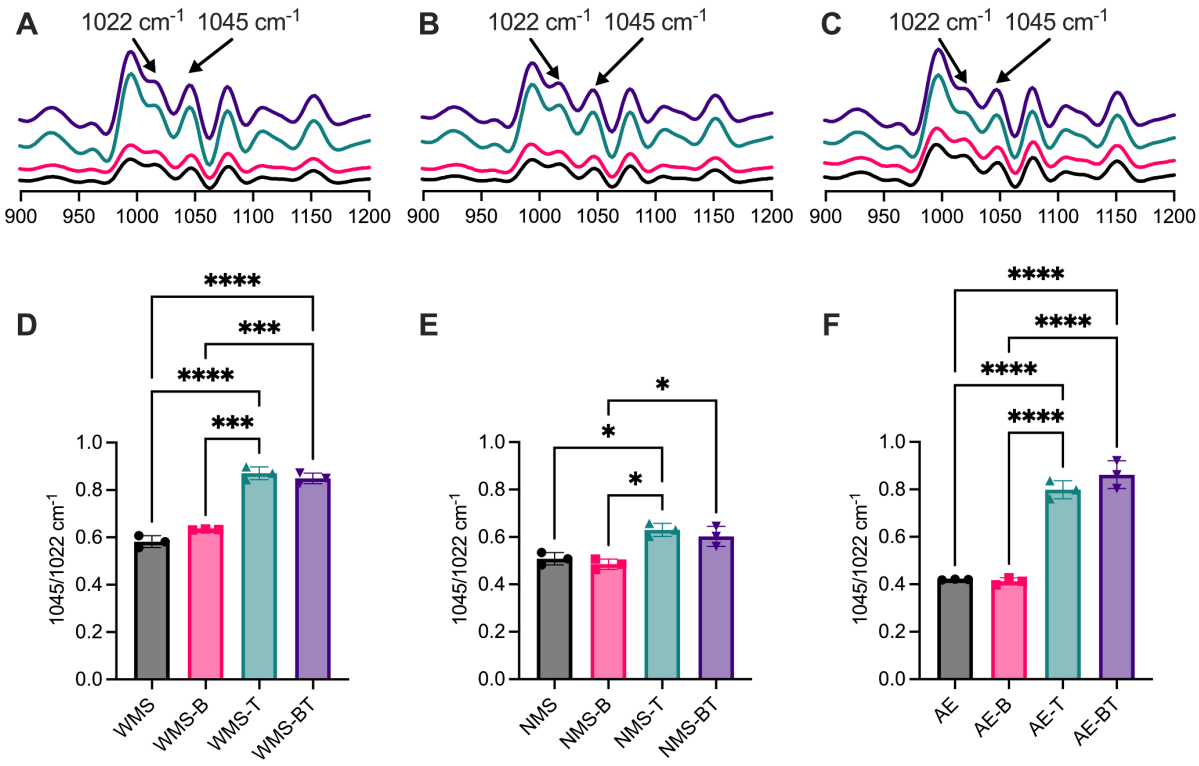

Figure 18. Fourier transform infrared - Attenuated total reflectance spectroscopy (FTIR–ATR) patterns and degree of order (1045/1022 cm^{-1}) of NSs (black), MS-Bs (red), MS-Ts (green), and MS-BTs (purple). FTIR–ATR patterns of (A) WMSs, (B) NMSs, and (C) AEs. Degree of order (1045/1022 cm^{-1}) of (A) WMSs, (B) NMSs, and (C) AEs.

4. Discussion

Structure/Modification Relationship of NMs and MSs

The interfacial kinetics showed increased $^{kin}\Gamma_{max}$ for MS-B whereas MS-T displayed a similar $^{kin}\Gamma_{max}$ compared to NSs. Based on the CLD, showing shortened side chains in both MS-B and MS-T compared to NSs, *Ro*BE catalyzed formation of new α-1,6-linkages on the granular surface. By contrast, TuαGT predominantly catalyzes hydrolysis and/or cyclization of branch chains on the starch granule surfaces. Notably, the increase in longer chains along with a decrease in shorter chains for MS-BT compared with MS-B is consistent with our previous study using TuαGT to modify gelatinized starches, and confirmed that TuαGT can catalyze disproportionation reactions on WMS-B and NMS-B [123,124].

The newly generated short side chains by *Ro*BE might disrupt the arrange of the crystalline region, leading to a decreased crystallinity for NMS-B and AE-B than native NMS and AE, respectively. However, the unchanged crystallinity for WMS-B than native WMS might be due to the naturally higher content of amylopectin and α-1,6-linkages in WMS. The newly formed side chains showed minor effects on the crystalline region [147,321,322]. Conversely, both NMS-B and AE-B showed decreased crystallinity compared to NMS and AE, respectively (Figure 17). This phenomenon could be attributed to the disparity between WMS and starches containing amylose (NMS and AE). In WMS, the α-1,6-linkages introduced by *Ro*BE comprised only a small fraction, exerting minimal influence on the overall crystallinity of the granules. NMS and AE, however, contained a higher amylose content than WMS, and α-1,6-branch chains generated by *Ro*BE on the amylose at the starch surface can disrupt the crystal arrangement, leading to a reduction in the crystallinity of starch granules [323].

For MS-T and MS-BT, crystallinity and surface order degree increased dramatically. This observation, coupled with the CLD results (Table 7), suggests that the enhanced crystallinity of MS-Ts compared to NSs was attributed to the hydrolysis and cyclization of starch granules by TuαGT, consistent with our previous study [274]. However, the situation for MS-BTs appears to be different, as TuαGT may not only catalyze hydrolysis and cyclization in the amorphous regions of starch, leading to a decrease in crystallinity, but also facilitate disproportionation reactions, elongating the short chains generated by *Ro*BE. This elongation of exterior chains contributes to an overall increase in crystallinity.

Structure/function Relationship by Molecular Docking

Based on the interfacial kinetics and CLD analysis, we concluded that *Ro*BE catalyzed formation of new α-1,6-linkages on the granular surface. In comparison, TuαGT predominantly

catalyzes hydrolysis and/or cyclization of branch chains on the starch granules, but catalyzes disproportionation of the *Ro*BE modified starches and gelatinized starches. To understand why *Ro*BE catalyze transglycosylation on both gelatinized and ungelatinized starch, while TuαGT reacted differently on these [274], molecular docking was done between *Ro*BE (PDB entry 6JOY as model) and maltododecaose (Figure 19A), and TuαGT (AlphaFold2 model) and a part (17 glucose units) of 34-meric cycloamylose (Figure 19C).

*Ro*BE has an open active site (Figure 19A) and when acting on gelatinized starch, donor and acceptor chains both are easily accommodated at the active site (Figure 19B), with formation of a new α-1,6-linkage. The donor and acceptor chain were also seen in a complex structure between rice branching enzyme and maltododecaose [324]. Despite the presence of double helical structure between α-glucan chains in granular starches, the open active site still allowed for the entry of chains and facilitated transglycosylation.

In TuαGT, the α-glucan chain slipped into the active center via the entrance cavity (Figure 19D) to the exit cavity (Figure 19E), which is partially blocked by the so-called 250 loop (blue, Figure 19E) [126]. For the reaction on gelatinized starches, a flexible α-glucan chain first gets into the active site, followed by cleavage with formation of a covalent intermediate. A new flexible α-glucan chain acting as acceptor enters the active site through the exit cavity and becomes elongated by transfer of donor chain from the covalent intermediate. For granular starch, probably the enzyme will first unwind a double helix and let a single chain into the active site [126], followed by cleaving of the donor chain. However, the non-reducing segment of donor α-glucans in a double helix is not flexible enough to get into the active site, while a water molecule can get into the active center leading to a hydrolysis/cyclization reaction. Alternatively, the non-reducing end of the formed intermediate is flexible and can enter the active center to undergo transglycosylation [126]. Examining the arrangement of the ligand in the active site of TuαGT (Figure 19F), we observed that for TuαGT to catalyze disproportionation, the acceptor chain needs to be at least of DP 4–5 (yellow dashed square in Figure 19F). As shown in Figure 15, MS-Bs showed a larger proportion with chains of DP 1–8 than NSs. These short side chains with DP 1–8 are unable to form a helical structure [8], making them flexible acceptors for TuαGT to catalyze disproportionation reaction and elongate these short chains.

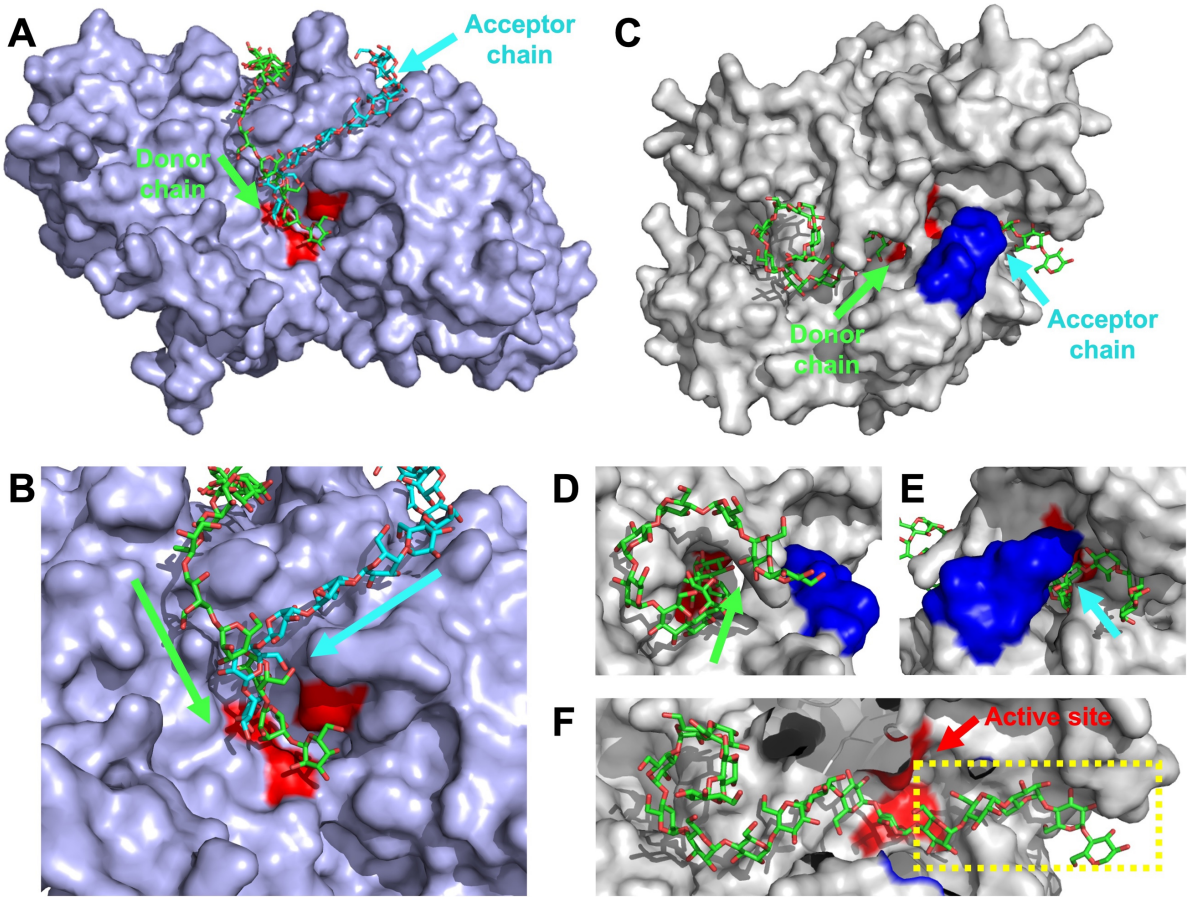

Figure 19. Molecular docking of *Ro*BE (PDB: 6JOY) and maltododecaose, and TuαGT (AlphaFold2 model) and 34-meric large-ring cyclodextrin (partial, 17 glucose units) using AutoDock Vina. (A) Docked complex between *Ro*BE (light blue) and maltododecaose (donor chain: green, acceptor chain: cyan). The active sites (red), and the entrance direction of the donor and acceptor chains to the active sites are highlighted. (B) Close-up of the *Ro*BE active site. (C) Model of complex between TuαGT (gray) and 34-meric large-ring cyclodextrin (partial, green sticks). The active site (red), the 250 loop (blue), and the entrance (green arrow) and exit (cyan arrow) of active sites are highlighted. (D) Close-up of entrance, (E) exit of the active site of TuαGT and (F) the layout of ligand in active site.

Application of Sabatier Principle in Designing Starch

The Sabatier principle describes the general relationship between binding strength and catalytic turnover, stating that catalysis is most effective when catalyst-reactant interactions exhibit moderate strength [264,308]. This weak binding leads to inadequate intermediate formation, whereas strong interactions delay the catalysis due to accumulation of stable intermediates. According to the Sabatier principle, the plots between catalyst-substrate affinity and the catalytic rate leads to the so-called “volcano plots” [263]. These plots exhibit highest

reaction at intermediate affinity (Figure 20). Volcano curves emerge when the free energies of intermediates and transition states simultaneously shift across different catalysts, signifying their catalytic efficiency [264,308].

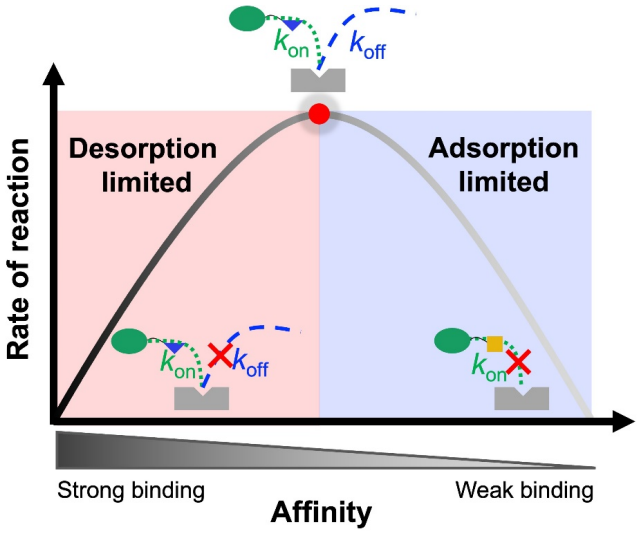

Figure 20. Volcano plot illustrating the Sabatier principle. The pink part represents desorption limited catalysis, where higher affinity for substrate leads to lower rate of reaction. The blue part represents adsorption limited catalysis, where higher affinity for substrate leads to higher rate of reaction. The red dot represents the best affinity of the enzyme for substrate leading to the highest rate of reaction. Figure inspired by a figure from Kari et al. [264].

The relationship between k_{cat}, $^{inv}k_{cat}$, and $\Delta\Delta G°$, $^{kin}\Gamma_{max}$ and $\Delta\Delta G°$ on different starch granules revealed that modification by *Ro*BE and TuαGT had a distinctive and biphasic effect on the catalytic performance of *Bl*Pul (Figure 21A). Firstly, it can be observed that MS-B, particularly AE-B, bind their enzyme too tightly for efficient catalysis. This strong affinity occurred together with a slow maximum turnover rate for AE-B (k_{cat}=0.62 s^{-1}), but when the interaction was weakened by TuαGT modification, leading to AE-BT, to a level of $K_{1/2}$ ~101 g/L, the k_{cat} dramatically increased to 3.96 s^{-1}). Similar results were found between NMS-B and NMS-BT. Despite the difference between maize starches, WMS, showing $K_{1/2}$ ~60.9 g/L and k_{cat}~8.62 s^{-1} represents the Sabatier optimum, where the lifetime of the enzyme−substrate complex attains a favorable, intermediate value (Figure 21A). This gained affinity might stem from the increase in $^{kin}\Gamma_{max}$ for *Bl*Pul on the surface of these starches (Figure 21C). Comparing the k_{cat} and $^{inv}k_{cat}$ (Figure 21A, B) for most of the starches showed similar relationship with $\Delta\Delta G°$, while WMS-B is out of the fitting in $^{inv}k_{cat}$-$\Delta\Delta G°$ (Figure 21B). The poor fit for WMS-B in $^{kin}\Gamma_{max}$-$\Delta\Delta G°$ may be explained by considering specific changes in ^{conv}MM and ^{inv}MM parameters. From our previous work, $^{inv}k_{cat}$ represents not only the catalytic rate (k_{cat}), but also the ability for the

enzyme to find attack sites ($^{kin}\Gamma_{max}$) on the surface of substrate. In the case of WMS-B, the lower k_{cat}, combined with higher $^{inv}k_{cat}$ compared to WMS, indicate that although *Bl*Pul catalyze WMS-B at a slower rate, it is capable of attacking more sites on WMS-B than on WMS, in accordance with the increase in branch point content.

To further explain the different behavior in k_{cat}-$\Delta\Delta G°$ and $^{inv}k_{cat}$-$\Delta\Delta G°$ fitting, the data for $^{kin}\Gamma_{max}$ and $\Delta\Delta G°$ were fitted (Figure 21C). It was observed that the $^{kin}\Gamma_{max}$ fits nicely with $\Delta\Delta G°$, proving that with higher $^{kin}\Gamma_{max}$ recognized by *Bl*Pul, the affinity between *Bl*Pul and starch will be higher. However, it should be noted that the dataset for WMS-B exhibited a noticeably weaker fit compared to the others. For WMS-B, the lower $\Delta\Delta G°$ caused the reduced k_{cat}, while higher $^{kin}\Gamma_{max}$ led to the dramatically increased $^{inv}k_{cat}$ as compared to WMS.

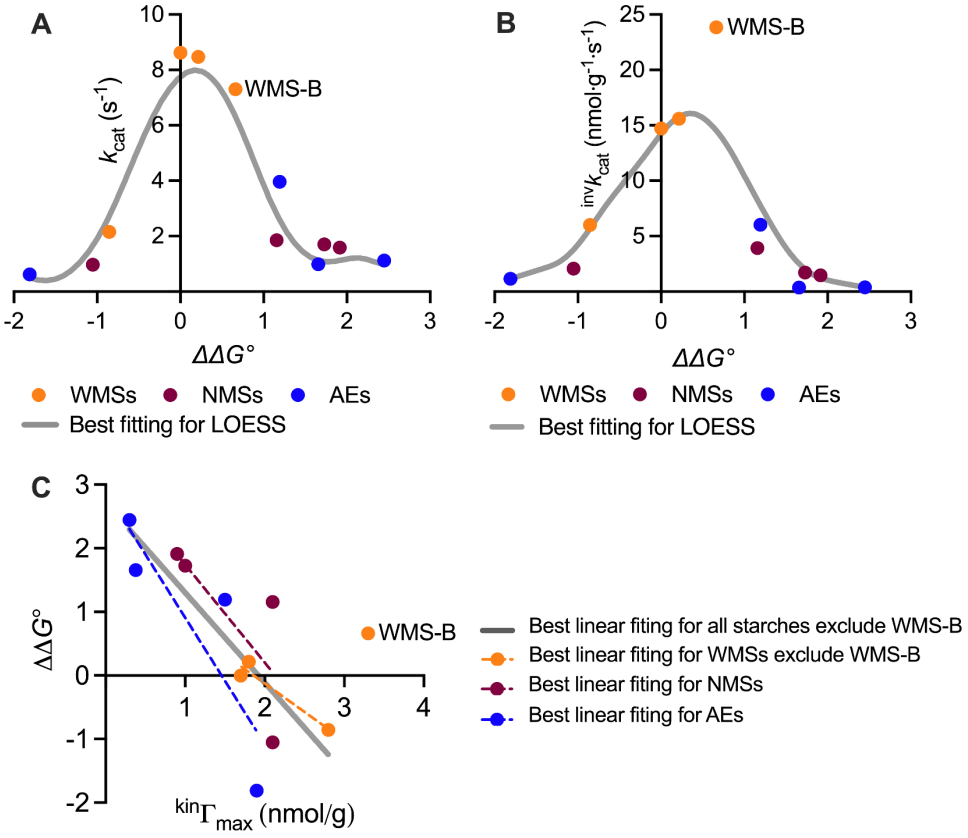

Figure 21. Fitting analysis of kinetic data. Fitting of (A) k_{cat} and (B) $^{inv}k_{cat}$ with $\Delta\Delta G°$ for *Bl*Pul acting on WMSs (orange), NMSs (brown), and AEs (blue). Gray line represents best fitting for locally weighted scatterplot smoothing (LOESS) to guide the eye. $K_{1/2}$ for WMS was selected as $K_{1/2,ref}$ to fix the $\Delta\Delta G°$ for WMS as zero (eq.5). (C) Linear fitting of $\Delta\Delta G°$ with $^{kin}\Gamma_{max}$ for *Bl*Pul acting on WMSs (orange), NMSs (brown), and AEs (blue). Gray line represents best linear fitting for all starches, WMS-B excluded. Orange, brown, and blue dashed lines represent best linear fitting for WMS (WMS-B excluded), NMSs, and AEs, respectively.

5. Conclusion

In the present work, the Sabatier principle as a tool to understand the enzymatic modification and the structure of starch granules. Based on the granule structure of NSs and MSs, *Ro*BE has capability to catalyze transglycosylation on starch granules, whereas TuαGT catalyze disproportionation on MS-B but hydrolysis and/or cyclization on NSs. The k_{cat}, $^{kin}\Gamma_{max}$, and $\Delta\Delta G°$ from interfacial kinetics demonstrated that starch modification by BE or 4αGT could alter the binding affinity between *Bl*Pul and starch granules, and affect the catalytic rate according to the Sabatier principle.

Author contributions

YW designed and performed the experiments, collected the data, and drafted the manuscript. YT and AB collected the data for CLD, XRD, and FTIR-ATR of starches. PW contributed to data analysis. MSM and BS developed the theoretical framework and edited the manuscript. All authors contributed to the revision and editing of the manuscript.

Abbreviations

4αGT, 4-α-glucanotransferase; BE, branching enzyme; *Bl*Pul, pullulanase from *Bacillus licheniformis*; CLD, chain length distribution; DP, degree of polymerization; NMS, normal maize starch; *Ro*BE, branching enzyme from *Rhodothermus obamensis*; TuαGT, 4-α-glucanotransferase from *Thermoproteus uzoniensis*; WMS, waxy maize starch.

Acknowledgements

Karina Jansen (Department of Biotechnology and Biomedicine, Technical University of Denmark) is gratefully thanked for technical assistance. We are thankful to Cargill for providing waxy maize starch, to Archer Daniels Midland for providing normal maize starch, and to Northwest A&F University for providing high amylose maize starch.

Funding

This work was supported by China Scholarship Council (CSC) grant #202006790033 and the Technical University of Denmark (YW), and by a China Scholarship Council (CSC) grant #202003250068 (YT).

2.3 Impact of Branching Enzyme and 4-α-Glucanotransferase Modification on Starch

This chapter is comprised of 1 paper (***Paper 4***), concerning modification on starches using *Ro*BE and TuαGT. In this chapter, *Ro*BE and TuαGT were used to modify gelatinized normal maize starch. This modified starch was used for encapsulation of curcumin.

Starch, a prevalent carbohydrate, serves vital roles in nutrition and food industry applications, including encapsulating sensitive bioactives [299,325]. Various encapsulation methods involve native starch granules, starch-stabilized emulsions, hydrogels, and microporous granules [326–329]. Enzymatic modification, like BE altering maize starch, elevates α-1,6-linkage for improved gastrointestinal resistance [108]. Gu et al. found highly branched starch prepared by BE enhances ascorbic acid retention [330]. We also had discovered previously that 4αGT elongates exterior amylopectin chains for slow retrogradation and gelation strength in tapioca starch hydrogels [128]. Combining starch with polysaccharides like alginate enhances the encapsulation of starch hydrogel [326,331,332]. The gel network of alginate, though permeable, benefits from starch addition, improving encapsulation efficiency [333,334]. The biocompatibility of alginate and the improved gel properties by addition of starch make these combinations promising for bioactive delivery [335].

In ***Paper 4***, a novel super-branched amylopectin was produced from normal maize starch by modification with *Ro*BE followed by TuαGT, and applied for co-entrapment of a curcumin-loaded emulsion in alginate beads. This modified starch was used to co-entrap a curcumin-loaded emulsion in alginate beads. The gel beads' network structure was formed through retrograded starch and Ca^{2+}-cross-linked alginate. The dual enzyme-modified starch had more and longer α-1,6-linked branch chains compared to single enzyme-modified and unmodified starches, and it exhibited higher resistance to digestive enzymes. Alginate beads with or without starch were similar in size (1.69–1.74 mm), but the presence of different starches improved curcumin retention 1.4–2.8 times. During *in vitro* simulated gastrointestinal digestion, 70%, 43%, and 22% of the curcumin were retained in the presence of modified, unmodified, or no starch, respectively. Molecular docking supported that curcumin and starch interacted through hydrogen bonding, hydrophobic contacts, and π-π stacking.

2.3.1 Paper 4 – Sequential Starch Modification by Branching Enzyme and 4-α-Glucanotransferase Improves Retention of Curcumin in Starch-Alginate Beads

This paper was accepted for publication in *Carbohydrate Polymers* on the 11th of September 2023. The paper presents results on a novel enzyme-modified starch using branching enzyme and 4-α-glucanotransferase, and application of this modified starch in encapsulation of curcumin with alginate. The supporting information can be found at the end of the paper. The permission to reuse this article in this PhD thesis was obtained from the publisher.

Carbohydrate Polymers 323 (2024) 121387

Contents lists available at ScienceDirect

Carbohydrate Polymers

journal homepage: www.elsevier.com/locate/carbpol

Sequential starch modification by branching enzyme and 4-α-glucanotransferase improves retention of curcumin in starch-alginate beads

Yu Wang [a,1], Chengfang Pang [b,1], Hossein Mohammad-Beigi [a], Xiaoxiao Li [c], Yazhen Wu [c], Marie Karen Tracy Hong Lin [d], Yuxiang Bai [c], Marie Sofie Møller [e,*], Birte Svensson [a,*]

[a] Enzyme and Protein Chemistry, Department of Biotechnology and Biomedicine, Technical University of Denmark, DK-2800 Kgs. Lyngby, Denmark
[b] Research Group for Genomic Epidemiology, National Food Institute, Technical University of Denmark, DK-2800 Kongens Lyngby, Denmark
[c] School of Food Science and Technology, Jiangnan University, Wuxi, Jiangsu 214122, China
[d] National Center for Nanofabrication and Characterization, Technical University of Denmark, Kgs. Lyngby DK-2800, Denmark
[e] Applied Molecular Enzyme Chemistry, Department of Biotechnology and Biomedicine, Technical University of Denmark, DK-2800 Kgs. Lyngby, Denmark

ARTICLE INFO

Keywords:
Enzymatic modification
Starch-alginate beads
Curcumin emulsion
In vitro digestion
Release models

ABSTRACT

A new super-branched amylopectin with longer exterior chains was produced from normal maize starch by modification with branching enzyme followed by 4-α-glucanotransferase, and applied for co-entrapment of a curcumin-loaded emulsion in alginate beads. The network structure of the gel beads was obtained with Ca^{2+}-cross-linked alginate and a modest load of retrograded starch. The dual enzyme modified starch contained more and longer α-1,6-linked branch chains than single enzyme modified and unmodified starches and showed superior resistance to digestive enzymes. Alginate beads with or without starch were of similar size (1.69–1.74 mm), but curcumin retention was improved 1.4–2.8-fold in the presence of different starches. Thus, subjecting the curcumin-loaded beads to *in vitro* simulated gastrointestinal digestion resulted in retention of 70, 43 and 22 % of the curcumin entrapped in the presence of modified, unmodified, or no starch, respectively. Molecular docking provided support for curcumin interacting with starch *via* hydrogen bonding, hydrophobic contacts and π-π stacking. The study highlights the potential of utilizing low concentration of dual-enzyme modified starch with alginate to create a versatile vehicle for controlled release and targeted delivery of bioactive compounds.

1. Introduction

Starch is one of the most abundant carbohydrates in nature and plays a major role in human nutrition as well as an ingredient in the food industry (Chi et al., 2021). Among numerous applications, starch has been successfully used for the encapsulation of vulnerable bioactive compounds (Zhu, 2017). Several encapsulation systems are reported, including the use of native starch granules (Chen et al., 2021; Han et al., 2015; López-Córdoba et al., 2014), starch granule-stabilized pickering emulsion (Marefati et al., 2015), starch hydrogels (Koev et al., 2022; Lu et al., 2021; Mun et al., 2015), and microporous starch granules (Chen et al., 2021; Xing et al., 2014).

Enzymatic modification of starch using transglycosylases attracted attention for production of starch derivatives with novel properties and improved encapsulation behavior. Thus, modification of maize starch by branching enzyme (BE) of glucoside hydrolase family 13 (GH13), catalyzing transfer of new branches (Tetlow & Emes, 2014), increased the content of α-1,6-linkages, which enhanced resistance to enzymes in the gastrointestinal tract (GIT) (Gu et al., 2021). For example, highly branched starch prepared using BE improved retention of encapsulated ascorbic acid during *in vitro* digestion (Gu et al., 2021). Additionally, starch gel strength has an important role in enzymatic digestion (Chen et al., 2022). We have discovered a 4-α-glucanotransferase (4αGT) of family GH77 from *Thermoproteus uzoniensis* that specifically elongates exterior branch chains in amylopectin by transfer of short fragments from amylose. This modification conferred tapioca starch hydrogel with desirable slowed down long-term retrogradation while still maintaining the short-term gelation strength (Wang et al., 2020). Recently, improved

* Corresponding authors.
E-mail addresses: msmo@dtu.dk (M.S. Møller), bis@bio.dtu.dk (B. Svensson).
[1] These authors contributed equally to this work.

https://doi.org/10.1016/j.carbpol.2023.121387
Received 1 June 2023; Received in revised form 30 August 2023; Accepted 11 September 2023
Available online 13 September 2023

UV stability and retarded release during *in vitro* digestion was reported for a curcumin emulsion-loaded hydrogel prepared from rice starch modified by 4αGT (Kang et al., 2021).

In addition to encapsulations based solely on starch or modified starch (Gu et al., 2021; Kang et al., 2021), combinations of native starch are reported with other polysaccharides, such as alginate (Bu et al., 2023; Chen et al., 2021; López-Córdoba et al., 2014; Singh et al., 2009) and pullulan (Liang & Gao, 2023). Alginates are composed of β-D-mannuronate and α-L-guluronate residues and form gel networks through ionic bridges with Ca^{2+} or other divalent cations (Hosseini et al., 2014). Alginates have been applied in preparation of hydrogel beads for the oral delivery of bioactive compounds because of its excellent biocompatibility, gelation properties, water retention and swelling capacity (Cong et al., 2018; Manzoor et al., 2022). However, the porous structure and hydrophilicity make alginate beads highly permeable causing rapid release of entrapped guest molecules. Notably, addition of starch has improved encapsulation efficacy of alginate beads (López-Córdoba et al., 2013).

Curcumin is a natural polyphenol that can serve as a flavoring and coloring food additive and which has various beneficial health effects due to its anti-inflammatory, anti-carcinogenic, and antioxidant properties. However, its poor water solubility (<0.1 mg/mL), sensitivity to acidic and alkaline conditions as well as to visible and UV light require attention. Compared with encapsulation of curcumin alone, curcumin Oil-in-Water (O/W) emulsion is preferable due to the significantly higher stability and solubility of curcumin in the oil phase. Additionally, O/W emulsions can be designed to have controlled release properties, allowing for sustained or targeted delivery of curcumin (Li et al., 2021; Ma et al., 2017).

At present, starch based beads are generally prepared with different types of starches. Several studies have reported the use of native starch in different concentrations to prepare starch-alginate hydrogels for encapsulation of guest compounds (Bu et al., 2023; Chen et al., 2021; Guedes Silva et al., 2021; López-Córdoba et al., 2013; Singh et al., 2009). Chemically modified starches have attracted attention as they exhibit reduced digestibility. Cationized starch and hydroxypropyl distarch phosphate made from tapioca starch have been used for preparing starch-alginate hydrogels (Lozano-Vazquez et al., 2015; Malakar et al., 2013). However, as environmental awareness and health consciousness have increased, enzyme-modified starch has gained prominence. Jain et al. thus modified rice starch using debranching enzyme followed by octenyl succinic anhydride (OSA) esterification, and used this modified starch to prepare lycopene loaded starch-alginate beads (Jain et al., 2020). Besides, Park et al. investigated the improvement of digestibility of starch-entrapped calcium alginate microspheres containing native or amylosucrase modified waxy maize starch (Park et al., 2014). However, there are still very few studies using the combination of alginate and enzymatically modified starch, especially investigating the relationship between molecular structure of modified starch and encapsulation efficiency of starch-alginate hydrogel beads. Notably, the starch concentration used in the above studies varies from 5 % to 33.3 % and usually the best behaving beads have the highest starch concentration (Bu et al., 2023; Jain et al., 2020; Park et al., 2014).

We hypothesize that a new super-branched amylopectin with longer exterior chains can be produced from normal maize starch (NMS) by transglycosylation with BE and 4αGT, and the derived hydrogel being applied for alginate encapsulation enabling controlled release of curcumin. In particular, the modified starch (MS) obtained by BE followed by 4αGT treatments improved UV stability and retention of encapsulated curcumin in an *in vitro* simulated GIT system. Molecular docking provided support for curcumin interacting with starch *via* hydrogen bonds, hydrophobic contacts and π-π stacking. The obtained starch-alginate bead encapsulations can serve as a new type of vehicle for delivery of bioactive compounds to the large intestine and are expected to have broad application prospects in functional foods and pharmaceutical industries.

2. Material and methods

2.1. Materials

NMS (20.7 % amylose content) was a kind gift of Archer Daniels Midland (ADM, Decatur, IL). BE from *Rhodothermus obamensis* (5.98 U/mg, Novozymes, Denmark) was a kind gift of Andreas Blennow, University of Copenhagen. The 4αGT from *Thermoproteus uzoniensis* was produced recombinantly and purified as described (Wang et al., 2020). Mucin from porcine stomach (M2378), porcine bile extract (B8631), pancreatin from porcine pancreas (P7545; 8 × USP), α-amylase from human saliva (A1031), amyloglucosidase from *Aspergillus niger* (A7095), trimethylsilylpropanoic acid (TMSP), curcumin, sodium alginate (180,947; M/G ratio: 1.56:1, molecular weight: 120,000–190,000 g/mol), and Tween 80 were purchased from Sigma-Aldrich Co. Ltd. (St. Louis, MO, USA) and pullulanase M2 (from *Bacillus licheniformis*, 900 U/mL) from Megazyme Co. Ltd. (Wicklow, Ireland). Sunflower oil was from a local supermarket (Netto, Denmark).

2.2. Preparation of modified maize starches (MSs)

NMS (6 %, w/v), suspended in 20 mM MES, 150 mM NaCl, 10 % glycerol, pH 6.0, was gelatinized (99 °C, 1100 rpm, 30 min) and incubated with either BE (1 U/g starch, 60 °C, 30 min) to obtain MS_B or 4αGT (1.5 U/g starch, 75 °C, 20 h) to obtain MS_T (Wang et al., 2023). NMS was also modified sequentially first by BE (1 U/g starch, 60 °C, 30 min), heated (100 °C, 30 min), cooled to 75 °C, and then added 1.5 U 4αGT/g starch (75 °C, 20 h) to obtain MS_{BT}. MSs were precipitated by three volumes of 96 % ethanol, kept overnight at 4 °C, centrifuged (4000*g*, 10 min), dried (40 °C, overnight) to remove ethanol, frozen (−80 °C, overnight), freeze-dried, and stored at room temperature.

2.3. Molecular structure of NMS and MSs

2.3.1. Starch-iodine complex spectra

Starch-iodine complexes were analyzed as described (Bai et al., 2015). NMS and MSs (10 mg) in 1 mL of MilliQ water were gelatinized (99 °C, 30 min) and 20 μL mixed with 200 μL iodine solution (0.001 g I_2, 0.01 g KI in 10 mL MilliQ water), incubated (25 °C, 2 min), and the absorbance recorded from 500 to 800 nm using a microplate reader (PowerWave XS, BIO-TEK).

2.3.2. Molecular weight distribution

The molecular size of NMS and MSs was determined by size exclusion chromatography-multi-angle laser light scattering-refractive index detector (SEC-MALLS-RI). Starch (5 mg/mL) suspended in DMSO:MilliQ water (9:1, v/v) was gelatinized on a boiling water bath for 1 h with

shaking every 10 min until the solution was clear and free from floc. The gelatinized starch was incubated (30 °C, 250 rpm, 48 h) to disrupt particles, re-boiled, filtered (0.45 μm filter) and 100 μL injected on a tandem column (Ohpak SB-804 HQ, Ohpak SB-806 HQ) using 0.1 M $NaNO_3$ (0.02 % NaN_3) as mobile phase at a flow rate of 0.6 mL/min and a column temperature set at 50 °C. Data were analyzed by ASTRA software version 5.3.4 (Wyatt Technologies).

2.3.3. Chain length distribution

Chain length distribution of NMS and MSs was determined by high performance anion exchange chromatography with pulsed amperometric detection (HPAEC-PAD) (Gu et al., 2021). Starch (5 mg/mL) suspended in 50 mM sodium acetate, pH 4.5 was gelatinized (99 °C, 30 min), debranched by pullulanase (0.036 U/mg, 42 °C, 12 h), and centrifuged (10,000g, 10 min). The supernatant (20 μL) was analyzed by HPAEC-PAD (ICS-5000+, Thermo Fisher Scientific, USA) equipped with a CarboPac PA-200 column. The relative content of chains was calculated according to the specific areas and the average DP was calculated from the values of the relative content of each chain.

2.3.4. ^1H NMR spectroscopy

1D ^1H NMR spectra were acquired using a 600 MHz NMR spectrometer (Bruker Avance III, Bruker Biospin, Rheinstetten, Germany) to assess contents of α-1,4 and α-1,6 linkages (Xue et al., 2022). NMS and MSs (5 mg/mL) suspended in D_2O were gelatinized (99 °C, 2 h), freeze-dried twice and dissolved in D_2O (with 0.03 % TMSP, 99 °C, 30 min) before analysis. The degree of branching was estimated from the areas of signals of anomeric protons (α-1,4: δ 5.35–5.45; α-1,6: δ 4.95–5.00).

2.3.5. Degree of starch digestibility

NMS and MSs (20 mg), suspended in 2 mL 50 mM sodium acetate, 5 mM $CaCl_2$, pH 5.5, were gelatinized (99 °C, 1100 rpm, 1 h), cooled to 37 °C and degraded as reported (Tian et al., 2021) by 2 mg/mL pancreatin and 3.6 μM amyloglucosidase (final enzyme concentrations) (37 °C, 300 rpm, 2 h). Aliquots (50 μL) were removed at 0, 20 and 120 min, mixed with 96 % ethanol (500 μL) and centrifuged (10,000g, 5 min). Glucose in the supernatant was quantified using the GOPOD assay (D-Glucose Assay Kit, Megazyme) with glucose as standard (Huggett, 1957). Rapidly digested starch (RDS) was defined as degraded within 0–20 min, slowly digested starch (SDS) as degraded within 20–120 min, and resistant starch (RS) as the remaining residue (Englyst et al., 1992):

$$\%RDS = G20/(\text{initial dry mass of sample}) \times (162/180) \times 100\%$$

$$\%SDS = (G120 - G20)/(\text{initial dry mass of sample}) \times (162/180) \times 100\%$$

$$\%RS = \text{initial dry mass of sample} - \%RDS - \%SDS$$

2.4. Rheological properties of NMS and MSs

NMS and MSs (60 mg/mL), suspended in MilliQ water, were completely gelatinized (99 °C, 1100 rpm, 60 min) (Wang et al., 2020) and kept (4 °C, 24 h) before dynamic rheological analysis using a rheometer (TA Instruments, Waters LLC, USA) equipped with a parallel-plate system (40 mm diameter) at a gap of 200 μm. Starch samples were transferred to the rheometer plate and excess removed with a spatula. The linear viscoelastic range was obtained by determining the oscillation amplitude at an oscillation strain range of 0.1–100 % at 25 °C. Dynamic shear data were obtained from frequency sweeps over 0.1–10 Hz in the linear viscoelastic range at 25 °C.

2.5. Preparation of curcumin-loaded starch-alginate beads (ABs)

NMS and MSs were dispersed (90 mg/mL, w/v) in MilliQ water, gelatinized (99 °C, 30 min) and cooled to room temperature. Stock curcumin O/W emulsion (1 mL 0.5 % curcumin, 10 % sunflower oil, 4 % Tween-80; for preparation see Supporting Information Section 1.2. and Fig. S1) was mixed with gelatinized starch (1 mL, 90 mg/mL) and sodium alginate (1 mL, 30 mg/mL) (Table 1) with gentle stirring. This mixture was injected dropwise from a 1 mL sterile syringe into cross-linking solution (25 mL, 0.5 M $CaCl_2$) with slow stirring (100 rpm, 25 °C, 15 min), and kept at 4 °C overnight for starch gelation. The ABs were collected by filtration, washed twice with MilliQ water, and kept in MilliQ water at 4 °C. The size of beads was analyzed using ImageJ software (version 1.50b, National Institutes of Health, USA). To determine the content of curcumin, ABs were isolated by filtration using filter paper and 50 mg was mixed with 0.5 mL acetone, incubated (25 °C, 1100 rpm, 5 min), added 25 mL 96 % ethanol and centrifuged (1300g, 10 min). Curcumin in the supernatant was quantified spectrophotometrically at 425 nm using 0.005–0.02 mg/mL curcumin in acetone as standard (Fig. S2). Curcumin content (%) of the beads (Table 1) was calculated according to Eq. (1), where V_1, C_1 and m_0 are the volume (0.5 mL), the concentration of curcumin in the supernatant (mg/mL), and the initial weight of beads (50 mg).

$$\text{Curcumin content } (\%) = \frac{V_1 \times C_1}{m_0} \times 100 \quad (1)$$

Table 1
Composition and properties of curcumin loaded starch-alginate beads (ABs).

Name	Alginate	Starch	Starch/alginate ratio (w/w)	Curcumin content (%)	Curcumin/polysaccharides ratio (w/w)	Size of beads (mm)	Diameter of pores (μm)
AB	√	×	ND	0.66 ± 0.03	0.073:1	1.69 ± 0.05[a]	0.51 ± 0.23[a]
S-AB	√	NMS	3:1	0.94 ± 0.02	0.078:1	1.73 ± 0.07[a]	0.05 ± 0.04[b]
MS_B-AB	√	MS_B	3:1	0.78 ± 0.02	0.065:1	1.70 ± 0.04[a]	0.35 ± 0.21[a]
MS_T-AB	√	MS_T	3:1	0.81 ± 0.02	0.068:1	1.72 ± 0.03[a]	0.47 ± 0.28[a]
MS_{BT}-AB	√	MS_{BT}	3:1	0.94 ± 0.02	0.078:1	1.74 ± 0.07[a]	0.19 ± 0.16[b]

Values are means ± standard deviation. Values with different letters in the same row are significantly different at $p < 0.05$.

2.6. Cryo-Scanning Electron Microscope (Cryo-SEM)

A bead was mounted for cryo-SEM on a sample holder attached to a transfer rod, rapidly frozen by plunging into slushed liquid nitrogen at −210 °C, and transferred to the preparation chamber stage at −180 °C (Quorum PP2000 Cryo Transfer System). The frozen sample was cleaved with a cold knife (facilitating an exposed surface in the fractured sample), sublimated at −80 °C for 15 min, and coated with Pt at a current of 4.5 mA for 30 s. The sample was then transferred under vacuum to the SEM stage in the Field Emission Scanning Electron Microscope (FEI Quanta 200 ESEM FEG) and imaged at 10 kV using an ETD detector. The pore size distribution of beads was analyzed using ImageJ software (version 1.50b, National Institutes of Health, USA).

2.7. UV stability

Stability of curcumin in ABs (100 mg in 10 mL MilliQ water) was determined using a UV irradiation chamber at room temperature with continuous stirring (120 rpm) and exposed to UVB light (TUV 30 W G30 TB, Philips) emitted at 254 nm for 6 h. Intact curcumin in the ABs was quantified according to Eq. (1) (Section 2.5).

2.8. Molecular docking

The single helix of A-type amylose (AmyA_double.pdb) was used to mimic the α-glucan chain conformation (https://polysac3db.cermav.cnrs.fr). The 3D structure of curcumin was obtained from ChemSpider (http://www.chemspider.com/). AutoDock version 1.5.7 (La Jolla, CA, USA), was used to add hydrogens to calculate Gasteiger charges and generate PDBQT files. The molecular docking was performed with AutoDock tools (ADT) version 1.5.7 (www.autodock.scrips.edu) and the complex was illustrated using PyMol (New York, USA).

2.9. In vitro digestion (INFOGEST)

A simulated GIT model composed of oral, gastric and intestinal phases (INFOGEST) was used to evaluate release of encapsulated curcumin from different alginate beads (ABs) during *in vitro* digestion (Brodkorb et al., 2019; Wang et al., 2021) with slight modification (see Supporting Information Section 1.3 for preparation of simulated saliva fluid (SSF), simulated gastric fluid (SGF) and simulated intestinal fluid (SIF)).

Oral phase: ABs (250 mg) was incubated in 10 mL SSF (with salivary α-amylase, 75 U/mL) at 37 °C with continuous stirring (300 rpm, 10 min). Aliquots (100 μL) were withdrawn after 10 min, diluted 100 times with ethanol (96 %), centrifuged (4000*g*, 5 min) and the absorbance of the supernatant was measured at 425 nm to quantify the curcumin content (see Section 2.5 and Fig. S2).

Gastric phase: Before starting the experiment, 640 mg pepsin was dissolved in 200 mL SGF and preheated (37 °C, 10 min). After 10 min of oral phase digestion, 15 mL SGF was added, followed by incubation with continuous stirring (300 rpm, 2 h). For gastric phase without enzyme, 15 mL SGF was replaced by SGF without pepsin. Aliquots (100 μL) were withdrawn every 15 min and analyzed for curcumin release as described above.

Small intestinal phase: After 2 h of gastric phase digestion, 25 mL SIF containing 7.5 mg/mL pancreatin was added, followed by incubation with continuous stirring (300 rpm, 2 h). Aliquots (100 μL) were withdrawn every 15 min and analyzed for curcumin release as described above.

2.10. Characterization of the mechanism of curcumin release from ABs

Data of curcumin release rate from ABs for the first 60 min in SGF and SIF were fitted to different mathematical models for drug release, where M_t is the amount of curcumin released at time t, M_∞ is the initial amount and k is the release rate constant.

In the zero-order model (Eq. (2)) release is independent of curcumin concentration (Bruschi, 2015):

$$\frac{M_t}{M_\infty} = kt \tag{2}$$

The first-order model (Eq. (3)) assumes that the curcumin content within the reservoir declines exponentially and the release rate is positively related to the residual content (Ehtezazi et al., 2000):

$$\frac{M_t}{M_\infty} = 1 - exp(-kt) \tag{3}$$

The Higuchi square root time model (Eq. (4)) is the most widely used (Higuchi, 1963) and suitable for describing curcumin release from matrices:

$$\frac{M_t}{M_\infty} = kt^{\frac{1}{2}} \tag{4}$$

The Korsmeyer–Peppas model (Eq. (5)) is based on a power law dependence of the fraction released with time (Korsmeyer et al., 1983):

$$\frac{M_t}{M_\infty} = kt^n \tag{5}$$

where n is the diffusional exponent ranging from 0.43 to 1 depending on the release mechanism and the shape of the delivery device. Based on the value of n, curcumin transport in spheres is classified either as Fickian or Case I diffusion ($n \leq 0.5$), non-Fickian or anomalous transport ($0.5 < n < 1$), or Case II transport ($n = 1$), where the dominant mechanism for release is polymer relaxation (erosion/degradation) during gel swelling. Anomalous transport occurs due to a coupling of Fickian diffusion and polymer relaxation (Ritger & Peppas, 1987).

Sum of squares for each model was calculated using GraphPad Prism 6 (GraphPad Software Inc) to determine the best fitting kinetic model (Malakar et al., 2013).

2.11. Statistical analysis

Experiments were performed in triplicate. The statistical significance was assessed with Two-way ANOVA using GraphPad Prism 6 (GraphPad Software Inc). p values < 0.05 were considered statistically significant throughout the study.

3. Results and discussion

3.1. Structure and digestibility of NMS before and after modification with BE and 4αGT

Treatment of NMS with BE and 4αGT, either individually or in sequence (BE followed by 4αGT), resulted in MSs containing amylopectin with altered branch structure.

3.1.1. Iodine-starch complexation

The absorption spectra of iodine complexes with helix cavities of α-glucans depend on the amount of captured iodine thus distinguishing cavity sizes and hence amylose and amylopectin. For instance, iodine yields a dark blue color (540–660 nm) with amylose and a purple color (500–540 nm) with amylopectin (Yu et al., 2021). Firstly, to determine the optimal modification duration, NMS was treated by BE from 10 to 120 min (Fig. S3). As the peak absorbance stabilized after shifting from 610 to 580 nm during the initial to 30 min this time was chosen for production of MS_B. In the case of MS_B, MS_T and MS_{BT}, iodine complex spectra showed increasing blue shifts with absorbance maxima of 580, 560, and 530 nm, respectively, compared to 630 nm of NMS (Fig. 1A). This suggests that iodine mainly bound to amylose in NMS and with branch chains in the MSs, where amylose had been consumed in

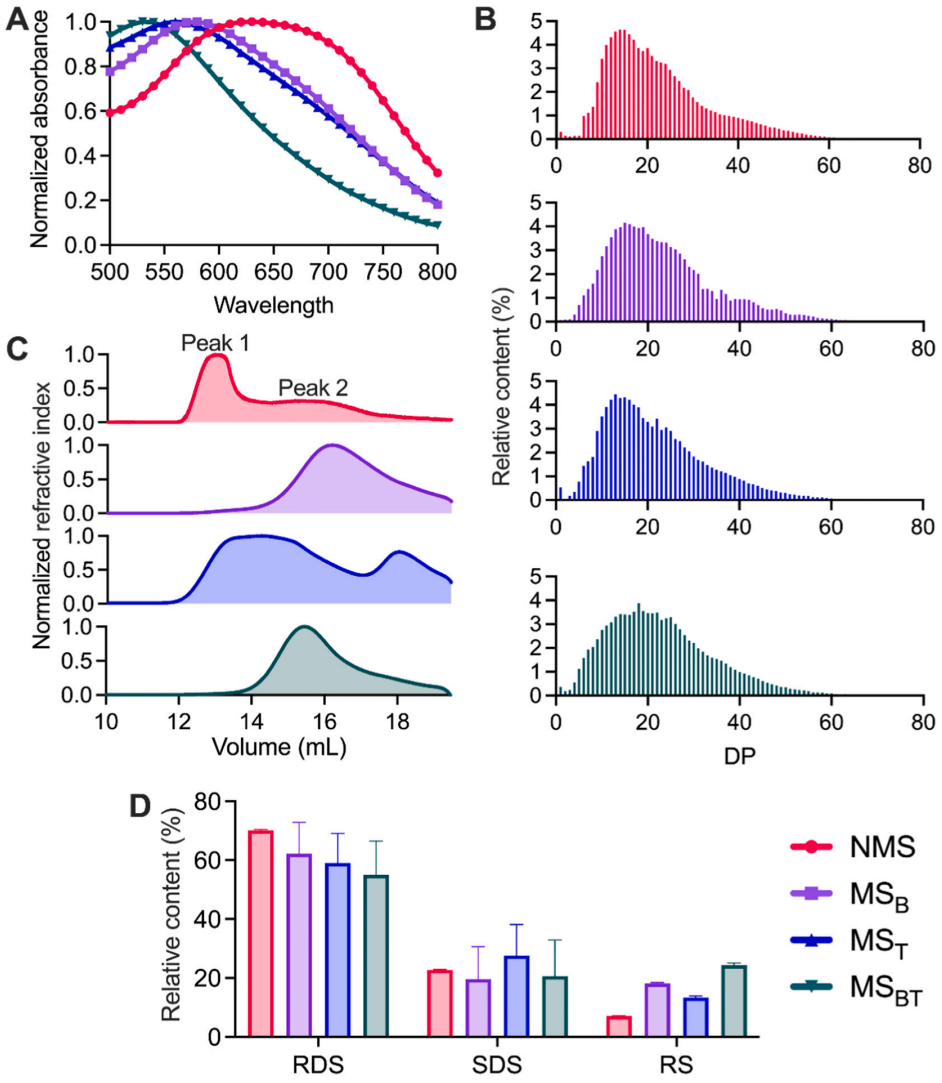

Fig. 1. Structural analyses of NMS (red), MSs modified by BE (MS_B, purple), 4αGT (MS_T, blue) and BE+4αGT (MS_{BT}, green). (A) Spectra of starch-iodine complexes; (B) Chain length distribution; (C) SEC analysis of molecular size distribution; (D) Contents of rapidly digested starch (RDS), slowly digested starch (SDS) and resistant starch (RS).

transglycosylation reactions. The larger blue shift to 530 nm of MS_{BT} compared to 580 nm of MS_B agrees well with utilization of amylose present in MS_B by 4αGT.

3.1.2. Chain length distribution

Treatment of NMS with BE, 4αGT, and BE followed by 4αGT to obtain MS_B, MS_T and MS_{BT} altered the chain length distribution of NMS (Fig. 1B) as evidenced from the relative amounts of A-, B1-, B2-, and B3-chain length categories (Table 2). The A-chains (DP <12) increased significantly by 4.2 percentage points (p.p.) in MS_B, while the B1-chains (DP 13–24) decreased by 3.6 p.p., in agreement with BE catalyzing transfer of new, rather short branches to the amylopectin, resulting in an overall higher content of shorter chains (Li et al., 2019). In MS_T, B1-chains decreased by 3.3 p.p., while B2- and B3-chains increased by 2.4 and 1.2 p.p., respectively, consistent with the mode of action of 4αGT (Li et al., 2023) and our previous finding that this 4αGT from *Thermoproteus uzoniensis* elongates exterior chains in amylopectin (Wang et al., 2020). Finally, in MS_{BT} B1-chains decreased by 3.2 p.p., while B2- and B3-chains both increased by 1.7 p.p., compared to MS_B, indicating that 4αGT as expected elongated branch chains in MS_B, the BE product of NMS. Earlier studies have explored the impact of BE and 4αGT on starch modification. For example, Kakutani et al. (2008) focused on preparing enzymatically synthesized glycogen (Kakutani et al., 2008), while Sorndech et al. (2016) found that the modified starch exhibited a highly branched amylopectin characterized by shorter branch chains (Sorndech et al., 2016), which could potentially hinder the effective network formation of starch-alginate hydrogels (Li et al., 2023; Liang et al., 2023).

Table 2
Percentage of different branch chain length categories, α-1,6−/α-1,4-linkage ratio, and contents of RDS, SDS and RS in NMS, MS_B, MS_T, and MS_{BT}.

Parameter	NMS	MS_B	MS_T	MS_{BT}
A-chain (DP 1–12)	18.4 ± 0.3[a]	22.6 ± 0.8[b]	18.0 ± 0.6[a]	19.8 ± 0.3[a]
B1-chain (DP 13–24)	48.1 ± 0.7[c]	44.5 ± 0.6[b]	44.8 ± 0.3[b]	41.6 ± 1.3[a]
B2-chain (DP 25–36)	19.8 ± 0.8[a]	21.5 ± 0.8[b]	22.2 ± 1.0[b]	23.9 ± 0.7[c]
B3-chain (DP >37)	14.1 ± 0.4[a]	11.8 ± 2.2[a]	15.3 ± 1.0[a]	15.2 ± 1.1[a]
α-1,6-/α-1,4-linkage ratio	3.9 ± 0.1[a]	5.3 ± 0.2[b]	4.1 ± 0.1[a]	5.1 ± 0.2[b]
RDS	70.2 ± 0.3[a]	62.2 ± 10.6[a]	59.0 ± 10.1[a]	55.0 ± 11.5[a]
SDS	22.8 ± 0.2[b]	19.6 ± 0.8[c]	27.6 ± 0.5[a]	20.6 ± 1.8[c]
RS	7.1 ± 0.1 d	18.1 ± 0.4 b	13.4 ± 0.5 c	24.4 ± 0.8 a

Values are means ± standard deviation. Values with different letters in the same row are significantly different at $p < 0.05$.

3.1.3. Molecular size distribution

The molecular weight (M_w) distribution of NMS was analyzed before and after BE and 4αGT treatments using SEC-MALLS-RI (Fig. 1C). The two typical peaks of amylopectin (Peak 1) and amylose (Peak 2) in NMS changed after BE modification to one broad later eluting peak (at 16.2 mL), indicating a decrease in M_w of MS_B. Notably, MS_{BT} eluted slightly earlier (at 15.4 mL) with a similar peak shape in accordance with 4αGT using amylose to extend amylopectin branches. MS_{BT} exhibited a narrower amylopectin peak than MS_B, suggesting greater uniformity. The elution profiles support the notion that BE generated amylopectin with more short branches than found in NMS and of lower M_w. 4αGT elongated native as well as newly formed branches reducing the A-chain content by 2.8 p.p. and increasing B2- and B3-chain contents by 2.4 and 3.4 p.p., representing the super-branched amylopectin of higher M_w. Conversely, in MS_T, 4αGT was primarily using amylose to elongate amylopectin chains without altering the branching pattern. Hence the amylose content was significantly decreased as supported by the blue shift in the iodine-starch complexation assay (Fig. 1A,C, Table 2).

3.1.4. α-1,6−/α-1,4-linkage ratio

To further characterize the MSs, their degree of branching was quantified by ^{1}H NMR spectroscopy using chemical shifts in the range of 4.6–5.6 ppm for protons at α-1,4 and α-1,6 linkages (Table 2). Compared with NMS, the α-1,6−/α-1,4-linkage ratio increased dramatically by 40 and 36 % in MS_B and MS_{BT}, respectively, due to formation of new branches in turn extended by 4αGT in transglycosylation reactions (Ban et al., 2020).

3.1.5. Contents of RDS, SDS, and RS in NMS and MSs

The changes in contents of rapidly digested starch (RDS), slowly digested starch (SDS), and resistant starch (RS) (Englyst et al., 1992) in the MSs clearly reflected the effect on the digestibility by α-amylase (in pancreatin) and amyloglucosidase of NMS by the BE and 4αGT treatments (Fig. 1D, Table 2). Thus MS_B and MS_T both gained RS and lost RDS compared to NMS, consistent with BE enhancing resistance to amylolytic degradation due to the increase in α-1,6-linkages and branch chains elongated by 4αGT (Jiang et al., 2014), assuming associative interactions hindering attack by α-amylase and glucoamylase (Ao et al., 2007). Notably, sequential BE and 4αGT modification generated 3.4- and 1.3-fold more RS in MS_{BT} than found in NMS and MS_B, respectively, as expected for a higher content and increased length of branches in amylopectin (Fig. 1B, Table 2).

3.2. Rheological properties of NMS and MS hydrogels

Once starches are subjected to gelatinization, they undergo a process of molecular reorganization and cross-linking of chains through hydrogen bonds. This results in formation of a locally more stable gel

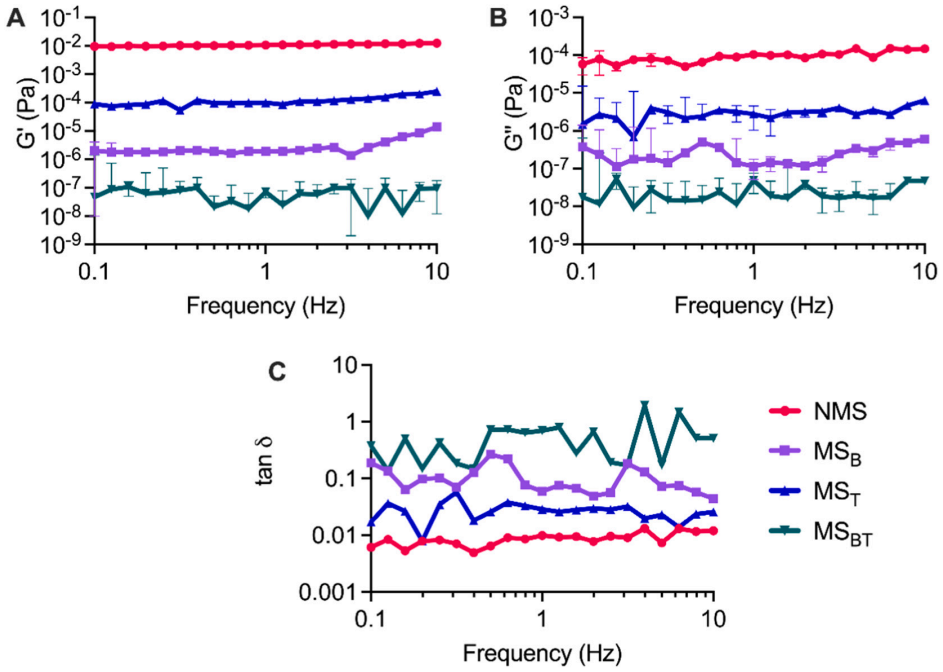

Fig. 2. Rheological properties of NMS (red) modified by BE (purple), 4αGT (blue) and BE+4αGT (green). Frequency-dependence is shown of (A) G′; (B) G″; and (C) tan δ.

network, which, upon cooling, transforms into a hydrogel (Yu et al., 2018). The storage modulus (G′) represents the elastic portion, and the loss modulus (G″) the viscous portion of the viscoelastic behavior. Tan δ is G″/G′, and higher tan δ corresponds to a less solid-like behavior. For example, G″ > G′ indicates a liquid-like response as seen for a polymer solution, referred to as a "true polymer solution", while G′ > G″ is observed in rheological tests for solid-like hydrogels (Kang et al., 2021; Tashiro et al., 2010). Changes in storage (G′) and loss (G″) moduli were measured during frequency sweeps in the range of 0.1–10 Hz to monitor the viscoelastic properties of semi-solid hydrogels prepared from NMS, MS_B, MS_T, and MS_{BT} (Fig. 2). Rheological tests were conducted at 25 °C to evaluate stability of the hydrogels intended for use in consolidating curcumin-loaded emulsions at room temperature. This approach is advantageous as it is energy-saving, while ensuring the desired performance of the hydrogels. First the strain dependence of G′ and G″ was evaluated to select a strain (1 %) for the samples to measure within a linear viscoelastic range (Fig. S4). All starches gave G′ > G″ indicating a solid-like response (Fig. 2). Compared to the three MSs, NMS had higher G′ and G″ but lowest tan δ values, indicating that this hydrogel was stronger than those prepared from the MSs. Moreover, a relatively stronger hydrogel was obtained for MS_T, followed by MS_{BT} and MS_B in that order. Based on our previous work, most of the amylose would be consumed in the 4αGT reaction (Li et al., 2023; Sun et al., 2020), leading to a lower gel strength of hydrogels prepared from the MSs, while higher amylose content in NMS contributes to the stronger hydrogen bonding in the gel network. The MS_{BT} hydrogel was stronger than that of MS_B (Fig. 2), probably due to its higher content of longer branch chains, enhancing hydrogen bonding in the starch hydrogel (Table 2).

During starch hydrogel formation, association of amylose *via* hydrogen bonds with amylopectin branch chains and other amylose molecules is important. As demonstrated by the molecular size distribution analysis, 4αGT significantly degraded amylose (Fig. 1C), and the structure of amylopectin in MS_T was reshaped compared to NMS (Fig. 1B). Amylose was also consumed by BE-catalyzed transglycosylation and served as both donor and acceptor to form MS_B (Li et al., 2019). However, the association of α-glucan chains decreased in MS_B compared to MS_T, resulting in a weaker hydrogel (Fig. 2). The looser gel network in MS_B-AB than MS_T-AB is suggested to be caused by the lower content of longer chains in amylopectin, leading to less hydrogen bond formation within starch or between starch and alginate (see Section 3.3). Notably, further treatment of MS_B by 4αGT, which increased the molecular size due to formation of longer amylopectin branches, resulted in higher gel strength for MS_{BT}.

3.3. Cryo-SEM of curcumin loaded starch-alginate beads

Mixtures of curcumin emulsion, NMS or MS hydrogels and alginate were used for encapsulation (see Section 2.5 and Table 1). Size and pore distribution, photographs and cryo-SEM images of the curcumin loaded starch-alginate beads are shown in Table 1, and Figs. 3 and 4.

All alginate beads (ABs) showed similar diameter from 1.69 to 1.74 mm, indicating that the addition of NMS and MSs did not affect the overall size of ABs (Fig. 3, Table 1). As shown by cryo-SEM gelatinized starch and alginate clumped together in the beads (ABs) and formed a three-dimensional network filled with the curcumin O/W emulsion (Fig. 4). The gelation of starch and alginate can occur *via* two main mechanisms: ionic gelation and physical gelation. In ionic gelation, calcium ions interact with the carboxylate groups of alginate, leading to the formation of a gel network. Physical gelation, on the other hand, involves the gel formation *via* hydrogen bonds between starch and alginate molecules (Ramírez et al., 2015). Notably, the ABs have very different surface roughness (Fig. 4A–E) and gel network compactness (Fig. 4F–J), the roughest surface being seen for the control without starch, AB (Fig. 4A) and for BE-modified starch containing beads, MS_B-AB (Fig. 4C), while sequentially BE- and 4αGT-modified beads, MS_{BT}-AB

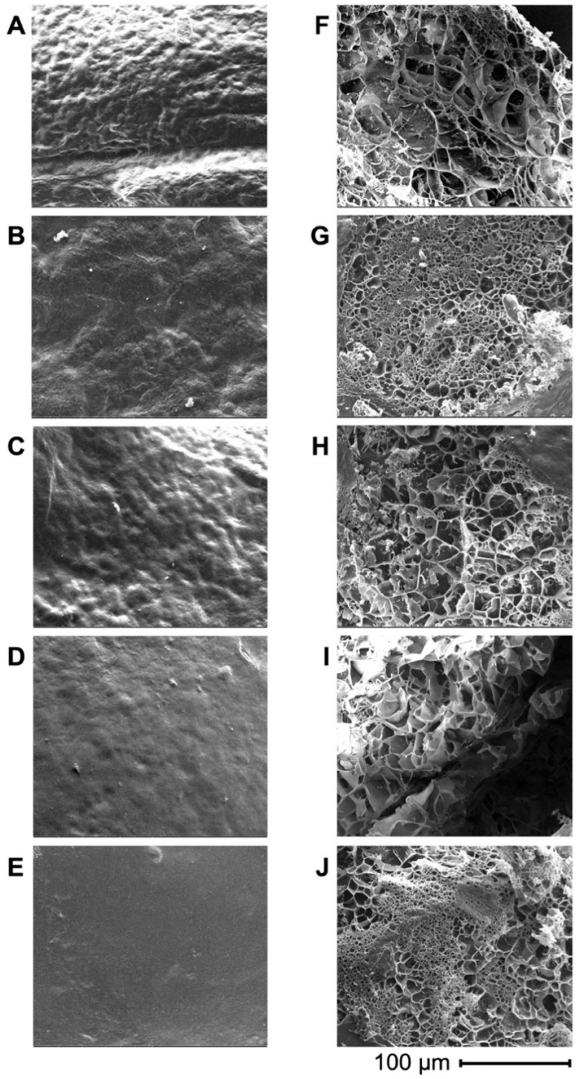

Fig. 4. Cryo-SEM curcumin-starch-alginate beads. Images of the surface of (A) AB (control without starch), (B) S-AB, (C) MS_B-AB, (D) MS_T-AB, and (E) MS_{BT}-AB and of the gel network in (F) AB, (G) S-AB, (H) MS_B-AB, (I) MS_T-AB, and (J) MS_{BT}-AB.

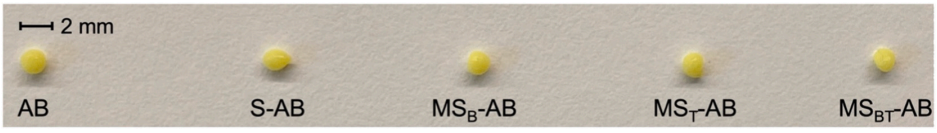

Fig. 3. Photographs of alginate beads (ABs) without and with modified starches (MSs), AB, S-AB, MS_B-AB, MS_T-AB, and MS_{BT}-AB.

(Fig. 4E) had the smoothest surface and maybe are harder for enzymes to attack, in accordance with the higher curcumin retention of MS_{BT}-AB in *in vitro* simulated digestion (see Section 3.5). A denser network having smaller pores was observed for beads containing unmodified NMS, S-AB (Fig. 4G) and MS_{BT}-AB (Fig. 4J), while MS_B-AB contained a partly compact network (Fig. 4H), and MS_T-AB had the loosest gel network (Fig. 4I, Table 1). Additionally, an inverse relationship was evident between amount of encapsulated curcumin and pore diameter of the beads, smaller pores correlating with higher curcumin contents as for S-AB and MS_{BT}-AB (Fig. S5, Table 1). Thus, the compactness of the network of the starch-alginate beads significantly varied with the starch modification and influenced the yield of encapsulation. The most compact gel network obtained for S-AB presumably reflects its higher content of amylose, which BE and 4αGT had consumed in the different MSs included in the other ABs. Thus, the most loose gel network, found in MS_B-AB and MS_T-AB, is suggested to stem from this consumption of amylose, leading to less hydrogen bond formation within starch or between starch and alginate. As for MS_{BT}-AB, the higher content of branches supported formation of hydrogen bonds, leading to a stronger gel network, probably especially involving 4αGT-elongated branch chains. The more compact gel network of NMS (S-AB, Fig. 4G) correlated with the highest gel strength (tan δ) (Fig. 2C).

3.4. Curcumin UV stability in ABs

Curcumin is susceptible to degradation by UV and visible light (Park et al., 2019), and in AB >50 % of the curcumin was lost after 1 h of UV exposure, which increased to around 70 % after 4 h (Fig. 6A). However, curcumin was clearly protected in ABs containing starch and best so in S-AB (>80 %, 6 h), likely reflecting that NMS gelates faster to form a stronger hydrogel than the three MSs (Fig. 2). Besides, the higher content of intact long-chain amylose in NMS can be related to the formation of giant or wormlike micelles formed by weak electrostatic interactions with tween-80 (Merta et al., 2001; Vernon-Carter et al., 2018). Notably, MS_T-AB and MS_{BT}-AB provided similar levels of protection of curcumin, while MS_B-AB was less effective (Fig. 5A). UV irradiation increases the bead temperature (Barkoula et al., 2008) resulting in weakened hydrogen bonding and double helix structure between starch molecular chains. Consequently, UV-irradiation can destroy the gel network (Bu et al., 2023). However, it seems that a strong starch hydrogel suppressed destruction of the gel network and prevented bead swelling, thus offering superior curcumin protection. S-AB and MS_{BT}-AB had a denser network with smaller pores compared to the other ABs (Fig. 4F–J, Table 1), which provided a better barrier against curcumin loss by UV irradiation (Balasubramanian et al., 2018).

All ABs containing starch maintained higher amounts of curcumin intact than the AB without starch (Fig. 5A). Moreover, it was observed that the presence of gels of starch and different types of modified starch in the ABs affected their compactness to different degree, having significant impact on the efficacy of curcumin encapsulation (Section 3.3). We further speculate that molecular interactions between curcumin and starch also affect the encapsulation rate (Table 1) and the apparent sensitivity of curcumin to UV light (Araiza-Calahorra et al., 2018). Thus, in the present work, molecular docking of curcumin to the cavity of a helical α-glucan chain support a carrier effect revealing several features likely improving the miscibility of curcumin in this system (Fig. 5C,D). Curcumin was completely entrapped in the α-glucan cavity with a free binding energy of −5.2 kcal/mol, indicating good stability of the complex. In the modelled complex hydrogen bonds of 3.1–4.1 Å were formed between the carbonyl oxygen of curcumin and sugar hydroxyl groups (Fig. 5E-G, red). Moreover, the central aliphatic carbon chain of curcumin (Fig. 5B) can make a hydrophobic contact with the single helix α-glucan (Fig. 5C). Finally, distances of π-π stacking interactions between an aromatic ring of curcumin and two adjacent glucose residues in the α-glucan were calculated to 4.7–5.1 Å (Fig. 5E,G, green), compatible with a previous study on reliable π-π interactions of <7 Å (Piovesan et al., 2016). Thus, hydrogen bonding, hydrophobic and π-π stacking interactions with the α-glucan chain improve embedding of curcumin by a starch gel in the alginate beads.

3.5. Curcumin retention in ABs during simulated in vitro GIT digestion

The cumulative release of curcumin from starch-alginate beads (ABs) was monitored in simulated salivary, gastric and intestinal fluids (SSF, SGF and SIF) using the INFOGEST protocol (Brodkorb et al., 2019) (Fig. 6). MS_{BT}-AB was most efficient and retained 70.2 % encapsulated curcumin after exposure to the simulated fluids of the GIT. MS_T-AB had a slightly lower retention of 57.6 %, followed by MS_B-AB, S-AB, and AB retaining 47.2 %, 42.5 %, and 22.4 %, respectively (Fig. 6G). The MS_{BT} gel had a particularly positive effect on curcumin retention in oral phase (SSF), which contains human salivary α-amylase, under acidic conditions in the SGF, and when exposed to digestive enzymes present in pancreatin (α-amylase and lipase) in the SIF. Thus, MS_{BT} offered effective encapsulation of curcumin in the simulated gut system. In

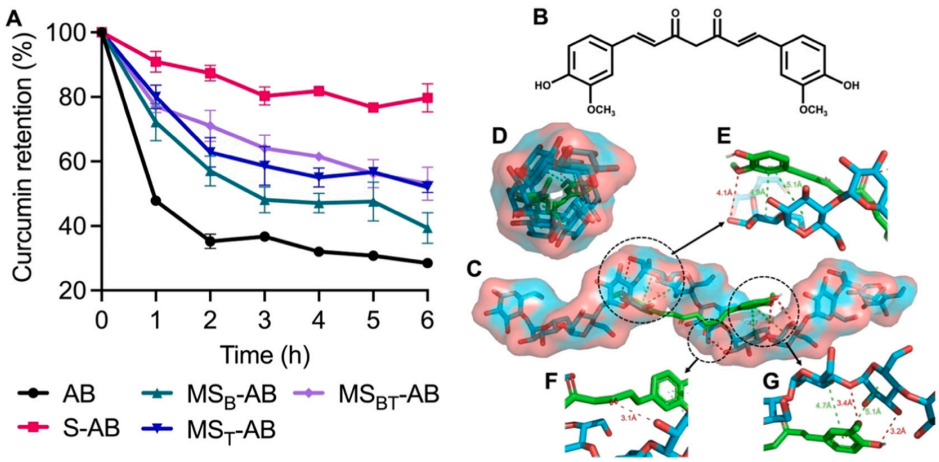

Fig. 5. Stability of curcumin in ABs. (A) Loss of curcumin during UV exposure. (B) Chemical structure of curcumin. (C) Molecular docking of curcumin (green) to an amylose single helix (blue) using AutoDock Vina. (D) Front end view of docked curcumin in the cavity of a single helix α-glucan chain. (E-G) Presentation of calculated hydrogen bond (red) and π-π stacking (green) interactions between curcumin and the α-glucan chain.

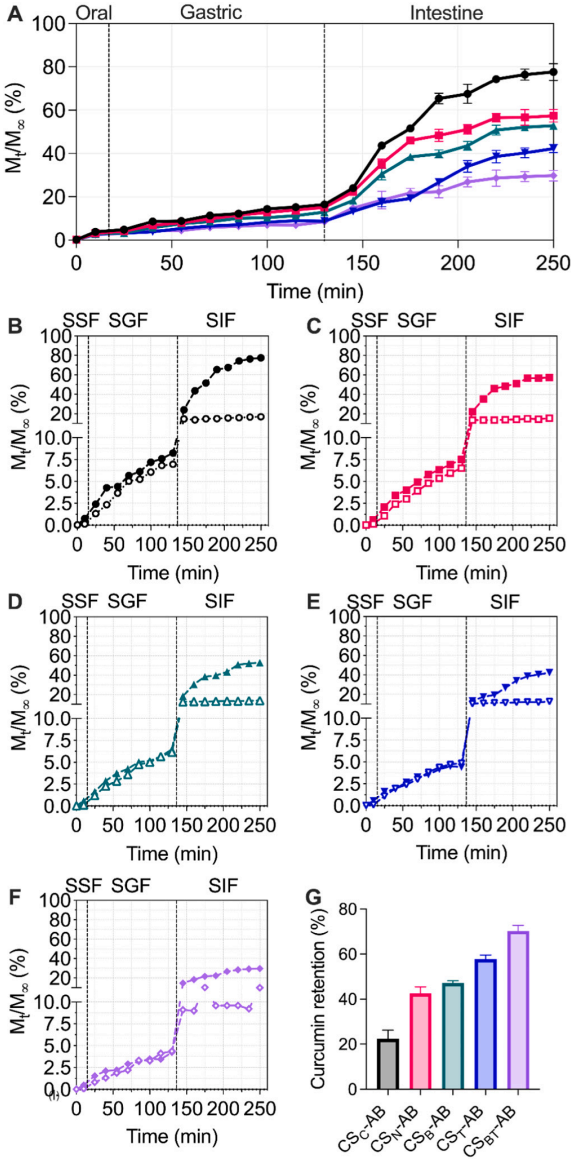

Fig. 6. Cumulative curcumin release from AB (black), S-AB (red), MS_B-AB (green), MS_T-AB (blue), and MS_{BT}-AB (purple) during *in vitro* digestion. M_t is the amount of curcumin released at time t and M_∞ is the initial amount of curcumin. (A) *In vitro* release profiles of curcumin from ABs with digestive enzymes at 37 °C. Individual, *in vitro* release profiles of curcumin from (B) AB, (C) S-AB, (D) MS_B-AB, (E) MS_T-AB, and (F) MS_{BT}-AB with (solid) or without (open) digestive enzymes at 37 °C. (G) Final retention (%) of curcumin in different ABs after *in vitro* digestion (250 min).

comparison, Bu et al. reported that alginate beads containing 33.3 % native pea starch retained ~25 % of proanthocyanidins following an *in vitro* release experiment (Bu et al., 2023). Besides, including 5 % rice starch modified by debranching and octyl succinic anhydride esterification in starch-alginate beads maintained ~60 % of lycopene during *in vitro* release experiment (Jain et al., 2020). However, excessive intake of starch with low digestibility would significantly increase intensity of abdominal cramps, flatulence, and fullness (Bergeron et al., 2016). Thus compared with the above high starch loads, the use of only 3 % starch for ABs in the present work reduced risk of undesirable intake of starch, while retaining higher contents of the guest compound (70.2 % for MS_{BT}-AB, Fig. 6).

The curcumin release data were fitted to different kinetic models (Eqs. (2)–(5); Section 2.10) to gain insights into the mechanism of release from ABs. The rate constant (k), diffusional exponent (n), correlation coefficient (R^2), and sum of squares (SS) are summarized in Table 3. According to the R^2 and SS, the Korsmeyer-Peppas model provided the best fit for all starch-containing ABs (Table 3). For this reason, only the Korsmeyer-Peppas model will be discussed.

In SGF with digestive enzymes (Table 3) $n < 0.5$, as found for MS_{BT}-AB ($n = 0.435$), suggested that curcumin is released primarily *via* Fickian diffusion, whereas for the other beads having $n > 0.5$ the release occurs *via* erosion/degradation and swelling. This behavior is consistent with MS_{BT} having highest RS content (24.4 %) (Fig. 1D, Table 2). However, n in the range of 0.55–0.65 for the other four bead types, AB, S-AB, MS_B-AB, and MS_T-AB, indicated an anomalous release mechanism to be prominent, clearly influenced by the destruction of the network caused by digestive enzymes. The higher n value of S-AB compared to MS_T-AB is consistent with S-AB forming a stronger gel (Fig. 2). For all bead types, the curcumin release in SGF without digestive enzymes showed a higher n than with digestive enzymes, suggesting an increased release *via* coupling of Fickian diffusion and erosion/degradation. Finally, the more prominent curcumin release in SIF for all ABs fitted the Korsmeyer-Peppas model with n values in the range 0.35–0.66 (Table 3). The n of 0.35 for MS_{BT}-AB again indicated release primarily *via* Fickian diffusion. For AB, S-AB, MS_B-AB, and MS_T-AB, n values of 0.52–0.66 reflect that curcumin release occurred by both polymer chain relaxation and Fickian diffusion through the hydrated layers of the matrix, which corresponded to the reported non-Fickian diffusion of curcumin from alginate-gelatin fiber (Sharma et al., 2020). MS_{BT}-AB had the lowest n value, followed by MS_T-AB. This observation suggests that the higher proportion of α-1,6-branch points in MS_{BT} and the longer branch chains in both MS_{BT} and MS_T (Table 2) led to the formation of stronger hydrogen bonding between starch and alginate. As a result, MS_{BT}-AB and MS_T-AB were less susceptible to the α-amylase in pancreatin. Remarkably, the data for AB, S-AB, and MS_B-AB in SIF gave very similar n values (Table 3), indicating that NMS and MS_B did not alter the release mechanism, although S-AB and MS_B-AB retained curcumin more efficiently than the control alginate beads, AB (Fig. 6). It should be noted that in the absence of digestive enzymes, the release of curcumin in SGF was considerably faster than in SIF. Similarly, Zhao et al. found that apigenin in microemulsion filled gellan gum hydrogel showed faster release in a low pH medium (Zhao & Wang, 2019). The faster release of drugs in a low pH medium might be related to the shrinkage of the hydrogel networks.

In summary, the fitting to the models indicated that the presence of MS_{BT} significantly decreased the release of curcumin by showing Fickian diffusion (that is representative for almost no erosion/degradation of the gel network) in both SGF and SIF, while the release of curcumin from the other ABs also occurred due to erosion/degradation of the network to different degree. The pharmacological activity of the released curcumin was not assessed in our study. However, previous literature suggests that if curcumin undergoes degradation, its absorbance within the 420–450 nm range may be compromised and difficult to determine (Aboudiab et al., 2020). Therefore, the observed absorbance at 425 nm, as employed in our study, serves as supporting evidence for the pharmacological activity of curcumin being retained. Embedding curcumin in emulsion within alginate beads with different starches, especially MS_{BT}-AB, has the potential to enable controlled release of curcumin in different sections of the intestinal tract, including the colon. Such targeted release is crucial for harnessing curcumin's anti-inflammatory and anti-tumor properties, which have been demonstrated by inhibiting growth of colon cancer cells (Selvam et al., 2019; Sripetthong et al., 2023).

Table 3
Kinetic parameters of curcumin release from different ABs in simulated *in vitro* digestion fitted to different mathematical models.

Phase	Sample	Zero order			First order			Higuchi			Korsmeyer-Peppas model			
		k (min^{-1})	R^2	SS[a]	k (min^{-1})	R^2	SS	k ($min^{1/2}$)	R^2	SS	k (min^{-n})	n	R^2	SS
Gastric phase (without digestive enzyme)	AB	0.012	0.994	0.427	0.015	0.983	17.8	0.068	0.914	1.08	0.013	0.972	0.995	0.338
	S-AB	0.010	0.984	0.169	0.015	0.983	11.8	0.075	0.923	0.416	0.019	0.848	0.993	0.052
	MS_B-AB	0.010	0.965	0.093	0.015	0.995	8.74	0.070	0.959	0.724	0.028	0.745	0.994	0.092
	MS_T-AB	0.011	0.950	0.054	0.016	0.993	3.98	0.075	0.969	0.373	0.036	0.696	0.994	0.047
	MS_{BT}-AB	0.010	0.959	0.159	0.012	0.993	2.50	0.061	0.966	0.694	0.027	0.720	0.996	0.102
Gastric phase (with digestive enzyme)	AB	0.013	0.794	0.916	0.020	0.919	14.2	0.086	0.933	0.316	0.072	0.548	0.935	0.275
	S-AB	0.012	0.854	0.169	0.018	0.949	11.8	0.081	0.953	0.416	0.057	0.594	0.960	0.052
	MS_B-AB	0.012	0.882	0.267	0.019	0.959	9.74	0.082	0.937	0.194	0.046	0.654	0.956	0.021
	MS_T-AB	0.013	0.784	0.063	0.022	0.885	1.56	0.091	0.902	0.373	0.068	0.576	0.907	0.063
	MS_{BT}-AB	0.013	0.630	0.066	0.021	0.820	0.631	0.087	0.894	0.195	0.111	0.435	0.899	0.064
Small intestinal phase	AB	0.016	0.865	115	0.026	0.935	34.8	0.097	0.912	28.6	0.056	0.656	0.928	19.2
	S-AB	0.019	0.870	91.3	0.033	0.928	20.6	0.114	0.915	11.4	0.066	0.658	0.932	11.4
	MS_B-AB	0.020	0.865	69.8	0.029	0.929	14.9	0.104	0.910	4.93	0.060	0.660	0.927	4.70
	MS_T-AB	0.011	0.727	16.2	0.017	0.837	58.9	0.076	0.894	66.0	0.071	0.517	0.894	4.22
	MS_{BT}-AB	0.019	0.574	3.32	0.035	0.831	20.5	0.114	0.875	7.31	0.191	0.350	0.896	2.75

[a] Sum of squares calculated using GraphPad Prism 6 (GraphPad Software Inc).

4. Conclusion

The presented sustainable encapsulation system developed for hydrogels of modified starch and alginate was shown to enable retention of curcumin under *in vitro* simulated GIT conditions. Transglycosylation by BE and 4αGT modified the NMS to MSs containing super-branched amylopectin, characterized by higher amounts of α-1,6-branch points and longer branch chains, increasing the starch hydrogel strength and contents of slowly digested starch (SDS) and resistant starch (RS). Curcumin encapsulation efficiency, UV stability, and retention of curcumin were improved by the presence of starches in alginate beads (ABs). Especially for MS_{BT}-AB, containing the super-branched amylopectin, the resistant to digestion in a simulated GIT according to the kinetics of the model indicated primarily release *via* Fickian diffusion and not *via* network erosion and bead swelling. A significantly higher content of curcumin was retained (70.2 %) at a lower starch concentration (3 %) than in related encapsulations. Besides, the cryo-SEM images proved that the smaller pore size correlated with the highest curcumin encapsulation rate for MS_{BT}-AB. Our findings provide proof-of-concept for this new starch-alginate encapsulation system using a modest starch load having potential to become a valuable tool for controlled delivery and protection of functional bioactive and ingredients such as drugs, vitamins, antioxidants, probiotics, and flavors *e.g.* in soft capsules to benefit end users.

Abbreviations

4αGT	4-α-glucanotransferase
BE	branching enzyme
MS_B-AB	curcumin-loaded MS_B alginate beads
MS_{BT}-AB	curcumin-loaded MS_{BT} alginate beads
AB	curcumin-loaded alginate beads
S-AB	curcumin-loaded NMS alginate beads
MS_T-AB	curcumin-loaded MS_T alginate beads
GIT	gastrointestinal tract
MS_B	NMS modified by BE
MS_T	NMS modified by 4αGT
MS_{BT}	NMS sequentially modified by branching enzyme followed by 4-α-glucanotransferase
NMS	normal maize starch
RDS	rapidly digested starch
RS	resistant starch
SDS	slowly digested starch
SGF	simulated gastric fluid
SIF	simulated intestinal fluid
SS	sum of squares
SSF	simulated salivary fluid

CRediT authorship contribution statement

Yu Wang designed and performed the experiments, collected the data, and drafted the manuscript.

Chengfang Pang, Marie Sofie Møller and Birte Svensson developed the theoretical framework and edited the manuscript.

Hossein Mohammad-Beigi collected cryo-SEM data and analyzed the *in vitro* digestion model.

Marie Karen Tracy Hong Lin assisted with cryo-SEM.

Xiaoxiao Li, Yazhen Wu and Yuxiang Bai analyzed starch structure.

All authors contributed to the editing and approved the final version of the manuscript.

Declaration of competing interest

The authors declare that they have no competing interests.

Data availability

Data will be made available on request.

Acknowledgements

Karina Jansen (Department of Biotechnology and Biomedicine, Technical University of Denmark) is gratefully thanked for technical assistance. We are grateful to Andreas Blennow (Department of Plant and Environmental Sciences, University of Copenhagen) for providing NMS and BE. This work was supported by a China Scholarship Council (CSC) grant #202006790033 (to Y. Wang), Technical University of Denmark, National Natural Science Foundation of China (No. 32072268) and Fundamental Research Funds for the Central Universities (JUSRP2050205). We are thankful to Archer Daniels Midland (ADM, Decatur, IL) for normal maize starch.

Appendix A. Supplementary data

Supplementary data to this article can be found online at https://doi.org/10.1016/j.carbpol.2023.121387.

References

Aboudiab, B., Tehrani-Bagha, A. R., & Patra, D. (2020). Curcumin degradation kinetics in micellar solutions: Enhanced stability in the presence of cationic surfactants. *Colloids and Surfaces A: Physicochemical and Engineering Aspects, 592*, 124602. https://doi.org/10.1016/j.colsurfa.2020.124602

Ao, Z., Simsek, S., Zhang, G., Venkatachalam, M., Reuhs, B. L., & Hamaker, B. R. (2007). Starch with a slow digestion property produced by altering its chain length, branch density, and crystalline structure. *Journal of Agricultural and Food Chemistry, 55*(11), 4540–4547. https://pubs.acs.org/doi/10.1021/jf063123x.

Araiza-Calahorra, A., Akhtar, M., & Sarkar, A. (2018). Recent advances in emulsion-based delivery approaches for curcumin: From encapsulation to bioaccessibility. *Trends in Food Science & Technology, 71*, 155–169. https://doi.org/10.1016/J.TIFS.2017.11.009

Bai, Y., van der Kaaij, R. M., Leemhuis, H., Pijning, T., van Leeuwen, S. S., Jin, Z., & Dijkhuizen, L. (2015). Biochemical characterization of the *Lactobacillus reuteri* glycoside hydrolase family 70 GTFB type of 4,6-α-glucanotransferase enzymes that synthesize soluble dietary starch fibers. *Applied and Environmental Microbiology, 81*(20), 7223–7232. https://doi.org/10.1128/AEM.01860-15

Balasubramanian, R., Kim, S. S., & Lee, J. (2018). Novel synergistic transparent κ-carrageenan/xanthan gum/gellan gum hydrogel film: Mechanical, thermal and water barrier properties. *International Journal of Biological Macromolecules, 118*, 561–568. https://doi.org/10.1016/j.ijbiomac.2018.06.110

Ban, X., Dhoble, A. S., Li, C., Gu, Z., Hong, Y., Cheng, L., … Li, Z. (2020). Bacterial 1,4-α-glucan branching enzymes: Characteristics, preparation and commercial applications. *Critical Reviews in Biotechnology, 40*(3), 380–396. https://doi.org/10.1080/07388551.2020.1713720

Barkoula, N. M., Alcock, B., Cabrera, N. O., & Peijs, T. (2008). Flame-retardancy properties of intumescent ammonium poly(phosphate) and mineral filler magnesium hydroxide in combination with graphene. *Polymers, 16*(2), 101–113. https://doi.org/10.1002/pc

Bergeron, N., Williams, P. T., Lamendella, R., Faghihnia, N., Grube, A., Li, X., … Krauss, R. M. (2016). Diets high in resistant starch increase plasma levels of trimethylamine-N-oxide, a gut microbiome metabolite associated with CVD risk. *British Journal of Nutrition, 116*(12), 2020–2029. https://doi.org/10.1017/S0007114516004165

Brodkorb, A., Egger, L., Alminger, M., Alvito, P., Assunção, R., Ballance, S., Bohn, T., Bourlieu-Lacanal, C., Boutrou, R., Carrière, F., Clemente, A., Corredig, M., Dupont, D., Dufour, C., Edwards, C., Golding, M., Karakaya, S., Kirkhus, B., Le Feunteun, S., … Recio, I. (2019). INFOGEST static in vitro simulation of gastrointestinal food digestion. *Nature Protocols, 14*(4), 991–1014. https://doi.org/10.1038/s41596-018-0119-1

Bruschi, M. L. (2015). *Strategies to modify the drug release from pharmaceutical systems*. Woodhead Publishing. https://doi.org/10.1016/B978-0-08-100092-2.00006-0

Bu, X., Guan, M., Dai, L., Ji, N., Qin, Y., Xu, X., & Xiong, L. (2023). Fabrication of starch-based emulsion gel beads by an inverse gelation technique for loading proanthocyanidin and curcumin. *Food Hydrocolloids, 137*, 108336. https://doi.org/10.1016/j.foodhyd.2022.108336

Chen, S., Qin, L., Chen, T., Yu, Q., Chen, Y., Xiao, W., Ji, X., & Xie, J. (2022). Modification of starch by polysaccharides in pasting, rheology, texture and in vitro digestion: A review. *International Journal of Biological Macromolecules, 207*, 81–89. https://doi.org/10.1016/j.ijbiomac.2022.02.170

Chen, Y., Song, H., Huang, K., & Guan, X. (2021). Novel porous starch/alginate hydrogels for controlled insulin release with dual response to pH and amylase. *Food & Function, 12*(19), 9165–9177. https://doi.org/10.1039/D1FO01411K

Chi, C., Li, X., Huang, S., Chen, L., Zhang, Y., Li, L., & Miao, S. (2021). Basic principles in starch multi-scale structuration to mitigate digestibility: A review. *Trends in Food Science and Technology, 109*, 154–168. https://doi.org/10.1016/j.tifs.2021.01.024

Cong, Z., Shi, Y., Wang, Y., Wang, Y., Niu, J., Chen, N., & Xue, H. (2018). A novel controlled drug delivery system based on alginate hydrogel/chitosan micelle composites. *International Journal of Biological Macromolecules, 107*(PartA), 855–864. https://doi.org/10.1016/j.ijbiomac.2017.09.065

Ehtezazi, T., Washington, C., & Melia, C. D. (2000). First order release rate from porous PLA microspheres with limited exit holes on the exterior surface. *Journal of Controlled Release, 66*(1), 27–38. https://doi.org/10.1016/S0168-3659(99)00255-2

Englyst, H. N., Kingman, S. M., & Cummings, J. H. (1992). Classification and measurement of nutritionally important starch fractions. *European Journal of Clinical Nutrition, 46*, S33–S50.

Gu, Z., Chen, B., & Tian, Y. (2021). Highly branched corn starch: Preparation, encapsulation, and release of ascorbic acid. *Food Chemistry, 343*, 128485. https://doi.org/10.1016/j.foodchem.2020.128485

Guedes Silva, K. C., Feltre, G., Dupas Hubinger, M., & Kawazoe Sato, A. C. (2021). Protection and targeted delivery of β-carotene by starch-alginate-gelatin emulsion-filled hydrogels. *Journal of Food Engineering, 290*, 110205. https://doi.org/10.1016/J.JFOODENG.2020.110205

Han, S., Choi, S.-H., Kim, W., Kim, B.-Y., & Baik, M.-Y. (2015). Infusion of catechin into native corn starch granules for drug and nutrient delivery systems. *Food Science and Biotechnology, 24*, 2035–2040. https://doi.org/10.1007/s10068-015-0270-1

Higuchi, T. (1963). Mechanism of sustained-action medication. Theoretical analysis of rate of release of solid drugs dispersed in solid matrices. *Journal of Pharmaceutical Sciences, 52*(12), 1145–1149. https://doi.org/10.1002/jps.2600521210

Hosseini, S. M., Hosseini, H., Mohammadifar, M. A., German, J. B., Mortazavian, A. M., Mohammadi, A., … Khaksar, R. (2014). Preparation and characterization of alginate and alginate-resistant starch microparticles containing nisin. *Carbohydrate Polymers, 103*, 573–580. https://doi.org/10.1016/j.carbpol.2013.12.078

Huggett, A. (1957). Enzymic determination of blood glucose. *The Biochemical Journal, 66*, 12P.

Jain, S., Winuprasith, T., & Suphantharika, M. (2020). Encapsulation of lycopene in emulsions and hydrogel beads using dual modified rice starch: Characterization, stability analysis and release behaviour during in-vitro digestion. *Food Hydrocolloids, 104*, 105730. https://doi.org/10.1016/j.foodhyd.2020.105730

Jiang, H., Miao, M., Ye, F., Jiang, B., & Zhang, T. (2014). Enzymatic modification of corn starch with 4-α-glucanotransferase results in increasing slow digestible and resistant starch. *International Journal of Biological Macromolecules, 65*, 208–214.

Kakutani, R., Adachi, Y., Kajiura, H., Takata, H., Ohno, N., & Kuriki, T. (2008). Stimulation of macrophage by enzymatically synthesized glycogen: The relationship between structure and biological activity. *Biocatalysis and Biotransformation, 26*(1–2), 152–160. https://doi.org/10.1080/10242420701804541

Kang, J., Kim, Y., Choi, S., Rho, S., & Kim, Y. (2021). Improving the stability and curcumin retention rate of curcumin-loaded filled hydrogel prepared using 4αGTase-treated rice starch. *Foods, 10*(1), 150. https://doi.org/10.3390/foods10010150

Koev, T. T., Harris, H. C., Kiamehr, S., Khimyak, Y. Z., & Warren, F. J. (2022). Starch hydrogels as targeted colonic drug delivery vehicles. *Carbohydrate Polymers, 289*, 119413. https://doi.org/10.1016/j.carbpol.2022.119413

Korsmeyer, R. W., Gurny, R., Doelker, E., Buri, P., & Peppas, N. A. (1983). Mechanisms of solute release from porous hydrophilic polymers. *International Journal of Pharmaceutics, 15*(1), 25–35. https://doi.org/10.1016/0378-5173(83)90064-9

Li, X., Wang, Y., Wu, J., Jin, Z., Dijkhuizen, L., Abou Hachem, M., & Bai, Y. (2023). *Thermoproteus uzoniensis* 4-α-glucanotransferase catalyzed production of a thermo-reversible potato starch gel with superior rheological properties and freeze-thaw stability. *Food Hydrocolloids, 134*, 108026. https://doi.org/10.1016/j.foodhyd.2022.108026

Li, Y., Li, C., Gu, Z., Cheng, L., Hong, Y., & Li, Z. (2019). Digestion properties of corn starch modified by α-D-glucan branching enzyme and cyclodextrin glycosyltransferase. *Food Hydrocolloids, 89*, 534–541. https://doi.org/10.1016/J.FOODHYD.2018.11.025

Li, Y. H., Wang, Y. S., Zhao, J. S., Li, Z. Y., & Chen, H. H. (2021). A pH-sensitive curcumin loaded microemulsion-filled alginate and porous starch composite gels: Characterization, in vitro release kinetics and biological activity. *International Journal of Biological Macromolecules, 182*, 1863–1873. https://doi.org/10.1016/J.IJBIOMAC.2021.05.174

Liang, Q., & Gao, Q. (2023). Effect of amylose content on the preparation for carboxymethyl starch/pullulan electrospun nanofibers and their properties as encapsulants of thymol. *Food Hydrocolloids, 136*, 108250. https://doi.org/10.1016/j.foodhyd.2022.108250

Liang, X., Chen, L., McClements, D. J., Jin, Z., & Miao, M. (2023). Polysaccharide-based hydrogels. In *Sustainable hydrogels: Synthesis, properties, and applications*. Elsevier Inc.. https://doi.org/10.1016/B978-0-323-91753-7.00003-X

López-Córdoba, A., Deladino, L., & Martino, M. (2013). Effect of starch filler on calcium-alginate hydrogels loaded with yerba mate antioxidants. *Carbohydrate Polymers, 95*(1), 315–323. https://doi.org/10.1016/J.CARBPOL.2013.03.019

López-Córdoba, A., Deladino, L., & Martino, M. (2014). Release of yerba mate antioxidants from corn starch-alginate capsules as affected by structure. *Carbohydrate Polymers, 99*, 150–157. https://doi.org/10.1016/j.carbpol.2013.08.026

Lozano-Vazquez, G., Lobato-Calleros, C., Escalona-Buendia, H., Chavez, G., Alvarez-Ramirez, J., & Vernon-Carter, E. J. (2015). Effect of the weight ratio of alginate-modified tapioca starch on the physicochemical properties and release kinetics of chlorogenic acid containing beads. *Food Hydrocolloids, 48*, 301–311. https://doi.org/10.1016/j.foodhyd.2015.02.032

Lu, Y., Zhang, Y., Yuan, F., Gao, Y., & Mao, L. (2021). Eco-friendly synthesis of hydrogels from starch, citric acid, and itaconic acid: Swelling capacity and metal chelation properties. *Food Hydrocolloids, 116*, 106637. https://doi.org/10.1016/J.FOODHYD.2021.106637

Ma, P., Zeng, Q., Tai, K., He, X., Yao, Y., Hong, X., & Yuan, F. (2017). Preparation of curcumin-loaded emulsion using high pressure homogenization: Impact of oil phase and concentration on physicochemical stability. *LWT, 84*, 34–46. https://doi.org/10.1016/J.LWT.2017.04.074

Malakar, J., Nayak, A. K., & Das, A. (2013). Modified starch (cationized)-alginate beads containing aceclofenac: Formulation optimization using central composite design. *Starch/Staerke, 65*(7–8), 603–612. https://doi.org/10.1002/star.201200231

Manzoor, A., Dar, A. H., Pandey, V. K., Shams, R., Khan, S., Panesar, P. S., … Khan, S. A. (2022). Recent insights into polysaccharide-based hydrogels and their potential applications in food sector: A review. *International Journal of Biological Macromolecules, 213*, 987–1006.

Marefati, A., Sjöö, M., Timgren, A., Dejmek, P., & Rayner, M. (2015). Fabrication of encapsulated oil powders from starch granule stabilized W/O/W Pickering emulsions by freeze-drying. *Food Hydrocolloids, 51*, 261–271. https://doi.org/10.1016/j.foodhyd.2015.04.022

Merta, J., Torkkeli, M., Ikonen, T., Serimaa, R., & Stenius, P. (2001). Structure of cationic starch (CS)/anionic surfactant complexes studied by small-angle X-ray scattering (SAXS). *Macromolecules, 34*(9), 2937–2946. https://doi.org/10.1021/ma001793c

Mun, S., Kim, Y.-R., & McClements, D. J. (2015). Control of β-carotene bioaccessibility using starch-based filled hydrogels. *Food Chemistry, 173*, 454–461. https://doi.org/10.1016/j.foodchem.2014.10.053

Park, H. R., Rho, S. J., & Kim, Y. R. (2019). Solubility, stability, and bioaccessibility improvement of curcumin encapsulated using 4-α-glucanotransferase-modified rice starch with reversible pH-induced aggregation property. *Food Hydrocolloids, 95*, 19–32. https://doi.org/10.1016/j.foodhyd.2019.04.012

Park, I., Kim, Y. K., Kim, B. H., & Moon, T. W. (2014). Encapsulated amylosucrase-treated starch with enhanced thermal stability: Preparation and susceptibility to digestion. *Starch/Staerke, 66*(1–2), 216–224. https://doi.org/10.1002/star.201300055

Piovesan, D., Minervini, G., & Tosatto, S. C. E. (2016). The RING 2.0 web server for high quality residue interaction networks. *Nucleic Acids Research, 44*(1), W367–W374. https://doi.org/10.1093/nar/gkw315

Ramírez, C., Millon, C., Nuñez, H., Pinto, M., Valencia, P., Acevedo, C., & Simpson, R. (2015). Study of effect of sodium alginate on potato starch digestibility during invitro digestion. *Food Hydrocolloids, 44*, 328–332. https://doi.org/10.1016/j.foodhyd.2014.08.023

Ritger, P. L., & Peppas, N. A. (1987). A simple equation for description of solute release II. Fickian and anomalous release from swellable devices. *Journal of Controlled Release, 5*(1), 37–42. https://doi.org/10.1016/0168-3659(87)90035-6

Selvam, C., Prabu, S. L., Jordan, B. C., Purushothaman, Y., Umamaheswari, A., Zare, M. S. H., & Thilagavathi, R. (2019). Molecular mechanisms of curcumin and its analogs in colon cancer prevention and treatment. *Life Sciences, 239*, 117032.

Sharma, A., Mittal, A., Puri, V., Kumar, P., & Singh, I. (2020). Curcumin-loaded, alginate–gelatin composite fibers for wound healing applications. *3 Biotech, 10*(11), 1–13. https://doi.org/10.1007/s13205-020-02453-5

Singh, B., Sharma, D. K., & Gupta, A. (2009). A study towards release dynamics of thiram fungicide from starch-alginate beads to control environmental and health hazards. *Journal of Hazardous Materials, 161*(1), 208–216. https://doi.org/10.1016/j.jhazmat.2008.03.074

Sorndech, W., Sagnelli, D., Meier, S., Jansson, A. M., Lee, B. H., Hamaker, B. R., … Blennow, A. (2016). Structure of branching enzyme- and amylomaltase modified starch produced from well-defined amylose to amylopectin substrates. *Carbohydrate Polymers, 152*, 51–61. https://doi.org/10.1016/j.carbpol.2016.06.097

Sripetthong, S., Eze, F. N., Sajomsang, W., & Ovatlarnporn, C. (2023). Development of pH-responsive N-benzyl-N-O-succinyl chitosan micelles loaded with a curcumin analog (cyqualone) for treatment of colon cancer. *Molecules, 28*(6), 2693. https://doi.org/10.3390/molecules28062693

Sun, L., Wang, Y., & Miao, M. (2020). Inhibition of α-amylase by polyphenolic compounds: Substrate digestion, binding interactions and nutritional intervention. *Trends in Food Science and Technology, 104*, 190–207. https://doi.org/10.1016/J.TIFS.2020.08.003

Tashiro, A., Hasegawa, A., Kohyama, K., Kumagai, H., & Kumagai, H. (2010). Relationship between the rheological properties of thickener solutions and their velocity through the pharynx as measured by the ultrasonic pulse Doppler method. *Bioscience, Biotechnology, and Biochemistry, 74*(8), 1598–1605. https://doi.org/10.1271/bbb.100192

Tetlow, I. J., & Emes, M. J. (2014). A review of starch-branching enzymes and their role in amylopectin biosynthesis. *IUBMB Life, 66*(8), 546–558. https://doi.org/10.1002/iub.1297

Tian, Y., Li, M., Liu, X., Jane, J. L., Guo, B., & Dhital, S. (2021). Storage temperature and time affect the enzyme resistance starch and glycemic response of cooked noodles. *Food Chemistry, 344*, 128702. https://doi.org/10.1016/J.FOODCHEM.2020.128702

Vernon-Carter, E. J., Alvarez-Ramirez, J., Bello-Perez, L. A., Garcia-Hernandez, A., Roldan-Cruz, C., & Garcia-Diaz, S. (2018). *In vitro* digestibility of normal and waxy corn starch is modified by the addition of Tween 80. *International Journal of Biological Macromolecules, 116*, 715–720. https://doi.org/10.1016/j.ijbiomac.2018.05.076

Wang, P., Luo, Z., & Xiao, Z. (2021). Preparation, physicochemical characterization and in vitro release behavior of resveratrol-loaded oxidized gellan gum/resistant starch hydrogel beads. *Carbohydrate Polymers, 260*, 117794. https://doi.org/10.1016/J.CARBPOL.2021.117794

Wang, Y., Li, X., Ji, H., Zheng, D., Jin, Z., Bai, Y., & Svensson, B. (2020). Thermophilic 4-α-glucanotransferase from *Thermoproteus uzoniensis* retards the long-term retrogradation but maintains the short-term gelation strength of tapioca starch. *Journal of Agricultural and Food Chemistry, 68*(20), 5658–5667. https://doi.org/10.1021/acs.jafc.0c00927

Wang, Y., Wu, Y., Christensen, S. J., Janeček, Š., Bai, Y., Møller, M. S., & Svensson, B. (2023). Impact of starch binding domain fusion on activities and starch product structure of 4-α-glucanotransferase. *Molecules, 23*, 1320. https://doi.org/10.3390/molecules28031320

Xing, Y., Xu, Q., Ma, Y., Che, Z., Cai, Y., & Jiang, L. (2014). Effect of porous starch concentrations on the microbiological characteristics of microencapsulated *Lactobacillus acidophilus*. *Food & Function, 5*(5), 972–983. https://doi.org/10.1039/C3FO60438A

Xue, N., Wang, Y., Li, X., & Bai, Y. (2022). Enzymatic synthesis, structure of isomalto/malto-polysaccharides from linear dextrins prepared by retrogradation. *Carbohydrate Polymers, 288*, 119350. https://doi.org/10.1016/j.carbpol.2022.119350

Yu, C., Tang, X., Liu, S., Yang, Y., Shen, X., & Gao, C. (2018). Laponite crosslinked starch/polyvinyl alcohol hydrogels by freezing/thawing process and studying their cadmium ion absorption. *International Journal of Biological Macromolecules, 117*, 1–6.

Yu, M., Liu, B., Zhong, F., Wan, Q., Zhu, S., Huang, D., & Li, Y. (2021). Interactions between caffeic acid and corn starch with varying amylose content and their effects on starch digestion. *Food Hydrocolloids, 114*, 106544. https://doi.org/10.1016/J.FOODHYD.2020.106544

Zhao, X., & Wang, Z. (2019). A pH-sensitive microemulsion-filled gellan gum hydrogel encapsulated apigenin: Characterization and in vitro release kinetics. *Colloids and Surfaces B: Biointerfaces, 178*, 245–252. https://doi.org/10.1016/j.colsurfb.2019.03.015

Zhu, F. (2017). Encapsulation and delivery of food ingredients using starch based systems. *Food Chemistry, 229*, 542–552. https://doi.org/10.1016/j.foodchem.2017.02.101

Supporting Information

Sequential starch modification by branching enzyme and 4-α-glucanotransferase improves retention of curcumin in starch-alginate beads

Yu Wang [a, 1], Chengfang Pang [b, 1], Hossein Mohammad-Beigi [a], Xiaoxiao Li [c], Yazhen Wu [c], Marie Karen Tracy Hong Lin [d], Yuxiang Bai [c], Marie Sofie Møller [e, *], Birte Svensson [a, *]

[a] Enzyme and Protein Chemistry, Department of Biotechnology and Biomedicine, Technical University of Denmark, DK-2800, Kgs. Lyngby, Denmark

[b] Research Group for Genomic Epidemiology, National Food Institute, Technical University of Denmark, DK-2800 Kongens Lyngby, Denmark

[c] School of Food Science and Technology, Jiangnan University, Wuxi, Jiangsu, 214122, China

[d] National Center for Nanofabrication and Characterization, Technical University of Denmark, Kgs. Lyngby, DK-2800, Denmark

[e] Applied Molecular Enzyme Chemistry, Department of Biotechnology and Biomedicine, Technical University of Denmark, DK-2800, Kgs. Lyngby, Denmark

[1] These authors contributed equally to this work.

[*] Corresponding authors:

Marie Sofie Møller: msmo@dtu.dk

Birte Svensson: bis@bio.dtu.dk

Experimental section

1.1. Standard activity assays

The activity of branching enzyme (BE, *Rhodothermus obamensis*, Novozymes) was determined as reported (Van Der Maarel et al., 2003) by incubating 1 mg/mL amylose type III (Sigma-Aldrich) in 900 µL 50 mM MES, 150 mM NaCl, pH 6.0 with 100 µL BE (final concentration: 0.01 mg/mL) at 60 °C for 10 min, followed by heating (99 °C, 15 min) to stop the reaction. Aliquots (20 µL) were mixed with 200 µL iodine reagent (0.001 g I_2, 0.01 g KI in 10 mL MilliQ water), and the absorbance at 530 nm was measured. One unit of enzyme activity was defined as the amount of BE that decreased A_{530} by 1% per min.

The activity of *Thermoproteus uzoniensis* 4αGT was determined as reported by incubating 1 mg/mL maltotriose in 900 µL 50 mM MES, 150 mM NaCl, pH 6.0 with 100 µL 4αGT (final concentration: 20 nM) at 75°C for 1 h (Wang et al., 2020). The rate of glucose released was determined using the GOPOD assay (D-Glucose Assay Kit, Megazyme) and glucose as standard. One unit of disproportionation activity was defined as the amount of 4αGT releasing 1 µmol of glucose per min under the above conditions.

1.2. Preparation of curcumin-loaded emulsion (CE)

The oil phase was made by adding curcumin in sunflower oil (1–20%, v/v) and emulsifier (Tween 80, 0.5–20%, v/v) to MilliQ water, heated (60 °C, 10 min) for complete dissolution of curcumin and sonicated (Ultra Sonicator, QSonica, LLC, USA) for 0.5–5 min with different amplitudes, 30 or 40%. The resulting emulsion was centrifuged (1300 *g*, 30 min). Curcumin in the emulsion was quantified spectrophotometrically at 425 nm at room temperature after 100-fold dilution with 95% ethanol using curcumin (0.005–0.02 mg/mL) in 95% ethanol as standard. The encapsulation rate was calculated according to eq. 1, where V_0 and C_0 is the initial volume and concentration of curcumin, and V_1 and C_1 is the volume and concentration of un-encapsulated curcumin.

$$\text{Encapsulation rate (\%)} = \frac{V_0 \times C_0 - V_1 \times C_1}{V_0 \times C_0} \times 100 \quad (1)$$

Optimization by varying oil content, surfactant content, sonication power and time resulted in highest encapsulation efficiency using 10% oil (Fig. S2A), 4% Tween-80 (Fig. S2B), and sonication at 40% amplitude (Fig. S2C) for 2 min (Fig. S2D).

1.3. In vitro digestion of CS-ABs

A simulated gastrointestinal tract (GIT) model consisting of oral, gastric and intestinal phases was used to evaluate the release rate of encapsulated curcumin during *in vitro* digestion as described in INFOGEST with slight modification (Brodkorb et al., 2019).

Simulated saliva fluid (SSF) was prepared by dissolving KCl (final concentration: 15.1 mM), KH_2PO_4 (3.7 mM), $NaHCO_3$ (13.6 mM), $MgCl_2(H_2O)_6$ (0.15 mM), $(NH_4)_2CO_3$ (0.06 mM), HCl (1.1 mM), $CaCl_2(H_2O)_2$ (1.5 mM) in 100 mL MilliQ water, followed by pH adjusting to 7.0.

Simulated gastric fluid (SGF) was prepared by dissolving KCl (6.9 mM), KH_2PO_4 (0.9 mM), $NaHCO_3$ (25 mM), NaCl (47.2 mM), $MgCl_2(H_2O)_6$ (0.12 mM), $(NH_4)_2CO_3$ (0.5 mM), HCl (15.6 mM) and $CaCl_2(H_2O)_2$ (0.15 mM) in MilliQ water and the pH was adjusted to 3.0 using HCl (1 M). Before starting the experiment, 640 mg pepsin was dissolved in 200 mL of SGF and preheated (37 °C, 10 min).

Simulated intestinal fluid (SIF) was prepared by dissolving KCl (6.8 mM), KH_2PO_4 (0.8 mM), $NaHCO_3$ (85 mM), NaCl (38.4 mM), $MgCl_2(H_2O)_6$ (0.33 mM), HCl (8.4 mM) and $CaCl_2(H_2O)_2$ (0.6 mM) in MilliQ water and pH was adjusted to 7.0.

Supplementary figures

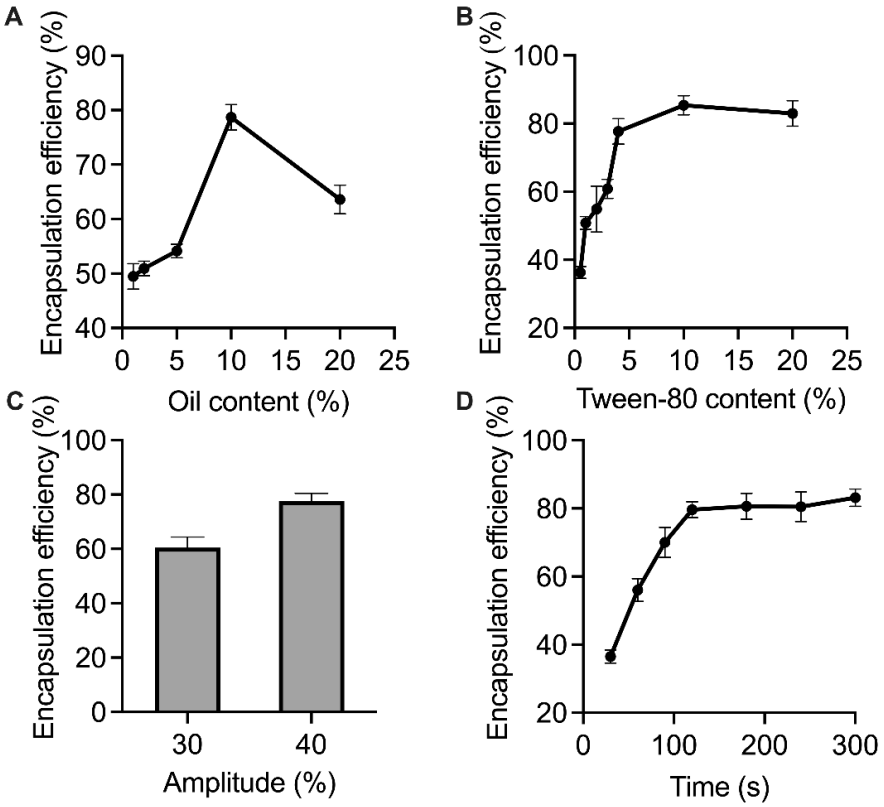

Fig. S1. Preparation of curcumin-loaded emulsion. Influence on the preparation of curcumin loaded emulsion of (A) sunflower oil content, (B) Tween-80 content, (C) sonication amplitude, and (D) sonication time at 40% amplitude.

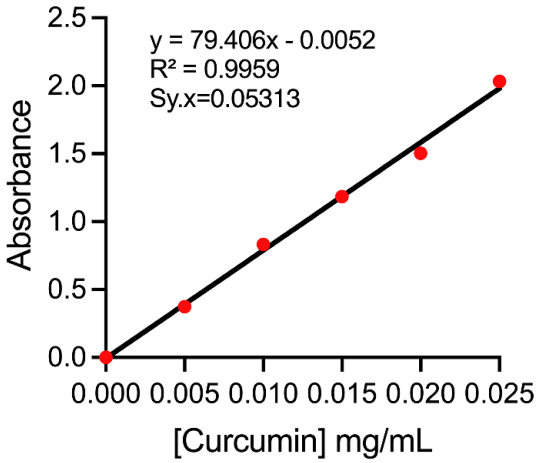

Fig. S2. The resulting standard curve for curcumin dissolved in acetone generated by plotting the absorbance *vs* concentration of curcumin. Red circles represent the data and the line the best linear fit. The slope, intercept, R^2, and standard deviation of the residuals (Sy.x) were calculated using GraphPad Prism 6 (GraphPad Software Inc).

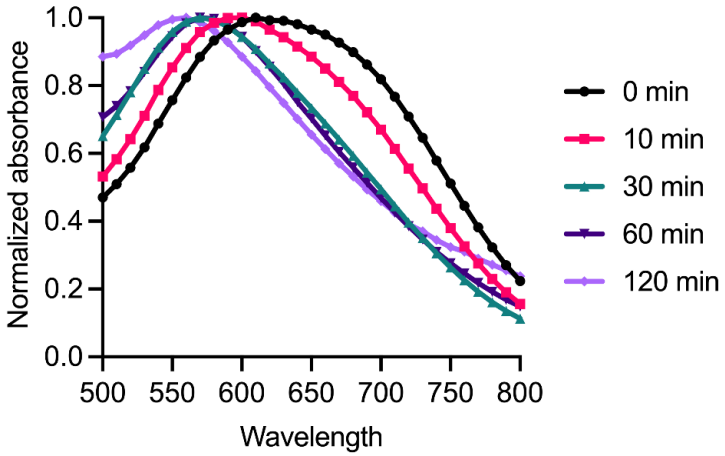

Fig. S3. Spectra of iodine complexes of starch modified by BE for different reaction times.

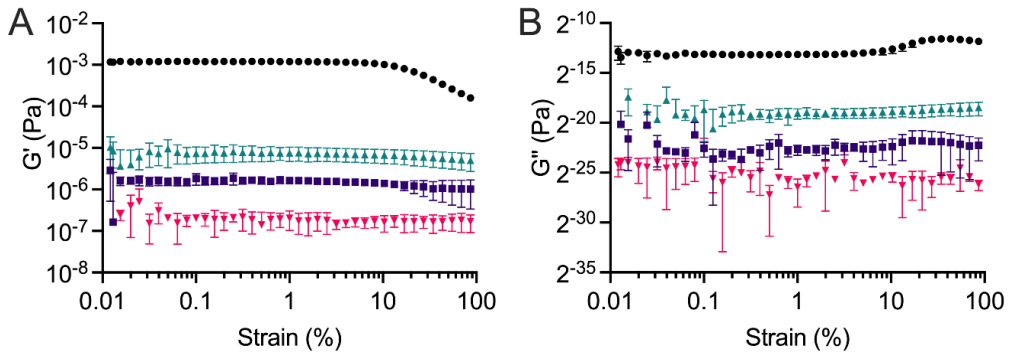

Fig. S4. Rheological properties of NMS modified by BE and 4αGT. Strain-dependence of (A) G' and (B) G'' for NMS (black) and MS_B (red), MS_T (green) and MS_{BT} (purple).

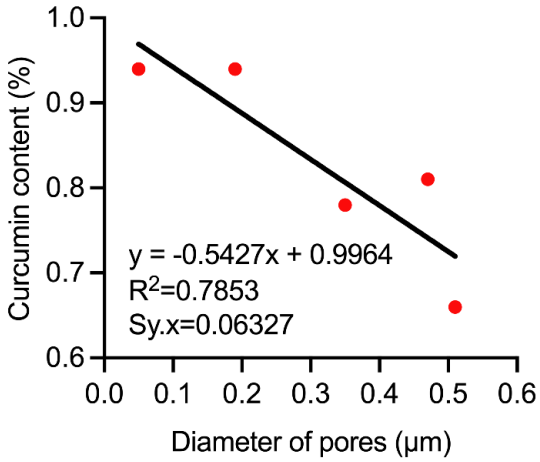

Fig. S5. Relationship between pore diameter and curcumin content of different ABs. Red circles represent the data (Table 1) and the line the best linear fit. The slope, intercept, R^2, and standard deviation of the residuals (Sy.x) were calculated using GraphPad Prism 6 (GraphPad Software Inc).

References

Brodkorb, A., Egger, L., Alminger, M., Alvito, P., Assunção, R., Ballance, S., Bohn, T., Bourlieu-Lacanal, C., Boutrou, R., Carrière, F., Clemente, A., Corredig, M., Dupont, D., Dufour, C., Edwards, C., Golding, M., Karakaya, S., Kirkhus, B., Le Feunteun, S., … Recio, I. (2019). INFOGEST static in vitro simulation of gastrointestinal food digestion. *Nature Protocols*, *14*(4), 991–1014. https://doi.org/10.1038/s41596-018-0119-1

Van Der Maarel, M., Vos, A., Sanders, P., & Dijkhuizen, L. (2003). Properties of the glucan branching enzyme of the hyperthermophilic bacterium *Aquifex aeolicus*. *Biocatalysis and Biotransformation*, *21*(4–5), 199–207. https://doi.org/https://doi.org/10.1080/10242420310001618528

Wang, Y., Li, X., Ji, H., Zheng, D., Jin, Z., Bai, Y., & Svensson, B. (2020). Thermophilic 4-α-glucanotransferase from *Thermoproteus uzoniensis* retards the long-term retrogradation but maintains the short-term gelation strength of tapioca starch. *Journal of Agricultural and Food Chemistry*, *68*(20), 5658–5667. https://doi.org/10.1021/acs.jafc.0c00927

Chapter 3: Discussion

Enzymatic conversion of starch by enzymes is relatively well understood. However, most knowledge is about enzymatic modification and degradation of gelatinized starch, and few studies report on the conversion of granular starch. In this thesis, we aimed to study the effect of starch binding domains (SBDs) on different starch-active enzymes (***Paper 1***, ***Paper 2***, and ***Manuscript 1***) with special focus on the interfacial catalysis of starch granules (***Paper 1***, ***Paper 3***, and ***Manuscript 1***). Different from analyzing the catalytic process for different enzymes, we also aimed to investigate the modification of starch using different enzymes, and the applications of these modified starches in encapsulation of bioactive compounds (***Paper 4***, and ***Manuscript 2***). The discussion will be divided into two sections.

Impact of SBDs on the starch-active enzymes

In ***Paper 1***, the fusion of SBDs to the α-amylase AHA demonstrated enhanced affinity towards granular starches, evidenced by reduced K_d and increased binding and attack site densities. While SBD-fusion improved the ability of enzymes to recognize attack sites, especially for high-amylose substrates, there was a greater population of adsorbed, but unproductive enzyme molecules in the fusions. This suggests that while SBDs aid in enzyme accumulation on granules and forming enzyme-substrate complexes, they do not always result in successful catalytic action. It is posited that while the CD interacts preferably with specific attack sites, SBDs might bind to non-productive sites. Such observations mirror results seen in cellulose degradation by certain cellobiohydrolases [6]. Comparatively, while AHA-SBD fusions showed enhanced activity on A- and B-type starches, a slight reduction in activity for soluble amylose was observed, potentially due to competition between SBDs and the active site for the substrate.

To further study the importance of SBDs in interfacial catalysis of granular starches by starch-active enzymes, the pullulanase *La*Pul was N-terminally truncated to remove CBM41 (Δ41-*La*Pul) or CBM41 and two DUFs (Δ(41+DUFs)-*La*Pul) (***Manuscript 1***). The truncation of CBM41 transitioned *La*Pul from a dimer to a monomer in solution, paralleling the behavior seen for a Thermus maltogenic amylase. CBM41, recognized for binding with α-glucans, stabilizes enzymes and enhances substrate affinity. Indeed, when CBM41 was removed from *La*Pul, there was an increase in K_M for soluble substrates, indicating reduced affinity. Interestingly, the removal also resulted in a boosted k_{cat}, showcasing a behavior termed as desorption limited reactions per the Sabatier principle. On starch granules, reactions were adsorption limited, highlighting substrate differences: soluble glucans are more flexible than the branches on starch granules. In examining DUFs, while not always functionally verified, they are crucial for the conformational stability. *La*Pul without CBM41 and DUFs regained

substrate affinity, possibly due to the truncation exposed certain aromatic residues, enhancing its interaction with substrates.

Given that type I pullulanase specifically targets α-1,6-linkages, the attack site density observed in the interfacial kinetics of granular starches using *La*Pul motivated us to employ the interfacial kinetic method to quantify α-1,6- branch points by using *Bl*Pul for hydrolysis (***Paper 3***). This new method was validated on starch granules pretreated by either *Ro*BE, or TuαGT. The $^{kin}\Gamma_{max}$ parameter, representing the density of accessible branch points, showed that WMS granules had denser branching than NMS. The CLD results, and 1.9- and 2.3-fold higher $^{kin}\Gamma_{max}$ for *Ro*BE-modified WMS and NMS granules indicated that RoBE importantly increased the number of short chains on starch granule surfaces. Surprisingly, the CLD results indicated that TuαGT did not elongate the chains on the surface of the starch granules, but rather catalyzed hydrolysis and / or cyclization, causing branch chain shortening. Despite enzymatic modification by either *Ro*BE or TuαGT, and before or after *Bl*Pul hydrolysis, the starch granule surfaces remained intact as seen by SEM imaging, supporting the notion that most reactions occurred on the granule surface without erosion in the form of e.g. pores and channels.

For further study of effects of SBDs on glucanotransferase, three different SBDs were N-terminally fused individually to TuαGT (***Paper 2***). The fusions showed significant impact both on the enzymatic activity and binding characteristics. It is particularly noteworthy that while the optimal activity for maltotriose disproportionation was hampered, the enzyme action on polysaccharides like amylose improved by the fusion. This diverse dual behavior might be attributed to the added SBDs enhancing substrate binding, hence increasing local substrate concentration, and perhaps guiding the substrate to the active site of the enzyme. Additionally, the modifications by the TuαGT and its SBD fusions altered the structural properties of maize starch, impacting both the CLD and the molecular weight. Interestingly, variations in the α-1,6/α-1,4-linkage ratio among the modified starches provide evidence of the unique mechanisms and actions of the enzymes.

In essence, while SBD enhancement did increase affinity for starch, it produced varied enzymatic results. For instance, AHA-SBD fusions and *La*Pul demonstrated improved catalytic efficiency on granular starch compared to AHA alone and Δ41- *La*Pul, respectively, and there was an increase in the thermostability of TuαGT. However, for Δ41-*La*Pul, an excessive increase in substrate affinity negatively impacted its catalytic efficiency on soluble pullulan and amylopectin than *La*Pul.

Application of enzymatically modified starches

In ***Paper 4***, gelatinized NMS was modified using *Ro*BE and then TuαGT, and transformed into MSs having a super-branched amylopectin structure. This structure is distinguished by its increase in α-1,6-branch point, and extended branch chains, which enhance the durability of the starch hydrogel and the levels of slowly digestible starch (SDS) and resistant starch (RS). These starch hydrogels were used to co-encapsulate a curcumin-infused emulsion within alginate beads (ABs). The ABs with dual enzyme modified starch showed the largest enhancement in encapsulation efficiency, UV stability and retention of curcumin in a simulated GIT.

Apart from modifying gelatinized starch using *Ro*BE and TuαGT (***Paper 4***), we also managed to modify maize starch granules with different amylose content (WMS, NMS, and AE) using *Ro*BE and TuαGT (***Manuscript 2***). Different from the effects of modification by either *Ro*BE or TuαGT on WMS and NMS (***Paper 3***), notably, TuαGT can catalyzed disproportionation on *Ro*BE-modified starches. Together with the molecular docking, it was observed that for TuαGT to catalyze disproportionation, the acceptor chain needs to be at least of DP 4–5. When employing the interfacial kinetics approach to study the degradation of starch granules with *Bl*Pul, it became evident that *Bl*Pul exhibited varying levels of affinity to different native starch granules. This divergence in affinity resulted in significantly different catalytic behaviors. Specifically, it gave rise to situations where the catalysis of starch granules debranching was constrained either by adsorption or desorption, in accordance with the Sabatier principle.

Chapter 4: Conclusion

In conclusion, this thesis has delved into the intricate world of enzymatic conversion and modification of starch, shedding light on various aspects of this complex process. The primary focus of the research was to investigate the impact of SBDs on starch-active enzymes and their catalytic behaviors with a particular emphasis on interfacial catalysis of starch granules. Additionally, the study extended its exploration to the applications of enzymatically modified starches in cp-encapsulation with alginate of bioactive compounds.

The introduction of SBDs into starch-active enzymes, as demonstrated in ***Paper 1***, ***Paper 2***, and ***Manuscript 1***, showcased both enhanced affinity for granular starches and the potential trade-offs that come with it. While SBD-fusion improved enzyme recognition of attack sites, it also led to a greater population of adsorbed but unproductive enzyme molecules. This observation underscores the complexity of enzyme-substrate interactions and highlights the need for a nuanced understanding of their effects.

Furthermore, the research expanded its horizons by examining the interfacial catalysis of starch granules using *Bl*Pul, revealing distinct affinity patterns for different native and mofidied starch granules and resulting in markedly different catalytic behaviors (***Paper 3*** and ***Manuscript 2***). This phenomenon, in accordance with the Sabatier principle, showcased situations where catalysis was constrained either by adsorption or desorption, emphasizing the critical role of enzyme-substrate interactions in starch degradation.

In the application-oriented section of the thesis, enzymatically modified starches exhibited their potential in the encapsulation of bioactive compounds, as demonstrated in ***Paper 4***. The modification of gelatinized starches led to the creation of starch hydrogels with super-branched amylopectin structures, enhancing starch durability and the levels of slowly digestible starch and resistant starch. These hydrogels were employed to encapsulate curcumin-infused emulsions, demonstrating improved encapsulation efficiency, UV stability, and retention of curcumin in alginate beads under simulated gastrointestinal conditions.

In essence, this comprehensive exploration of starch enzymatic conversion, modification, and application has provided valuable and new insights into the intricate world of enzymatic interactions with starch substrates. It underscores the importance of considering the nuanced effects of SBDs on enzyme behavior, the complex dynamics of interfacial catalysis on starch granules, and the potential applications of enzymatically modified starches in the field of co-encapsulation technology. These findings not only contribute to our fundamental understanding of enzymatic processes but also offer practical implications for the development of novel starch-based products with enhanced functionality and nutritional value.

Chapter 5: Future Perspectives

This thesis provided insight into interfacial catalysis of granular starches by different starch-active enzymes, as well as the enzymatic modification of starches and the application of these modified starches.

In ***Paper 1***, we devised AHA-SBD fusions guided by the Sabatier principle to enhance activity. Although we achieved increased affinity of AHA for the substrate, we fell short of reaching the Sabatier optimum. This leaves us uncertain whether higher affinity and activity can be achieved. Although we designed other AHA-SBD fusions aiming for further increase in affinity, none of them were produced successfully. It would be of great interest to find the optimum SBD-fusion according to Sabatier principle.

Paper 2 saw success as we improved affinity and catalytic efficiency by fusing SBDs to the N-terminus of TuαGT. This advancement was extended to starch modification with BE in ***Paper 4***. Regrettably, due to poor yield and instability of recombinant proteins, we could not use SBD-TuαGT fusions for modifying starch to be used in starch-alginate hydrogel beads. Despite minor changes in starch structure, investigating the impact of fused SBDs on TuαGT in terms of starch product structure, particularly for providing more exterior chains through BE for TuαGT extension, remains a compelling avenue.

In ***Manuscript 1***, compared to the challenges with AHA-SBD and SBD-TuαGT fusions, the NTDs truncation variants of *La*Pul exhibited promising yields. We hypothesized that the enhanced substrate affinity for ∆(41+DUFs)-*La*Pul could be attributed to the exposure of aromatic amino acids on CBM48 and CD surfaces after DUFs truncation, an unprecedented finding. This hypothesis was built on the AlphaFold2 model. For the future perspective, there are two ways to experimentally prove this hypothesis: (1) Mutate these for aromatic amino acids on the surface of CBM48 and CD and investigate the affinity between the mutatants and starch; (2) Crystallize to confirm the structure of the two truncation variants (∆41-*La*Pul and ∆(41+DUFs)-*La*Pul).

The application of interfacial kinetics approach in starch degradation by *Bl*Pul demonstrated that the modification of starch granules by glucanotransferases is a complicated process (***Paper 3*** and ***Manuscript 2***). To further investigate the modification process, future research prospects from this paper encompass: (1) understand the interaction between the *Bl*Pul and the surface of starch granules, and (2) investigate the detailed molecular structure of the surface of starch granules.

Differing from the investigation into the catalytic processes for various starch-active enzymes, ***Paper 4*** showcased the creation of super-branched amylopectin with elongated exterior

chains from NMS using BE and 4αGT. This unique starch structure found application in curcumin encapsulation within alginate hydrogel beads. Future research prospects from this paper encompass: (1) manipulating starch structure by exploring enzyme quantity, reaction time, and conditions, (2) assessing pharmacological activity of curcumin during UV treatment, in vitro digestion, and shelf storage, (3) testing the efficacy of encapsulation of different compounds.

References

1. Smith, A.M.; Zeeman, S.C. Starch: A flexible, adaptable carbon store coupled to plant growth. Annu. Rev. Plant Biol. 2020, 71, 217–245.
2. Baghurst, P.A.; Baghurst, K.I.; Record, S.J. Dietary fibre, non-starch polysaccharides and resistant starch: a review. Food Aust. 1996, 48, S3–S35.
3. Padi, R.K.; Chimphango, A.; Roskilly, A.P. Economic and environmental analysis of waste-based bioenergy integration into industrial cassava starch processes in Africa. Sustain. Prod. Consum. 2022, 31, 67–81.
4. Punia Bangar, S.; Ashogbon, A.O.; Singh, A.; Chaudhary, V.; Whiteside, W.S. Enzymatic modification of starch: A green approach for starch applications. Carbohydr. Polym. 2022, 287, 119265.
5. Tian, Y.; Wang, Y.; Zhong, Y.; Møller, M.S.; Westh, P.; Svensson, B.; Blennow, A. Interfacial catalysis during amylolytic degradation of starch granules : Current understanding and kinetic approaches. Molecules 2023, 28, 3799.
6. Kari, J.; Andersen, M.; Borch, K.; Westh, P. An inverse Michaelis-Menten approach for interfacial enzyme kinetics. ACS Catal. 2017, 7, 4904–4914.
7. Damager, I.; Engelsen, S.B.; Blennow, A.; Lindberg Møller, B.; Motawia, M.S. First principles insight into the α-glucan structures of starch: Their synthesis, conformation, and hydration. Chem. Rev. 2010, 110, 2049–2080.
8. Bertoft, E. Understanding starch structure: Recent progress. Agronomy 2017, 7, 56.
9. Spinozzi, F.; Ferrero, C.; Perez, S. The architecture of starch blocklets follows phyllotaxic rules. Sci. Rep. 2020, 10, 1–16.
10. Zhong, Y.; Li, Z.; Qu, J.; Bertoft, E.; Li, M.; Zhu, F.; Blennow, A.; Liu, X. Relationship between molecular structure and lamellar and crystalline structure of rice starch. Carbohydr. Polym. 2021, 258, 117616.
11. Nakamura, Y.; Kainuma, K. On the cluster structure of amylopectin. Plant Mol. Biol. 2022, 108, 291–306.
12. Jane, J. Current understanding on starch granule structures. J. Appl. Glycosci. 2006, 53, 205–213.
13. Jane, J.; Ao, Z.; Duvick, S.A.; Wiklund, M.; Yoo, S.-H.; Wong, K.-S.; Gardner, C. Structures of amylopectin and starch granules: How are they synthesized? J. Appl. Glycosci. 2003, 50, 167–172.
14. Alcázar-Alay, S.C.; Meireles, M.A.A. Physicochemical properties, modifications and applications of starches from different botanical sources. Food Sci. Technol. 2015, 35, 215–236.
15. Jane, J.; Kasemsuwan, T.; Leas, S.; Zobel, H.; Robyt, J.F. Anthology of starch granule morphology by scanning electron microscopy. Starch-Stärke 1994, 46, 121–129.
16. Hall, D.M.; Sayre, J.G. A scanning electron-microscope study of starches: Part III: Miscellaneous starches. Text. Res. J. 1971, 41, 880–894.
17. Pérez, S.; Bertoft, E. The molecular structures of starch components and their contribution to the architecture of starch granules: A comprehensive review. Starch/Staerke 2010, 62, 389–420.
18. French, D. Chemical and physical properties of starch. J. Anim. Sci. 1973, 37, 1048–1061.
19. Lindeboom, N.; Chang, P.R.; Tyler, R.T. Analytical, biochemical and physicochemical aspects of starch granule size, with emphasis on small granule starches: a review. Starch-Stärke 2004, 56, 89–99.
20. Jiang, H.; Campbell, M.; Blanco, M.; Jane, J.-L. Characterization of maize amylose-extender (ae) mutant starches: Part II. Structures and properties of starch residues remaining after enzymatic hydrolysis at boiling-water temperature. Carbohydr. Polym. 2010, 80, 1–12.
21. Lin, L.; Guo, D.; Zhao, L.; Zhang, X.; Wang, J.; Zhang, F.; Wei, C. Comparative structure of starches from high-amylose maize inbred lines and their hybrids. Food Hydrocoll. 2016, 52, 19–28.
22. Cai, C.; Zhao, L.; Huang, J.; Chen, Y.; Wei, C. Morphology, structure and gelatinization properties of

heterogeneous starch granules from high-amylose maize. Carbohydr. Polym. 2014, 102, 606–614.
23. Fannon, J.E.; Hauber, R.J.; BeMILLER, J.N. Surface pores of starch granules. Cereal Chem 1992, 69, 284–288.
24. Zhang, B.; Dhital, S.; Gidley, M.J. Synergistic and antagonistic effects of α-amylase and amyloglucosidase on starch digestion. Biomacromolecules 2013, 14, 1945–1954.
25. Dhital, S.; Butardo Jr, V.M.; Jobling, S.A.; Gidley, M.J. Rice starch granule amylolysis–Differentiating effects of particle size, morphology, thermal properties and crystalline polymorph. Carbohydr. Polym. 2015, 115, 305–316.
26. Huber, K.C.; BeMiller, J.N. Visualization of channels and cavities of corn and sorghum starch granules. Cereal Chem. 1997, 74, 537–541.
27. Fannon, J.E.; Gray, J.A.; Gunawan, N.; Huber, K.C.; BeMiller, J.N. Heterogeneity of starch granules and the effect of granule channelization on starch modification. Cellulose 2004, 11, 247–254.
28. Gidley, M.J.; Bociek, S.M. Molecular organization in starches: A carbon 13 CP/MAS NMR study. J. Am. Chem. Soc. 1985, 107, 7040–7044.
29. Blennow, A.; Hansen, M.; Schulz, A.; Jørgensen, K.; Donald, A.M.; Sanderson, J. The molecular deposition of transgenically modified starch in the starch granule as imaged by functional microscopy. J. Struct. Biol. 2003, 143, 229–241.
30. Tang, P.C.; Ash, J.S.; Bates, D.W.; Overhage, J.M.; Sands, D.Z. Personal health records: definitions, benefits, and strategies for overcoming barriers to adoption. J. Am. Med. Informatics Assoc. 2006, 13, 121–126.
31. Tang, H.; Mitsunaga, T.; Kawamura, Y. Molecular arrangement in blocklets and starch granule architecture. Carbohydr. Polym. 2006, 63, 555–560.
32. Baker, A.A.; Miles, M.J.; Helbert, W. Internal structure of the starch granule revealed by AFM. Carbohydr. Res. 2001, 330, 249–256.
33. Dang, J.M.C.; Copeland, L. Imaging rice grains using atomic force microscopy. J. Cereal Sci. 2003, 37, 165–170.
34. Barrera, G.N.; Calderón-Domínguez, G.; Chanona-Pérez, J.; Gutiérrez-López, G.F.; León, A.E.; Ribotta, P.D. Evaluation of the mechanical damage on wheat starch granules by SEM, ESEM, AFM and texture image analysis. Carbohydr. Polym. 2013, 98, 1449–1457.
35. Chen, L.; McClements, D.J.; Ma, Y.; Yang, T.; Ren, F.; Tian, Y.; Jin, Z. Analysis of porous structure of potato starch granules by low-field NMR cryoporometry and AFM. Int. J. Biol. Macromol. 2021, 173, 307–314.
36. Baldwin, P.M.; Davies, M.C.; Melia, C.D. Starch granule surface imaging using low-voltage scanning electron microscopy and atomic force microscopy. Int. J. Biol. Macromol. 1997, 21, 103–107.
37. Chen, L.; Ma, R.; Zhang, Z.; Huang, M.; Cai, C.; Zhang, R.; McClements, D.J.; Tian, Y.; Jin, Z. Comprehensive investigation and comparison of surface microstructure of fractionated potato starches. Food Hydrocoll. 2019, 89, 11–19.
38. Ridout, M.J.; Parker, M.L.; Hedley, C.L.; Bogracheva, T.Y.; Morris, V.J. Atomic force microscopy of pea starch granules: Granule architecture of wild-type parent, r and rb single mutants, and the rrb double mutant. Carbohydr. Res. 2003, 338, 2135–2147.
39. Hsieh, C.-F.; Liu, W.; Whaley, J.K.; Shi, Y.-C. Structure and functional properties of waxy starches. Food Hydrocoll. 2019, 94, 238–254.
40. Shi, Y.-C.; Seib, P.A. The structure of four waxy starches related to gelatinization and retrogradation. Carbohydr. Res. 1992, 227, 131–145.
41. Carciofi, M.; Blennow, A.; Jensen, S.L.; Shaik, S.S.; Henriksen, A.; Buléon, A.; Holm, P.B.; Hebelstrup,

K.H. Concerted suppression of all starch branching enzyme genes in barley produces amylose-only starch granules. BMC Plant Biol. 2012, 12, 1–16.
42. Sagnelli, D.; Chessa, S.; Mandalari, G.; Di Martino, M.; Sorndech, W.; Mamone, G.; Vincze, E.; Buillon, G.; Nielsen, D.S.; Wiese, M. Low glycaemic index foods from wild barley and amylose-only barley lines. J. Funct. Foods 2018, 40, 408–416.
43. Wang, S.; Guo, P. *Botanical Sources of Starch*; 2020; ISBN 9789811506215.
44. Jane, J.; Shen, J.J. Internal structure of the potato starch granule revealed by chemical gelatinization. Carbohydr. Res. 1993, 247, 279–290.
45. Pan, D.D.; Jane, J.-L. Internal Structure of Normal Maize Starch Granules Revealed by Chemical Surface Gelatinization. Biomacromolecules 2000, 1, 126–132.
46. Bertoft, E. Composition of clusters and their arrangement in potato amylopectin. Carbohydr. Polym. 2007, 68, 433–446.
47. Aberle, T.; Burchard, W.; Vorwerg, W.; Radosta, S. Conformational contributions of amylose and amylopectin to the structural properties of starches from various sources. Starch-Stärke 1994, 46, 329–335.
48. Lelievre, J.; Lewis, J.A.; Marsden, K. The size and shape of amylopectin: A study using analytical ultracentrifugation. Carbohydr. Res. 1986, 153, 195–203.
49. Hanashiro, I.; Abe, J.; Hizukuri, S. A periodic distribution of the chain length of amylopectin as revealed by high-performance anion-exchange chromatography. Carbohydr. Res. 1996, 283, 151–159.
50. Drula, E.; Garron, M.L.; Dogan, S.; Lombard, V.; Henrissat, B.; Terrapon, N. The carbohydrate-active enzyme database: Functions and literature. Nucleic Acids Res. 2022, 50, D571–D577.
51. Janeček, Š.; Svensson, B. How many α-amylase GH families are there in the CAZy database? Amylase 2022, 6, 1–10.
52. Nichols, B.L.; Avery, S.; Sen, P.; Swallow, D.M.; Hahn, D.; Sterchi, E. The maltase-glucoamylase gene: common ancestry to sucrase-isomaltase with complementary starch digestion activities. Proc. Natl. Acad. Sci. 2003, 100, 1432–1437.
53. Stam, M.R.; Danchin, E.G.J.; Rancurel, C.; Coutinho, P.M.; Henrissat, B. Dividing the large glycoside hydrolase family 13 into subfamilies: Towards improved functional annotations of α-amylase-related proteins. Protein Eng. Des. Sel. 2006, 19, 555–562.
54. Janeček, Š.; Svensson, B.; MacGregor, E.A. α-Amylase: an enzyme specificity found in various families of glycoside hydrolases. Cell. Mol. Life Sci. 2014, 71, 1149–1170.
55. Wu, X.; Hu, M.; Hu, X.; Ding, H.; Gong, D.; Zhang, G. Inhibitory mechanism of epicatechin gallate on α-amylase and α-glucosidase and its combinational effect with acarbose or epigallocatechin gallate. J. Mol. Liq. 2019, 290, 111202.
56. Jespersen, H.M.; Macgregor, E.A.; Sierks, M.R.; Svensson, B. Comparison of the domain-level organization of starch hydrolases and related enzymes. Biochem. J 1991, 280, 51–55.
57. Tao, X.; Jang, M.S.; Kim, K.S.; Yu, Z.; Lee, Y.C. Molecular cloning, expression and characterization of α-amylase gene from a marine bacterium *Pseudoalteromonas* sp. MY-1. Indian J. Biochem. Biophys. 2008, 45, 305–309.
58. Brayer, G.D.; Luo, Y.; Withers, S.G. The structure of human pancreatic α-amylase at 1.8 Å resolution and comparisons with related enzymes. Protein Sci. 1995, 4, 1730–1742.
59. Dey, T.B.; Kumar, A.; Banerjee, R.; Chandna, P.; Kuhad, R.C. Improvement of microbial α-amylase stability: strategic approaches. Process Biochem. 2016, 51, 1380–1390.
60. Na, S.; Park, M.; Jo, I.; Cha, J.; Ha, N.-C. Structural basis for the transglycosylase activity of a GH57-type glycogen branching enzyme from Pyrococcus horikoshii. Biochem. Biophys. Res. Commun. 2017,

484, 850–856.
61. Imamura, H.; Fushinobu, S.; Yamamoto, M.; Kumasaka, T.; Jeon, B.S.; Wakagi, T.; Matsuzawa, H. Crystal structures of 4-α-glucanotransferase from *Thermococcus litoralis* and its complex with an inhibitor. J. Biol. Chem. 2003, 278, 19378–19386.
62. Kim, J.W.; Flowers, L.O.; Whiteley, M.; Peeples, T.L. Biochemical confirmation and characterization of the family-57-like α-amylase of *Methanococcus jannaschii*. Folia Microbiol. (Praha). 2001, 46, 467–473.
63. Watanabe, H.; Nishimoto, T.; Kubota, M.; Chaen, H.; Fukuda, S. Cloning, sequencing, and expression of the genes encoding an isocyclomaltooligosaccharide glucanotransferase and an α-amylase from a *Bacillus circulans* strain. Biosci. Biotechnol. Biochem. 2006, 70, 2690–2702.
64. Ficko-Blean, E.; Stuart, C.P.; Boraston, A.B. Structural analysis of CPF_2247, a novel α-amylase from *Clostridium perfringens*. Proteins Struct. Funct. Bioinforma. 2011, 79, 2771–2777.
65. Boel, E.; Brady, L.; Brzozowski, A.M.; Derewenda, Z.; Dodson, G.G.; Jensen, V.J.; Petersen, S.B.; Swift, H.; Thim, L.; Woldike, H.F. Calcium binding in. alpha.-amylases: an x-ray diffraction study at 2.1-Å resolution of two enzymes from Aspergillus. Biochemistry 1990, 29, 6244–6249.
66. Machius, M.; Declerck, N.; Huber, R.; Wiegand, G. Activation of *Bacillus licheniformis* α-amylase through a disorder→order transition of the substrate-binding site mediated by a calcium–sodium–calcium metal triad. Structure 1998, 6, 281–292.
67. Robert, X.; Haser, R.; Gottschalk, T.E.; Ratajczak, F.; Driguez, H.; Svensson, B.; Aghajari, N. The structure of barley α-amylase isozyme 1 reveals a novel role of domain C in substrate recognition and binding: a pair of sugar tongs. Structure 2003, 11, 973–984.
68. Linden, A.; Mayans, O.; Meyer-Klaucke, W.; Antranikian, G.; Wilmanns, M. Differential regulation of a hyperthermophilic α-amylase with a novel (Ca, Zn) two-metal center by zinc*. J. Biol. Chem. 2003, 278, 9875–9884.
69. Timmins, J.; Leiros, H.-K.S.; Leonard, G.; Leiros, I.; McSweeney, S. Crystal structure of maltooligosyltrehalose trehalohydrolase from *Deinococcus radiodurans* in complex with disaccharides. J. Mol. Biol. 2005, 347, 949–963.
70. Pereira, P.J.B.; Lozanov, V.; Patthy, A.; Huber, R.; Bode, W.; Pongor, S.; Strobl, S. Specific inhibition of insect α-amylases: Yellow meal worm α-amylase in complex with the amaranth α-amylase inhibitor at 2.0 Å resolution. Structure 1999, 7, 1079–1088.
71. Family, H.; Park, J.; Woo, E. The distinctive permutated domain structure of periplasmic α-amylase (MalS) from glycoside hydrolase family 13 subfamily 19. 2023.
72. Ohtaki, A.; Iguchi, A.; Mizuno, M.; Tonozuka, T.; Sakano, Y.; Kamitori, S. Mutual conversion of substrate specificities of *Thermoactinomyces vulgaris* R-47 α-amylases TVAI and TVAII by site-directed mutagenesis. Carbohydr. Res. 2003, 338, 1553–1558.
73. Hirano, Y.; Tsukamoto, K.; Ariki, S.; Naka, Y.; Ueda, M.; Tamada, T. X-ray crystallographic structural studies of α-amylase I from *Eisenia fetida*. Acta Crystallogr. Sect. D Struct. Biol. 2020, 76, 834–844.
74. Fujimoto, Z.; Takase, K.; Doui, N.; Momma, M.; Matsumoto, T.; Mizuno, H. Crystal structure of a catalytic-site mutant α-amylase from *Bacillus subtilis* complexed with maltopentaose 11Edited by R. Huber. J. Mol. Biol. 1998, 277, 393–407.
75. Aghajari, N.; Feller, G.; Gerday, C.; Haser, R. Crystal structures of the psychrophilic α-amylase from *Alteromonas haloplanctis* in its native form and complexed with an inhibitor. Protein Sci. 1998, 7, 564–572.
76. Koropatkin, N.M.; Smith, T.J. SuSG: A unique cell-membrane-associated α-amylase from a prominent human gut symbiont targets complex starch molecules. Structure 2010, 18, 200–215.
77. Liu, Y.; Yu, J.; Li, F.; Peng, H.; Zhang, X.; Xiao, Y.; He, C. Crystal structure of a raw-starch-degrading

bacterial α-amylase belonging to subfamily 37 of the glycoside hydrolase family GH13. Sci. Rep. 2017, 7, 44067.

78. Chai, K.P.; Othman, N.F.B.; Teh, A.-H.; Ho, K.L.; Chan, K.-G.; Shamsir, M.S.; Goh, K.M.; Ng, C.L. Crystal structure of *Anoxybacillus* α-amylase provides insights into maltose binding of a new glycosyl hydrolase subclass. Sci. Rep. 2016, 6, 23126.
79. Gobius, K.S.; Pemberton, J.M. Molecular cloning, characterization, and nucleotide sequence of an extracellular amylase gene from *Aeromonas hydrophila*. J. Bacteriol. 1988, 170, 1325–1332.
80. Hutcheon, G.W.; Vasisht, N.; Bolhuis, A. Characterisation of a highly stable α-amylase from the halophilic archaeon *Haloarcula hispanica*. Extremophiles 2005, 9, 487–495.
81. Møller, M.S.; Henriksen, A.; Svensson, B. Structure and function of α-glucan debranching enzymes. Cell. Mol. Life Sci. 2016, 73, 2619–2641.
82. Møller, M.S.; Goh, Y.J.; Rasmussen, K.B.; Cypryk, W.; Celebioglu, H.U.; Klaenhammer, T.R.; Svensson, B.; Abou Hachem, M. An extracellular cell-attached pullulanase confers branched α-glucan utilization in human gut *Lactobacillus acidophilus*. Appl. Environ. Microbiol. 2017, 83, 1–13.
83. Cockburn, D.W.; Kibler, R.; Brown, H.A.; Duvall, R.; Moraïs, S.; Bayer, E.; Koropatkin, N.M. Structure and substrate recognition by the *Ruminococcus bromii* amylosome pullulanases. J. Struct. Biol. 2021, 213, 107765.
84. Cockburn, D.W.; Koropatkin, N.M. Polysaccharide degradation by the intestinal microbiota and its influence on human health and disease. J. Mol. Biol. 2016, 428, 3230–3252.
85. Vester-Christensen, M.B.; Holck, J.; Rejzek, M.; Perrin, L.; Tovborg, M.; Svensson, B.; Field, R.A.; Møller, M.S. Exploration of the transglycosylation activity of barley limit dextrinase for production of novel glycoconjugates. Molecules 2023, 28.
86. Xia, W.; Chen, S.; Wu, J. Production and the Applications in Preparation of Branched Sugar Products of Starch Debranching Enzymes. In *Industrial Starch Debranching Enzymes*; Springer, 2023; pp. 61–71.
87. Saha, B.C.; Zeikus, J.G. Novel highly thermostable pullulanase from thermophiles. Trends Biotechnol. 1989, 7, 234–239.
88. Xia, W.; Wang, L.; Wu, J. Sequence, Structure, and Engineering of Microbial Starch Debranching Enzymes. In *Industrial Starch Debranching Enzymes*; Springer, 2023; pp. 41–60.
89. Kuriki, T.; Imanaka, T. The concept of the α-amylase family: Structural similarity and common catalytic mechanism. J. Biosci. Bioeng. 1999, 87, 557–565.
90. Shoseyov, O.; Shani, Z.; Levy, I. Carbohydrate binding modules: Biochemical properties and novel applications. Microbiol. Mol. Biol. Rev. 2006, 70, 283–295.
91. Dumbrepatil, A.B.; Choi, J.H.; Park, J.T.; Kim, M.J.; Kim, T.J.; Woo, E.J.; Park, K.H. Structural features of the *Nostoc punctiforme* debranching enzyme reveal the basis of its mechanismm and suostrate specificity. Proteins Struct. Funct. Bioinforma. 2010, 78, 348–356.
92. Duan, X.; Wu, J. Enhancing the secretion efficiency and thermostability of a *Bacillus deramificans* pullulanase mutant (D437H/D503Y) by N-terminal domain truncation. Appl. Environ. Microbiol. 2015, 81, 1926–1931.
93. Gilding, E.K.; Frere, C.H.; Cruickshank, A.; Rada, A.K.; Prentis, P.J.; Mudge, A.M.; Mace, E.S.; Jordan, D.R.; Godwin, I.D. Allelic variation at a single gene increases food value in a drought-tolerant staple cereal. Nat. Commun. 2013, 4, 1483.
94. Gourlay, L.J.; Santi, I.; Pezzicoli, A.; Grandi, G.; Soriani, M.; Bolognesi, M. Group B *Streptococcus* pullulanase crystal structures in the context of a novel strategy for vaccine development. J. Bacteriol. 2009, 191, 3544–3552.
95. Lammerts Van Bueren, A.; Ficko-Blean, E.; Pluvinage, B.; Hehemann, J.H.; Higgins, M.A.; Deng, L.;

Ogunniyi, A.D.; Stroeher, U.H.; El Warry, N.; Burke, R.D.; et al. The conformation and function of a multimodular glycogen-degrading pneumococcal virulence factor. Structure 2011, 19, 640–651.
96. Møller, M.S.; Abou Hachem, M.; Svensson, B.; Henriksen, A. Structure of the starch-debranching enzyme barley limit dextrinase reveals homology of the N-terminal domain to CBM21. Acta Crystallogr. Sect. F Struct. Biol. Cryst. Commun. 2012, 68, 1008–1012.
97. Mikami, B.; Iwamoto, H.; Malle, D.; Yoon, H.-J.; Demirkan-Sarikaya, E.; Mezaki, Y.; Katsuya, Y. Crystal structure of pullulanase: Evidence for parallel binding of oligosaccharides in the active site. J. Mol. Biol. 2006, 359, 690–707.
98. East, A.; Mechaly, A.E.; Huysmans, G.H.M.; Bernarde, C.; Tello-Manigne, D.; Nadeau, N.; Pugsley, A.P.; Buschiazzo, A.; Alzari, P.M.; Bond, P.J. Structural basis of pullulanase membrane binding and secretion revealed by X-ray crystallography, molecular dynamics and biochemical analysis. Structure 2016, 24, 92–104.
99. Saka, N.; Iwamoto, H.; Malle, D.; Takahashi, N.; Mizutani, K.; Mikami, B. Elucidation of the mechanism of interaction between *Klebsiella pneumoniae* pullulanase and cyclodextrin. Acta Crystallogr. Sect. D Struct. Biol. 2018, 74, 1115–1123.
100. Saka, N.; Malle, D.; Iwamoto, H.; Takahashi, N.; Mizutani, K.; Mikami, B. Relationship between the induced-fit loop and the activity of *Klebsiella pneumoniae* pullulanase. Acta Crystallogr. Sect. D Struct. Biol. 2019, 75, 792–803.
101. Xu, J.; Ren, F.; Huang, C.H.; Zheng, Y.; Zhen, J.; Sun, H.; Ko, T.P.; He, M.; Chen, C.C.; Chan, H.C.; et al. Functional and structural studies of pullulanase from *Anoxybacillus* sp. LM18-11. Proteins Struct. Funct. Bioinforma. 2014, 82, 1685–1693.
102. Turkenburg, J.P.; Brzozowski, A.M.; Svendsen, A.; Borchert, T. V; Davies, G.J.; Wilson, K.S. Structure of a pullulanase from *Bacillus acidopullulyticus*. Proteins Struct. Funct. Bioinforma. 2009, 76, 516–519.
103. Malle, D.; Itoh, T.; Hashimoto, W.; Murata, K.; Utsumi, S.; Mikami, B. Overexpression, purification and preliminary X-ray analysis of pullulanase from *Bacillus subtilis* strain 168. Acta Crystallogr. Sect. F Struct. Biol. Cryst. Commun. 2006, 62, 381–384.
104. Huang, P.; Wu, S.; Yang, S.; Yan, Q.; Jiang, Z. Structural basis of carbohydrate binding in domain C of a type I pullulanase from *Paenibacillus barengoltzii*. Acta Crystallogr. Sect. D Struct. Biol. 2020, 76, 447–457.
105. Li, L.; Dong, F.; Lin, L.; He, D.; Wei, W.; Wei, D. N-terminal domain truncation and domain insertion-based engineering of a novel thermostable type I pullulanase from *Geobacillus thermocatenulatus*. J. Agric. Food Chem. 2018, 66, 10788–10798.
106. Chen, A.; Sun, Y.; Zhang, W.; Peng, F.; Zhan, C.; Liu, M.; Yang, Y.; Bai, Z. Downsizing a pullulanase to a small molecule with improved soluble expression and secretion efficiency in *Escherichia coli*. Microb. Cell Fact. 2016, 15, 1–10.
107. Chen, A.; Liu, X.; Dai, X.; Zhan, J.; Peng, F.; Li, L.; Wang, F.; Li, S.; Yang, Y.; Bai, Z. Effect of N-terminal truncation of *Bacillus acidopullulyticus* pullulanase on enzyme properties and functions. Shengwu Gongcheng Xuebao/Chinese J. Biotechnol. 2016, 32, 355–364.
108. Tetlow, I.J.; Emes, M.J. A review of starch-branching enzymes and their role in amylopectin biosynthesis. IUBMB Life 2014, 66, 546–558.
109. Feng, L.; Fawaz, R.; Hovde, S.; Sheng, F.; Nosrati, M.; Geiger, J.H. Crystal structures of *Escherichia coli* branching enzyme in complex with cyclodextrins. Acta Crystallogr. Sect. D Struct. Biol. 2016, 72, 641–647.
110. Santos, C.R.; Tonoli, C.C.C.; Trindade, D.M.; Betzel, C.; Takata, H.; Kuriki, T.; Kanai, T.; Imanaka, T.; Arni, R.K.; Murakami, M.T. Structural basis for branching-enzyme activity of glycoside hydrolase family

57: Structure and stability studies of a novel branching enzyme from the hyperthermophilic archaeon *Thermococcus Kodakaraensis* KOD1. Proteins Struct. Funct. Bioinforma. 2011, 79, 547–557.

111. Feng, L.; Fawaz, R.; Hovde, S.; Gilbert, L.; Chiou, J.; Geiger, J.H. Crystal structures of *Escherichia coli* branching enzyme in complex with linear oligosaccharides. Biochemistry 2015, 54, 6207–6218.
112. Ban, X.; Dhoble, A.S.; Li, C.; Gu, Z.; Hong, Y.; Cheng, L.; Holler, T.P.; Kaustubh, B.; Li, Z. Bacterial 1,4-α-glucan branching enzymes: characteristics, preparation and commercial applications. Crit. Rev. Biotechnol. 2020, 40, 380–396.
113. Idaka, M.; Terada, T.; Murayama, K.; Yamaguchi, H.; Nureki, O.; Ishitani, R.; Kuramitsu, S.; Shirouzu, M.; Yokoyama, S. Crystal Structure of TT1467 from *Thermus thermophilus* HB8. Nicht publiziert 2003.
114. Courseaux, A.; George, O.; Deschamps, P.; Bompard, C.; Duchêne, T.; Dauvillée, D. BE3 is the major branching enzyme isoform required for amylopectin synthesis in *Chlamydomonas reinhardtii*. Front. Plant Sci. 2023, 14, 1201386.
115. Wang, L.; Wang, Y.; Makhmoudova, A.; Nitschke, F.; Tetlow, I.J.; Emes, M.J. CRISPR–Cas9-mediated editing of starch branching enzymes results in altered starch structure in *Brassica napus*. Plant Physiol. 2022, 188, 1866–1886.
116. Adeva-Andany, M.M.; González-Lucán, M.; Donapetry-García, C.; Fernández-Fernández, C.; Ameneiros-Rodríguez, E. Glycogen metabolism in humans. BBA Clin. 2016, 5, 85–100.
117. Barbetti, F.; Rocchi, M.; Bossolasco, M.; Cordera, R.; Sbraccia, P.; Finelli, P.; Consalez, G.G. The human skeletal muscle glycogenin gene: Cdna, tissue expression, and chromosomal localization. Biochem. Biophys. Res. Commun. 1996, 220, 72–77.
118. Hayashi, M.; Suzuki, R.; Colleoni, C.; Ball, S.G.; Fujita, N.; Suzuki, E. Bound substrate in the structure of cyanobacterial branching enzyme supports a new mechanistic model. J. Biol. Chem. 2017, 292, 5465–5475.
119. Abad, M.C.; Binderup, K.; Rios-Steiner, J.; Arni, R.K.; Preiss, J.; Geiger, J.H. The X-ray crystallographic structure of *Escherichia coli* branching enzyme. J. Biol. Chem. 2002, 277, 42164–42170.
120. Pal, K.; Kumar, S.; Sharma, S.; Garg, S.K.; Alam, M.S.; Xu, H.E.; Agrawal, P.; Swaminathan, K. Crystal structure of full-length Mycobacterium tuberculosis H37Rv glycogen branching enzyme: Insights of N-terminal β-sandwich in substrate specificity and enzymatic activity. J. Biol. Chem. 2010, 285, 20897–20903.
121. Wang, Z.; Xin, C.; Li, C.; Gu, Z.; Cheng, L.; Hong, Y.; Ban, X.; Li, Z. Expression and characterization of an extremely thermophilic 1, 4-α-glucan branching enzyme from *Rhodothermus obamensis* STB05. Protein Expr. Purif. 2019, 164, 105478.
122. Weiss, S.C.; Skerra, A.; Schiefner, A. Structural basis for the interconversion of maltodextrins by MalQ, the amylomaltase of *Escherichia coli*. J. Biol. Chem. 2015, 290, 21352–21364.
123. Joo, S.; Kim, S.; Seo, H.; Kim, K.J. Crystal Structure of Amylomaltase from *Corynebacterium glutamicum*. J. Agric. Food Chem. 2016, 64, 5662–5670.
124. Barends, T.R.M.; Bultema, J.B.; Kaper, T.; van der Maarel, M.J.E.C.; Dijkhuizen, L.; Dijkstra, B.W. Three-way stabilization of the covalent intermediate in amylomaltase, an α-Amylase-like transglycosylase. J. Biol. Chem. 2007, 282, 17242–17249.
125. Kaper, T.; Leemhuis, H.; Uitdehaag, J.C.M.; van der Veen, B.A.; Dijkstra, B.W.; van der Maarel, M.J.E.C.; Dijkhuizen, L. Identification of acceptor substrate binding subsites+ 2 and+ 3 in the amylomaltase from *Thermus thermophilus* HB8. Biochemistry 2007, 46, 5261–5269.
126. Roth, C.; Weizenmann, N.; Bexten, N.; Saenger, W.; Zimmermann, W.; Maier, T.; Sträter, N. Amylose recognition and ring-size determination of amylomaltase. Sci. Adv. 2017, 3, 1–10.
127. Juers, D.H.; Huber, R.E.; Matthews, B.W. Structural comparisons of TIM barrel proteins suggest

functional and evolutionary relationships between β-galactosidase and other glycohydrolases. Protein Sci. 1999, 8, 122–136.
128. Wang, Y.; Li, X.; Ji, H.; Zheng, D.; Jin, Z.; Bai, Y.; Svensson, B. Thermophilic 4-α-glucanotransferase from *Thermoproteus uzoniensis* retards the long-term retrogradation but maintains the short-term gelation strength of tapioca starch. J. Agric. Food Chem. 2020, 68, 5658–5667.
129. Li, X.; Wang, Y.; Wu, J.; Jin, Z.; Dijkhuizen, L.; Abou Hachem, M.; Bai, Y. *Thermoproteus uzoniensis* 4-α-glucanotransferase catalyzed production of a thermo-reversible potato starch gel with superior rheological properties and freeze-thaw stability. Food Hydrocoll. 2023, 134, 108026.
130. Lloyd, J.R.; Blennow, A.; Burhenne, K.; Kossmann, J. Repression of a novel isoform of disproportionating enzyme (stDPE2) in potato leads to inhibition of starch degradation in leaves but not tubers stored at low temperature. Plant Physiol. 2004, 134, 1347–1354.
131. Andersen, S.; Møller, M.S.; Poulsen, J.C.N.; Pichler, M.J.; Svensson, B.; Leggio, L. Lo; Goh, Y.J.; Hachem, M.A. An 1,4-α-glucosyltransferase defines a new maltodextrin catabolism scheme in *Lactobacillus acidophilus*. Appl. Environ. Microbiol. 2020, 86.
132. Jiang, H.; Miao, M.; Ye, F.; Jiang, B.; Zhang, T. Enzymatic modification of corn starch with 4-α-glucanotransferase results in increasing slow digestible and resistant starch. Int. J. Biol. Macromol. 2014, 65, 208–214.
133. Barends, T.R.M.; Korf, H.; Kaper, T. Structural influences on product specificity in amylomaltase from *Aquifex aeolicus* 2005.
134. Przylas, I.; Tomoo, K.; Terada, Y.; Takaha, T.; Fujii, K.; Saenger, W.; Sträter, N. Crystal structure of amylomaltase from *Thermus aquaticus*, a glycosyltransferase catalysing the production of large cyclic glucans. J. Mol. Biol. 2000, 296, 873–886.
135. Jung, J.; Jung, T.; Seo, D.; Yoon, S.; Choi, H.; Park, B.C.; Park, C.; Woo, E. Structural and functional analysis of substrate recognition by the 250s loop in amylomaltase from *Thermus brockianus*. Proteins Struct. Funct. Bioinforma. 2011, 79, 633–644.
136. O'Neill, E.C.; Stevenson, C.E.M.; Tantanarat, K.; Latousakis, D.; Donaldson, M.I.; Rejzek, M.; Nepogodiev, S.A.; Limpaseni, T.; Field, R.A.; Lawson, D.M. Structural dissection of the maltodextrin disproportionation cycle of the *Arabidopsis plastidial* disproportionating enzyme 1 (DPE1). J. Biol. Chem. 2015, 290, 29834–29853.
137. Imamura, K.; Matsuura, T.; Nakagawa, A.; Kitamura, S.; Kusunoki, M.; Takaha, T.; Unno, H. Structural analysis and reaction mechanism of the disproportionating enzyme (D-enzyme) from potato. Protein Sci. 2020, 29, 2085–2100.
138. Gangoiti, J.; Van Leeuwen, S.S.; Gerwig, G.J.; Duboux, S.; Vafiadi, C.; Pijning, T.; Dijkhuizen, L. 4,3-α-Glucanotransferase, a novel reaction specificity in glycoside hydrolase family 70 and clan GH-H. Sci. Rep. 2017, 7, 1–15.
139. Hara, M.; Sawada, T.; Ito, A.; Ito, F.; Kuboi, T. A major β-amylase expressed in radish taproots. Food Chem. 2009, 114, 523–528.
140. Svensson, B.; Larsen, K.; Svendsen, I.; Boel, E. The complete amino acid sequence of the glycoprotein, glucoamylase G1, from *Aspergillus niger*. Carlsberg Res. Commun. 1983, 48, 529–544.
141. Das, M.; Rajan, N.; Biswas, P.; Banerjee, R. A novel approach for resistant starch production from green banana flour using amylopullulanase. LWT 2022, 153, 112391.
142. Miao, M.; Bemiller, J.N. Enzymatic approaches for structuring starch to improve functionality. Annu. Rev. Food Sci. Technol. 2023, 14, 1–25.
143. Hj. Latip, D.N.; Samsudin, H.; Utra, U.; Alias, A.K. Modification methods toward the production of porous starch: A review. Crit. Rev. Food Sci. Nutr. 2021, 61, 2841–2862.

144. Gamvros, R.J.; Blekas, G.A. Legal Aspects and Specifications of Biopolymers Used in Foods. In *Developments in Food Science*; Elsevier, 2000; Vol. 41, pp. 419–439 ISBN 0167-4501.
145. Nguyen, T.T.H.; Cho, J.-Y.; Seo, Y.-S.; Woo, H.-J.; Kim, H.-K.; Kim, G.J.; Jhon, D.-Y.; Kim, D. Production of a low calorie mandarin juice by enzymatic conversion of constituent sugars to oligosaccharides and prevention of insoluble glucan formation. Biotechnol. Lett. 2015, 37, 711–716.
146. Nimpiboon, P.; Tumhom, S.; Nakapong, S.; Pongsawasdi, P. Amylomaltase from Thermus filiformis: expression in *Saccharomyces cerevisiae* and its use in starch modification. J. Appl. Microbiol. 2020, 129, 1287–1296.
147. Zhong, Y.; Herburger, K.; Kirkensgaard, J.J.K.; Khakimov, B.; Hansen, A.R.; Blennow, A. Sequential maltogenic α-amylase and branching enzyme treatment to modify granular corn starch. Food Hydrocoll. 2021, 120, 106904.
148. Ren, J.; Chen, S.; Li, C.; Gu, Z.; Cheng, L.; Hong, Y.; Li, Z. A two-stage modification method using 1, 4-α-glucan branching enzyme lowers the *in vitro* digestibility of corn starch. Food Chem. 2020, 305, 125441.
149. Keeratiburana, T.; Hansen, A.R.; Soontaranon, S.; Blennow, A.; Tongta, S. Pre-treatment of granular rice starch to enhance branching enzyme catalysis. Carbohydr. Polym. 2020, 247, 116741.
150. Dura, A.; Rosell, C.M. Physico-chemical properties of corn starch modified with cyclodextrin glycosyltransferase. Int. J. Biol. Macromol. 2016, 87, 466–472.
151. Yoshioka, Y.; Hasegawa, K.; Matsuura, Y.; Katsube, Y.; Kubota, M. Crystal structures of a mutant maltotetraose-forming exo-amylase cocrystallized with maltopentaose. J. Mol. Biol. 1997, 271, 619–628.
152. Hashim, S.O.; Delgado, O.D.; Martínez, M.A.; Kaul, R.-H.; Mulaa, F.J.; Mattiasson, B. Alkaline active maltohexaose-forming α-amylase from *Bacillus halodurans* LBK 34. Enzyme Microb. Technol. 2005, 36, 139–146.
153. Kamon, M.; Sumitani, J.; Tani, S.; Kawaguchi, T.; Kamon, M.; Sumitani, J.; Tani, S.; Kawaguchi, T. Characterization and gene cloning of a maltotriose-forming exo-amylase from *Kitasatospora* sp. MK-1785. Appl. Microbiol. Biotechnol. 2015, 99, 4743–4753.
154. Lv, Q.-Q.; Cao, J.-J.; Liu, R.; Chen, H.-Q. Structural characterization, α-amylase and α-glucosidase inhibitory activities of polysaccharides from wheat bran. Food Chem. 2021, 341, 128218.
155. Wang, R.; Liu, P.; Cui, B.; Kang, X.; Yu, B.; Qiu, L.; Sun, C. Effects of pullulanase debranching on the properties of potato starch-lauric acid complex and potato starch-based film. Int. J. Biol. Macromol. 2020, 156, 1330–1336.
156. Liu, P.; Gao, W.; Zhang, X.; Wu, Z.; Yu, B.; Cui, B. Physicochemical properties of pea starch-lauric acid complex modified by maltogenic amylase and pullulanase. Carbohydr. Polym. 2020, 242, 116332.
157. Krishnan, V.; Awana, M.; Kulshreshta, A.; Praveen, S.; Singh, A. A quick and simple gel diffusion assay to visualize and quantify pullulanase activity for resistant starch content in food crops. J. Plant Biochem. Biotechnol. 2023, 32, 189–195.
158. Van Der Maarel, M.J.E.C.; Van Der Veen, B.; Uitdehaag, J.C.M.; Leemhuis, H.; Dijkhuizen, L. Properties and applications of starch-converting enzymes of the α-amylase family. J. Biotechnol. 2002, 94, 137–155.
159. Takata, H.; Ohdan, K.; Takaha, T.; Kuriki, T.; Okada, S. Properties of branching enzyme from hyperthermophilic bacterium, Aquifex aeolicus, and its potential for production of highly-branched cyclic dextrin. J. Appl. Glycosci. 2003, 50, 15–20.
160. Bhuiyan, S.H.; Kitaoka, M.; Hayashi, K. A cycloamylose-forming hyperthermostable 4-α-glucanotransferase of *Aquifex aeolicus* expressed in Escherichia coli. J. Mol. Catal. B Enzym. 2003, 22, 45–53.

161. Li, X.; Jiang, T.; Wang, Y.; Dong, J.; Jin, Z.; Bai, Y. Exploring the roles of amylopectin in starch modification with *Limosilactobacillus reuteri* 121 4, 6-α-glucanotransferase via developed methods. Int. J. Biol. Macromol. 2023, 243, 125040.
162. Ueda, S. Fungal glucoamylases and raw starch digestion. Trends Biochem. Sci. 1981, 6, 89–90.
163. Søgaard, M.; Kadziola, A.; Haser, R.; Svensson, B. Site-directed mutagenesis of histidine 93, aspartic acid 180, glutamic acid 205, histidine 290, and aspartic acid 291 at the active site and tryptophan 279 at the raw starch binding site in barley alpha-amylase 1. J. Biol. Chem. 1993, 268, 22480–22484.
164. Zhang, X.; Caner, S.; Kwan, E.; Li, C.; Brayer, G.D.; Withers, S.G. Evaluation of the significance of starch surface binding sites on human pancreatic α-amylase. Biochemistry 2016, 55, 6000–6009.
165. Puspasari, F.; Radjasa, O.K.; Noer, A.S.; Nurachman, Z.; Syah, Y.M.; van der Maarel, M.; Dijkhuizen, L.; Janeček, S.; Natalia, D. Raw starch-degrading α-amylase from *Bacillus aquimaris* MKSC 6.2: Isolation and expression of the gene, bioinformatics and biochemical characterization of the recombinant enzyme. J. Appl. Microbiol. 2013, 114, 108–120.
166. Janeček, Š.; Mareček, F.; MacGregor, E.A.; Svensson, B. Starch-binding domains as CBM families–history, occurrence, structure, function and evolution. 2019, 1–15.
167. Hayashida, S.; Kunisaki, S.; Nakao, M.; Flor, P.Q. Evidence for raw starch-affinity site on *Aspergillus awamori* glucoamylase I. Agric. Biol. Chem. 1982, 46, 83–89.
168. Svensson, B.; Svendsen, T.G.; Svendsen, I.B.; Sakai, T.; Ottesen, M. Characterization of two forms of glucoamylase from *Aspergillus niger*. Carlsberg Res. Commun. 1982, 47, 55–69.
169. Ashkari, T.; Nakamura, N.; Tanaka, Y.; Kiuchi, N.; Shibano, Y.; Tanaka, T.; Amachi, T.; Yoshizumi, H. *Rhizopus* raw-starch-degrading glucoamylase: Its cloning and expression in yeast. Agric. Biol. Chem. 1986, 50, 957–964.
170. Tanaka, Y.; Ashikari, T.; Nakamura, N.; Kiuchi, N.; Shibano, Y.; Amachi, T.; Yoshizumi, H. Comparison of amino acid sequences of three glucoamylases and their structure-function relationships. Agric. Biol. Chem. 1986, 50, 965–969.
171. Brown, H.A.; Deveaux, A.L.; Juliano, B.R.; Photenhauer, A.L.; Boulinguiez, M.; Bornschein, R.E.; Wawrzak, Z.; Ruotolo, B.T.; Terrapon, N.; Koropatkin, N.M. BoGH13A Sus from Bacteroides ovatus represents a novel α-amylase used for *Bacteroides* starch breakdown in the human gut. Cell. Mol. Life Sci. 2023.
172. Photenhauer, A.L.; Cerqueira, F.M.; Villafuerte-Vega, R.; Armbruster, K.M.; Mareček, F.; Chen, T.; Wawrzak, Z.; Hopkins, J.B.; Vander Kooi, C.W.; Janeček, Š.; et al. The *Ruminococcus bromii* amylosome protein Sas6 binds single and double helical α-glucan structures in starch. bioRxiv 2022, 2022.11.20.514607.
173. Juge, N.; Le Gal-Coëffet, M.F.; Furniss, C.S.M.; Gunning, A.P.; Kramhøft, B.; Morris, V.J.; Williamson, G.; Svensson, B. The starch binding domain of glucoamylase from *Aspergillus niger*: Overview of its structure, function, and role in raw-starch hydrolysis. Biol. - Sect. Cell. Mol. Biol. 2002, 57, 239–245.
174. Stephen, P.; Cheng, K.-C.; Lyu, P.-C. Crystal structure of circular permuted *Ro*CBM21 (CP90): Dimerisation and proximity of binding sites. PLoS One 2012, 7, e50488.
175. Huang, X.F.; Nazarian, F.; Vincken, J.P.; Visser, R.G.F.; Trindade, L.M. A tandem CBM25 domain of α-amylase from *Microbacterium aurum* as potential tool for targeting proteins to starch granules during starch biosynthesis. BMC Biotechnol. 2017, 17, 1–8.
176. Valk, V.; Lammerts van Bueren, A.; van der Kaaij, R.M.; Dijkhuizen, L. Carbohydrate-binding module 74 is a novel starch-binding domain associated with large and multidomain α-amylase enzymes. FEBS J. 2016, 283, 2354–2368.
177. Paldi, T.; Levy, I.; Shoseyov, O. Glucoamylase starch-binding domain of *Aspergillus niger* B1: Molecular

cloning and functional characterization. Biochem. J. 2003, 372, 905–910.
178. Southall, S.M.; Simpson, P.J.; Gilbert, H.J.; Williamson, G.; Williamson, M.P. The starch-binding domain from glucoamylase disrupts the structure of starch. FEBS Lett. 1999, 447, 58–60.
179. Sorimachi, K.; Le Gal-Coëffet, M.-F.; Williamson, G.; Archer, D.B.; Williamson, M.P. Solution structure of the granular starch binding domain of *Aspergillus niger* glucoamylase bound to β-cyclodextrin. Structure 1997, 5, 647–661.
180. Penninga, D.; Van Der Veen, B.A.; Knegtel, R.M.A.; Van Hijum, S.A.F.T.; Rozeboom, H.J.; Kalk, K.H.; Dijkstra, B.W.; Dijkhuizen, L. The raw starch binding domain of cyclodextrin glycosyltransferase from *Bacillus circulans* strain 251. J. Biol. Chem. 1996, 271, 32777–32784.
181. Abt, M.R.; Zeeman, S.C. Evolutionary innovations in starch metabolism. Curr. Opin. Plant Biol. 2020, 55, 109–117.
182. Tung, J.Y.; Chang, M.D.T.; Chou, W.I.; Liu, Y.Y.; Yeh, Y.H.; Chang, F.Y.; Lin, S.C.; Qiu, Z.L.; Sun, Y.J. Crystal structures of the starch-binding domain from *Rhizopus oryzae* glucoamylase reveal a polysaccharide-binding path. Biochem. J. 2008, 416, 27–36.
183. Boraston, A.B.; Healey, M.; Klassen, J.; Ficko-Blean, E.; van Bueren, A.L.; Law, V. A structural and functional analysis of α-glucan recognition by family 25 and 26 carbohydrate-binding modules reveals a conserved mode of starch recognition. J. Biol. Chem. 2006, 281, 587–598.
184. Cockburn, D.W.; Suh, C.; Medina, K.P.; Duvall, R.M.; Wawrzak, Z.; Henrissat, B.; Koropatkin, N.M. Novel carbohydrate binding modules in the surface anchored α-amylase of *Eubacterium rectale* provide a molecular rationale for the range of starches used by this organism in the human gut. Mol. Microbiol. 2018, 107, 249–264.
185. Abe, A.; Tonozuka, T.; Sakano, Y.; Kamitori, S. Complex structures of *Thermoactinomyces vulgaris* R-47 α-amylase 1 with malto-oligosaccharides demonstrate the role of domain N acting as a starch-binding domain. J. Mol. Biol. 2004, 335, 811–822.
186. Polekhina, G.; Gupta, A.; van Denderen, B.J.W.; Feil, S.C.; Kemp, B.E.; Stapleton, D.; Parker, M.W. Structural basis for glycogen recognition by AMP-activated protein kinase. Structure 2005, 13, 1453–1462.
187. Arnal, G.; Cockburn, D.W.; Brumer, H.; Koropatkin, N.M. Structural basis for the flexible recognition of α-glucan substrates by *Bacteroides thetaiotaomicron* SusG. Protein Sci. 2018, 27, 1093–1101.
188. Zhang, W.; Yu, J.; Zhang, X.; Peng, H.; Li, X.; Zhang, J.; Sun, H.; Tu, X. Ligand induced folding of the first identified CBM69 starch binding domain AmyP-SBD. Protein Pept. Lett. 2018, 25, 362–367.
189. Machovič, M.; Janeček, Š. Starch-binding domains in the post-genome era. Cell. Mol. Life Sci. 2006, 63, 2710–2724.
190. Long, C.M.; Virolle, M.-J.; Chang, S.-Y.; Chang, S.; Bibb, M.J. Alpha-Amylase gene of *Streptomyces limosus*: Nucleotide sequence, expression motifs, and amino acid sequence homology to mammalian and invertebrate alpha-amylases. J. Bacteriol. 1987, 169, 5745–5754.
191. Wang, N.; Zhang, Y.; Wang, Q.; Liu, J.; Wang, H.; Xue, Y.; Ma, Y. Gene cloning and characterization of a novel α-amylase from alkaliphilic *Alkalimonas amylolytica*. Biotechnol. J. Healthc. Nutr. Technol. 2006, 1, 1258–1265.
192. MacGregor, E.A.; Janeček, Š.; Svensson, B. Relationship of sequence and structure to specificity in the α-amylase family of enzymes. Biochim. Biophys. Acta (BBA)-Protein Struct. Mol. Enzymol. 2001, 1546, 1–20.
193. Mikami, B.; Adachi, M.; Kage, T.; Sarikaya, E.; Nanmori, T.; Shinke, R.; Utsumi, S. Structure of raw starch-digesting *Bacillus cereus* β-amylase complexed with maltose. Biochemistry 1999, 38, 7050–7061.
194. Giardina, T.; Gunning, A.P.; Juge, N.; Faulds, C.B.; Furniss, C.S.M.; Svensson, B.; Morris, V.J.;

Williamson, G. Both binding sites of the starch-binding domain of Aspergillus niger glucoamylase are essential for inducing a conformational change in amylose. J. Mol. Biol. 2001, 313, 1149–1159.
195. Janeček, Š.; Kuchtová, A. In silico identification of catalytic residues and domain fold of the family GH119 sharing the catalytic machinery with the α-amylase family GH57. FEBS Lett. 2012, 586, 3360–3366.
196. Raththagala, M.; Brewer, M.K.; Kooi, C.W. Vander; Gentry, M.S.; Raththagala, M.; Brewer, M.K.; Parker, M.W.; Sherwood, A.R.; Wong, B.K.; Hsu, S.; et al. Structural mechanism of laforin function in glycogen dephosphorylation and lafora disease. Mol. Cell 2015, 57, 261–272.
197. Nekiunaite, L.; Isaksen, T.; Vaaje-Kolstad, G.; Abou Hachem, M. Fungal lytic polysaccharide monooxygenases bind starch and β-cyclodextrin similarly to amylolytic hydrolases. FEBS Lett. 2016, 590, 2737–2747.
198. Christiansen, C.; Abou Hachem, M.; Glaring, M.A.; Viksø-Nielsen, A.; Sigurskjold, B.W.; Svensson, B.; Blennow, A. A CBM20 low-affinity starch-binding domain from glucan, water dikinase. FEBS Lett. 2009, 583, 1159–1163.
199. Lee, S.-P.; Morikawa, M.; Takagi, M.; Imanaka, T. Cloning of the aapT gene and characterization of its product, alpha-amylase-pullulanase (AapT), from thermophilic and alkaliphilic *Bacillus* sp. strain XAL601. Appl. Environ. Microbiol. 1994, 60, 3764–3773.
200. Saburi, W.; Morimoto, N.; Mukai, A.; Kim, D.H.; Takehana, T.; Koike, S.; Matsui, H.; Mori, H. A thermophilic alkalophilic α-amylase from *Bacillus* sp. AAH-31 shows a novel domain organization among glycoside hydrolase family 13 enzymes. Biosci. Biotechnol. Biochem. 2013, 77, 1867–1873.
201. Orengo, C.A.; Pearl, F.M.G.; Bray, J.E.; Todd, A.E.; Martin, A.C.; Lo Conte, L.; Thornton, J.M. The CATH Database provides insights into protein structure/function relationships. Nucleic Acids Res. 1999, 27, 275–279.
202. Hashimoto, H. Recent structural studies of carbohydrate-binding modules. Cell. Mol. Life Sci. C. 2006, 63, 2954–2967.
203. Engelberts, K.; Schmidt, E.; Reineke, W. Degradation of o-toluate by *Pseudomonas* sp. strain WR401. FEMS Microbiol. Lett. 1989, 59, 35–38.
204. Janeček, Š.; Majzlová, K.; Svensson, B.; MacGregor, E.A. The starch-binding domain family CBM41—An in silico analysis of evolutionary relationships. Proteins Struct. Funct. Bioinforma. 2017, 85, 1480–1492.
205. Pereira, G. V.; Abdel-Hamid, A.M.; Dutta, S.; D'Alessandro-Gabazza, C.N.; Wefers, D.; Farris, J.A.; Bajaj, S.; Wawrzak, Z.; Atomi, H.; Mackie, R.I.; et al. Degradation of complex arabinoxylans by human colonic Bacteroidetes. Nat. Commun. 2021, 12.
206. Kooi, C.W.V.; Taylor, A.O.; Pace, R.M.; Meekins, D.A.; Guo, H.F.; Kim, Y.; Gentry, M.S. Structural basis for the glucan phosphatase activity of Starch Excess4. Proc. Natl. Acad. Sci. U. S. A. 2010, 107, 15379–15384.
207. Seung, D.; Boudet, J.; Monroe, J.; Schreier, T.B.; David, L.C.; Abt, M.; Lu, K.J.; Zanella, M.; Zeeman, S.C. Homologs of PROTEIN TARGETING TO STARCH control starch granule initiation in *Arabidopsis* leaves. Plant Cell 2017, 29, 1657–1677.
208. Yang, S.J.; Lee, H.S.; Park, C.S.; Kim, Y.R.; Moon, T.W.; Park, K.H. Enzymatic analysis of an amylolytic enzyme from the hyperthermophilic archaeon *Pyrococcus furiosus* reveals its novel catalytic properties as both an α-amylase and a cyclodextrin-hydrolyzing enzyme. Appl. Environ. Microbiol. 2004, 70, 5988–5995.
209. Mesbah, N.M.; Wiegel, J. Biochemical characterization of halophilic, alkalithermophilic amylopullulanase PulD7 and truncated amylopullulanases PulD7ΔN and PulD7ΔC. Int. J. Biol. Macromol. 2018, 111, 632–638.
210. Zhao, Y.; Liu, Y.; Fu, Q.; Zhou, Y.; Qin, R.; Xiong, H.; Wang, Y. Domain analysis and site-directed

mutagenesis of a thermophilic pullulanase from *Thermotoga maritima* MSB8. 2023, 1–11.
211. Belshaw, N.J.; Williamson, G. Specificity of the binding domain of glucoamylase 1. Eur. J. Biochem. 1993, 211, 717–724.
212. Belshaw, N.J.; Williamson, G. Interaction of β-cyclodextrin with the granular starch binding domain of glucoamylase. Biochim. Biophys. Acta (BBA)-Protein Struct. Mol. Enzymol. 1991, 1078, 117–120.
213. Williamson, M.P.; Le Gal-Coëffet, M.-F.; Sorimachi, K.; Furniss, C.S.M.; Archer, D.B.; Williamson, G. Function of conserved tryptophans in the *Aspergillus niger* glucoamylase 1 starch binding domain. Biochemistry 1997, 36, 7535–7539.
214. Williamson, G.; Belshaw, N.J.; Williamson, M.P. O-glycosylation in *Aspergillus* glucoamylase. Conformation and role in binding. Biochem. J. 1992, 282, 423–428.
215. Van Bueren, A.L.; Higgins, M.; Wang, D.; Burke, R.D.; Boraston, A.B. Identification and structural basis of binding to host lung glycogen by streptococcal virulence factors. Nat. Struct. Mol. Biol. 2007, 14, 76–84.
216. Koay, A.; Woodcroft, B.; Petrie, E.J.; Yue, H.; Emanuelle, S.; Bieri, M.; Bailey, M.F.; Hargreaves, M.; Park, J.T.; Park, K.H.; et al. AMPK β subunits display isoform specific affinities for carbohydrates. FEBS Lett. 2010, 584, 3499–3503.
217. Mobbs, J.I.; Koay, A.; Di Paolo, A.; Bieri, M.; Petrie, E.J.; Gorman, M.A.; Doughty, L.; Parker, M.W.; Stapleton, D.I.; Griffin, M.D.W.; et al. Determinants of oligosaccharide specificity of the carbohydrate-binding modules of AMP-activated protein kinase. Biochem. J. 2015, 468, 245–257.
218. Hedin, N.; Barchiesi, J.; Gomez-Casati, D.F.; Iglesias, A.A.; Ballicora, M.A.; Busi, M. V. Identification and characterization of a novel starch branching enzyme from the picoalgae *Ostreococcus tauri*. Arch. Biochem. Biophys. 2017, 618, 52–61.
219. Palmer, E.; Freeman, T. Investigation into the use of C- and N-terminal GFP fusion proteins for subcellular localization studies using reverse transfection microarrays. Comp. Funct. Genomics 2004, 5, 342–353.
220. Hartl, F.U.; Hayer-Hartl, M. Molecular chaperones in the cytosol: From nascent chain to folded protein. Science (80-.). 2002, 295, 1852–1858.
221. Juge, N.; Nøhr, J.; Le Gal-Coëffet, M.F.; Kramhøft, B.; Furniss, C.S.M.; Planchot, V.; Archer, D.B.; Williamson, G.; Svensson, B. The activity of barley α-amylase on starch granules is enhanced by fusion of a starch binding domain from *Aspergillus niger* glucoamylase. Biochim. Biophys. Acta - Proteins Proteomics 2006, 1764, 275–284.
222. Hua, Y.W.; Chi, M.C.; Lo, H.F.; Hsu, W.H.; Lin, L.L. Fusion of Bacillus stearothermophilus leucine aminopeptidase II with the raw-starch-binding domain of *Bacillus* sp. TS-23 α-amylase generates a chimeric with enhanced thermostability and catalytic activity. J. Ind. Microbiol. Biotechnol. 2004, 31, 273–277.
223. Jia, X.; Guo, Y.; Lin, X.; You, M.; Lin, C.; Chen, L.; Chen, J. Fusion of a family 20 carbohydrate-binding module (CBM20) with cyclodextrin glycosyltransferase of *Geobacillus* sp. CHB1 improves catalytic efficiency. J. Basic Microbiol. 2017, 57, 471–480.
224. Reddy Chichili, V.P.; Kumar, V.; Sivaraman, J. Linkers in the structural biology of protein-protein interactions. Protein Sci. 2013, 22, 153–167.
225. Argos, P. An investigation of oligopeptides linking domains in protein tertiary structures and possible candidates for general gene fusion. J. Mol. Biol. 1990, 211, 943–958.
226. Bai, Y.; Shen, W.-C. Improving the oral efficacy of recombinant granulocyte colony-stimulating factor and transferrin fusion protein by spacer optimization. Pharm. Res. 2006, 23, 2116–2121.
227. Sabourin, M.; Tuzon, C.T.; Fisher, T.S.; Zakian, V.A. A flexible protein linker improves the function of

epitope-tagged proteins in Saccharomyces cerevisiae. Yeast 2007, 24, 39–45.
228. Jeong, W.H.; Lee, H.; Song, D.H.; Eom, J.H.; Kim, S.C.; Lee, H.S.; Lee, H.; Lee, J.O. Connecting two proteins using a fusion alpha helix stabilized by a chemical cross linker. Nat. Commun. 2016, 7, 1–9.
229. Arai, R.; Ueda, H.; Kitayama, A.; Kamiya, N.; Nagamune, T. Design of the linkers which effectively separate domains of a bifunctional fusion protein. Protein Eng. Des. Sel. 2001, 14, 529–532.
230. George, R.A.; Heringa, J. An analysis of protein domain linkers: their classification and role in protein folding. Protein Eng. Des. Sel. 2002, 15, 871–879.
231. Chen, X.; Bai, Y.; Zaro, J.L.; Shen, W.-C. Design of an in vivo cleavable disulfide linker in recombinant fusion proteins. Biotechniques 2010, 49, 513–518.
232. Leriche, G.; Chisholm, L.; Wagner, A. Cleavable linkers in chemical biology. Bioorg. Med. Chem. 2012, 20, 571–582.
233. Takamatsu, N.; Watanabe, Y.; Yanagi, H.; Meshi, T.; Shiba, T.; Okada, Y. Production of enkephalin in tobacco protoplasts using tobacco mosaic virus RNA vector. FEBS Lett. 1990, 269, 73–76.
234. Amet, N.; Lee, H.-F.; Shen, W.-C. Insertion of the designed helical linker led to increased expression of tf-based fusion proteins. Pharm. Res. 2009, 26, 523–528.
235. Oliveira, C.; Carvalho, V.; Domingues, L.; Gama, F.M. Recombinant CBM-fusion technology — Applications overview. Biotechnol. Adv. 2015, 33, 358–369.
236. Chen, L.; Ford, C.; Kusnadi, A.; Nikolov, Z.L. Improved adsorption to starch of a β-galactosidase fusion protein containing the starch-binding domain from *Aspergillus* glucoamylase. Biotechnol. Prog. 1991, 7, 225–229.
237. Dalmia, B.K.; Nikolov, Z.L. Characterization of a β-galactosidase fusion protein containing the starch-binding domain of *Aspergillus* glucoamylase. Ann. N. Y. Acad. Sci. 1994, 721, 160–167.
238. Nazarian Firouzabadi, F.; Kok-Jacon, G.A.; Vincken, J.P.; Ji, Q.; Suurs, L.C.J.M.; Visser, R.G.F. Fusion proteins comprising the catalytic domain of mutansucrase and a starch-binding domain can alter the morphology of amylose-free potato starch granules during biosynthesis. Transgenic Res. 2007, 16, 645–656.
239. Guillén, D.; Moreno-Mendieta, S.; Aguilera, P.; Sánchez, S.; Farres, A.; Rodríguez-Sanoja, R. The starch-binding domain as a tool for recombinant protein purification. Appl. Microbiol. Biotechnol. 2013, 97, 4141–4148.
240. Huang, H. Bin; Chi, M.C.; Hsu, W.H.; Liang, W.C.; Lin, L.L. Construction and one-step purification of *Bacillus kaustophilus* leucine aminopeptidase fused to the starch-binding domain of *Bacillus* sp. strain TS-23 α-amylase. Bioprocess Biosyst. Eng. 2005, 27, 389–398.
241. Peng, H.; Li, R.; Li, F.; Zhai, L.; Zhang, X.; Xiao, Y.; Gao, Y. Extensive hydrolysis of raw rice starch by a chimeric α-amylase engineered with α-amylase (AmyP) and a starch-binding domain from *Cryptococcus* sp. S-2. Appl. Microbiol. Biotechnol. 2018, 102, 743–750.
242. Yamaguchi, R.; Ishibashi, M.; Tokunaga, H.; Arakawa, T.; Tokunaga, M. Halophilic starch-binding domain as a novel fusion protein partner for efficient recombinant protein expression. 2015, 384–385.
243. Moreno-Mendieta, S.A.; Guillén, D.; Espitia, C.; Hernández-Pando, R.; Sanchez, S.; Rodríguez-Sanoja, R. A novel antigen-carrier system: The *Mycobacterium tuberculosis* Acr protein carried by raw starch microparticles. Int. J. Pharm. 2014, 474, 241–248.
244. Moreira, S.M.; Andrade, F.K.; Domingues, L.; Gama, M. Development of a strategy to functionalize a dextrin-based hydrogel for animal cell cultures using a starch-binding module fused to RGD sequence. 2008, 8, 1–8.
245. Zhang, Y.F.; Tang, Y.L.; Jiang, M.J.; Ji, Q. Effect of glgB/GASBD fusion gene expression on increased branching degree of potato starch and changes in physicochemical properties of starch. Int. J. Food

Prop. 2020, 23, 533–548.
246. Hua, Y.; Chi, M.; Lo, H.; Kuo, L.; Ku, K.; Lin, L. Adsorption-elution purification of chimeric *Bacillus stearothermophilus* leucine aminopeptidase II with raw-starch-binding activity. World J. Microbiol. Biotechnol. 2005, 21, 689–694.
247. Hu, H.; Yang, J.; Chen, J.; Chi, M.; Lin, L.; Ggt, B.; Amy, N.; Ggt, B.; Amy, N.; Ggt, B.; et al. Enzyme and Microbial Technology Enzymatic characterization of Bacillus licheniformis γ-glutamyltranspeptidase fused with N-terminally truncated forms of Bacillus sp TS-23 alpha-amylase. Enzyme Microb. Technol. 2012, 51, 86–94.
248. Latorre-García, L.; Adam, A.C.; Manzanares, P.; Polaina, J. Improving the amylolytic activity of *Saccharomyces cerevisiae* glucoamylase by the addition of a starch binding domain. J. Biotechnol. 2005, 118, 167–176.
249. Han, R.; Li, J.; Shin, H.D.; Chen, R.R.; Du, G.; Liu, L.; Chen, J. Carbohydrate-binding module-cyclodextrin glycosyltransferase fusion enables efficient synthesis of 2-O-d-glucopyranosyl-l-ascorbic acid with soluble starch as the glycosyl donor. Appl. Environ. Microbiol. 2013, 79, 3234–3240.
250. Park, J.H.; Kim, H.J.; Kim, Y.H.; Cha, H.; Kim, Y.W.; Kim, T.J.; Kim, Y.R.; Park, K.H. The action mode of *Thermus aquaticus* YT-1 4-α-glucanotransferase and its chimeric enzymes introduced with starch-binding domain on amylose and amylopectin. Carbohydr. Polym. 2007, 67, 164–173.
251. Zhong, Y.; Sagnelli, D.; Topbjerg, H.B.; Hasler-sheetal, H.; Andrzejczak, O.A.; Hooshmand, K.; Gislum, R.; Jiang, D.; Møller, I.M.; Blennow, A.; et al. Expression of starch-binding factor CBM20 in barley plastids controls the number of starch granules and the level of CO 2 fixation. 2020, 71, 234–246.
252. Levy, I.; Paldi, T.; Shoseyov, O. Engineering a bifunctional starch-cellulose cross-bridge protein. Biomaterials 2004, 25, 1841–1849.
253. Han, X.; Ding, N.; Ban, X.; Gu, Z.; Cheng, L.; Hong, Y.; Li, C.; Li, Z. Fusion of maltooligosaccharide-forming amylases from two origins for the improvement of maltopentaose synthesis. Food Res. Int. 2021, 150.
254. Lin, S.C.; Lin, I.P.; Chou, W.I.; Hsieh, C.A.; Liu, S.H.; Huang, R.Y.; Sheu, C.C.; Chang, M.D.T. CBM21 starch-binding domain: A new purification tag for recombinant protein engineering. Protein Expr. Purif. 2009, 65, 261–266.
255. Martín, M.; Wayllace, N.Z.; Valdez, H.A.; Gomez-Casati, D.F.; Busi, M. V. Improving the glycosyltransferase activity of *Agrobacterium tumefaciens* glycogen synthase by fusion of N-terminal starch binding domains (SBDs). Biochimie 2013, 95, 1865–1870.
256. Gorodetskii, V.; Lauterbach, J.; Rotermund, H.-H.; Block, J.H.; Ertl, G. Coupling between adjacent crystal planes in heterogeneous catalysis by propagating reaction–diffusion waves. Nature 1994, 370, 276–279.
257. Shaik, S.S.; Obata, T.; Hebelstrup, K.H.; Schwahn, K.; Fernie, A.R.; Mateiu, R. V; Blennow, A. Starch granule re-structuring by starch branching enzyme and glucan water dikinase modulation affects caryopsis physiology and metabolism. PLoS One 2016, 11, e0149613.
258. Blennow, A.; Skryhan, K.; Tanackovic, V.; Krunic, S.L.; Shaik, S.S.; Andersen, M.S.; Kirk, H.G.; Nielsen, K.L. Non-GMO potato lines, synthesizing increased amylose and resistant starch, are mainly deficient in isoamylase debranching enzyme. Plant Biotechnol. J. 2020, 18, 2096.
259. Lancaster, L.; Abdallah, W.; Banta, S.; Wheeldon, I. Engineering enzyme microenvironments for enhanced biocatalysis. Chem. Soc. Rev. 2018, 47, 5177–5186.
260. Feller, B.E.; Kellis, J.T.; Cascão-Pereira, L.G.; Robertson, C.R.; Frank, C.W. Interfacial biocatalysis on charged and immobilized substrates: The roles of enzyme and substrate surface charge. Langmuir 2011, 27, 250–263.
261. Christiansen, C.; Abou Hachem, M.; Janeček, Š.; Viksø-Nielsen, A.; Blennow, A.; Svensson, B. The

carbohydrate-binding module family 20-diversity, structure, and function. FEBS J. 2009, 276, 5006–5029.
262. Zhang, J.; Li, C.; Wang, G.; Cao, J.; Yang, X.; Liu, X.; Sun, L. α-Amylase inhibition of a certain dietary polyphenol is predominantly affected by the concentration of α-1, 4-glucosidic bonds in starchy and artificial substrates. Food Res. Int. 2022, 157, 111210.
263. Fersht, A.R. Catalysis, binding and enzyme-substrate complementarity. Proc. R. Soc. London. Ser. B. Biol. Sci. 1974, 187, 397–407.
264. Kari, J.; Olsen, J.P.; Jensen, K.; Badino, S.F.; Krogh, K.B.R.M.; Borch, K.; Westh, P. Sabatier principle for interfacial (heterogeneous) enzyme catalysis. ACS Catal. 2018, 8, 11966–11972.
265. Warren, F.J.; Royall, P.G.; Gaisford, S.; Butterworth, P.J.; Ellis, P.R. Binding interactions of α-amylase with starch granules: The influence of supramolecular structure and surface area. Carbohydr. Polym. 2011, 86, 1038–1047.
266. Tahir, R.; Ellis, P.R.; Butterworth, P.J. The relation of physical properties of native starch granules to the kinetics of amylolysis catalysed by porcine pancreatic α-amylase. Carbohydr. Polym. 2010, 81, 57–62.
267. Karamitros, C.S.; Murray, K.; Winemiller, B.; Lamb, C.; Stone, E.M.; D'Arcy, S.; Johnson, K.A.; Georgiou, G. Leveraging intrinsic flexibility to engineer enhanced enzyme catalytic activity. Proc. Natl. Acad. Sci. 2022, 119, e2118979119.
268. Wang, X.; Nie, Y.; Xu, Y. Improvement of the activity and stability of starch-debranching pullulanase from Bacillus naganoensis via tailoring of the active sites lining the catalytic pocket. J. Agric. Food Chem. 2018, 66, 13236–13242.
269. Zaera, F. Designing sites in heterogeneous catalysis: Are we reaching selectivities competitive with those of homogeneous catalysts? Chem. Rev. 2022, 122, 8594–8757.
270. Furukawa, M.; Kawakami, N.; Tomizawa, A.; Miyamoto, K. Efficient degradation of poly (ethylene terephthalate) with *Thermobifida fusca* cutinase exhibiting improved catalytic activity generated using mutagenesis and additive-based approaches. Sci. Rep. 2019, 9, 16038.
271. Arnling Bååth, J.; Jensen, K.; Borch, K.; Westh, P.; Kari, J. Sabatier principle for rationalizing enzymatic hydrolysis of a synthetic polyester. JACS Au 2022, 2, 1223–1231.
272. Zhang, B.; Dhital, S.; Gidley, M.J. Densely packed matrices as rate determining features in starch hydrolysis. Trends Food Sci. Technol. 2015, 43, 18–31.
273. Wang, Y.; Tian, Y.; Zhong, Y.; Suleiman, M.A.; Feller, G.; Westh, P.; Blennow, A.; Møller, M.S.; Svensson, B. Improved hydrolysis of granular starches by a psychrophilic α-amylase starch binding domain-fusion. J. Agric. Food Chem. 2023, 71, 9040–9050.
274. Wang, Y.; Tian, Y.; Christensen, S.J.; Blennow, A.; Svensson, B.; Møller, M.S. An enzymatic approach to quantify branching on the surface of starch granules by interfacial catalysis. Food Hydrocoll. 2024, 146.
275. Zhong, Y.; Bertoft, E.; Li, Z.; Blennow, A.; Liu, X. Amylopectin starch granule lamellar structure as deduced from unit chain length data. Food Hydrocoll. 2020, 108, 106053.
276. Blennow, A.; Wischmann, B.; Houborg, K.; Ahmt, T.; Jørgensen, K.; Engelsen, S.B.; Bandsholm, O.; Poulsen, P. Structure function relationships of transgenic starches with engineered phosphate substitution and starch branching. Int. J. Biol. Macromol. 2005, 36, 159–168.
277. Kozlov, S.S.; Blennow, A.; Krivandin, A. V; Yuryev, V.P. Structural and thermodynamic properties of starches extracted from GBSS and GWD suppressed potato lines. Int. J. Biol. Macromol. 2007, 40, 449–460.
278. Htoon, A.; Shrestha, A.K.; Flanagan, B.M.; Lopez-Rubio, A.; Bird, A.R.; Gilbert, E.P.; Gidley, M.J. Effects of processing high amylose maize starches under controlled conditions on structural organisation and amylase digestibility. Carbohydr. Polym. 2009, 75, 236–245.
279. Tian, Y.; Qu, J.; Zhou, Q.; Ding, L.; Cui, Y.; Blennow, A.; Zhong, Y.; Liu, X. High pressure/temperature

pasting and gelling of starch related to multilevel structure-analyzed with RVA 4800. Carbohydr. Polym. 2022, 295, 119858.
280. Feller, G.; Le Bussy, O.; Gerday, C. Expression of psychrophilic genes in mesophilic hosts: Assessment of the folding state of a recombinant-amylase. Appl. Environ. Microbiol. 1998, 64, 1163–1165.
281. Letunic, I.; Bork, P. Interactive Tree Of Life (iTOL) v5: An online tool for phylogenetic tree display and annotation. Nucleic Acids Res. 2021, 49, W293–W296.
282. Huang, Y.; Niu, B.; Gao, Y.; Fu, L.; Li, W. CD-HIT Suite: A web server for clustering and comparing biological sequences. Bioinformatics 2010, 26, 680–682.
283. Huang, L.; Zhang, H.; Wu, P.; Entwistle, S.; Li, X.; Yohe, T.; Yi, H.; Yang, Z.; Yin, Y. DbCAN-seq: A database of carbohydrate-active enzyme (CAZyme) sequence and annotation. Nucleic Acids Res. 2018, 46, D516–D521.
284. Sayers, E.W.; Cavanaugh, M.; Clark, K.; Pruitt, K.D.; Schoch, C.L.; Sherry, S.T.; Karsch-Mizrachi, I. GenBank. Nucleic Acids Res. 2021, 49, D92–D96.
285. UniProt: The universal protein knowledgebase in 2021. Nucleic Acids Res. 2021, 49, D480–D489.
286. Janeček, Š.; Svensson, B.; MacGregor, E.A. Structural and evolutionary aspects of two families of non-catalytic domains present in starch and glycogen binding proteins from microbes, plants and animals. Enzyme Microb. Technol. 2011, 49, 429–440.
287. Kuchtová, A.; Janeček, Š. In silico analysis of family GH77 with focus on amylomaltases from borreliae and disproportionating enzymes DPE2 from plants and bacteria. Biochim. Biophys. Acta - Proteins Proteomics 2015, 1854, 1260–1268.
288. Kuchtov, A.; Gentry, M.S.; Cek, S.J.; Cek, S.J. The unique evolution of the carbohydrate-binding module CBM20 in laforin. 2018, 592, 586–598.
289. Knegtel, R.M.A.; Strokopytov, B.; Penninga, D.; Faber, O.G.; Rozeboom, H.J.; Kalk, K.H.; Dijkhuizen, L.; Dijkstra, B.W. Crystallographic studies of the interaction of cyclodextrin glycosyltransferase from *Bacillus circulans* strain 251 with natural substrates and products. J. Biol. Chem. 1995, 270, 29256–29264.
290. Sievers, F.; Wilm, A.; Dineen, D.; Gibson, T.J.; Karplus, K.; Li, W.; Lopez, R.; McWilliam, H.; Remmert, M.; Söding, J. Fast, scalable generation of high-quality protein multiple sequence alignments using Clustal Omega. Mol. Syst. Biol. 2011, 7, 539.
291. Felsenstein, J. Confidence limits on phylogenies: An approach using the bootstrap. Evolution (N. Y). 1985, 39, 783–791.
292. Kumar, S.; Stecher, G.; Li, M.; Knyaz, C.; Tamura, K. MEGA X: Molecular evolutionary genetics analysis across computing platforms. Mol. Biol. Evol. 2018, 35, 1547.
293. Schiano-di-Cola, C.; Røjel, N.; Jensen, K.; Kari, J.; Sørensen, T.H.; Borch, K.; Westh, P. Systematic deletions in the cellobiohydrolase (CBH) Cel7A from the fungus *Trichoderma reesei* reveal flexible loops critical for CBH activity. J. Biol. Chem. 2019, 294, 1807–1815.
294. Ernst, O.; Zor, T. Linearization of the Bradford protein assay. J. Vis. Exp. 2010, e1918.
295. Christensen, S.J.; Madsen, M.S.; Zinck, S.S.; Hedberg, C.; Sørensen, O.B.; Svensson, B.; Meyer, A.S. Enzymatic potato starch modification and structure-function analysis of six diverse GH77 4-alpha-glucanotransferases. Int. J. Biol. Macromol. 2022, 224, 105–1149.
296. Kaimal, A.M.; Mujumdar, A.S.; Thorat, B.N. Resistant starch from millets: Recent developments and applications in food industries. Trends Food Sci. Technol. 2021, 111, 563–580.
297. Ståhl, M.; Berghel, J.; Frodeson, S.; Granström, K.; Renström, R. Effects on pellet properties and energy use when starch is added in the wood-fuel pelletizing process. Energy and Fuels 2012, 26, 1937–1945.
298. Tian, Y.; Wang, Y.; Liu, X.; Herburger, K.; Westh, P.; Møller, M.S.; Svensson, B.; Zhong, Y.; Blennow, A. Interfacial enzyme kinetics reveals degradation mechanisms behind resistant starch. Food Hydrocoll.

2023, 28, 108621.
299. Chi, C.; Li, X.; Huang, S.; Chen, L.; Zhang, Y.; Li, L.; Miao, S. Basic principles in starch multi-scale structuration to mitigate digestibility: A review. Trends Food Sci. Technol. 2021, 109, 154–168.
300. Zhai, Y.; Li, X.; Bai, Y.; Jin, Z.; Svensson, B. Maltogenic α-amylase hydrolysis of wheat starch granules: Mechanism and relation to starch retrogradation. Food Hydrocoll. 2022, 124, 107256.
301. Zhong, Y.; Xu, J.; Liu, X.; Ding, L.; Svensson, B.; Herburger, K.; Guo, K.; Pang, C.; Blennow, A. Recent advances in enzyme biotechnology on modifying gelatinized and granular starch. Trends Food Sci. Technol. 2022, 123, 343–354.
302. Liu, X.; Luan, H.; Jinglin, Y.; Wang, S.; Wang, S.; Copeland, L. A method for characterizing short-range molecular order in amorphous starch. Carbohydr. Polym. 2020, 242, 116405.
303. Li, X.; Wang, Y.; Wu, J.; Jin, Z.; Dijkhuizen, L.; Svensson, B.; Bai, Y. Designing starch derivatives with desired structures and functional properties via rearrangements of glycosidic linkages by starch-active transglycosylases. Crit. Rev. Food Sci. Nutr. 2023, 1–14.
304. Guo, L.; Deng, Y.; Lu, L.; Zou, F.; Cui, B. Synergistic effects of branching enzyme and transglucosidase on the modification of potato starch granules. Int. J. Biol. Macromol. 2019, 130, 499–507.
305. Gui, Y.; Zou, F.; Li, J.; Tang, J.; Guo, L.; Cui, B. Corn starch modification during endogenous malt amylases: The impact of synergistic hydrolysis time of α-amylase and β-amylase and limit dextrinase. Int. J. Biol. Macromol. 2021, 190, 819–826.
306. Li, Y.; Ren, J.; Liu, J.; Sun, L.; Wang, Y.; Liu, B.; Li, C.; Li, Z. Modification by α-D-glucan branching enzyme lowers the *in vitro* digestibility of starch from different sources. Int. J. Biol. Macromol. 2018, 107, 1758–1764.
307. Sabatier, P. *La Catalyse En Chimie Organique*; C. Béranger, 1920; Vol. 3;.
308. Kari, J.; Schaller, K.; Molina, G.A.; Borch, K.; Westh, P. The Sabatier principle as a tool for discovery and engineering of industrial enzymes. Curr. Opin. Biotechnol. 2022, 78, 102843.
309. Wei, R.; Weber, G. Performance of PET hydrolases with tethered binding modules in large-scale applications. Chem Catal. 2022, 2, 2406–2408.
310. Medford, A.J.; Vojvodic, A.; Hummelshøj, J.S.; Voss, J.; Abild-Pedersen, F.; Studt, F.; Bligaard, T.; Nilsson, A.; Nørskov, J.K. From the Sabatier principle to a predictive theory of transition-metal heterogeneous catalysis. J. Catal. 2015, 328, 36–42.
311. Wang, Y.; Pang, C.; Mohammad-beigi, H.; Li, X.; Wu, Y.; Karen, M.; Hong, T.; Bai, Y.; Sofie, M.; Svensson, B. Sequential starch modification by branching enzyme and 4- α -glucanotransferase improves retention of curcumin in starch-alginate beads. 2024, 323.
312. Wang, Y.; Wu, Y.; Christensen, S.J.; Janeček, Š.; Bai, Y.; Møller, M.S.; Svensson, B. Impact of starch binding domain fusion on activities and starch product structure of 4-α-glucanotransferase. Molecules 2023, 23, 1320.
313. Brückner, S. Pulwin: A program for analyzing powder x-ray diffraction patterns. Powder Diffr. 2000, 15, 218–219.
314. Cramer, P. AlphaFold2 and the future of structural biology. Nat. Struct. Mol. Biol. 2021, 28, 704–705.
315. Wang, Z.; Xin, C.; Li, C.; Gu, Z.; Cheng, L.; Hong, Y.; Ban, X.; Li, Z. Expression and characterization of an extremely thermophilic 1,4-α-glucan branching enzyme from *Rhodothermus obamensis* STB05. Protein Expr. Purif. 2019, 164, 105478.
316. Xu, J.; Blennow, A.; Li, X.; Chen, L.; Liu, X. Gelatinization dynamics of starch in dependence of its lamellar structure, crystalline polymorphs and amylose content. Carbohydr. Polym. 2020, 229, 115481.
317. Yuryev, V.P.; Krivandin, A. V; Kiseleva, V.I.; Wasserman, L.A.; Genkina, N.K.; Fornal, J.; Blaszczak, W.; Schiraldi, A. Structural parameters of amylopectin clusters and semi-crystalline growth rings in wheat

starches with different amylose content. Carbohydr. Res. 2004, 339, 2683–2691.
318. Singh, N.; Singh, J.; Kaur, L.; Sodhi, N.S.; Gill, B.S. Morphological, thermal and rheological properties of starches from different botanical sources. Food Chem. 2003, 81, 219–231.
319. Capron, I.; Robert, P.; Colonna, P.; Brogly, M.; Planchot, V. Starch in rubbery and glassy states by FTIR spectroscopy. Carbohydr. Polym. 2007, 68, 249–259.
320. Van Soest, J.J.G.; Tournois, H.; de Wit, D.; Vliegenthart, J.F.G. Short-range structure in (partially) crystalline potato starch determined with attenuated total reflectance Fourier-transform IR spectroscopy. Carbohydr. Res. 1995, 279, 201–214.
321. Lopez-Rubio, A.; Clarke, J.M.; Ben Scherer; Topping, D.L.; Gilbert, E.P. Structural modifications of granular starch upon acylation with short-chain fatty acids. Food Hydrocoll. 2009, 23, 1940–1946.
322. Tian, Y.; Liu, X.; Judas, J.; Kirkensgaard, K.; Khakimov, B.; Enemark-rasmussen, K.; Henrik, K.; Blennow, A.; Zhong, Y. Characterization of different high amylose starch granules. Part I : Multi-scale structures and relationships to thermal properties. Food Hydrocoll. 2024, 146, 109286.
323. Vermeylen, R.; Goderis, B.; Reynaers, H.; Delcour, J.A. Amylopectin molecular structure reflected in macromolecular organization of granular starch. Biomacromolecules 2004, 5, 1775–1786.
324. Gavgani, H.N.; Fawaz, R.; Ehyaei, N.; Walls, D.; Pawlowski, K.; Fulgos, R.; Park, S.; Assar, Z.; Ghanbarpour, A.; Geiger, J.H. A structural explanation for the mechanism and specificity of plant branching enzymes I and IIb. J. Biol. Chem. 2022, 298, 101395.
325. Zhu, F. Encapsulation and delivery of food ingredients using starch based systems. Food Chem. 2017, 229, 542–552.
326. Chen, Y.; Song, H.; Huang, K.; Guan, X. Novel porous starch/alginate hydrogels for controlled insulin release with dual response to pH and amylase. Food Funct. 2021, 12, 9165–9177.
327. Marefati, A.; Sjöö, M.; Timgren, A.; Dejmek, P.; Rayner, M. Fabrication of encapsulated oil powders from starch granule stabilized W/O/W Pickering emulsions by freeze-drying. Food Hydrocoll. 2015, 51, 261–271.
328. Koev, T.T.; Harris, H.C.; Kiamehr, S.; Khimyak, Y.Z.; Warren, F.J. Starch hydrogels as targeted colonic drug delivery vehicles. Carbohydr. Polym. 2022, 289, 119413.
329. Xing, Y.; Xu, Q.; Ma, Y.; Che, Z.; Cai, Y.; Jiang, L. Effect of porous starch concentrations on the microbiological characteristics of microencapsulated *Lactobacillus acidophilus*. Food Funct. 2014, 5, 972–983.
330. Gu, Z.; Chen, B.; Tian, Y. Highly branched corn starch: Preparation, encapsulation, and release of ascorbic acid. Food Chem. 2021, 343, 128485.
331. Bu, X.; Guan, M.; Dai, L.; Ji, N.; Qin, Y.; Xu, X.; Xiong, L. Fabrication of starch-based emulsion gel beads by an inverse gelation technique for loading proanthocyanidin and curcumin. Food Hydrocoll. 2023, 137, 108336.
332. López-Córdoba, A.; Deladino, L.; Martino, M. Release of yerba mate antioxidants from corn starch-alginate capsules as affected by structure. Carbohydr. Polym. 2014, 99, 150–157.
333. Manzoor, A.; Dar, A.H.; Pandey, V.K.; Shams, R.; Khan, S.; Panesar, P.S.; Kennedy, J.F.; Fayaz, U.; Khan, S.A. Recent insights into polysaccharide-based hydrogels and their potential applications in food sector: A review. Int. J. Biol. Macromol. 2022, 213, 987–1006.
334. Cong, Z.; Shi, Y.; Wang, Y.; Wang, Y.; Niu, J.; Chen, N.; Xue, H. A novel controlled drug delivery system based on alginate hydrogel/chitosan micelle composites. Int. J. Biol. Macromol. 2018, 107, 855–864.
335. López-Córdoba, A.; Deladino, L.; Martino, M. Effect of starch filler on calcium-alginate hydrogels loaded with yerba mate antioxidants. Carbohydr. Polym. 2013, 95, 315–323.

Appendix 1 – Poster presentations

Poster 1: “Enhanced Interfacial Catalysis of Granular Starch by Starch Binding Domain Fusions”. **Yu Wang**, Yu Tian, Yuyue Zhong, Mohammad A. Suleiman, Georges Feller, Peter Westh, Andreas Blennow, Marie Sofie Møller, Birte Svensson. Poster created and presented by Yu Wang at the following events:

The 8th Symposium on the Alpha-Amylase Family - ALAMY_8, Slovakia, October 9 to 13, 2022.

Enzyme Future-Enzyme Discovery and Engineering, DTU Bioengineering, Denmark, October 27, 2022.

Linderstrøm-Lang Symposium, Copenhagen Biocenter, Denmark, November 18, 2022.

Poster 2: “Enzymatic Degradation of Starch Granules by Interfacial Catalysis” **Yu Wang**, Yu Tian, Yuyue Zhong, Georges Feller, Xinxun Liu, Klaus Herburger, Peter Westh, Andreas Blennow, Marie Sofie Møller, **Birte Svensson**. Gordon Research Conference, Poster Academy, New Hampshire, USA, July 23 to 28, 2023. Poster created by Yu Wang and presented by Birte Svensson.

DTU Bioengineering
Department of Biotechnology and Biomedicine

Yu Wang
yuawa@dtu.dk

Enhanced Interfacial Catalysis of Granular Starch by Starch Binding Domain Fusions

Yu Wang [1], Yu Tian [3], Yuyue Zhong [3], Mohammad A. Suleiman [1], Georges Feller [4], Peter Westh [5], Andreas Blennow [3], Marie S. Møller [2,*], Birte Svensson [1,*]

1: Enzyme and Protein Chemistry, Technical University of Denmark, Denmark, 2: Applied Molecular Enzyme Chemistry, Technical University of Denmark, Denmark, 3: Department of Plant and Environmental Sciences, University of Copenhagen, Denmark, 4: Center for Protein Engineering-InBioS, University of Liège, Belgium, 5: Interfacial Enzymology, Technical University of Denmark, Denmark
* Corresponding authors: Marie S. Møller: msmo@dtu.dk, Birte Svensson: bis@bio.dtu.dk

INTRODUCTION: To improve activity of a psychrophilic α-amylase from *Pseudoalteromonas haloplanktis* TAB23 (AHA) [1] towards starch granule, an SBD of CBM20 either from *Aspergillus niger* glucoamylase (SBD_{GA}) or *Arabidopsis thaliana* phosphoglucan, water dikinase (SBD_{GWD3}) was fused to the C-terminus of AHA. The interfacial catalysis towards five maize starches was analyzed by combined conventional and inverse Michaelis-Menten kinetics. The SBD-fusion increased the number of binding sites and attack sites by 3-7 and 2-5 fold, respectively. Interestingly, the fused SBD changed the substrate specificity of AHA.

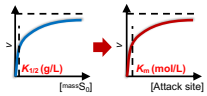

$K_m = {}^{kin}\Gamma_{max} \cdot K_{1/2}$

$K_{1/2}$: The mass load at half-saturation.
K_M: The molar concentration of attack sites at half-saturation.
${}^{kin}\Gamma_{max}$: Density of attack sites (mol/g).
${}^{ads}\Gamma_{max}$: Density of binding sites (mol/g).

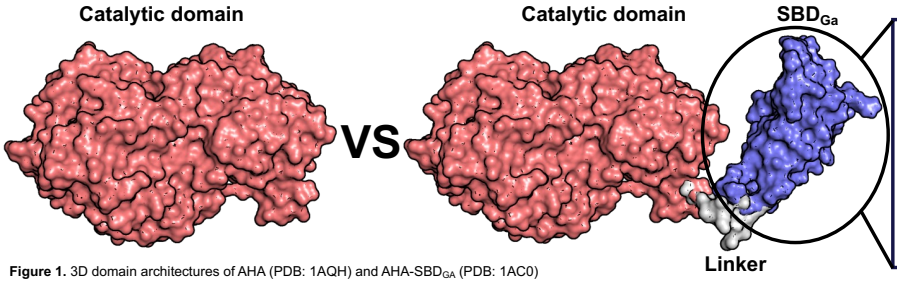

Figure 1. 3D domain architectures of AHA (PDB: 1AQH) and AHA-SBD_{GA} (PDB: 1AC0)

Enhanced binding capacity

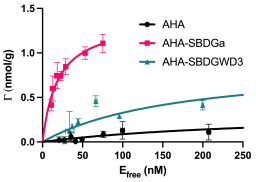

Figure 2. Binding isotherms on WMS granules by AHAs.

Increased density of attack site (${}^{kin}\Gamma_{max}$)

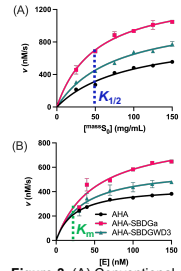

${}^{kin}\Gamma_{max} = \frac{K_m}{K_{1/2}}$

AHA	$k_{cat}/K_{1/2}$ (L·[g·s]$^{-1}$)	0.32 ± 0.03
	${}^{kin}\Gamma_{max}$ (nmol/g)	0.28 ± 0.02
	${}^{ads}\Gamma_{max}$ (nmol/g)	0.35 ± 0.08
	A/B ratio (%)	79.92
AHA-SBD_{GA}	$k_{cat}/K_{1/2}$ (L·[g·s]$^{-1}$)	0.69 ± 0.13
	${}^{kin}\Gamma_{max}$ (nmol/g)	0.86 ± 0.04
	${}^{ads}\Gamma_{max}$ (nmol/g)	1.36 ± 0.24
	A/B ratio (%)	63.10
AHA-SBD_{GWD3}	$k_{cat}/K_{1/2}$ (L·[g·s]$^{-1}$)	0.42 ± 0.06
	${}^{kin}\Gamma_{max}$ (nmol/g)	0.61 ± 0.17
	${}^{ads}\Gamma_{max}$ (nmol/g)	0.97 ± 0.03
	A/B ratio (%)	62.60

Figure 3. (A) Conventional and (B) inverse kinetics of WMS granules by AHA and SBD fusions.

Application of Sabatier principle

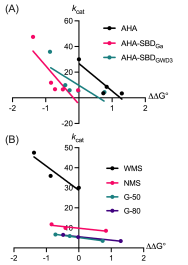

Figure 4. Fitting of k_{cat} with ΔΔG° for AHA and AHA-SBD fusions (A) or starch granules (B).

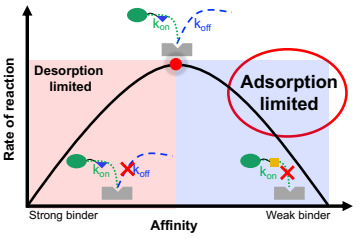

Figure 5. The volcano plot illustrating the Sabatier principle. This figure is inspired by Kari [2].

Changed substrate specificity

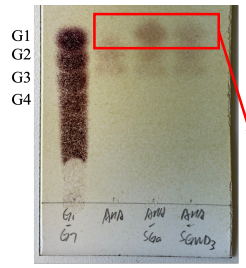

Enzyme	[Glucose] (μM)
AHA	218 ± 30
AHA-SBD_{Ga}	1854 ± 28
AHA-SBD_{GWD3}	986 ± 64

Figure 6. Product of AHAs from WMS granule.

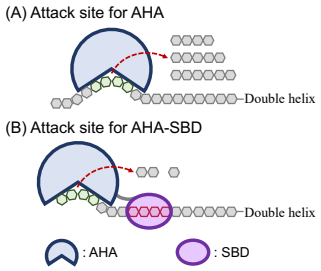

Figure 7. Definition of attack site for AHA (A) and SBD fusions (B).

CONCLUSION

- Catalytic efficiency of AHA on starch granules was much improved because of the increased density of attack site.
- Substrate specificity changed by the SBD fusions.

PROSPECT

- Screen SBDs with higher affinity and construct fusions with AHA, which can show desorption limitation.
- Understand the changes on substrate specificity by SBD fusion.

References

[1] Feller, G., et al.. Stability and Structural Analysis of α-amylase from the Antarctic Psychrophile *Alteromonas Haloplanctis* A23. Eur. J. Biochem. 1994, 222 (2), 441–447.
[2] Kari, J., et al.. Sabatier Principle for Interfacial (Heterogeneous) Enzyme Catalysis. ACS Catal. 2018, 8 (12), 11966–11972.

Acknowledgements

Enzyme and Protein Chemistry Group (Technical University of Denmark)
Travel grant from William Demant Foundation (Case no. 22-2985)

Funding

To be published

DTU Bioengineering
Department of Biotechnology and Biomedicine

Enzymatic Degradation of Starch Granules by Interfacial Catalysis

Yu Wang [1], Yu Tian [2], Stefan Jarl Christensen [3], Yuyue Zhong [2], Georges Feller [4], Xinxun Liu [5], Klaus Herburger [6], Peter Westh [7], Andreas Blennow [2], Marie S. Møller [8,*], Birte Svensson [1,*]

1: Enzyme and Protein Chemistry, DTU Bioengineering, Technical University of Denmark, Denmark; 2: Department of Plant and Environmental Sciences, University of Copenhagen, Denmark; 3: Enzyme Technology, DTU Bioengineering; 4: Center for Protein Engineering-InBioS, University of Liège, Belgium; 5: College of Food Science and Engineering, Nanjing University of Finance and Economics, China; 6: Institute of Biosciences, University of Rostock, Germany; 7: Interfacial Enzymology, DTU Bioengineering; 8: Applied Molecular Enzyme Chemistry, DTU Bioengineering
* Corresponding authors: Marie S. Møller: msmo@dtu.dk, Birte Svensson: bis@bio.dtu.dk

INTRODUCTION: Enzymatic modification of starch granules occurs naturally through heterogenous catalysis during biosynthesis and degradation. Thus, in Nature mobilization and utilization of storage starch in seeds and tubers during germination as well as during digestion by enzymes from the gut microbiota rely on intimate binding of enzymes onto starch granules.

We investigated, inspired by cellulase-crystalline cellulose interfacial kinetics [1,2], how different amylolytic enzymes degrade waxy maize starch (WMS) granules by using a combination of conventional Michaelis-Menten kinetics having substrate in excess, with inverse Michaelis-Menten kinetics having enzyme in excess, and a Langmuir isotherm binding to determine kinetic parameters (k_{cat} and K_m) as well as the densities of attack sites ($^{kin}\Gamma_{max}$) and enzyme binding sites ($^{ads}\Gamma_{max}$) [3,4].

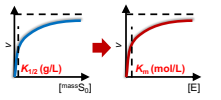

$K_m = {}^{kin}\Gamma_{max} \cdot K_{1/2}$ [1]

$K_{1/2}$: The mass load at half-saturation.
K_M: The molar concentration of attack sites at half-saturation.
$^{kin}\Gamma_{max}$: Density of attack sites (mol/g).

Enhanced Interfacial Catalysis of a Psychrophilic α-Amylase by SBD-Fusion [3]

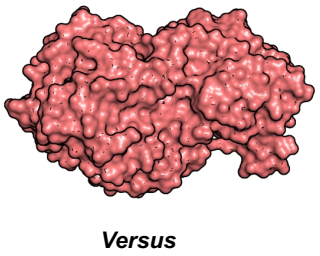

Versus

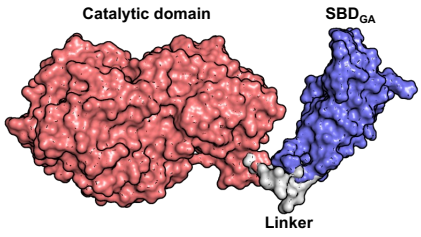

Figure 1. 3D domain architecture models of AHA α-amylase from *Pseudoalteromonas haloplanktis* (PDB: 1AQH) and AHA fused with CBM20 starch binding domain from *Aspergillus niger* glucoamylase, SBD_{GA} (PDB: 1AC0)

Increased density of attack sites ($^{kin}\Gamma_{max}$) and binding sites ($^{ads}\Gamma_{max}$)

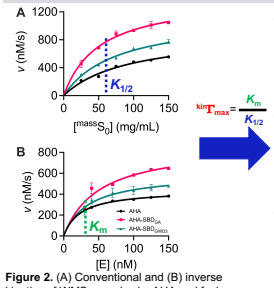

Figure 2. (A) Conventional and (B) inverse kinetics of WMS granules by AHA and fusions with CBM20 SBDs from *A. niger* glucoamylase and potato glucan, water dikinase 3

AHA	$k_{cat}/K_{1/2}$ (L·[g·s]$^{-1}$)	0.32 ± 0.03 (**1**)
	$^{kin}\Gamma_{max}$ (nmol/g)	0.28 ± 0.02 (**1**)
	$^{ads}\Gamma_{max}$ (nmol/g)	0.35 ± 0.08 (**1**)
	A/B ratio (%)	79.92
AHA-SBD_{GA}	$k_{cat}/K_{1/2}$ (L·[g·s]$^{-1}$)	0.69 ± 0.13 (**2.2**)
	$^{kin}\Gamma_{max}$ (nmol/g)	0.86 ± 0.04 (**3.1**)
	$^{ads}\Gamma_{max}$ (nmol/g)	1.36 ± 0.24 (**3.9**)
	A/B ratio (%)	63.10
AHA-SBD_{GWD3}	$k_{cat}/K_{1/2}$ (L·[g·s]$^{-1}$)	0.42 ± 0.06 (**1.3**)
	$^{kin}\Gamma_{max}$ (nmol/g)	0.61 ± 0.17 (**2.2**)
	$^{ads}\Gamma_{max}$ (nmol/g)	0.97 ± 0.03 (**2.8**)
	A/B ratio (%)	62.60

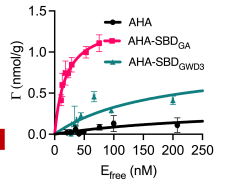

Figure 3. Binding isotherms on WMS granules by AHA and AHA SBD-fusions.

Enzyme	AHA	AHA-SBD_{GA}	AHA-SBD_{GWD3}
K_d (nM)	293 ± 52 (15.4)	19 ± 8 (1)	128 ± 54 (6.7)

Changed substrate specificity

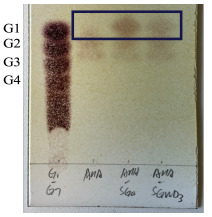

Figure 4. Products of AHA, AHA-SBD_{GA} and AHA-SBD_{GWD3} from WMS granules

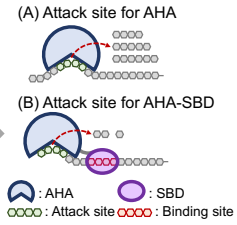

Figure 5. Definition of attack site for (A) AHA and (B) AHA SBD-fusions

Sabatier principle

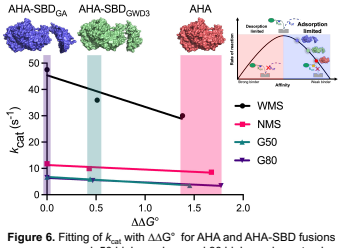

Figure 6. Fitting of k_{cat} with ΔΔG° for AHA and AHA-SBD fusions on waxy, normal, 50 high-amylose and 80 high-amylose starch granules. This shows adsorption-limited catalysis

Application of Interfacial Kinetics

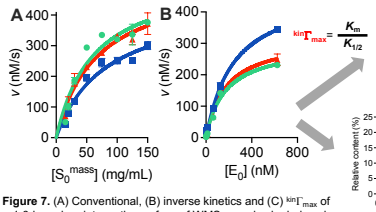

Figure 7. (A) Conventional, (B) inverse kinetics and (C) $^{kin}\Gamma_{max}$ of α-1,6-branch points on the surface of WMS granules hydrolysed by pullulanase from *Bacillus licheniformis*. Green: WMS; Blue: branching enzyme modified WMS; red: 4-α-glucanotransferase modified WMS

Figure 8. Chain length distribution released by *Bl*Pul from WMS and modified WMS granules

CONCLUSION and PROSPECTS

- Catalytic efficiency of AHA on starch granules improved by SBD-fusion because of the increased density of attack sites. The Sabatier principle indicated adsorption-limited catalysis, i.e. higher affinity elicits higher activity;
- Substrate specificity changed by the SBD-fusion;
- We implemented a novel approach to quantify α-1,6-branch points by measuring the attack site density ($^{kin}\Gamma_{max}$) for the debranching enzyme *Bl*Pul acting on the surface of starch granules using interfacial catalysis.
- In the future: screen for SBDs with higher affinity to construct fusions with AHA, which show desorption-limited catalysis;
- Identify more changes of substrate specificity on different starch granules for AHA and *Bl*Pul and related enzymes by SBD fusion.

References
[1] Kari et al. ACS Catal. 2017, 7, 4904–14
[2] Kari et al. ACS Catal. 2018, 8, 11966–72
[3] Wang et al. J Agric Food Chem. 2023, 71, 9040–9050
[4] Tian et al. Food Hydrocoll. 2023, 140, 108621

Acknowledgements
Enzyme and Protein Chemistry Group (Technical University of Denmark)

Funding
Innovation Fund Denmark